REPORT NO.
UC SESM 73-4

STRUCTURES AND MATERIALS RESEARCH
DEPARTMENT OF CIVIL ENGINEERING

IDENTIFICATION OF NONLINEAR MATERIALS BY FINITE ELEMENT METHODS

by

ROBERT H. IDING

JANUARY 1973

STRUCTURAL ENGINEERING LABORATORY
UNIVERSITY OF CALIFORNIA
BERKELEY CALIFORNIA

Structures and Materials Research
Department of Civil Engineering
Division of Structural Engineering
and Structural Mechanics

IDENTIFICATION OF NONLINEAR MATERIALS BY FINITE ELEMENT METHODS

by

Robert H. Iding

Dissertation Committee

R. L. Taylor
K. S. Pister
J. N. Distefano

Professors of Civil Engineering
University of California, Berkeley

R. J. Devogelaere

Professor of Computer Science
University of California, Berkeley

Structural Engineering Laboratory
University of California
Berkeley, California

January 1973

Effective Writing in Corporate Security

Custom Workshop for

Bank of America

ABSTRACT

A method is developed to identify nonlinear material behavior. Discussed are the types of functionals that characterize various classes of nonlinear thermomechanical materials, the types of experiments needed to generate data capable of identifying nonlinear material constitutive functionals, and the inverse boundary value problem that models the identification problem. A new technique of material parameterization that utilizes finite elements defined over the multi-dimensional domain of the material operator is found to give very useful results. The identification problem is expressed as a system of nonlinear algebraic equations that couples the set of experimentally observed measurements and the discretized boundary value problem.

A computer program is developed for the special case of isotropic, incompressible elastic materials. A wide range of numerical examples are studied to determine the accuracy and stability of this material identification algorithm.

TABLE OF CONTENTS

I. NONLINEAR THEORY OF THERMOMECHANICS

1.1 Introduction

In recent years a comprehensive theory of nonlinear continuum mechanics has been developed [1, 2, 3] which generalizes the traditional linearized field theories of the nineteenth century. Parts of this theory involve material constitutive functionals which describe the response characteristics of materials undergoing certain processes. The constitutive theory of materials gives information about the general form these functions must take, but in the end the exact determination of the response functionals for any particular material must come from actual experiments conducted upon samples of that material. It is an extremely complex problem to devise adequate experiments that are performable and to use the information to identify the material response functionals. Only a few very simple types of nonlinear materials have yielded to successful identification [4, 5, 6], and to date virtually all numerical applications of nonlinear field theory have employed either these simple materials or other assumed constitutive functionals which may or may not describe any real material [7 - 10]. This dissertation develops material identification techniques capable of dealing with materials that are as generalized as the current nonlinear field theory.

The remainder of this chapter will summarize the parts of nonlinear continuum mechanics theory underlying this study.

1.2 Motion and Deformation

In continuum theory a material body is represented as a set of particles in one-to-one correspondence with a region of Euclidean space. The motion of a body is a succession of configurations - the regions in space occupied by the set of particles. In each configuration $\mathcal{B}_{\underset{\sim}{x}}$ each particle p can be placed in one-to-one correspondence with an ordered triplet $\underset{\sim}{x}$ - the spatial coordinates, or position of the particle p. The motion of the whole body (the set of all particles) can be mathematically expressed by the function or mapping

$$\underset{\sim}{x} = \underset{\sim}{\chi}(p, t) \tag{1.1}$$

where t is the time when particle p occupies the position $\underset{\sim}{x}$, and $\underset{\sim}{\chi}$ is called a deformation function. Motion can be expressed in a more mathematically usable form if some particular configuration of particles is chosen as a reference configuration (denoted by $\mathcal{B}_{\underset{\sim}{\kappa}}$) and the position $\underset{\sim}{X}$ of the particles in that configuration made to identify the particles themselves. Hence the motion of the body with respect to a reference configuration $\mathcal{B}_{\underset{\sim}{\kappa}}$ is defined by

$$\underset{\sim}{x} = \underset{\sim}{\chi}(\underset{\sim}{X}, t) \tag{1.2}$$

where the functional form of $\underset{\sim}{\chi}$ will depend on the particular configuration chosen as reference. The deformation function in (1.2) in effect maps the reference configuration $\mathcal{B}_{\underset{\sim}{\kappa}}$ into the configuration $\mathcal{B}_{\underset{\sim}{x}}$ occupied by the body at time t, as shown below in Figure 1.1.

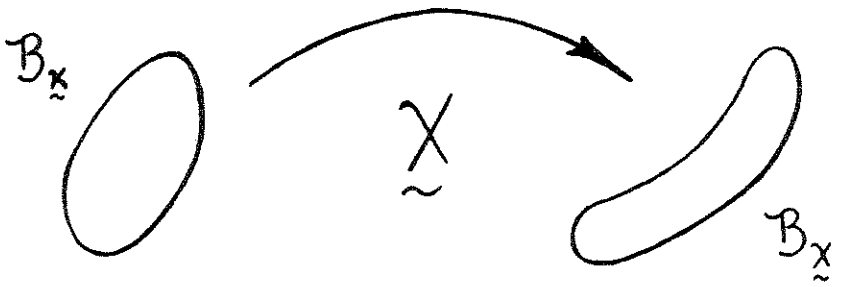

Fig. 1.1

Another description of motion is given by the displacement field $\underset{\sim}{u}(\underset{\sim}{X},t)$, which defines a particle's relative motion from its position in $\mathcal{B}_{\underset{\sim}{K}}$. Displacement and deformation fields are related by

$$\underset{\sim}{u}(\underset{\sim}{X},t) = \underset{\sim}{\chi}(\underset{\sim}{X},t) - \underset{\sim}{X}. \tag{1.3}$$

Motion has a local description as well as the global description above. That is, as the reference configuration $\mathcal{B}_{\underset{\sim}{K}}$ is mapped into the configuration $\mathcal{B}_{\underset{\sim}{\chi}}$, the neighborhood of a particle p is mapped from $N_{\underset{\sim}{K}}$ to $N_{\underset{\sim}{\chi}}$. That is, a material point $\underset{\sim}{X} + d\underset{\sim}{X}$ in $N_{\underset{\sim}{K}}$ moves to $\underset{\sim}{\chi} + d\underset{\sim}{\chi}$ in $N_{\underset{\sim}{\chi}}$. The relation between the two differential elements,

$$d\underset{\sim}{\chi} = \underset{\sim}{F} \cdot d\underset{\sim}{X}, \tag{1.4}$$

is expressed by the linear transformation (or tensor) $\underset{\sim}{F}$, called the deformation gradient and defined by

$$\underset{\sim}{F}(\underset{\sim}{X},t) = \nabla\underset{\sim}{\chi}(\underset{\sim}{X},t). \tag{1.5}$$

The transformation $\underset{\sim}{F}$ maps a neighborhood $N_{\underset{\sim}{K}}$ in $\mathcal{B}_{\underset{\sim}{K}}$ into a neighborhood $N_{\underset{\sim}{\chi}}$ in $\mathcal{B}_{\underset{\sim}{\chi}}$, as shown below in Figure 1.2.

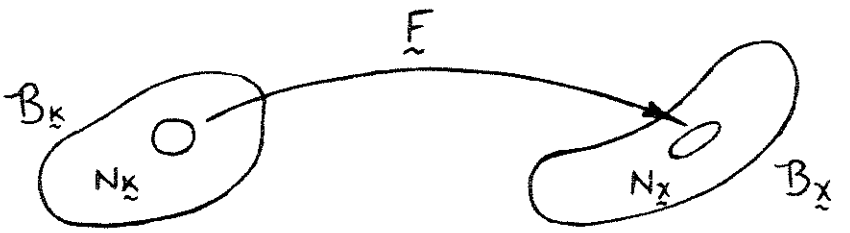

Fig. 1.2

Another local measure of deformation, which has the advantage of being a symmetric tensor, is the Cauchy-Green deformation tensor, defined by

$$\underset{\sim}{C} = \underset{\sim}{F}^T \cdot \underset{\sim}{F}. \tag{1.6}$$

A symmetric tensor such as $\underset{\sim}{C}$ has the property that certain quantities associated with it are invariant under orthogonal transformation. One set of invariants, called the principal invariants, is defined by

$$I_1 = \mathrm{tr}\,\underset{\sim}{C} \tag{1.7a}$$

$$I_2 = \det\underset{\sim}{C} \cdot \mathrm{tr}\,\underset{\sim}{C}^{-1} \tag{1.7b}$$

$$I_3 = \det\underset{\sim}{C} \tag{1.7c}$$

and is particularly useful in material constitutive theory. The tensor $\underset{\sim}{C}$, of course, has other sets of invariants, such as the principal values of $\underset{\sim}{C}$ or the principal moments of $\underset{\sim}{C}$ [11].

Another strain measure whose domain is the reference configuration $\mathcal{B}_K$ is the Lagrangian strain tensor $\underset{\sim}{E}$, defined by

$$2\underset{\sim}{E}(\underset{\sim}{X},t) = \underset{\sim}{C}(\underset{\sim}{X},t) - \underset{\sim}{I} \tag{1.8}$$

where $\underset{\sim}{I}$ is the identity transformation tensor. Lagrangian strain and displacement are related by the expression

$$\underset{\sim}{E} = \frac{1}{2}\left[\nabla\underset{\sim}{u} + \nabla\underset{\sim}{u}^{T} + \nabla\underset{\sim}{u}^{T}\cdot\nabla\underset{\sim}{u} \right], \tag{1.9}$$

a direct result of substituting (1.6), (1.5), (1.4) and the gradient of (1.3) into the definition of $\underset{\sim}{E}$ (1.8). This choice of strain measure is particularly convenient due to its symmetry and direct correlation with an intuitive sense of deformation [12]. Earlier nonlinear elasticity theory and numerical applications of the current theory tend to be expressed in terms of Lagrangian strain (1.9) rather than deformation gradient (1.5).

For situations in which the motion of the body is infinitesimal (i. e., when the inequality

$$\| \underset{\sim}{x} - \underset{\sim}{X} \| \ll 1 \tag{1.10}$$

holds at all points in the body at all times t) the reference configuration $\mathcal{B}_{\underset{\sim}{X}}$ and the deformed configuration $\mathcal{B}_{\underset{\sim}{x}}$ differ only by the infinitesimal displacement vector $\underset{\sim}{u}(\underset{\sim}{X}, t)$. Hence the Lagrangian strain (1.9) becomes linear in $\nabla\underset{\sim}{u}$ and is called the infinitesimal strain tensor $\underset{\sim}{\epsilon}$, such that

$$\underset{\sim}{\epsilon} = \frac{1}{2}\left[\nabla\underset{\sim}{u} + \nabla\underset{\sim}{u}^{T} \right]. \tag{1.11}$$

Note that the spatial domain of $\underset{\sim}{\epsilon}$ can be taken to be either $\mathcal{B}_{\underset{\sim}{X}}$ or $\mathcal{B}_{\underset{\sim}{x}}$, since the motion is infinitesimal. The assumption of infinitesimal strain and the linear strain-displacement equation (1.11) resulting from this assumption is one of the key linearizing assumptions that underlie the linear field theories of

continuum mechanics.

All of these kinematic quantities can be differentiated with respect to time. To be compatible with the reference configuration domains of other kinematic variables, time differentiation is usually carried out in $\mathcal{B}_{\underset{\sim}{K}}$ rather than in $\mathcal{B}_{\underset{\sim}{\chi}}$ and is denoted by a dot. For example, the first two derivatives of the motion $\underset{\sim}{\chi}(\underset{\sim}{X},t)$ are

$$\dot{\underset{\sim}{\chi}}(\underset{\sim}{X},t) = \frac{d}{dt}\underset{\sim}{\chi}(\underset{\sim}{X},t) \tag{1.12a}$$

$$\ddot{\underset{\sim}{\chi}}(\underset{\sim}{X},t) = \frac{d^2}{dt^2}\underset{\sim}{\chi}(\underset{\sim}{X},t), \tag{1.12b}$$

called the velocity and acceleration at time t of a point (or particle) $\underset{\sim}{X}$ in $\mathcal{B}_{\underset{\sim}{K}}$.

1.3 Force and Mass

External surroundings can exert force on a body in two different ways - by a body force $\underset{\sim}{b}$ distributed over the interior of the body or by a traction vector $\underset{\sim}{t}$ distributed over the surface of the body. Either type of force can be referred to either the reference configuration $\mathcal{B}_{\underset{\sim}{K}}$ or deformed configuration $\mathcal{B}_{\underset{\sim}{\chi}}$. That is, $\underset{\sim}{t}_{\underset{\sim}{K}}(\underset{\sim}{X})$ with $\underset{\sim}{X} \in \partial\mathcal{B}_{\underset{\sim}{K}}$ refers to the force per unit surface area of the body in its reference configuration $\mathcal{B}_{\underset{\sim}{K}}$, whereas $\underset{\sim}{t}_{\underset{\sim}{\chi}}(\underset{\sim}{\chi})$ (or commonly $\underset{\sim}{t}$) with $\underset{\sim}{\chi} \in \partial\mathcal{B}_{\underset{\sim}{\chi}}$ refers to the force per unit area of the body in its deformed configuration $\mathcal{B}_{\underset{\sim}{\chi}}$.

The internal forces at a point inside the body are characterized by stress tensors. The Cauchy stress (measured in the actual deformed configuration of the body) is defined by the Cauchy stress principle

$$\underset{\sim}{t}(\underset{\sim}{x}) = \underset{\sim}{T}(\underset{\sim}{x}) \cdot \underset{\sim}{n}(\underset{\sim}{x}) \tag{1.13}$$

where $\underset{\sim}{t}$ is the force vector on the surface at $\underset{\sim}{x}$ defined by the unit normal $\underset{\sim}{n}$. The stress measure which permits both forces and geometry to be expressed in terms of the reference configuration is called the Piola-Kirchhoff stress tensor, defined by

$$\underset{\sim}{P}(\underset{\sim}{x}) = (\det \underset{\sim}{F}) \underset{\sim}{F}^{-1} \underset{\sim}{T} (\underset{\sim}{F}^{-1})^{T} \tag{1.14}$$

which results in the following form of Cauchy's stress principle:

$$\underset{\sim}{t}_{K}(\underset{\sim}{x}) = \left(\underset{\sim}{F}(\underset{\sim}{x}) \cdot \underset{\sim}{P}(\underset{\sim}{x})\right) \cdot \underset{\sim}{n}_{K}(\underset{\sim}{x}) \tag{1.15}$$

where $\underset{\sim}{t}_{K}$ is the force vector on the surface at point $\underset{\sim}{x}$ defined by the unit normal $\underset{\sim}{n}_{K}$. Either $\underset{\sim}{T}$ or $\underset{\sim}{P}$ completely characterizes the state of stress at a point.

In infinitesimal field theory the distinction between Cauchy stress and Piola-Kirchhoff stress disappears, since the distinction between a reference configuration domain $\mathcal{B}_{K}$ and deformed configuration domain $\mathcal{B}_{x}$ disappears.

Also associated with a body $\mathcal{B}$ is a quantity called mass, defined such that

$$\int_{\mathcal{B}} dm = \text{mass of } \mathcal{B} \tag{1.16}$$

Mass is indicated in continua by the distributed quantity ρ, called mass density, such that

$$\int_{\mathcal{B}_{x}} \rho(\underset{\sim}{x}) dV = \text{mass of body}, \tag{1.17}$$

or if mass density referred to the reference configuration is used

$$\int_{\mathcal{B}_K} \rho_K(\underset{\sim}{X})\, dV = \text{mass of body.} \tag{1.18}$$

1.4 Temperature, Entropy, and Heat

Several other variables are needed to describe the thermomechanical state of a body. Temperature is a measure of molecular thermal agitation and is indicated by the scalar $\theta(\underset{\sim}{X},t)$. Specific entropy $\eta(\underset{\sim}{X},t)$ is a measure of thermodynamic disorder, and specific internal energy $e(\underset{\sim}{X},t)$ is a distributed measure of the thermomechanical energy contained within the deformed body. Temperature gradient may be defined by

$$\underset{\sim}{G}(\underset{\sim}{X},t) = \underset{\sim}{\nabla}\theta(\underset{\sim}{X},t), \tag{1.19}$$

where the differentiation here is with respect to the reference configuration.

Heat energy can be supplied to the body in two direct ways - by an internal heat supply $r(\underset{\sim}{X},t)$ distributed throughout the body, or a surface heat flux $Q_n(\underset{\sim}{X},t)$, $\underset{\sim}{X} \in \partial\mathcal{B}_K$, the rate of heat flow across a unit area of the surface of $\mathcal{B}_K$. The state of heat flow at a point $\underset{\sim}{X}$ in the body is completely specified by the heat flux vector, defined by

$$Q_n(\underset{\sim}{X},t) = \underset{\sim}{Q}(\underset{\sim}{X},t) \cdot \underset{\sim}{n}_K(\underset{\sim}{X}) \tag{1.20}$$

where $\underset{\sim}{n}_K$ is the unit normal to the surface across which Q_n is measured.

Another useful measure of the internal energy of a body is the scalar functional of $\underset{\sim}{X}$ and t, the specific free energy,

defined by

$$\psi = e - \theta\eta . \tag{1.21}$$

1.5 Balance Laws and Entropy Production Inequality

The balance principles relevant to thermomechanical continua, expressed in terms of a body's reference configuration $\mathcal{B}_K$, are

1) balance of linear momentum

$$\int_{\partial\mathcal{B}_K} \underset{\sim}{t}_K \, dS + \int_{\mathcal{B}_K} \rho_K \underset{\sim}{b}_K \, dV = \int_{\mathcal{B}_K} \rho_K \ddot{\underset{\sim}{\chi}} \, dV \tag{1.22a}$$

2) balance of angular momemtum

$$\int_{\partial\mathcal{B}_K} \underset{\sim}{\chi} \times \underset{\sim}{t}_K \, dS + \int_{\mathcal{B}_K} \rho_K \underset{\sim}{\chi} \times \underset{\sim}{b}_K \, dV = \int_{\mathcal{B}_K} \rho_K \dot{(\underset{\sim}{\chi} \times \dot{\underset{\sim}{\chi}})} \, dV \tag{1.22b}$$

3) balance of energy

$$\int_{\partial\mathcal{B}_K} (\underset{\sim}{t}_K \cdot \dot{\underset{\sim}{\chi}} - Q_n) dS + \int_{\mathcal{B}_K} \rho_K (\underset{\sim}{b}_K \cdot \dot{\underset{\sim}{\chi}} + r) dV = \int_{\mathcal{B}_K} \rho_K (\dot{e} + \dot{\underset{\sim}{\chi}} \cdot \ddot{\underset{\sim}{\chi}}) dV . \tag{1.22c}$$

The entropy production inequality, also expressed in terms of a body's reference configuration $\mathcal{B}_K$, is

$$\int_{\mathcal{B}_K} \rho_K \dot{\eta} \, dV - \int_{\mathcal{B}_K} \frac{\rho_K r}{\theta} dV + \int_{\partial\mathcal{B}_K} \frac{Q_n}{\theta} dS \geq 0. \tag{1.22d}$$

The conservation of mass principle

$$\frac{d}{dt} \int_{\mathcal{B}} dm = 0 \tag{1.23}$$

has been assumed in expressing (1.22a-d).

The balance principles and entropy production inequality above can be localized if certain smoothness conditions on the field variables are satisfied [1]. These local balance laws,

valid at every point in $\mathcal{B}_K$, are respectively

$$(\underset{\sim}{F}\cdot\underset{\sim}{P})\cdot\underset{\sim}{\nabla} + \rho_K \underset{\sim}{b}_K = \rho_K \ddot{\underset{\sim}{\chi}} \tag{1.24a}$$

$$\underset{\sim}{P}^T = \underset{\sim}{P} \tag{1.24b}$$

$$\rho_K \dot{e} - \rho_K r - \tfrac{1}{2}\,\mathrm{tr}(\underset{\sim}{P}\cdot\dot{\underset{\sim}{C}}) + \underset{\sim}{Q}\cdot\underset{\sim}{\nabla} = \underset{\sim}{0}, \tag{1.24c}$$

and the localized entropy production inequality is

$$\rho_K \dot{\eta} - \rho_K \frac{r}{\theta} + \frac{1}{\theta}\underset{\sim}{Q}\cdot\underset{\sim}{\nabla} - \frac{\underset{\sim}{Q}\cdot\underset{\sim}{G}}{\theta^2} \geq 0. \tag{1.24d}$$

If infinitesimal motion is assumed, the momentum balance (1.24a) is linearized and the energy balance (1.24c) becomes a quadratic functional, resulting in the linear balance laws

$$\underset{\sim}{T}\cdot\underset{\sim}{\nabla} + \rho\underset{\sim}{b} = \rho\ddot{\underset{\sim}{\chi}} \tag{1.25a}$$

$$\underset{\sim}{T}^T = \underset{\sim}{T} \tag{1.25b}$$

$$\rho\dot{e} - \rho r - \mathrm{tr}(\underset{\sim}{T}\cdot\underset{\sim}{\epsilon}) + \underset{\sim}{Q}\cdot\underset{\sim}{\nabla} = \underset{\sim}{0}. \tag{1.25c}$$

1.6 Material Constitutive Equations

A thermomechanical material is mathematically characterized by four response functionals $\hat{\psi}$, $\hat{\eta}$, $\underset{\sim}{\mathcal{F}}$, and $\hat{\underset{\sim}{Q}}$, all of which in the most general case are dependent on deformation history, temperature history, temperature gradient history, and time; i. e., for a point $\underset{\sim}{X}$ in the body $\mathcal{B}_K$ the functional form of the constitutive equations is

$$f\left(\underset{\sim}{X},\ \underset{\sim}{\chi}(\hat{\underset{\sim}{X}},t-s),\ \theta(\hat{\underset{\sim}{X}},t-s),\ \nabla\theta(\hat{\underset{\sim}{X}},t-s),\ t\right) \tag{1.26}$$

where $\hat{\underset{\sim}{X}}$ refers to any $\underset{\sim}{X} \in \mathcal{B}_K$, and $0 \leq s < \infty$.

For a homogeneous body composed of a simple material (a material whose response at a point $\underset{\sim}{x}$ is affected only by the motion and temperature in a small neighborhood around that point $\underset{\sim}{x}$) the response functionals reduce to the form

$$f\left(\underset{\sim}{F}(\underset{\sim}{x},t-s), \theta(\underset{\sim}{x},t-s), \underset{\sim}{\nabla}\theta(\underset{\sim}{x},t-s), t \right) \tag{1.27}$$

where the notation $\underset{\sim}{F}(\underset{\sim}{x},t-s)$, $0 \leq s < \infty$ refers to all deformation gradient states at point $\underset{\sim}{x}$ before time t and the deformation gradient state at time t .

The exact form of the four constitutive functionals must be determined by experiment. However, certain underlying principles that govern the nature of the response of a material can lead to constraints on constitutive equations. Five particularly useful principles, described in great detail in [1], are the principles of determinism and local action (already incorporated into (1.27)), the principle of material frame indifference, the invariance of material symmetry, and the entropy production inequality (1.24d). The last three principles permit simplification of the constitutive characterization of a general thermomechanical material to the following equations:

$$\psi(\underset{\sim}{x},t) = \hat{\psi}\left(\underset{\sim}{C}(\underset{\sim}{x},t-s), \theta(\underset{\sim}{x},t-s), t\right) \tag{1.28a}$$

$$\eta(\underset{\sim}{x},t) = \hat{\eta}\left(\underset{\sim}{C}(\underset{\sim}{x},t-s), \theta(\underset{\sim}{x},t-s), t\right) \tag{1.28b}$$

$$\underset{\sim}{P}(\underset{\sim}{x},t) = \underset{\sim}{\hat{P}}\left(\underset{\sim}{C}(\underset{\sim}{x},t-s), \theta(\underset{\sim}{x},t-s), t\right) \tag{1.28c}$$

$$\underset{\sim}{Q}(\underset{\sim}{x},t) = \underset{\sim}{\hat{Q}}\left(\underset{\sim}{C}(\underset{\sim}{x},t-s), \theta(\underset{\sim}{x},t-s), \underset{\sim}{\nabla}\theta(\underset{\sim}{x},t-s), t\right). \tag{1.28d}$$

The mathematical characterization of a material can be

simplified by making certain assumptions about its behavior. For example, a material whose behavior at a time t depends on the value of $\underset{\sim}{C}$, θ, and $\nabla\theta$ at time t only, rather than on the history of these variables, is defined as thermoelastic. Such a material can be completely characterized by the two material functionals

$$\psi(\underset{\sim}{x},t) = \hat{\psi}(\underset{\sim}{C}(\underset{\sim}{x},t), \theta(\underset{\sim}{x},t)) \tag{1.29a}$$

$$\underset{\sim}{Q}(\underset{\sim}{x},t) = \hat{\underset{\sim}{Q}}(\underset{\sim}{C}(\underset{\sim}{x},t), \theta(\underset{\sim}{x},t), \nabla\theta(\underset{\sim}{x},t)) \tag{1.29b}$$

since the other two field variables in (1.28) are derivable from $\hat{\psi}$ as follows:

$$\underset{\sim}{P}(\underset{\sim}{x},t) = 2\rho_R \frac{\partial}{\partial \underset{\sim}{C}} \hat{\psi}(\underset{\sim}{C},\theta) \tag{1.29c}$$

$$\eta(\underset{\sim}{x},t) = -\frac{\partial}{\partial\theta}\hat{\psi}(\underset{\sim}{C},\theta). \tag{1.29d}$$

Detailed derivation of (1.29) is available in [1, 14].

A material whose behavior is assumed to be unaffected by thermal effects or a material undergoing an isothermal process can be completely characterized by just one function:

$$\underset{\sim}{P}(\underset{\sim}{x},t) = \underset{\sim}{\mathcal{F}}(\underset{\sim}{C}(\underset{\sim}{x},t-s)). \tag{1.30}$$

If the material is also elastic (1.30) reduces to

$$\underset{\sim}{P}(\underset{\sim}{x},t) = \underset{\sim}{\mathcal{F}}(\underset{\sim}{C}(\underset{\sim}{x},t)) \tag{1.31a}$$

or, if the constitution of the material is defined by a strain energy functional $\hat{\psi}$,

$$\underset{\sim}{P}(\underset{\sim}{x},t) = 2\rho_R \frac{\partial}{\partial \underset{\sim}{C}} \hat{\psi}(\underset{\sim}{C}(\underset{\sim}{x},t)). \tag{1.31b}$$

Further restrictions on (1.29) are possible if material symmetry is considered. For example, if a thermoelastic material is considered mechanically and thermally isotropic (with respect to the reference configuration) the constitutive equations must be form invariant under any orthogonal transformation [2]; hence (1.29) takes the form

$$\psi = \hat{\psi}(I_1, I_2, I_3, \theta) \tag{1.32a}$$

$$\underset{\sim}{Q} = -\underset{\sim}{K}(\underset{\sim}{C}, \theta, \nabla\theta)\cdot\nabla\theta \tag{1.32b}$$

where I_1, I_2, and I_3 are the three invariants of $\underset{\sim}{C}$ (1.7) and $\underset{\sim}{K}$ (thermal conductivity) is the tensor function

$$\underset{\sim}{K} = \alpha_0\underset{\sim}{I} + \alpha_1\underset{\sim}{C} + \alpha_2\underset{\sim}{C}^2, \tag{1.33}$$

where α_0, α_1, and α_2 are scalar functions of I_1, I_2, I_3, θ, $\nabla\theta^2$, $\nabla\theta(\underset{\sim}{C}\cdot\nabla\theta)$, and $\nabla\theta(\underset{\sim}{C}^2\cdot\nabla\theta)$ [10]. For isotropic, elastic materials not subject to temperature effects (1.32) simplifies to one energy functional which completely characterizes the material:

$$W = \hat{W}(I_1, I_2, I_3) \tag{1.34}$$

where stress is derivable from the expression

$$\underset{\sim}{P} = 2\rho_k\frac{\partial}{\partial\underset{\sim}{C}}\hat{W} \tag{1.35}$$

$$= 2\rho_k\left[\frac{\partial\hat{W}}{\partial I_1}\frac{\partial I_1}{\partial\underset{\sim}{C}} + \frac{\partial\hat{W}}{\partial I_2}\frac{\partial I_2}{\partial\underset{\sim}{C}} + \frac{\partial\hat{W}}{\partial I_3}\frac{\partial I_3}{\partial\underset{\sim}{C}}\right]. \tag{1.36}$$

That is, the material can be characterized by three scalar functions of the three scalar variables I_1, I_2, I_3. The

stress-strain relation (1.36) can also be expressed without reference to a strain energy functional [1]:

$$\underset{\sim}{P} = \mathcal{J}_0 \underset{\sim}{I} + \mathcal{J}_1 \underset{\sim}{C} + \mathcal{J}_2 \underset{\sim}{C}^2, \tag{1.37}$$

$\mathcal{J}_0$, $\mathcal{J}_1$, $\mathcal{J}_2$ being scalar functions of I_1, I_2, I_3 as in (1.36). Refer to [15] for a full discussion of material symmetry and its effects on the general elastic constitutive relation (1.31).

Another important class of elastic materials are those assumed to be capable only of isochoric motions. A deformation is said to be isochoric if

$$\det \underset{\sim}{C} = 1. \tag{1.38}$$

A material of this type is called incompressible and is characterized by the stress constitutive equation

$$\underset{\sim}{P} = -h \underset{\sim}{C}^{-1} + \underset{\sim}{\mathcal{F}}(\underset{\sim}{C}) \tag{1.39}$$

or, if a strain energy functional $\hat{W}$ exists for the material,

$$\underset{\sim}{P} = -h \underset{\sim}{C}^{-1} + 2\rho_R \frac{\partial}{\partial \underset{\sim}{C}} \hat{W}(\underset{\sim}{C}). \tag{1.40}$$

The scalar function $h(\underset{\sim}{X}, t)$, defined over the whole reference configuration domain $\mathcal{B}_R$, is called the hydrostatic pressure and is indeterminate in the stress constitutive equation (1.40) until the information contained in the incompressibility constraint equation (1.38) and the balance laws (1.24) is utilized.

If an incompressible, elastic material is also isotropic, the stress constitutive equations (1.39) or (1.40) reduce to the

simplified forms

$$\underset{\sim}{P} = -h\underset{\sim}{C}^{-1} + \gamma_0(I_1, I_2)\underset{\sim}{I} + \gamma_1(I_1, I_2)\underset{\sim}{C} \tag{1.41}$$

or

$$\underset{\sim}{P} = -h\underset{\sim}{C}^{-1} + 2\rho_{\kappa}\frac{\partial}{\partial \underset{\sim}{C}}\hat{W}(I_1, I_2) \tag{1.42}$$

$$= -h\underset{\sim}{C}^{-1} + 2\rho_{\kappa}\left[\frac{\partial \hat{W}}{\partial I_1}\frac{\partial I_1}{\partial \underset{\sim}{C}} + \frac{\partial \hat{W}}{\partial I_2}\frac{\partial I_2}{\partial \underset{\sim}{C}}\right]. \tag{1.43}$$

Hence, the response of incompressible, isotropic elastic materials can be completely specified by the two scalar functions C_1 and C_2, such that

$$\frac{\partial}{\partial I_1}\hat{W}(I_1, I_2) = \frac{1}{\rho_{\kappa}} C_1(I_1, I_2) \tag{1.44a}$$

$$\frac{\partial}{\partial I_2}\hat{W}(I_1, I_2) = \frac{1}{\rho_{\kappa}} C_2(I_1, I_2) \tag{1.44b}$$

or

$$\gamma_0(I_1, I_2) = 2\left[C_1(I_1, I_2) + I_1 C_2(I_1, I_2)\right] \tag{1.45a}$$

$$\gamma_1(I_1, I_2) = -2\, C_2(I_1, I_2). \tag{1.45b}$$

Experimental evidence has shown that natural and synthetic rubbers are isotropic, elastic, and nearly incompressible. Since the material functions (1.44) describing these rubbers are relatively simple, numerous investigators have proposed particular forms for C_1 and C_2. The simplest, based on a theoretical model of the behavior of rubber molecules, is

$$C_1(I_1, I_2) = \text{constant} \tag{1.46a}$$

$$C_2(I_1, I_2) = 0 \tag{1.46b}$$

and is called Neo-Hookean [16]. Another form is

$$C_1(I_1, I_2) = \text{constant} \tag{1.47a}$$

$$C_2(I_1, I_2) = \text{constant}, \tag{1.47b}$$

called a Mooney-Rivlin material [17], very commonly used as the basis for studies of nonlinear elastic behavior because of its simplicity. Rivlin and Saunders [4], in an extensive series of tests on various rubbers, determined that the material functions' proper forms are

$$C_1(I_1, I_2) = \text{constant} \tag{1.48a}$$

$$C_2(I_1, I_2) = f(I_2). \tag{1.48b}$$

Note that because of (1.44) these functions imply a strain energy functional of the form

$$\hat{W}(I_1, I_2) = C_1 \cdot (I_1 - 3) + f(I_2 - 3). \tag{1.49}$$

Many other forms have been postulated and are fully discussed in a paper by Alexander [6].

For generations the usual approach to elasticity problems has been to assume that materials are linear and that deformations are infinitesimal. This assumes a strain energy functional of the form

$$\hat{W}(\underset{\sim}{\epsilon}) = \tfrac{1}{2}\underset{\sim}{\epsilon} \cdot \underset{\sim}{\mathcal{E}} \cdot \underset{\sim}{\epsilon} \tag{1.50}$$

where $\underset{\sim}{\epsilon}$ is the infinitesimal strain tensor (1.11) and $\underset{\sim}{\mathcal{E}}$ is a constant tensor of rank four called the elasticity of the material. The particular form of the 81 elements of $\underset{\sim}{\mathcal{E}}$ will depend on the type of material symmetry existing in the material $\underset{\sim}{\mathcal{E}}$ is

meant to characterize. The functional (1.50) leads to the linearized stress constitutive equation

$$\underset{\sim}{T} = \rho_{\kappa} \underset{\sim}{\mathcal{E}} \cdot \underset{\sim}{\epsilon} . \tag{1.51}$$

If the linearized material is also isotropic, only two constants are needed to define the elasticity $\underset{\sim}{\mathcal{E}}$: Young's modulus E and Poisson's ratio ν . Therefore, (1.51) can be simply expressed as

$$\underset{\sim}{T} = \frac{E\nu}{(1+\nu)(1-2\nu)} \operatorname{tr}\underset{\sim}{\epsilon}\, \underset{\sim}{I} + \frac{E}{1+\nu} \underset{\sim}{\epsilon}, \tag{1.52}$$

the familiar stress-strain law that completely characterizes a linear, isotropic elastic material.

1.7 Thermomechanical Process

A thermomechanical state is defined by the set of state variables $\{\underset{\sim}{\chi}, e, \underset{\sim}{P}, \underset{\sim}{b}, \theta, \eta, \underset{\sim}{Q}, r\}$ - all functions of $\underset{\sim}{X} \in \mathcal{B}_{\kappa}$ and a specified interval of time $t_{min} \leq t \leq t_{max}$. If these state variables satisfy the balance principles (1.24a-c) and the entropy production inequality (1.24d) at every point in domain $\mathcal{B}_{\kappa}$ and for the interval of time $t_{min} \leq t \leq t_{max}$, they define a thermomechanical process. For a given material body such a process is called admissible if additionally it satisfies the constitutive functionals (1.28) that characterize that material.

1.8 Initial Boundary Value Problem of Thermoelasticity

The thermomechanical state of a body subjected to a process is completely defined by a set of state variables $\{\underset{\sim}{\chi}, \underset{\sim}{C}, \underset{\sim}{P}, \underset{\sim}{b}, \theta, \eta, \psi, \underset{\sim}{G}, \underset{\sim}{Q}, r\}$ - all functions with domain $\underset{\sim}{X}$ in

$\mathcal{B}_K$ and $t_{min} \leq t \leq t_{max}$. Normally the body force $\underset{\sim}{b}(\underset{\sim}{X}, t)$ and the internal heat source $r(\underset{\sim}{X}, t)$ are assigned functions. The remaining state variables $R(\underset{\sim}{X}, t) : \{ \underset{\sim}{\chi}, \underset{\sim}{C}, \underset{\sim}{P}, \Theta, \eta, \psi, \underset{\sim}{G}, \underset{\sim}{Q} \}$ must then satisfy two further conditions:

I: R must be an admissible thermomechanical process. That is, for all $\underset{\sim}{X}$ in $\mathcal{B}_K$ and for $t_{min} \leq t \leq t_{max}$ must satisfy the following field equations:

1) definitions of strain, temperature gradient, and specific free energy

$$\underset{\sim}{C} = \nabla\underset{\sim}{\chi}^T \cdot \nabla\underset{\sim}{\chi} \tag{1.53a}$$

$$\underset{\sim}{G} = \nabla\Theta \tag{1.53b}$$

$$\psi = e - \Theta\eta \tag{1.53c}$$

2) balance laws

$$(\nabla\underset{\sim}{\chi} \cdot \underset{\sim}{P}) \cdot \nabla + \rho_K \underset{\sim}{b} = \rho_K \ddot{\underset{\sim}{\chi}} \tag{1.53d}$$

$$\underset{\sim}{P}^T = \underset{\sim}{P} \tag{1.53e}$$

$$\tfrac{1}{2} tr(\underset{\sim}{P} \cdot \dot{\underset{\sim}{C}}) + \rho_K r - \underset{\sim}{Q} \cdot \nabla = \rho_K \dot{e} \tag{1.53f}$$

3) material constitutive equations for a thermoelastic material

$$\psi = \hat{\psi}(\underset{\sim}{C}, \Theta) \tag{1.53g}$$

$$\underset{\sim}{Q} = \hat{\underset{\sim}{Q}}(\underset{\sim}{C}, \Theta, \underset{\sim}{G}) \tag{1.53h}$$

$$\underset{\sim}{P} = 2\rho_K \frac{\partial}{\partial \underset{\sim}{C}} \hat{\psi}(\underset{\sim}{C}, \Theta) \tag{1.53i}$$

$$\eta = -\frac{\partial}{\partial \Theta}\hat{\psi}(\underset{\sim}{C},\Theta) \tag{1.53j}$$

II: $\mathcal{R}$ must correctly reflect the prescribed process, represented by initial conditions and boundary conditions. That is, $\mathcal{R}$ must satisfy the following equations:

1) boundary conditions

$$\underset{\sim}{\chi}(\underset{\sim}{X},t) = \hat{\underset{\sim}{\chi}}(\underset{\sim}{X},t) \qquad \underset{\sim}{X} \in \partial\mathcal{B}_{\underset{\sim}{\kappa}}^{\mathrm{I}} \tag{1.54a}$$

$$(\underset{\sim}{\nabla}\underset{\sim}{\chi}\cdot\underset{\sim}{P})\cdot\underset{\sim}{n}_{\underset{\sim}{\kappa}} = \hat{\underset{\sim}{t}}_{\underset{\sim}{\kappa}}(\underset{\sim}{X},t) \qquad \underset{\sim}{X} \in \partial\mathcal{B}_{\underset{\sim}{\kappa}}^{\mathrm{II}} \tag{1.54b}$$

$$\Theta(\underset{\sim}{X},t) = \hat{\Theta}(\underset{\sim}{X},t) \qquad \underset{\sim}{X} \in \partial\mathcal{B}_{\underset{\sim}{\kappa}}^{\mathrm{III}} \tag{1.54c}$$

$$\underset{\sim}{Q}\cdot\underset{\sim}{n}_{\underset{\sim}{\kappa}} = \hat{Q}_n(\underset{\sim}{X},t) \qquad \underset{\sim}{X} \in \partial\mathcal{B}_{\underset{\sim}{\kappa}}^{\mathrm{IV}} \tag{1.54d}$$

where $\hat{\underset{\sim}{t}}_{\underset{\sim}{\kappa}}$, $\hat{\underset{\sim}{\chi}}$, $\hat{Q}_n$, $\hat{\Theta}$ are prescribed functions of time (over the interval $t_{min} \le t \le t_{max}$) for traction, motion, heat flow, and temperature on the boundaries of the body such that

$$\partial\mathcal{B}_{\underset{\sim}{\kappa}}^{\mathrm{I}} + \partial\mathcal{B}_{\underset{\sim}{\kappa}}^{\mathrm{II}} = \partial\mathcal{B}_{\underset{\sim}{\kappa}}^{\mathrm{III}} + \partial\mathcal{B}_{\underset{\sim}{\kappa}}^{\mathrm{IV}} = \partial\mathcal{B}_{\underset{\sim}{\kappa}} \tag{1.55}$$

2) initial conditions

$$\underset{\sim}{\chi}(\underset{\sim}{X},t_{min}) = \hat{\underset{\sim}{\chi}}_o(\underset{\sim}{X}) \qquad \underset{\sim}{X} \in \mathcal{B}_{\underset{\sim}{\kappa}} \tag{1.56a}$$

$$\dot{\underset{\sim}{\chi}}(\underset{\sim}{X},t_{min}) = \hat{\underset{\sim}{v}}_o(\underset{\sim}{X}) \qquad \underset{\sim}{X} \in \mathcal{B}_{\underset{\sim}{\kappa}} \tag{1.56b}$$

$$\Theta(\underset{\sim}{X},t_{min}) = \hat{\Theta}_o(\underset{\sim}{X}) \qquad \underset{\sim}{X} \in \mathcal{B}_{\underset{\sim}{\kappa}} \tag{1.56c}$$

where $\hat{\underset{\sim}{\chi}}_o$, $\hat{\underset{\sim}{v}}_o$, $\hat{\Theta}_o$ are prescribed functions for configuration, velocity, and temperature at $t = t_{min}$.

Determination of the process $\mathcal{R}$ that satisfies all these conditions is called the initial boundary value problem of

thermoelasticity.

The initial boundary value problem for more complex materials can be formulated by use of the generalized constitutive functionals (1.28) in place of (1.53f-j). Inelastic material behavior can also be represented by the introduction of internal state variables in the constitutive functionals. A paper by Coleman and Gurtin [14] contains a full development of this approach.

1.9 Boundary Value Problem of Elasticity

If thermal and dynamic effects are ignored a simpler, more specialized boundary value problem can be defined. That is, the thermomechanical state of a loaded elastic body is completely defined by the set $R(\underset{\sim}{X}) : \{ \underset{\sim}{X}, \underset{\sim}{C}, \underset{\sim}{P} \}$ that satisfies at every point $\underset{\sim}{X}$ in $\mathcal{B}_{\underset{\sim}{K}}$ the field equations

$$\underset{\sim}{C} = \nabla\underset{\sim}{X}^{T} \cdot \nabla\underset{\sim}{X} \tag{1.57a}$$

$$(\nabla\underset{\sim}{X} \cdot \underset{\sim}{P}) \cdot \nabla + \rho_{\underset{\sim}{K}} \underset{\sim}{b} = \underset{\sim}{0} \tag{1.57b}$$

$$\underset{\sim}{P}^{T} = \underset{\sim}{P} \tag{1.57c}$$

$$\underset{\sim}{P} = \underset{\sim}{\mathcal{F}}(\underset{\sim}{C}) \tag{1.57d}$$

and the boundary conditions

$$(\nabla\underset{\sim}{X} \cdot \underset{\sim}{P}) \cdot \underset{\sim}{n}_{\underset{\sim}{K}} = \hat{\underset{\sim}{t}}_{\underset{\sim}{K}} \qquad \underset{\sim}{X} \in \partial\mathcal{B}^{I}_{\underset{\sim}{K}} \tag{1.58a}$$

$$\underset{\sim}{X} = \hat{\underset{\sim}{X}} \qquad \underset{\sim}{X} \in \partial\mathcal{B}^{II}_{\underset{\sim}{K}} \tag{1.58b}$$

where

$$\partial\mathcal{B}^{I}_{\underset{\sim}{K}} + \partial\mathcal{B}^{II}_{\underset{\sim}{K}} = \partial\mathcal{B}_{\underset{\sim}{K}}. \tag{1.59}$$

If the elastic material is isotropic, the constitutive equation (1.57d) simplifies to the form (1.36); that is,

$$\underset{\sim}{P} = 2\rho_{\underset{\sim}{K}}\left[\frac{\partial\hat{W}}{\partial I_1}(I_1,I_2,I_3)\frac{\partial I_1}{\partial \underset{\sim}{C}} + \frac{\partial\hat{W}}{\partial I_2}(I_1,I_2,I_3)\frac{\partial I_2}{\partial \underset{\sim}{C}} + \frac{\partial W}{\partial I_3}(I_1,I_2,I_3)\frac{\partial I_3}{\partial \underset{\sim}{C}}\right]. \quad (1.60)$$

Note the mathematical structure of this boundary value problem - a system of nonlinear partial differential equations (1.57) defined over the three-dimensional domain $\underset{\sim}{X} \in \mathcal{B}_{\underset{\sim}{K}}$ with independent variables $\underset{\sim}{X}$, $\underset{\sim}{C}$, and $\underset{\sim}{P}$ and with the boundary conditions (1.58).

1.10 Boundary Value Problem of Linear Elasticity

If an isotropic, elastic material is assumed to behave linearly, as in (1.52), and the motion of the body is infinitesimal, as in (1.11) and (1.25), the boundary value problem of classical elasticity results. That is, find the state $R(\underset{\sim}{X})$: $\{\underset{\sim}{U}, \underset{\sim}{\epsilon}, \underset{\sim}{T}\}$ which satisfies the field equations

$$\underset{\sim}{\epsilon} = \tfrac{1}{2}\left[\nabla\underset{\sim}{U} + \nabla\underset{\sim}{U}^{T}\right] \quad (1.61a)$$

$$\underset{\sim}{T}\cdot\nabla + \rho_{\underset{\sim}{K}}\underset{\sim}{b} = \underset{\sim}{0} \quad (1.61b)$$

$$\underset{\sim}{T} = \frac{E\nu}{(1+\nu)(1-2\nu)}\operatorname{tr}\underset{\sim}{\epsilon}\,\underset{\sim}{I} + \frac{E}{1+\nu}\underset{\sim}{\epsilon} \quad (1.61c)$$

and the boundary conditions

$$\underset{\sim}{T}\cdot\underset{\sim}{n}_{\underset{\sim}{K}} = \hat{\underset{\sim}{t}}_{\underset{\sim}{K}} \qquad \underset{\sim}{X} \in \partial\mathcal{B}^{I}_{\underset{\sim}{K}} \quad (1.62a)$$

$$\underset{\sim}{U} = \hat{\underset{\sim}{U}} \qquad \underset{\sim}{X} \in \partial\mathcal{B}^{II}_{\underset{\sim}{K}} \quad (1.62b)$$

where

$$\partial\mathcal{B}^{I}_{\underset{\sim}{K}} + \partial\mathcal{B}^{II}_{\underset{\sim}{K}} = \partial\mathcal{B}_{\underset{\sim}{K}}. \quad (1.63)$$

Note that a much simpler mathematical problem results due to linearization - a system of 15 linear partial differential equations (1.61) defined over the three-dimensional domain $\mathcal{B}_R$ with independent variables $\underset{\sim}{U}$, $\underset{\sim}{\epsilon}$, $\underset{\sim}{T}$ and the boundary conditions (1.62). The solution of boundary value problem (1.61) is far simpler than the solution of boundary value problem (1.57) because of the equations' linearity and because of the material's very simple description in terms of the two easily determined constants E and ν.

1.11 Boundary Value Problem of Incompressible Elasticity

In Section 1.6 materials capable only of isochoric motion were discussed. The boundary value problem associated with an isotropic, elastic, incompressible material is to find the set of 16 state variables $R(\underset{\sim}{X}) : \{\underset{\sim}{\chi}, \underset{\sim}{C}, \underset{\sim}{P}, h\}$ that satisfies the field equations

$$\underset{\sim}{C} = \nabla\underset{\sim}{\chi}^T \cdot \nabla\underset{\sim}{\chi} \tag{1.64a}$$

$$(\nabla\underset{\sim}{\chi} \cdot \underset{\sim}{P}) \cdot \nabla + \rho_R \underset{\sim}{b} = \underset{\sim}{0} \tag{1.64b}$$

$$\underset{\sim}{P} = -h\underset{\sim}{C}^{-1} + 2\left(C_1(I_1, I_2)\frac{\partial I_1}{\partial \underset{\sim}{C}} + C_2(I_1, I_2)\frac{\partial I_2}{\partial \underset{\sim}{C}}\right) \tag{1.64c}$$

$$\det \underset{\sim}{C} = 1 \tag{1.64d}$$

and the boundary conditions

$$(\nabla\underset{\sim}{\chi} \cdot \underset{\sim}{P}) \cdot \underset{\sim}{n}_R = \hat{\underset{\sim}{t}}_R \qquad \underset{\sim}{X} \in \partial\mathcal{B}_R^I \tag{1.65a}$$

$$\underset{\sim}{\chi} = \hat{\underset{\sim}{\chi}} \qquad \underset{\sim}{X} \in \partial\mathcal{B}_R^{II} \tag{1.65b}$$

where

$$\partial\mathcal{B}_{\underset{\sim}{K}}^{I} + \partial\mathcal{B}_{\underset{\sim}{K}}^{II} = \partial\mathcal{B}_{\underset{\sim}{K}}. \tag{1.65c}$$

Note how the indeterminate constant h in the stress constitutive equation (1.64c) must be treated as an additional state variable, necessitating the addition of another field equation, the incompressibility constraint equation (1.64d). When the definitions (1.7a-b) are expanded, I_1 and I_2 can be expressed as

$$I_1 = C_{11} + C_{22} + C_{33} \tag{1.66a}$$

$$I_2 = C_{11}C_{33} + C_{22}C_{33} + C_{11}C_{22} - C_{12}^2 - C_{13}^2 - C_{23}^2. \tag{1.66b}$$

If $\partial I_1/\partial \underset{\sim}{C}$ and $\partial I_2/\partial \underset{\sim}{C}$ are evaluated the stress constitutive equation (1.64c) can be written as

$$\underset{\sim}{P} = -h\underset{\sim}{C}^{-1} + 2C_1(I_1,I_2)\begin{bmatrix}1&0&0\\0&1&0\\0&0&1\end{bmatrix} + 2C_2(I_1,I_2)\begin{bmatrix}C_{22}+C_{33} & -C_{12} & -C_{13}\\ -C_{12} & C_{11}+C_{33} & -C_{23}\\ -C_{13} & -C_{23} & C_{11}+C_{22}\end{bmatrix}. \tag{1.67}$$

Using a variational approach to this boundary value problem [10,18], it can be rephrased in a way that is more suitable for numerical solution techniques. That is, to find the state $R(\underset{\sim}{X}) : \{\underset{\sim}{\chi}, \underset{\sim}{C}, \underset{\sim}{P}, h\}$ that satisfies the field equations

$$\underset{\sim}{C} = \nabla\underset{\sim}{\chi}^{T} \cdot \nabla\underset{\sim}{\chi} \tag{1.68a}$$

$$\underset{\sim}{P} = -h\underset{\sim}{C}^{-1} + 2\left(C_1(I_1,I_2)\frac{\partial I_1}{\partial \underset{\sim}{C}} + C_2(I_1,I_2)\frac{\partial I_2}{\partial \underset{\sim}{C}}\right) \tag{1.68b}$$

and the boundary condition

$$\underset{\sim}{\chi} = \hat{\underset{\sim}{\chi}} \qquad \underset{\sim}{X} \in \partial\mathcal{B}_{\underset{\sim}{K}}^{II} \tag{1.68c}$$

results in a solution if the state R also minimizes the variational functional $\Phi(\underset{\sim}{\chi}, h)$, i. e.,

$$\delta\Phi(\underset{\sim}{\chi}, h) = \int_{B_K} \tfrac{1}{2}\underset{\sim}{P} : \delta\underset{\sim}{C}\, dV - \int_{B_K} (\det\underset{\sim}{C} - 1)\delta h\, dV - \int_{B_K} \rho_K \underset{\sim}{b}\cdot\delta\underset{\sim}{\chi}\, dV - \int_{\partial B_K^T} \hat{\underset{\sim}{t}}_K \cdot \delta\underset{\sim}{\chi}\, dS = 0. \tag{1.68d}$$

Equation (1.68d) is a generalized virtual work theorem for incompressible elasticity, and the state $\{\underset{\sim}{\chi}, \underset{\sim}{C}, \underset{\sim}{P}, h\}$ which satisfies it is precisely the same $\{\underset{\sim}{\chi}, \underset{\sim}{C}, \underset{\sim}{P}, h\}$ which would satisfy the balance equations (1.64b), incompressibility constraint equation (1.64d), and the traction boundary condition (1.65a). Hence boundary value problem (1.68) is equivalent to boundary value problem (1.64-5).

1.12 Boundary Value Problem for Isotropic, Incompressible Elastic Materials in a State of Plane Stress

If restrictive assumptions are made about the kinematic or thermal behavior of the bodies discussed above, simpler, yet significant, boundary value problems often result. A useful assumption is that the body is in a state of plane stress. That is, a body in the shape of a thin planar sheet, unloaded on its plane surfaces, is assumed to sustain no stresses on planes perpendicular to the plane of the sheet. For the body below in Figure 1.3 the plane stress assumption states:

$$\underset{\sim}{t}_K = \underset{\sim}{0} \qquad \text{for} \quad z = \pm\frac{T}{2} \tag{1.69a}$$

or

$$P_{33} = P_{32} = P_{31} = 0, \quad \forall \underset{\sim}{X} \in B_K. \tag{1.69b}$$

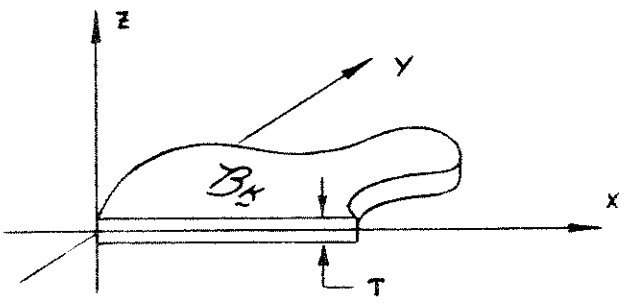

Fig. 1.3

Substitution of assumptions (1.69b) into the stress constitutive equation (1.67) of the isotropic, incompressible elastic boundary value problem of Section 1.11 results in the following constraints on $\underset{\sim}{C}$ and h:

$$C_{13} = 0 \tag{1.70a}$$

$$C_{23} = 0 \tag{1.70b}$$

$$h = 2C_{33}C_1(I_1, I_2) + 2C_{33}(C_{11}+C_{22})C_2(I_1, I_2). \tag{1.70c}$$

If motion perpendicular to the x-y plane of the body is represented by an extension ratio $\lambda(x, y)$, such that

$$\lambda^2(x, y) = C_{33}(x, y), \tag{1.71}$$

then all field variables in a plane stress problem are functions of only two variables, with domain $\mathcal{B}_{\underset{\sim}{K}}$ - the portion of the x-y plane the body occupies in its reference state $\mathcal{B}_{\underset{\sim}{K}}$.

Substituting (1.70c) into the three-dimensional constitutive equation (1.67) and writing the x- and y-components of the field equations (1.64), we can derive the two-dimensional plane stress boundary value problem of isotropic, incompressible elasticity. That is, for a prescribed body under prescribed loading condi-

tions find the set of 9 state variables $R(x,y) : \{ \chi_1, \chi_2, C_{11}, C_{12}, C_{22}, \lambda, P_{11}, P_{12}, P_{22} \}$ that satisfies at all (x,y) in the two-dimensional domain $\mathcal{B}_\kappa$ the field equations

$$\underset{\sim}{C} = \nabla \underset{\sim}{\chi}^T \cdot \nabla \underset{\sim}{\chi} \tag{1.72a}$$

$$(\nabla \underset{\sim}{\chi} \cdot \underset{\sim}{P}) \cdot \nabla + \rho_\kappa \underset{\sim}{b} = \underset{\sim}{0} \tag{1.72b}$$

$$\underset{\sim}{P} = 2C_1(I_1, I_2)\left\{ \begin{bmatrix} 1 & 0 \\ 0 & 1 \end{bmatrix} - \frac{\lambda^4}{\det \underset{\sim}{C}} \begin{bmatrix} C_{22} & -C_{12} \\ -C_{12} & C_{11} \end{bmatrix} \right\}$$

$$+ 2C_2(I_1, I_2)\left\{ \lambda^2 \begin{bmatrix} 1 & 0 \\ 0 & 1 \end{bmatrix} + \left(1 - \frac{\lambda^4 (C_{11} + C_{22})}{\det \underset{\sim}{C}}\right) \begin{bmatrix} C_{22} & -C_{12} \\ -C_{12} & C_{11} \end{bmatrix} \right\} \tag{1.72c}$$

$$\det \underset{\sim}{C} = 1 \tag{1.72d}$$

and the boundary conditions

$$(\nabla \underset{\sim}{\chi} \cdot \underset{\sim}{P}) \cdot \underset{\sim}{n}_\kappa = \hat{\underset{\sim}{t}}_\kappa \qquad \underset{\sim}{X} \in \partial \mathcal{B}_\kappa^{I} \tag{1.73a}$$

$$\underset{\sim}{\chi} = \hat{\underset{\sim}{\chi}} \qquad \underset{\sim}{X} \in \partial \mathcal{B}_\kappa^{II} \tag{1.73b}$$

where

$$\partial \mathcal{B}_\kappa^{I} + \partial \mathcal{B}_\kappa^{II} = \partial \mathcal{B}_\kappa . \tag{1.74}$$

Note that the plane stress assumption is a kinematic restriction, not a material restriction; the material functions $C_1(I_1, I_2)$ and $C_2(I_1, I_2)$ are precisely the same as those in the three-dimensional incompressible boundary value problem (1.64-5).

It is often more useful to express the plane stress boundary value problem (1.72-3) in terms of displacement $\underset{\sim}{u}(x,y)$ and Lagrangian strain $\underset{\sim}{E}(x,y)$, since this nonlinear formulation originally evolved as an extension of a linear plane stress boundary value problem. Also, numerical solution techniques are

easier to apply when $\underset{\sim}{U}$ and $\underset{\sim}{E}$ are state variables. Therefore, rephrasing (1.72-4), we seek the mechanical state $R(X,Y)$: $\{U_1, U_2, E_{11}, E_{12}, E_{22}, \lambda, P_{11}, P_{12}, P_{22}\}$ that satisfies at all points (X,Y) in $\mathcal{B}_K$ the field equations

$$\underset{\sim}{E} = \tfrac{1}{2}\left[\nabla\underset{\sim}{U} + \nabla\underset{\sim}{U}^T + \nabla\underset{\sim}{U}^T\cdot\nabla\underset{\sim}{U}\right] \tag{1.75a}$$

$$\left((\underset{\sim}{I} + \nabla\underset{\sim}{U})\cdot\underset{\sim}{P}\right)\cdot\nabla + \rho_K\underset{\sim}{b} = \underset{\sim}{0} \tag{1.75b}$$

$$\underset{\sim}{P} = 2C_1(I_1,I_2)\left\{\begin{bmatrix}1&0\\0&1\end{bmatrix} - \frac{\lambda^4}{\det(2\underset{\sim}{E}+\underset{\sim}{I})}\begin{bmatrix}2E_{22}+1 & -2E_{12}\\ -2E_{12} & 2E_{11}+1\end{bmatrix}\right\}$$
$$+ 2C_2(I_1,I_2)\left\{\lambda^2\begin{bmatrix}1&0\\0&1\end{bmatrix} + \left(1 + \frac{2\lambda^4(E_{11}+E_{22}+1)}{\det(2\underset{\sim}{E}+\underset{\sim}{I})}\right)\begin{bmatrix}2E_{22}+1 & -2E_{12}\\ -2E_{12} & 2E_{11}+1\end{bmatrix}\right\} \tag{1.75c}$$

$$\det(2\underset{\sim}{E} + \underset{\sim}{I}) = 1 \tag{1.75d}$$

and the boundary conditions

$$\left((\nabla\underset{\sim}{U} + \underset{\sim}{I})\cdot\underset{\sim}{P}\right)\cdot\underset{\sim}{n}_K = \hat{\underset{\sim}{t}}_K \qquad (X,Y) \in \partial\mathcal{B}_K^{I} \tag{1.76a}$$

$$\underset{\sim}{U} = \hat{\underset{\sim}{U}} \qquad (X,Y) \in \partial\mathcal{B}_K^{II} \tag{1.76b}$$

where

$$\partial\mathcal{B}_K^{I} + \partial\mathcal{B}_K^{II} = \partial\mathcal{B}_K. \tag{1.77}$$

Note the mathematical structure of boundary value problem (1.75-6): 9 nonlinear partial differential equations with two-dimensional domain $\mathcal{B}_K$, boundary conditions (1.76), and 9 unknown field variables $\underset{\sim}{U}$, $\underset{\sim}{E}$, λ and $\underset{\sim}{P}$.

A variational formulation for this boundary value problem is obtained by replacing the balance law (1.75b) and the traction boundary condition (1.76a) by the virtual work principle

$$\delta\Phi(\underset{\sim}{U}) = \int_{\mathcal{B}_K}\underset{\sim}{P}:\delta\underset{\sim}{E}\,dV - \int_{\mathcal{B}_K}\rho_K\underset{\sim}{b}\,dV - \int_{\partial\mathcal{B}_K^{I}}\hat{\underset{\sim}{t}}_K\cdot\delta\underset{\sim}{U}\,dS = \underset{\sim}{0}. \tag{1.78}$$

II. IDENTIFICATION OF NONLINEAR MATERIALS

2.1 Identification of Material Behavior

Application of the continuum mechanics concepts and boundary value problems developed in the previous chapter is predicated on the ability to identify the behavior of thermomechanical materials. That is, actual physical specimens of materials must be loaded and measured, and the observed data used to identify explicitly the appropriate constitutive functionals that mathematically characterize the materials. Nonlinear continuum mechanics theory is very useful in determining the format of the constitutive response functionals for various special classes of materials, but how to find explicitly these functions from experimentally obtained data is still an open question.

To identify a nonlinear material two separate steps are involved:

1) Design an experiment which will both supply adequate input information to identify the material of the specimen and be physically possible to conduct in the laboratory.

2) Design a mathematical model capable of representing the identification experiment. Observed experimental measurements are input to this model and identified material response is output.

The general material response functionals of Section 1.6 are tensor-valued functionals with tensor-valued arguments involving field histories. Even the far simpler response functionals for thermoelastic (1.29) or elastic (1.31) materials are tensor-

valued functionals with tensor-valued arguments. Consequently, traditional testing techniques (measuring a material specimen loaded in such a way that the strain and temperature fields (or field histories if a nonelastic material) are spatially uniform in the measured area of the specimen) will not generate sufficient information to determine the material operator - except for the very special cases to be discussed in Section 2.3. For example, in order that the general elastic response functional

$$\underset{\sim}{\mathcal{F}}(\underset{\sim}{C})$$

be determined from a uniform strain experiment (where $\underset{\sim}{C}(\underset{\sim}{X})$ is constant throughout the measured part of the specimen) for a particular argument $\underset{\sim}{C}$, 6 independent measurements in different directions must be taken - an impossible task in a loaded three-dimensional specimen.

Therefore, a general identification technique must utilize the input-output response for a material specimen in which strain and temperature field histories are not spatially uniform throughout the body. Hence the problem of material identification is coupled with the problem of solving boundary value problems (Sections 1.8-1.12). That is, a very complex system is needed to describe the material characterization experiment, one that imposes relationships upon both spatial field variables and material response functionals. We will refer to this input-output system as the material identification inverse problem. A more formal and more complete discussion of this approach to the material identification problem can be found in a paper by Pister [24].

Since material response functionals have different values for different strain and temperature arguments, the results of one identification experiment cannot be blindly applied to any stress analysis problem. Usually numerous different types of experiments are necessary to define a constitutive functional over a significant portion of its argument space, since the results of any single experiment (or associated inverse problem) will be valid only for those strain and temperature states (or histories) that exist in that experiment. Extrapolation of results to other strain states is facilitated by the constitutive theory of Section 1.6, but it is extrapolation nonetheless.

We shall now turn to the expression of a material identification problem in terms of the concepts of Chapter I.

2.2 Inverse Boundary Value Problem

Let us examine more closely the mathematical structure of the inverse problem involved in material identification. The inverse problem for a general thermomechanical material has the following elements:

Input - a geometric description of the specimen, a specified loading process ($\underset{\sim}{b}(\underset{\sim}{X},t)$, $\hat{\underset{\sim}{t}}_{\kappa}(\underset{\sim}{X},t)$, $r(\underset{\sim}{X},t)$, $Q_n(\underset{\sim}{X},t)$), and a description of the motion and temperature histories resulting from this loading process ($\underset{\sim}{\chi}(\underset{\sim}{X},t)$, $\Theta(\underset{\sim}{X},t)$).

Output - the four material functionals $\hat{\psi}$, $\hat{\eta}$, $\underset{\sim}{\mathcal{T}}$, $\hat{\underset{\sim}{Q}}$ that characterize the material of the specimen, defined for the strain and temperature histories that occur in the experiment.

Since the motion and temperature field histories that serve as input above cannot be measured continuously (in time and space) in an actual experiment, it is necessary to modify the inverse problem in such a way that the motion and temperature field histories are also unknowns, as well as the material operators, in the problem. Thus, a series of experimental observations of the field histories $\underset{\sim}{\chi}(\underset{\sim}{X},t)$ and $\Theta(\underset{\sim}{X},t)$ serve as input to the identification problem, from which the continuous field histories $\underset{\sim}{\chi}(\underset{\sim}{X},t)$, $\Theta(\underset{\sim}{X},t)$ and the material functionals are determined. This inverse boundary value problem can be stated more precisely as follows:

Input - a geometric description of the specimen, a specified loading process ($\underset{\sim}{b}(\underset{\sim}{X},t)$, $\hat{\underset{\sim}{t}}_{\underset{\sim}{x}}(\underset{\sim}{X},t)$, $r(\underset{\sim}{X},t)$, $Q_n(\underset{\sim}{X},t)$), relevant boundary conditions and initial conditions, and a description (through a finite set of experimental measurements) of the motion and temperature histories resulting from this loading process, i. e.,

$$\underset{\sim}{\chi}(\underset{\sim}{X},t) = \hat{\underset{\sim}{\chi}}(\underset{\sim}{X},t) \tag{2.1a}$$

$$\Theta(\underset{\sim}{X},t) = \hat{\Theta}(\underset{\sim}{X},t). \tag{2.1b}$$

Output - the material functionals that characterize the material of the specimen,

$$\psi(\underset{\sim}{X},t) = \hat{\psi}\left(\underset{\sim}{C}(\underset{\sim}{X},t-s), \Theta(\underset{\sim}{X},t-s)\right) \tag{2.2a}$$

$$\eta(\underset{\sim}{X},t) = \hat{\eta}\left(\underset{\sim}{C}(\underset{\sim}{X},t-s), \Theta(\underset{\sim}{X},t-s)\right) \tag{2.2b}$$

$$\underset{\sim}{P}(\underset{\sim}{X},t) = \underset{\sim}{\mathcal{F}}\left(\underset{\sim}{C}(\underset{\sim}{X},t-s),\Theta(\underset{\sim}{X},t-s)\right) \qquad (2.2c)$$

$$\underset{\sim}{Q}(\underset{\sim}{X},t) = \hat{\underset{\sim}{Q}}\left(\underset{\sim}{C}(\underset{\sim}{X},t-s),\Theta(\underset{\sim}{X},t-s),\underset{\sim}{G}(\underset{\sim}{X},t-s)\right) \qquad (2.2d)$$

defined for the strain and temperature histories that occur in the experiment, the motion $\underset{\sim}{\chi}(\underset{\sim}{X},t)$ and temperature $\Theta(\underset{\sim}{X},t)$, and any other field histories involved in the observed thermomechanical process that are derived as intermediate steps in determining the material functionals - such as strain history $\underset{\sim}{C}(\underset{\sim}{X},t-s)$.

The solution (output) of the general thermomechanical inverse boundary value problem is found by use of the field equations (1.53a-f) discussed in Section 1.8 and the input data described above. Needless to say, the mathematical nature of this general inverse boundary value problem is extremely complex and a general analytical solution is not possible.

The inverse boundary value problems associated with the forward-direction boundary value problems for more specialized materials (Sections 1.9-1.11) can be easily derived and take forms similar to that of the general problem just discussed. Here we will state precisely the inverse problem only for an isotropic, incompressible elastic material in a state of plane stress (equations (1.75-1.78) of Section 1.12) since we will refer to this problem frequently in later chapters because of its relative mathematical simplicity.

From an experiment on a body described by a two-dimensional reference configuration $\mathcal{B}_{\underset{\sim}{K}}$, subject to a prescribed body force

$\underset{\sim}{b}(\underset{\sim}{X},t)$, and whose deformed configuration is specified (through a finite number of experimental measurements) as

$$\underset{\sim}{U}(X,Y) = \hat{\underset{\sim}{U}}(X,Y) \qquad (X,Y) \in \mathcal{B}_{\underset{\sim}{K}} \tag{2.3a}$$

$$\lambda(X,Y) = \hat{\lambda}(X,Y) \qquad (X,Y) \in \mathcal{B}_{\underset{\sim}{K}}, \tag{2.3b}$$

find the material constitutive functions $C_1(I_1,I_2)$ and $C_2(I_1,I_2)$ and the thermomechanical state $R(X,Y):\{U_1, U_2, E_{11}, E_{12}, E_{22}, \lambda, P_{11}, P_{12}, P_{22}\}$ which satisfy at all (X,Y) in $\mathcal{B}_{\underset{\sim}{K}}$ the field equations

$$\underset{\sim}{E} = \tfrac{1}{2}\left[\nabla\underset{\sim}{U} + \nabla\underset{\sim}{U}^T + \nabla\underset{\sim}{U}^T\cdot\nabla\underset{\sim}{U}\right] \tag{2.4a}$$

$$\underset{\sim}{P} = 2C_1(I_1,I_2)\left\{\begin{bmatrix}1&0\\0&1\end{bmatrix} - \frac{\lambda^4}{\det(2\underset{\sim}{E}+\underset{\sim}{I})}\begin{bmatrix}2E_{22}+1 & -2E_{12}\\ -2E_{12} & 2E_{11}+1\end{bmatrix}\right\}$$

$$+ 2C_2(I_1,I_2)\left\{\lambda^2\begin{bmatrix}1&0\\0&1\end{bmatrix} + \left(1+\frac{2\lambda^4(E_{11}+E_{22}+1)}{\det(2\underset{\sim}{E}+\underset{\sim}{I})}\right)\begin{bmatrix}2E_{22}+1 & -2E_{12}\\ -2E_{12} & 2E_{11}+1\end{bmatrix}\right\} \tag{2.4b}$$

$$\det(2\underset{\sim}{E}+\underset{\sim}{I}) = 1, \tag{2.4c}$$

the boundary condition

$$\underset{\sim}{U}(X,Y) = \hat{\underset{\sim}{U}}(X,Y) \qquad (X,Y) \in \partial\mathcal{B}_{\underset{\sim}{K}}^{II} \tag{2.4d}$$

and the virtual work principle

$$\delta\Phi(\underset{\sim}{U}) = \int_{\mathcal{B}_{\underset{\sim}{K}}} \underset{\sim}{P}:\delta\underset{\sim}{E}\,dV - \int_{\mathcal{B}_{\underset{\sim}{K}}} \rho_{\underset{\sim}{K}}\,\underset{\sim}{b}\cdot\delta\underset{\sim}{U}\,dV$$

$$- \int_{\partial\mathcal{B}_{\underset{\sim}{K}}^{I}} \hat{\underset{\sim}{t}}_{\underset{\sim}{K}}\cdot\delta\underset{\sim}{U}\,dS = 0, \tag{2.4e}$$

where the strain invariants are directly related to $\underset{\sim}{E}$ and λ by the relations

$$I_1 = 2(E_{11} + E_{22} + 1) + \lambda^2 \tag{2.5a}$$

$$I_2 = 2\lambda^2(E_{11} + E_{22} + 1) + (2E_{11} + 1)(2E_{22} + 1) - 4E_{12}^2 . \tag{2.5b}$$

Note that the possibility of mixed boundary conditions is provided for in the expression

$$\partial\mathcal{B}_{\underset{\sim}{K}}^{I} + \partial\mathcal{B}_{\underset{\sim}{K}}^{II} = \partial\mathcal{B}_{\underset{\sim}{K}} . \tag{2.6}$$

The material functions C_1 and C_2 will, of course, not be identified over all possible points (I_1, I_2) but only over those points derivable from the output state $R(x,y)$.

Note the extensive amount of mathematical modelling that is necessary to express the isotropic, incompressible elastic material characterization problem in terms of the inverse boundary value problem (2.3-2.6):

1) The physical body is idealized as a homogeneous continuum representable by a set $\mathcal{B}_{\underset{\sim}{K}}$ in Euclidean space.

2) The loads upon the body are idealized as distributed loading functions $\underset{\sim}{b}(x,y)$ and $\hat{\underset{\sim}{t}}_{\underset{\sim}{K}}(x,y)$.

3) The way the body is connected to its environment is idealized by the geometric boundary conditions $\hat{\underset{\sim}{U}}$.

4) The material function $\underset{\sim}{\mathcal{F}}(\underset{\sim}{C})$ reflects the assumptions of perfect elasticity: behavior depends only on current configuration and shows no temperature effects.

5) The body is two-dimensionalized by the plane stress model.

6) The material is idealized as isotropic and incompressible.

The solution $C_i(I_1, I_2)$ of the inverse boundary value problem (2.3-2.6) will accurately portray the experimental material only if the mathematical model accurately represents the experimental situation. The material assumptions in 4) and 6) above should be thoroughly tested, and an experimental body and loading process should be designed in a way that permits accurate modelling.

Note the basic difference between the forward-direction boundary value problem of elasticity and the associated inverse boundary value problem. In the forward-direction boundary value problem we seek to determine the motion (Figure 2.1) of the body when the material operator (Figure 2.2) is known. On the other

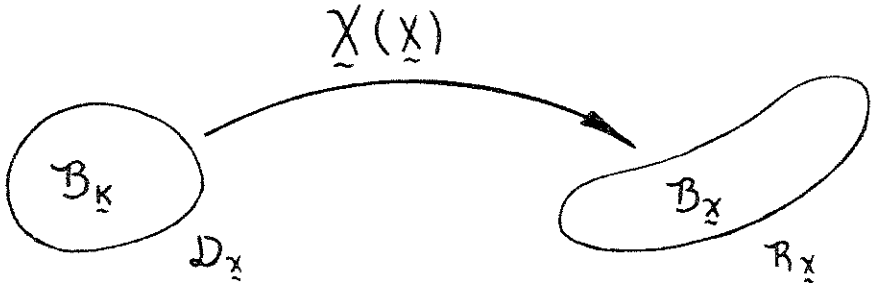

Fig. 2.1

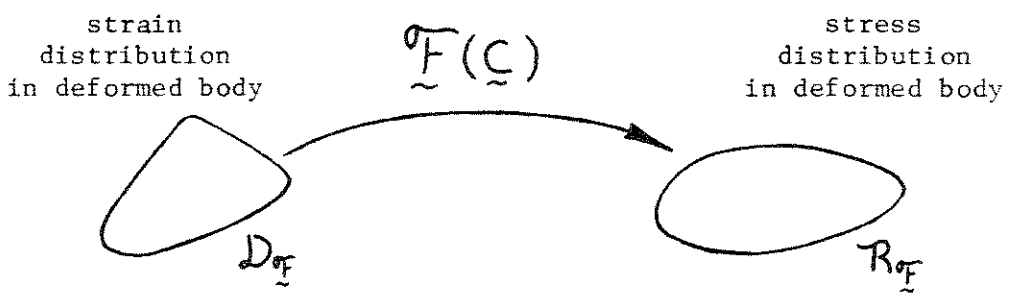

Fig. 2.2

hand, in the inverse boundary value problem we seek to determine both the motion and the material operator when an experimental description of the motion is known. The inverse problem is far more difficult since the domain of the material operator is unknown *a priori*.

2.3 Analytical Solution of the Inverse Problem

Stress analysis has always demanded some sort of mathematical characterization of engineering materials. For centuries this demand has been met by assuming linear material behavior - at least in the strain ranges involved in engineering design. Material identification for linear elastic materials is a very simple affair, since the material response functions (1.51) are expressed in terms of constant elastic moduli completely independent of the strain domain of the operator. Hence, identifying the elastic parameters through any experiment will produce a material characterization that is valid in any other strain state. Thus, a simple homogeneous strain experiment will suffice to identify a linear elastic material and solution of the inverse boundary value problem is a trivial algebraic operation.

For example, most engineering materials are assumed to be isotropic, linear elastic (1.52); therefore, the boundary value problem (1.61-1.63) describes the behavior of any body composed of this material and finding the two material moduli E and ν requires the solution of the associated inverse problem. Since identifying E and ν in any strain state will produce results valid for all strain states, a simple uniaxial stress experiment is usually used, as in Figure 2.3.

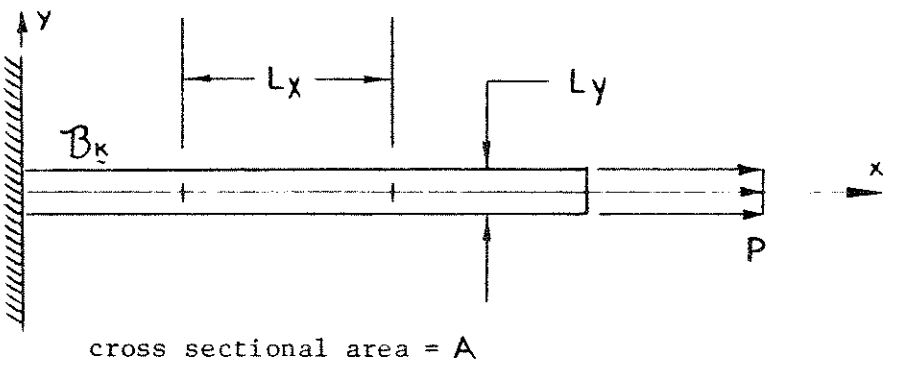

Fig. 2.3

The solution of the inverse problem is an extremely simple analytical process, resulting in

$$E = P \cdot L_x / A \cdot \Delta L_x \tag{2.7a}$$

$$\nu = \Delta L_y \cdot L_x / \Delta L_x \cdot L_y \tag{2.7b}$$

where ΔL_x and ΔL_y are measured displacements or data from strain gauges.

Numerous irrational nonlinear material characterization techniques have been developed using a nonlinear functional form for E . The exact form of $E(\epsilon)$ is then determined from a uniaxial or other simple homogeneous strain experiment. However, applying an identified $E(\epsilon)$ to a stress analysis problem involving strain states different from those of the identifying experiment is a gross approximation unless the strain invariant domain of the stress analysis problem is a subset of the strain invariant domain of the experiment that derived $E(\epsilon)$. A nonlinear isotropic elastic material characterization that will be valid in all strain states must be based on the general elastic constitutive relation (1.37).

The isotropic, incompressible inverse boundary value problem (2.3-2.6) can be solved analytically for bodies in a state of biaxial homogeneous strain, making possible the identification of the functions $C_i(I_1, I_2)$ for all strain states except those producing buckling in a thin sheet. A body in biaxial strain is shown in Figure 2.4.

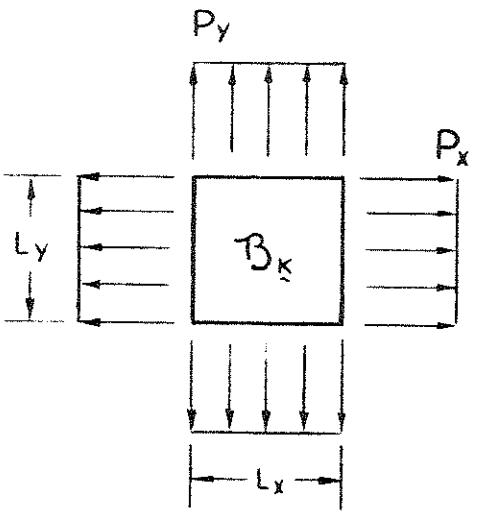

h = thickness of sheet

λ_x = extension ratio for deformation in the x-direction

λ_y = extension ratio for deformation in the y-direction

Fig. 2.4

If traction boundary conditions are given by

$$t_x = \frac{P_x \cdot \lambda_x}{L_y \cdot h} \tag{2.8a}$$

$$t_y = \frac{P_y \cdot \lambda_y}{L_x \cdot h} \tag{2.8b}$$

then the inverse boundary value problem applied to the homogeneous body of Figure 2.4 reduces to the two algebraic equations

$$\begin{aligned} t_x &= 2\left(\lambda_x^2 - \frac{1}{\lambda_x^2 \lambda_y^2}\right)\left(C_1 + \lambda_y^2 C_2\right) \\ t_y &= 2\left(\lambda_y^2 - \frac{1}{\lambda_x^2 \lambda_y^2}\right)\left(C_1 + \lambda_x^2 C_2\right) \end{aligned} \tag{2.9}$$

which can be solved directly for C_1 and C_2. The strain invariant values corresponding to the measured extension ratio pair (λ_x, λ_y) - and hence the domain (I_1, I_2) of the calculated C_1 and C_2 - is given by

$$I_1 = \lambda_x^2 + \lambda_y^2 + \frac{1}{\lambda_x^2 \lambda_y^2}$$
$$I_2 = \frac{1}{\lambda_x^2} + \frac{1}{\lambda_y^2} + \lambda_x^2 \lambda_y^2 . \tag{2.10}$$

Conducting the biaxial experiment for other loading combinations (P_x, P_y) will define $C_i(I_1, I_2)$ at other points in its domain. A thorough investigation of rubber-like materials using (2.9) has been carried out by Rivlin and Saunders [4] with excellent results. Consequently, the material constitution of rubber is quite well understood and numerous functional forms for $C_i(I_1, I_2)$ have been proposed [6].

If an incompressible material is subjected to a uniaxial stress experiment (Figure 2.3), the inverse boundary value problem (2.3-2.6) reduces to the single algebraic equation

$$P = 2A\left(\lambda - \frac{1}{\lambda^2}\right)\left(C_1 + \frac{1}{\lambda} C_2\right) \tag{2.11}$$

where λ is the measured extension ratio

$$\lambda = \Delta L_x + L_x \tag{2.12}$$

and the strain invariants are given by

$$I_1 = \lambda^2 + \frac{2}{\lambda}$$
$$I_2 = 2\lambda + \frac{1}{\lambda^2} . \tag{2.13}$$

Therefore, the material functions are indeterminate in a uniaxial stress experiment; only enough information for determination of the total stiffness $(C_1 + \frac{1}{\lambda} C_2)$ is given, and even the identified total stiffness is valid only for the strain invariant states derivable from (2.13). For an infinitesimal strain uniaxial experiment (where $\lambda \doteq 1$ and hence $I_1, I_2 \doteq 3$) the total stiffness is related to the traditional Young's modulus by

$$C_1 + C_2 = \frac{E}{6} . \tag{2.14}$$

To identify a compressible elastic material, characterized by the response functional $C_i(I_1, I_2, I_3)$, by a homogeneous strain experiment a fully triaxial strain state (as shown in Figure 2.5)

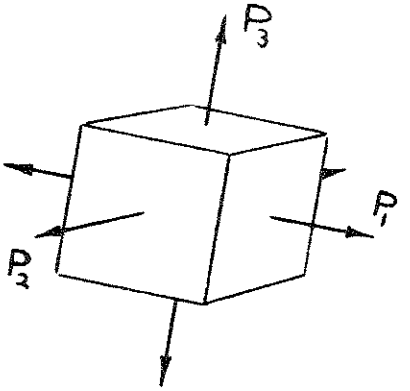

Fig. 2.5

would be needed. However, an experiment of this type cannot be designed in a way that makes measurement of the three extension ratios physically possible. A nonhomogeneous strain state is needed to identify $C_i(I_1, I_2, I_3)$, a situation much too complicated for analytical solution.

More general materials (1.28, 1.30, 1.32) also require complex

nonhomogeneous inverse boundary value problems to identify their response functionals - situations too difficult to solve analytically. Consequently, some sort of numerical solution will be necessary to identify all but the simplest nonlinear materials.

III. SOLUTION OF INVERSE PROBLEM BY DISCRETIZATION

3.1 Introduction

The inverse problem that must be solved to identify even the simplest of nonlinear materials is extremely complex. To solve the continuous inverse boundary value problems discussed in Section 2.2 is virtually impossible without approximate methods that eventually lead to linearized algebraic problems. The continuous nonlinear identification problem requires two very different types of numerical approximation: (1) transformation of the continuous partial differential equations to a system of discrete algebraic equations, and (2) transformation of the nonlinear equations to a sequence of solvable linear equations. The integration of these two operations can be accomplished in either of the following ways:

1) Quasilinearize the nonlinear inverse boundary value problem, and solve each linear step by means of some sort of discretization technique that converts the linear partial differential equations of each step into a system of linear algebraic equations.

2) Discretize the nonlinear continuous inverse boundary value problem at the outset to obtain a system of nonlinear algebraic equations, and solve these by a numerical method which converts them to a sequence of linear algebraic equations.

The second strategy seems to be the easiest approach, since it permits one to leave behind the extremely intractable continuous inverse boundary value problem at the earliest possible

moment. The method developed in this chapter will follow this second approach. The reader is referred to [19,20] for a full discussion of quasilinearization as applied to nonlinear boundary value problems.

Therefore, following the first strategy above, the first step in solving an inverse boundary value problem is to convert it to an algebraic problem. Three levels of discretization are necessary to accomplish this:

1) Space-time discretization of the kinematic and temperature state variables involved in the thermomechanical process $R(\underset{\sim}{X},t)$ is required. In practice, if the motion $\underset{\sim}{\chi}(\underset{\sim}{X},t)$ and temperature history $\Theta(\underset{\sim}{X},t)$ are discretized, then the strain, stress, and temperature gradient state variables can be expressed in discrete form by use of appropriate field equations in (1.53). Any of the standard methods of approximating an infinite-dimensional function by a finite number of elements in a subspace could be used, such as polynomial or finite difference approximations. One of the most successful discretization methods for nonlinear boundary value problems is the finite element method, which represents each function in terms of a finite number of very localized coordinate functions with scalar coefficients. For example, temperature can be discretized in terms of a finite element basis as follows:

$$\Theta(\underset{\sim}{X},t) \doteq \sum_{i=1}^{n} \Theta_i \varphi_i(\underset{\sim}{X},t). \tag{3.1}$$

In the simplest, most intuitive situations each coefficient Θ_i is the value of temperature at a certain sample point or node

in the domain of $\Theta(\underset{\sim}{X},t)$ - that is $\mathcal{B}_K$ and $t_{min} \leq t \leq t_{max}$. And the functions $\varphi_i(\underset{\sim}{X},t)$ simply interpolate between these nodal values of temperature to define an approximation to the temperature field $\Theta(\underset{\sim}{X},t)$. Each of the three components of motion $\underset{\sim}{\chi}(\underset{\sim}{X},t)$ can be discretized similarly to (3.1).

This level of discretization (which we will refer to as geometric discretization) is the only level needed to completely discretize the forward-direction boundary value problems of Sections 1.8-1.12, in which material properties are known and only the thermomechanical process $\mathcal{R}$ is sought. For example, in the thermoelastic initial boundary value problem (1.52-56) discretization of $\Theta(\underset{\sim}{X},t)$ and $\underset{\sim}{\chi}(\underset{\sim}{X},t)$ as in (3.1) leads directly to the expression of the entire continuous problem as a system of algebraic equations.

Solution of forward-direction nonlinear boundary value problems by the finite element method is a well-established procedure - especially for elastic materials [7-10,13]. A full theoretical development of the finite element method and its application to continuum analysis can be found in any of the standard texts [21,22].

2) Secondly, discretization of the information that describes the deformed configuration and temperature of the experimental body, the information contained in (2.1a-b), is needed. The continuous inverse problem assumes that $\underset{\sim}{\chi}$ and Θ are known exactly at every space-time point $(\underset{\sim}{X},t)$, whereas in an actual experiment it is possible to know them only at a finite number of points - points where measurements are taken. The way in

which these experimental data (2.1a-b) are described - the number and distribution of observations and the precise types of measurements of strain or temperature input - constitute the second level of discretization of the inverse boundary value problem.

3) Finally, discretization of the material constitutive functionals (2.2) is required. As discussed in Chapter II, the domain of the material functions will not be all $(\underset{\sim}{C}, \theta, \underset{\sim}{G})$ but only those sets $(\underset{\sim}{C}, \theta, \underset{\sim}{G})$ that occur in the thermomechanical process $R(\underset{\sim}{x}, t)$ for the particular inverse boundary value problem. Hence $\hat{\psi}$, $\hat{\eta}$, $\underset{\sim}{\mathcal{F}}$, and $\hat{\underset{\sim}{Q}}$ can be discretized only over the subset $(\underset{\sim}{C}, \theta, \underset{\sim}{G})$ that constitutes the proper domain for the particular experiment. The way in which the material constitutive functions are parameterized is the third level of discretization of the inverse boundary value problem. In this dissertation we shall examine in great detail the idea of representing the material functions in terms of finite element bases. For example, the stress constitutive equation (2.2c) can be expressed in terms of a finite element expansion by

$$\underset{\sim}{\mathcal{F}}\left(\underset{\sim}{C}(\underset{\sim}{x}, t-s), \theta(\underset{\sim}{x}, t-s)\right) \doteq \sum_{i=1}^{m} \underset{\sim}{\mathcal{F}}_i \varphi_i\left(\underset{\sim}{C}(\underset{\sim}{x}, t-s), \theta(\underset{\sim}{x}, t-s)\right) \qquad (3.2)$$

where $\underset{\sim}{\mathcal{F}}_i$ are values of the stress constitutive functional $\underset{\sim}{\mathcal{F}}\left(\underset{\sim}{C}(\underset{\sim}{x}, t-s), \theta(\underset{\sim}{x}, t-s)\right)$ at various "nodes" or points in its domain, and $\varphi_i\left(C(\underset{\sim}{x}, t-s), \theta(\underset{\sim}{x}, t-s)\right)$ are coordinate functions defined over the material operator $\underset{\sim}{\mathcal{F}}$'s domain for the particular experiment.

The general thermomechanical inverse problem is extremely

complex and demands very complicated and extensive discretization. Therefore, to develop and test solution techniques for the inverse problem we shall in the sequel consider the much simpler inverse boundary value problem (2.3-2.6) for an isotropic, incompressible elastic body in a state of plane stress. Application of the technique to the general thermomechanical problem will be discussed in Chapter V.

Let us here summarize the parts of the continuous inverse problem that must be discretized in each of the three levels indicated above:

1) Thermomechanical Inverse Problem

   a) geometric: $\underset{\sim}{\chi}(\underset{\sim}{X},t)$, $\Theta(\underset{\sim}{X},t)$

   b) experimental measurements: $\hat{\underset{\sim}{\chi}}$, $\hat{\Theta}$

   c) material: $\hat{\psi}(\underset{\sim}{C},\Theta)$, $\hat{\eta}(\underset{\sim}{C},\Theta)$, $\hat{\underset{\sim}{T}}(\underset{\sim}{C},\Theta)$, $\hat{\underset{\sim}{Q}}(\underset{\sim}{C},\Theta,\underset{\sim}{G})$

2) Incompressible Elastic Plane Stress Inverse Problem

   a) geometric: $\underset{\sim}{\upsilon}(x,y)$, $\lambda(x,y)$

   b) experimental measurements: $\hat{\underset{\sim}{\upsilon}}$, $\hat{\lambda}$

   c) material: $c_1(I_1,I_2)$, $c_2(I_1,I_2)$

The next three sections will examine each of these levels of discretization in detail for the incompressible elastic inverse problem and will indicate how the resulting discretized problem effects an approximate identification of the two material functions.

3.2 Finite Element Geometric Discretization

As a discretization choice for the kinematic field variables of the incompressible elastic inverse problem (2.3-2.6), consider the representations

$$\underset{\sim}{u}(x,y) \doteq \sum_{i=1}^{N} \underset{\sim}{u}_i \phi_i(x,y) \tag{3.3a}$$

$$\lambda(x,y) \doteq \sum_{i=1}^{M} \lambda_i \varphi_i(x,y) \tag{3.3b}$$

where N and M are the number of degrees of freedom (or nodes) in the discretizations for $\underset{\sim}{u}(x,y)$ and $\lambda(x,y)$ respectively. The finite element coordinate basis $\phi_i(x,y)$ must satisfy the geometric boundary conditions (2.4d). The distributed body force $\underset{\sim}{b}_K$ and the boundary traction loading $\hat{\underset{\sim}{t}}_K$ found in (2.4e) must also be discretized in some way consistent with (3.3a), preferably with the same basis. Consider the following expansions:

$$\underset{\sim}{b}_K(x,y) \doteq \sum_{i=1}^{N} \underset{\sim}{b}_{Ki} \phi_i(x,y) \tag{3.4a}$$

$$\hat{\underset{\sim}{t}}_K(x,y) \doteq \sum_{i=1}^{\partial N} \underset{\sim}{R}_i \phi_i(x,y) \tag{3.4b}$$

where ∂N refers to the boundary nodes of the discretization for $\underset{\sim}{u}(x,y)$.

Substitution of the discretized field variables (3.3-3.4) into the field equations (2.4) leads directly to a discretized energy functional which must be minimized with respect to each discrete nodal displacement and extension ratio, leading to the $2 \times N$ algebraic equations

$$\underset{\sim}{f}_{EQ}(\underset{\sim}{u}, \underset{\sim}{\lambda}) = \underset{\sim}{R} \tag{3.5}$$

and the continuous incompressibility constraint equation (2.4c) in the form of M discrete equations

$$\underset{\sim}{f}_{INC}(\underset{\sim}{U}, \underset{\sim}{\lambda}) = \underset{\sim}{1} . \tag{3.6}$$

In the notation of equations (3.5) and (3.6) $\underset{\sim}{U}$ is a $2\times N$-dimensional vector composed of all nodal values of displacement $\underset{\sim}{U}_i$, and $\underset{\sim}{\lambda}$ is an M-dimensional vector composed of all nodal values of extension ratio λ_i. The $2\times N$-dimensional vector $\underset{\sim}{R}$ represents the discretized prescribed loading b_{ki} and $\hat{t}_{ki}$, and the M-dimensional vector $\underset{\sim}{1}$ is a unit vector.

The force equilibrium equations (3.5) and the incompressibility constraint equations (3.6) can be written together in the form

$$\begin{Bmatrix} \underset{\sim}{f}_{EQ}(\underset{\sim}{U}, \underset{\sim}{\lambda}) \\ \underset{\sim}{f}_{INC}(\underset{\sim}{U}, \underset{\sim}{\lambda}) \end{Bmatrix} = \begin{Bmatrix} \underset{\sim}{R} \\ \underset{\sim}{1} \end{Bmatrix}, \tag{3.7}$$

or more compactly

$$\underset{\sim}{f}(\underset{\sim}{U}, \underset{\sim}{\lambda}) = \underset{\sim}{P} , \tag{3.8}$$

a system of $(2\times N+M)$ nonlinear algebraic equations that completely discretizes the continuous boundary value problem.

In actual practice the global finite element method coordinate functions $\phi_i(x,y)$, defined over the whole domain of the boundary value problem $\mathcal{B}_k$, are not used. Rather local element coordinate functions (called interpolation functions) $\psi_j(x,y)$ are defined over each element, such that the value of $\underset{\sim}{U}$ and $\underset{\sim}{\lambda}$ in each element is given by

$$U_k(x,y) \doteq \sum_{j=1}^{N} U_{kj}\,\psi_j(x,y) \tag{3.9}$$

(where $U_1(x,y)$ is the x-displacement, $U_2(x,y)$ the y-displacement, N the number of nodes in the element, and U_{kj} the elements of $\underset{\sim}{U}$ that are represented in this particular element) and

$$\lambda(x,y) \doteq \sum_{i=1}^{M} \lambda_i\,\xi_i(x,y) \tag{3.10}$$

(where M is the number of extension ratio nodes in the element and λ_i are the elements of $\underset{\sim}{\lambda}$ that are represented in this particular element). If a constant-strain finite element [21] is chosen to discretize $\underset{\sim}{U}(x,y)$ and a constant-λ triangular finite element is chosen to discretize $\lambda(x,y)$ the shape of the two-dimensional element is as shown in Figure 3.1

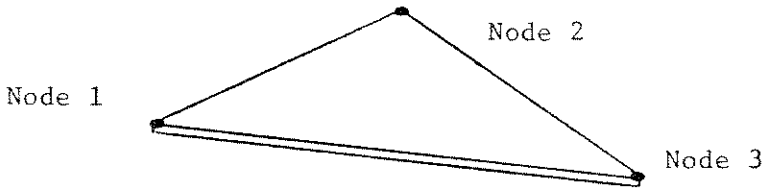

Fig. 3.1

and the local coordinate functions are as shown in Figure 3.2. Hence, the deformation in the element can be represented by

$$U_1(x,y) \doteq U_{11}\psi_1(x,y) + U_{12}\psi_2(x,y) + U_{13}\psi_3(x,y) \tag{3.11a}$$

$$U_2(x,y) \doteq U_{21}\psi_1(x,y) + U_{22}\psi_2(x,y) + U_{23}\psi_3(x,y) \tag{3.11b}$$

$$\lambda(x,y) \doteq \lambda\xi(x,y). \tag{3.11c}$$

The relevant field equations (2.4a-c) and the virtual work principle (2.4e) must be satisfied within each element. Substi-

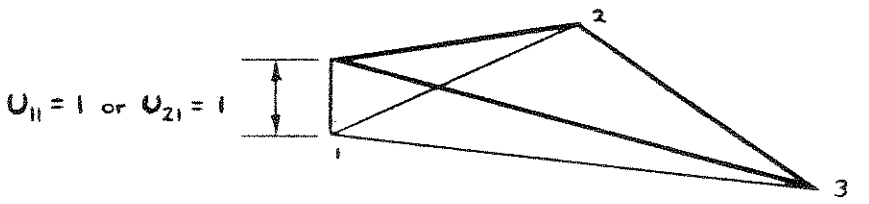

$\psi_1(x, y)$

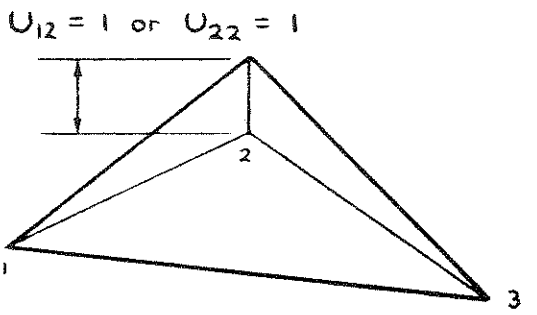

$\psi_2(x, y)$

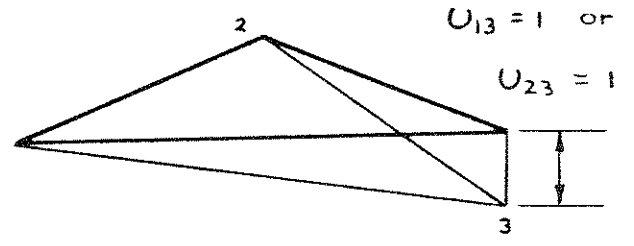

$\psi_3(x, y)$

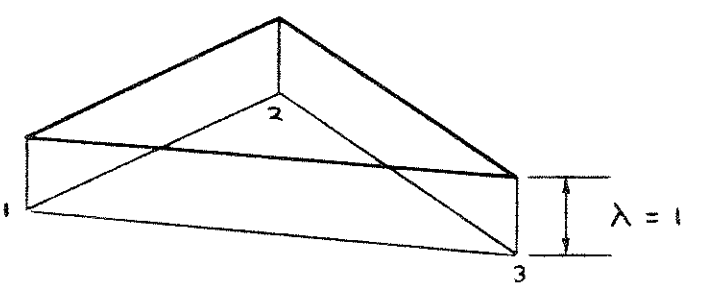

$\xi(x, y)$

FINITE ELEMENT LOCAL COORDINATE FUNCTIONS

Fig. 3.2

tution of the discretizations (3.11) into the former equations and minimization of the energy functional $\Phi(\underset{\sim}{U})$ result in a set of 6 force equilibrium equations and one incompressibility constraint equation for each triangular element:

$$\int_v P_{\alpha\beta}\psi_{N,\alpha}\left(\delta_{\beta K} + \psi_{M,\beta}U_{KM}\right)dV = \int_v \rho \underset{\sim}{b}_K \psi_N dV + \int_S \hat{t}_K \psi_N dS \tag{3.12}$$

and

$$\int_v \det\left[2E_{\alpha\beta} + \delta_{\alpha\beta}\right]dV = 1, \tag{3.13}$$

where $\alpha,\beta,K = 1,2$ and $N,M = 1,2,3$ and

$$E_{\alpha\beta} = \tfrac{1}{2}\left[\psi_{N,\beta}U_{\alpha N} + \psi_{N,\alpha}U_{\beta N} + \psi_{N,\alpha}U_{KN}\psi_{M,\beta}U_{KM}\right] \tag{3.14}$$

$$P_{\alpha\beta} = 2C_1(I_1,I_2)\left\{\left(1-\frac{\lambda^4\xi^4}{\det(C_{K\ell})}\right)\delta_{\alpha\beta} - \frac{2\lambda^4\xi^4}{\det(C_{K\ell})}\begin{bmatrix} E_{22} & -E_{12} \\ -E_{12} & E_{11}\end{bmatrix}\right\} + 2C_2(I_1,I_2)\left\{\lambda^2\xi^2\delta_{\alpha\beta} + \left(1+\frac{2\lambda^4\xi^4(E_{11}+E_{22}+1)}{\det(C_{K\ell})}\right)\begin{bmatrix} 2E_{22}+1 & -2E_{12} \\ -2E_{12} & 2E_{11}+1\end{bmatrix}\right\}. \tag{3.15}$$

When the algebraic equations (3.12-3.13) are calculated for each element in the mesh and assembled into a global system of equations encompassing all the nodes in the body, expression (3.8) again results:

$$\underset{\sim}{f}(\underset{\sim}{U},\underset{\sim}{\lambda}) = \underset{\sim}{P}. \tag{3.8}$$

All the numerical examples analyzed in this dissertation utilize this constant-strain, constant-λ element formulation.

3.3 Discretization of Deformed Configuration of Experiment

A continuous inverse problem requires as input a complete description of the deformed configuration $\mathcal{B}_{\underset{\sim}{\chi}}$ of the experimental body, expressed by the two continuous prescribed functions $\hat{\underset{\sim}{\upsilon}}(x,y)$ and $\hat{\lambda}(x,y)$, as illustrated in Figure 3.3.

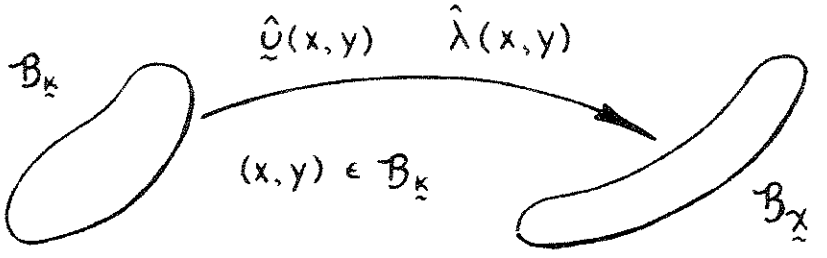

Fig. 3.3

Since an infinite number of measurements would be needed to determine $\mathcal{B}_{\underset{\sim}{\chi}}$ exactly, the identification problem was restated in terms of an inverse boundary value problem, permitting the deformed configuration $\mathcal{B}_{\underset{\sim}{\chi}}$ to be specified by a finite number of observations. The second level of discretization for plane stress inverse boundary value problem (2.3-2.6), therefore, is to choose a finite set of experimentally observed measurements that will in some sense adequately represent $\mathcal{B}_{\underset{\sim}{\chi}}$. These measurements can be in many forms:

1) A statement of the x- or y-displacement of some point on the body's surface (in the reference configuration $\mathcal{B}_{\underset{\sim}{\kappa}}$). This is the type of measurement used as input for the example of Appendix A.

2) The amount of deformation (in some specified direction)

between any two points on the surface of the body, as measured on an experimental specimen. This is the type of information used as input for the example of Appendix D.

3) A direct measurement of the strain state at some point in the body (e. g., elements of $\underset{\sim}{C}$ or $\underset{\sim}{E}$) by the use of some sort of strain gauge.

4) A measurement of the extension ratio at some point in the domain $\mathcal{B}_{\underset{\sim}{k}}$.

These actual physical measurements must be converted to mathematical expressions involving the same discrete variables $\underset{\sim}{\upsilon}$ and $\underset{\sim}{\lambda}$ used to discretize the kinematic variables of the boundary value problem - the vectors $\underset{\sim}{\upsilon}$ and $\underset{\sim}{\lambda}$ defined by (3.3). That is, each observed measurement of $\mathcal{B}_{\underset{\sim}{\chi}}$ must be expressed by an algebraic equation of the form

$$g(\underset{\sim}{\upsilon}, \underset{\sim}{\lambda}) = \delta . \tag{3.16}$$

In practical situations it is simplest to design the geometric finite element mesh in such a way that each measured point coincides with a node, making the mathematical description of the system of observed experimental measurements very obvious. For example, if the item of input δ_1 is the change in distance in the x-direction between points A and B (as shown in Figure 3.4), where point A lies on node 19 and point B lies on node 27, the input equation is

$$g_1(\underset{\sim}{\upsilon}, \underset{\sim}{\lambda}) = \upsilon_{27} - \upsilon_{19} = \delta_1 . \tag{3.17}$$

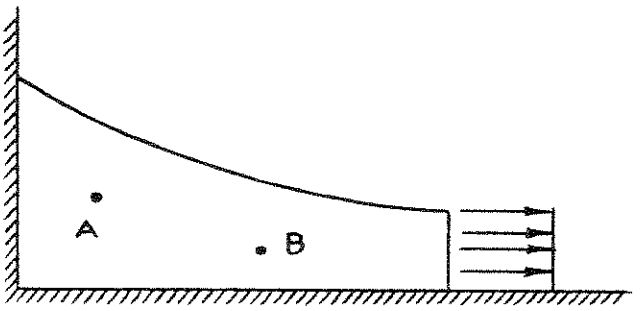

Fig. 3.4

The full set of q input measurements is expressed as

$$\underset{\sim}{g}(\underset{\sim}{\upsilon},\underset{\sim}{\lambda}) = \underset{\sim}{\delta} \tag{3.18}$$

where $\underset{\sim}{\delta}$ is a vector with as many elements as there are items of input. If a strain is measured in the body it must be expanded in terms of its finite element bases to obtain $\underset{\sim}{g}(\underset{\sim}{\upsilon},\underset{\sim}{\lambda})$.

Therefore, the set of q algebraic equations (3.18) completely discretizes the description of the deformed configuration $\mathcal{B}_{\underset{\sim}{x}}$ of the experimental body, described in the continuous inverse boundary value problem by

$$\underset{\sim}{\upsilon}(x,y) = \hat{\underset{\sim}{\upsilon}}(x,y) \tag{3.19a}$$

$$\lambda(x,y) = \hat{\lambda}(x,y). \tag{3.19b}$$

In other words, the information contained in $\underset{\sim}{\delta}$ is an experimental approximation to the exactly prescribed configuration $\hat{\underset{\sim}{\upsilon}}(x,y)$ and $\hat{\lambda}(x,y)$. As the dimension of $\underset{\sim}{\delta}$ increases to infinity, the discretized description of $\mathcal{B}_{\underset{\sim}{x}}$ (3.18) coincides with the continuous description (3.19).

3.4 Finite Element Material Discretization

The two material functions, $C_1(I_1, I_2)$ and $C_2(I_1, I_2)$, which characterize an isotropic, incompressible elastic material can be expressed in terms of a finite set of material parameters in several ways. We shall label this set of unknown material parameters by the q-dimensional vector $\underset{\sim}{C}$. The following three techniques warrant investigation:

1) Expand $C_i(I_1, I_2)$ in a polynomial in terms of the strain invariants:

$$C_i(I_1,I_2) = C_{i1} + C_{i2}(I_1-3) + C_{i3}(I_2-3) + C_{i4}(I_1-3)^2 + C_{i5}(I_2-3)^2 + C_{i6}(I_1-3)(I_2-3) + \cdots \tag{3.20}$$

Here the vector of material parameters $\underset{\sim}{C}$ is composed of all polynomial coefficients C_{ij}. This discretization technique works very well if there are only one or two terms in the polynomial; however, in larger, more realistic problems the higher-order terms make the inverse problem hopelessly hypersensitive. Consequently, although this approach is constantly mentioned in theoretical work it has not been very successfully used as the basis of a material identification method.

In addition, the polynomial expansion method gives the experimenter very little control over his material discretization. The domain of (3.20) is the whole (I_1, I_2) plane - not just the domain of the specific inverse boundary value problem that models the experiment. Hence inclusion of higher-order coefficients in $\underset{\sim}{C}$ tends to create a very unstable and usually

unusable material discretization.

A traditional way of parameterizing isotropic, incompressible materials is to express the energy functional (1.42) in terms of a polynomial

$$\hat{W}(I_1, I_2) = \sum_{i=0}^{n} \sum_{j=0}^{m} a_{ij} (I_1 - 3)^i (I_2 - 3)^j, \tag{3.21}$$

where C_i are the derivatives (1.43a) and hence expressible in terms of the parameters a_{ij}. However, (3.21) suffers from the sensitivities of (3.20) plus the added sensitivity of knowing C_1 and C_2 only through the derivatives of $\hat{W}$ - derivatives which must be obtained numerically and are extremely ill-conditioned with respect to a_{ij}. For discussion of an application of the polynomial expansion (3.21) to material identification the reader is referred to a paper by Kavanaugh [23].

2) Discretize C_1 and C_2 spatially by means of a finite element basis in $\mathcal{B}_{\underset{\sim}{K}}$. That is, let

$$C_1(x, y) = \sum_{i=1}^{r} c_i \varphi_i(x, y) \tag{3.22a}$$

$$C_2(x, y) = \sum_{i=r+1}^{q} c_i \varphi_i(x, y) \tag{3.22b}$$

at every point in the body. For example, if $C_1(x, y)$ for the body illustrated in Figure 3.4 is discretized by means of two quadrilateral elements with linear interpolation functions, 6 degrees of freedom result, as indicated in Figure 3.5. Hence, in physical terms the elements of the q-degree-of-freedom vector $\underset{\sim}{c}$ which describes in parametric terms the two material functions are simply the nodal values of the approximate material functions.

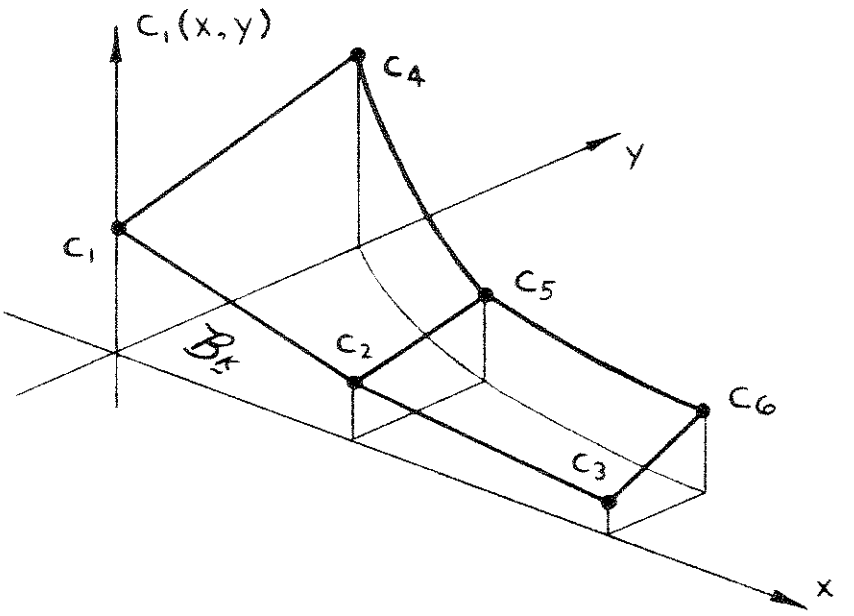

Fig. 3.5

The location of these nodal values of the material variables will depend on the material meshes chosen. Since the strain invariants I_1 and I_2 are also known in discretized form at all points in $\mathcal{B}_K$, the parameters $\underset{\sim}{C}$ also establish an approximation to $C_i(I_1, I_2)$.

The discrete $C_i(x,y)$ method needs very many degrees of freedom in $\underset{\sim}{C}$ to reasonably approximate the spatial material functions, which means each material node has only one or two measurements taken in its vicinity; hence the resulting algebraic system of equations tends to be ill-conditioned - even with virtually perfect discretizations and exact input measurements, as the example in Appendix A shows. In that example any input error at all (even 0 01%) in $\underset{\sim}{\delta}$ caused divergence. The main difficulty is that functional continuity with respect to I_1 and I_2 is not enforced, causing results very difficult to use when an identification contains error; however, there are some benefits to this

procedure since the scatter in the data (as in Figures A.7 and A.8) gives an indication of how reliable the identification is.

3) Discretize $C_1(I_1, I_2)$ and $C_2(I_1, I_2)$ directly in terms of the two strain invariants by setting up a finite element mesh in the (I_1, I_2) plane. That is, let

$$C_1(I_1, I_2) = \sum_{i=1}^{n_1} c_i \varphi_i(I_1, I_2) \tag{3.23a}$$

$$C_2(I_1, I_2) = \sum_{i=n_1+1}^{n_m} c_i \varphi_i(I_1, I_2). \tag{3.23b}$$

For example, in an experimental body loaded such that the strain invariant range involved is the area crosshatched in Figure 3.6

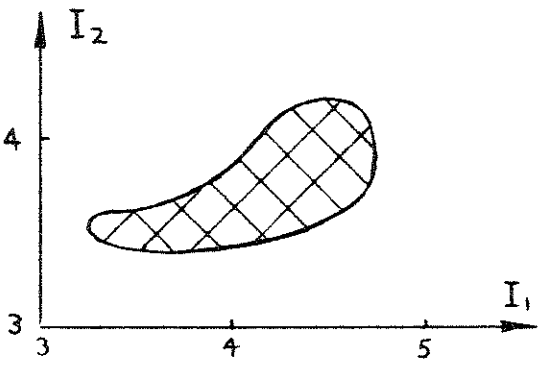

Fig. 3.6

a feasible finite element material mesh would be the 10 degree-of-freedom discretization shown in Figure 3.7. Note that these finite element bases permit extrapolation beyond the elements themselves and are a bit unorthodox. However, when viewed in terms of the global definition of discretization (3.23a-b) extrapolation is perfectly consistent, since the finite element coordinate functions $\varphi_i(I_1, I_2)$ are defined over an unbounded domain. For example, in the 10 degree-of-freedom mesh of

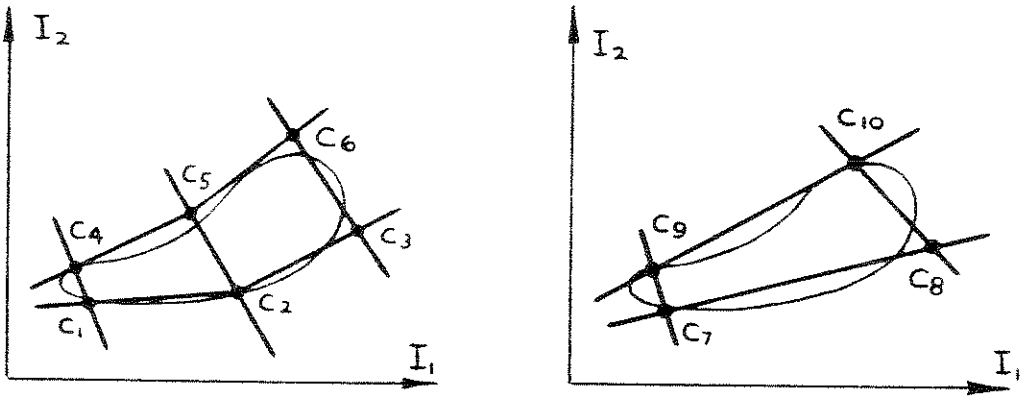

domain of $C_1(I_1, I_2)$ domain of $C_2(I_1, I_2)$

Fig. 3.7

Figure 3.7 the basis $\varphi_4(I_1, I_2)$ is as sketched in Figure 3.8 and is defined over the whole (I_1, I_2) plane. Note that this particular choice of element (a quadrilateral treated as two triangular elements with linear material interpolation functions) gives φ's that are discontinuous in parts of their domain that lie outside the elements themselves; however, this is quite acceptable and leads to no particular difficulties, especially since the strain states that must be dealt with in the identifi-

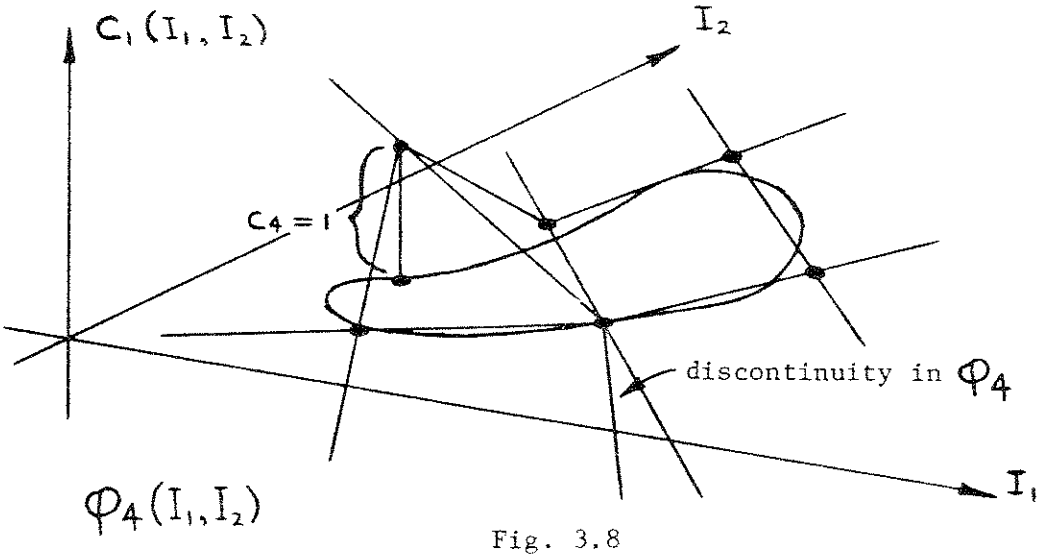

Fig. 3.8

cation problem lie almost entirely within the elements.

An isometric representation of $C_i(I_1, I_2)$ as discretized in Figure 3.7 is shown below in Figure 3.9 (with discontinuities in extrapolation ignored).

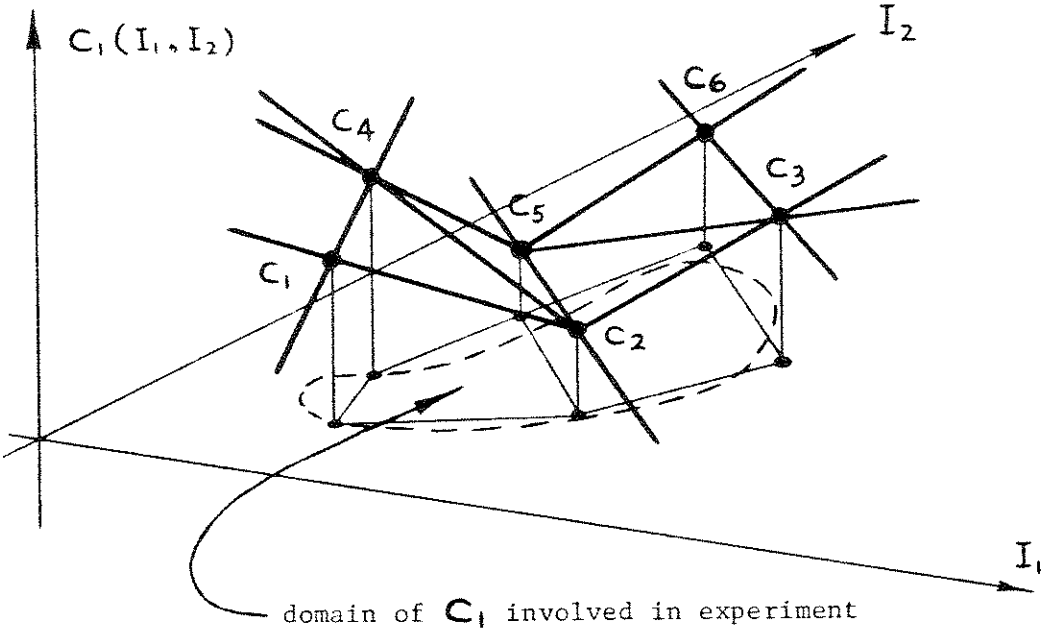

Fig. 3.9

From the previous discussion it is obvious that the elements of the material parameter vector $\underset{\sim}{C}$ are nodal values of C_1 or C_2 at various points (I_1, I_2) in the domain of $C_i(I_1, I_2)$.

At first glance a difficulty of this type of discretization might appear to be the large number of nodes needed for a full two-dimensional discretization of $C_i(I_1, I_2)$. In practical situations only a very small part of the total (I_1, I_2) domain of the general functions is involved in any particular experiment; hence only a few nodes are usually needed. The strain states

involved in the experiment can be very effectively estimated a priori by solving the forward-direction boundary value problem using a crude guess at the material functions - a guess perhaps arrived at from the simple experiments of Section 2.3. This information is then used to design an appropriate material mesh.

It is an interesting phenomenon that in technically feasible experiments the material operator will have a domain that involves only a near lineal sliver of the (I_1, I_2) plane; hence a one-dimensional discretization of $C_i(I_1, I_2)$ is normally sufficient. For example, the three very common homogeneous strain states shown below in Figure 3.10

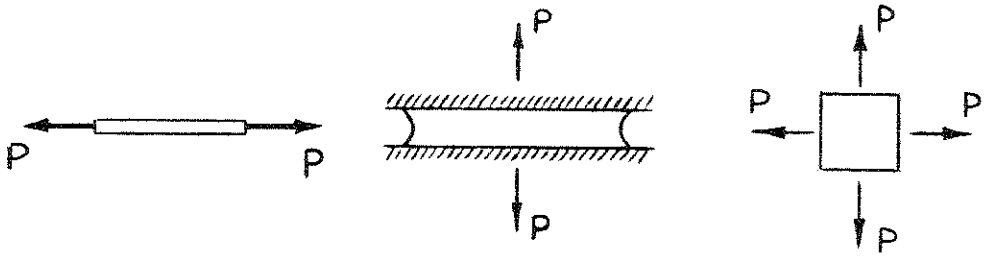

pure extension pure shear biaxial extension

Fig. 3.10

can only generate strain invariant states (as P increases from zero) which lie on the lines shown below in Figure 3.11.

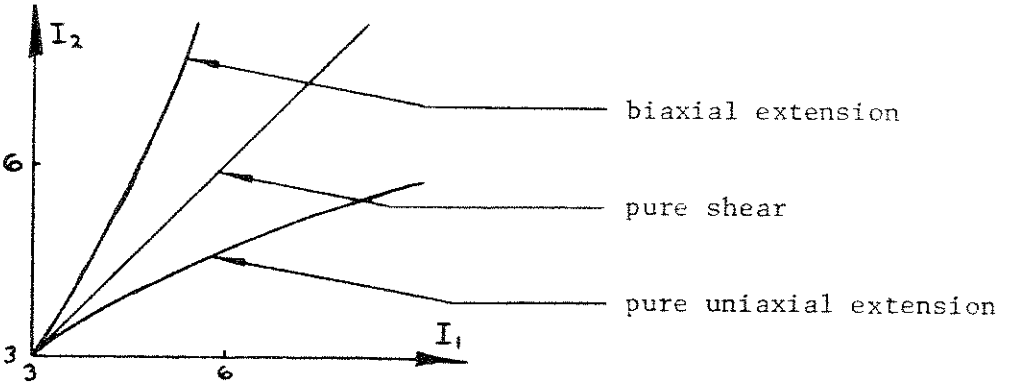

Fig. 3.11

Nonhomogeneous experiments designed with some forethought will have similar near one-dimensional distributions. For example, the specimen of Figure 3.12

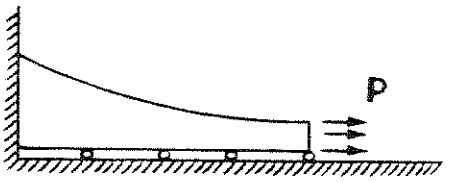

Fig. 3.12

will have a strain invariant distribution domain as in Figure 3.13,

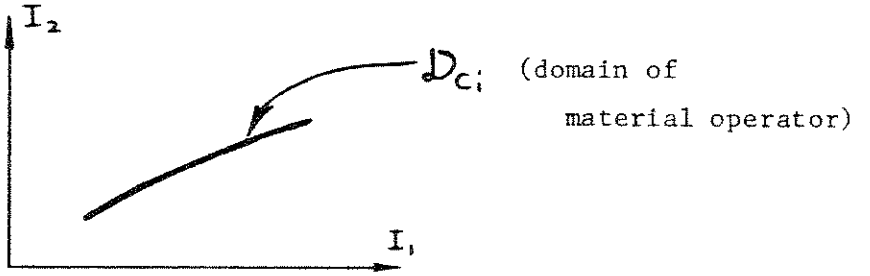

Fig. 3.13

which can be discretized by the one-dimensional elements shown below in Figure 3.14

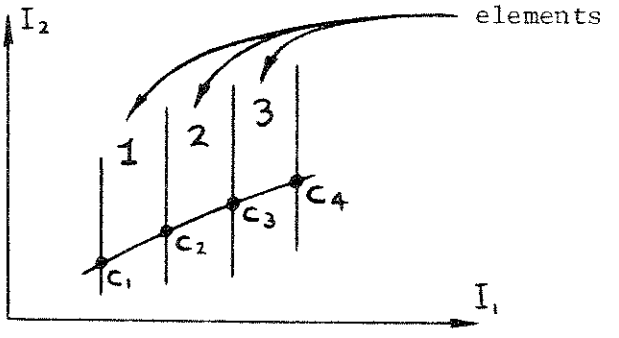

Fig. 3.14

Note that these elements define the material functions $C_i(I_1, I_2)$

over the entire (I_1, I_2) plane - should any intermediate step in the solution require a value of $C_i(I_1, I_2)$ for a point (I_1, I_2) not in the basically one-dimensional domain of C_i. These discretized material functions can be visualized isometrically as shown below in Figure 3.15.

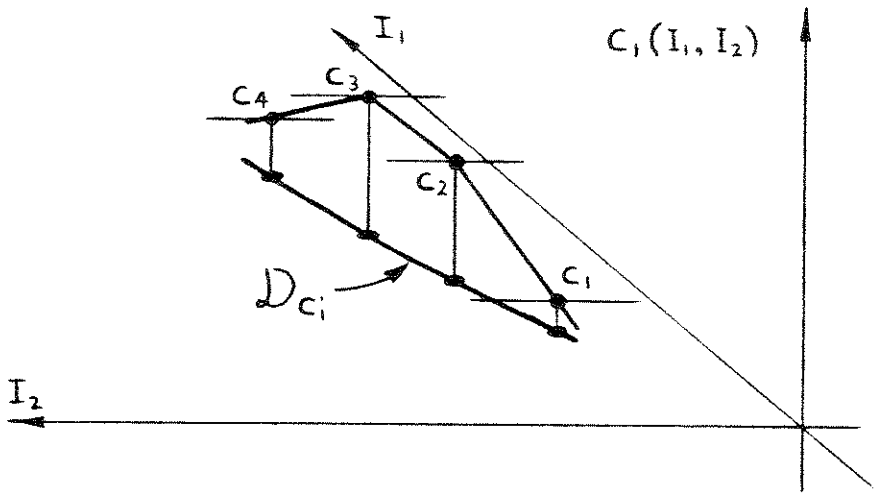

Fig. 3.15

The experiment of Appendix D is solved with the one-dimensional material discretization of Figure 3.14. Note how the domain of the material functions (Figure D.5) is ideally suited for one-dimensional material meshes.

Even experiments with very complicated nonhomogeneous strain states tend to have near lineal material operator domains. For example, a thin rubber sheet with a hole at its center is loaded as in Figure 3.16.

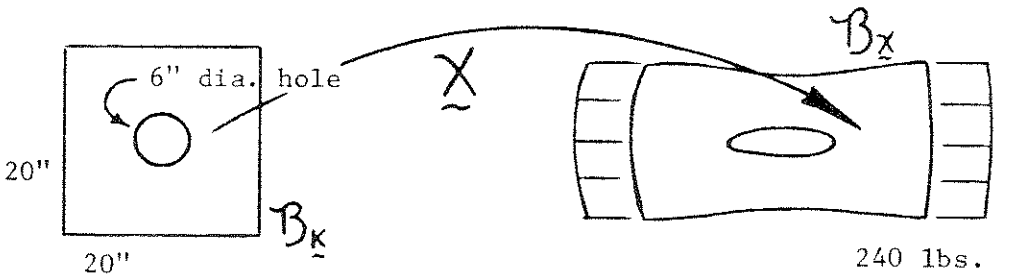

Fig. 3.16

Assume a Mooney-Rivlin material description with

$$\begin{aligned} C_1(I_1, I_2) &= 80 \text{ psi.} \\ C_2(I_1, I_2) &= 20 \text{ psi.} \end{aligned} \tag{3.24}$$

and adopt the geometric mesh shown in Figure 3.17. Analysis shows that the material operator has the domain indicated in Figure 3.18 - a virtually lineal (I_1, I_2) distribution. Other experiments with isotropic, incompressible elastic materials show this same phenomenon, making it very simple to effect a simple, stable material discretization. However, very little is known about the behavior of compressible or other more general materials; it may be necessary to discretize the material operator in several dimensions even in a relatively simple experimental situation. Refer to Chapter V for a discussion of material meshes for these more complicated materials.

The third discretization method - utilizing a finite element mesh defined directly over the domain of $C_i(I_1, I_2)$ - was found to be far superior to the other two methods. Excellent material identifications have been obtained using it - even with very poor input data in $\underset{\sim}{\delta}$. See Appendices B, C, and D for a summary of the results of various tests of this type of finite element material mesh. Note also that in Appendices A and B the same example is solved using both the second and third discretization methods and the relative merits of each solution compared.

Whichever system of material discretization is chosen, the continuous material functions $C_i(I_1, I_2)$ in the field equations of the inverse boundary value problem (2.4) must be expressed in

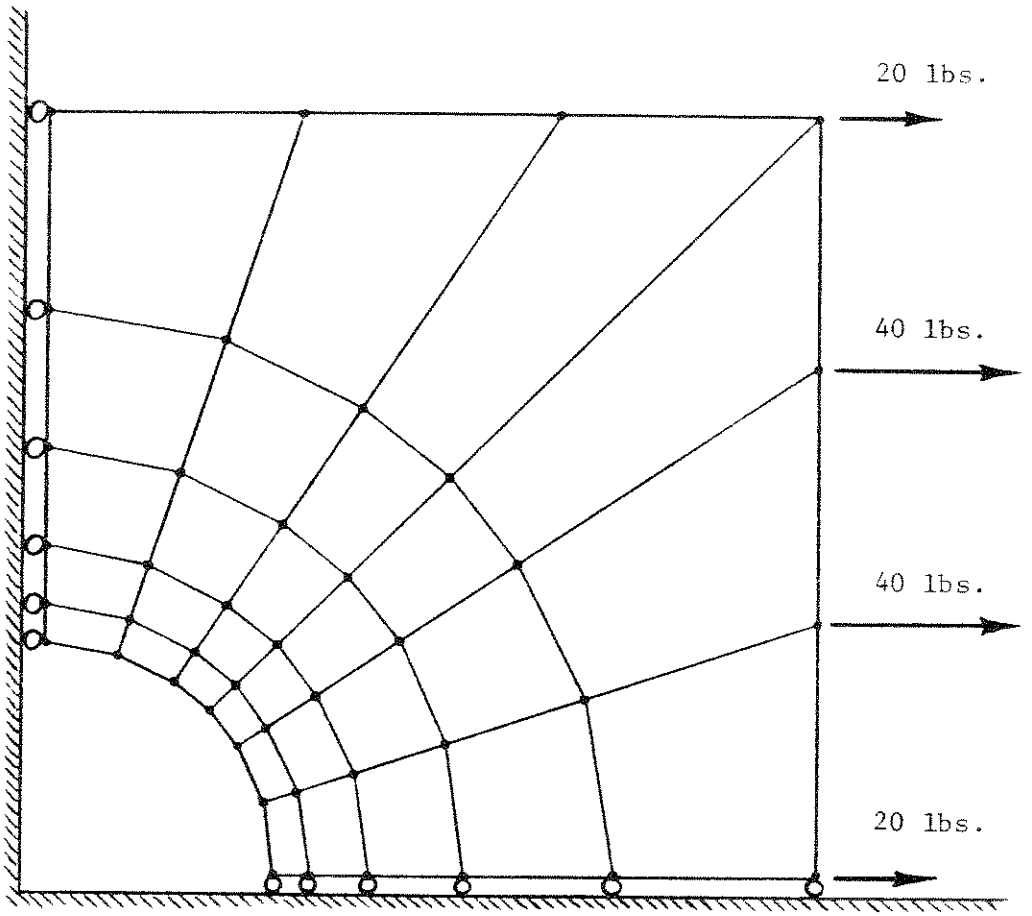

RUBBER SHEET WITH HOLE

30 ELEMENT GEOMETRIC MESH

Fig. 3.17

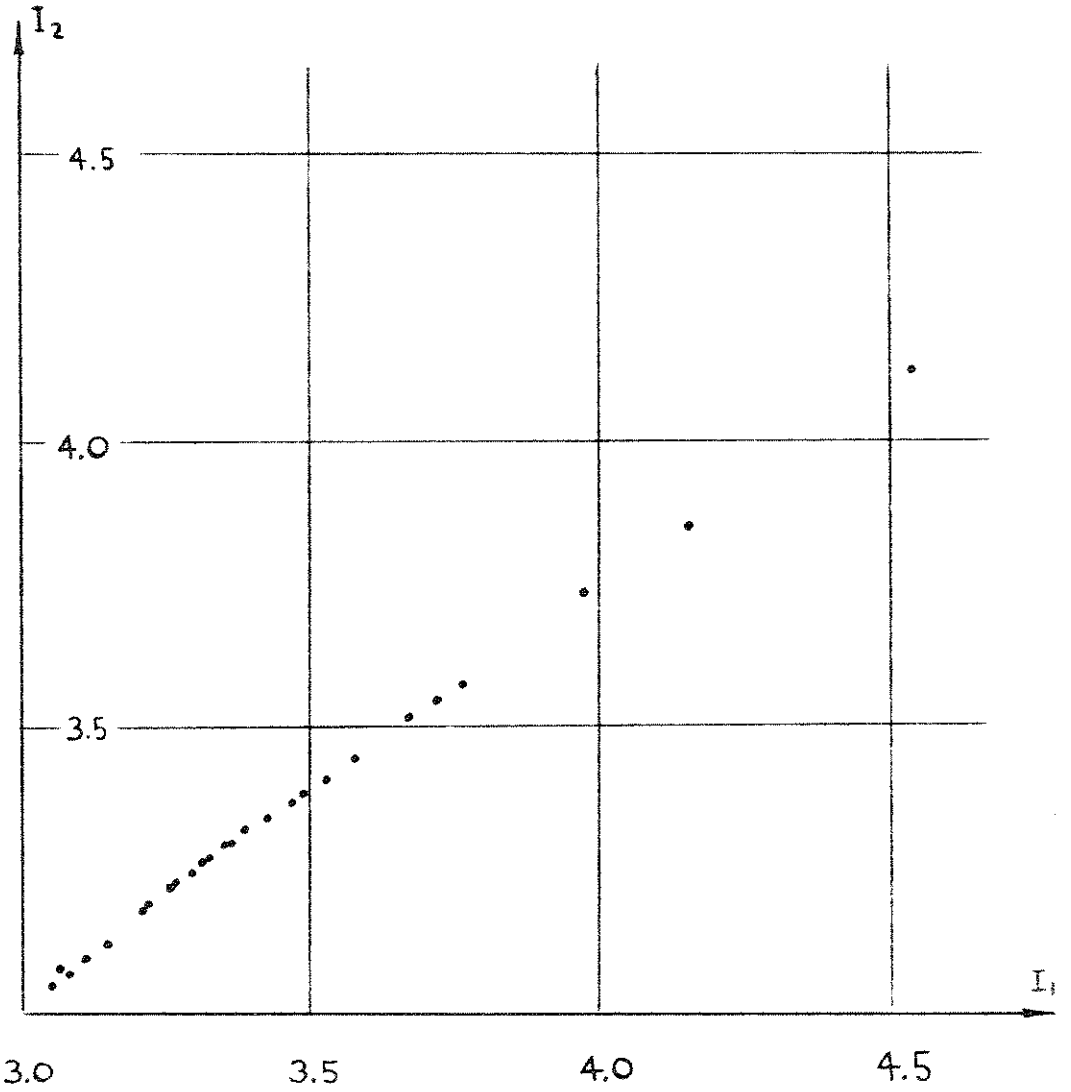

RUBBER SHEET WITH HOLE MODELLED BY 30 FINITE ELEMENTS

DOMAIN OF MATERIAL FUNCTIONS $C_i(I_1, I_2)$

Fig. 3.18

terms of the discrete material parameter vector $\underset{\sim}{c}$. This is done most simply by direct substitution of (3.20), (3.22), or (3.23) into the geometrically discretized field equations (3.8):

$$\underset{\sim}{f}(\underset{\sim}{u}, \underset{\sim}{\lambda}, \underset{\sim}{c}) = \underset{\sim}{P}. \tag{3.25}$$

If

$$\dim(\underset{\sim}{u}, \underset{\sim}{\lambda}) = n_u \tag{3.26a}$$

$$\dim \underset{\sim}{c} = n_m \tag{3.26b}$$

then (3.25) is a system of n_u algebraic equations in $n_u + n_m$ variables. Adding to (3.25) the mathematical description of the q experimental measurements (3.18), we obtain the system of nonlinear algebraic equations that fully defines the discretized inverse problem:

$$\begin{Bmatrix} \underset{\sim}{f}(\underset{\sim}{u}, \underset{\sim}{\lambda}, \underset{\sim}{c}) \\ \underset{\sim}{g}(\underset{\sim}{u}, \underset{\sim}{\lambda}) \end{Bmatrix} = \begin{Bmatrix} \underset{\sim}{P} \\ \underset{\sim}{\delta} \end{Bmatrix} \tag{3.27}$$

a global total of $n_u + q$ equations and $n_u + n_m$ independent variables. For the constant-strain finite element upon which (3.12-13) are based (and upon which all the test examples of this dissertation are based) expression (3.27) represents a global total of two force equilibrium equations for each node in the geometric mesh, one incompressibility constraint equation for each element, and an equation for each experimental measurement used as input.

The system of algebraic equations (3.27) is the discretized version of the continuous inverse boundary value problem (2.3-2.6).

Its solution $(\underset{\sim}{U}, \underset{\sim}{\lambda}, \underset{\sim}{C})$ is the discretized version of the continuous solution to (2.3-2.6), i. e., $\underset{\sim}{U}(x,y)$, $\lambda(x,y)$, $C_1(I_1,I_2)$, and $C_2(I_1,I_2)$. This discretized solution $(\underset{\sim}{U},\underset{\sim}{\lambda},\underset{\sim}{C})$ is physically determinate if the number of parameters in $\underset{\sim}{C}$ is equal to the number of experimental measurements; numerical solution techniques will be discussed in Section 3.6. The final identification of the material constitutive functions follows directly from interpolation between the elements of the discrete material solution $\underset{\sim}{C}$ using the appropriate finite element basis:

$$C_1(I_1,I_2) = \sum_{i=1}^{n_1} c_i \varphi_i(I_1,I_2) \tag{3.23a}$$

$$C_2(I_1,I_2) = \sum_{i=n_1+1}^{n_m} c_i \varphi_i(I_1,I_2). \tag{3.23b}$$

3.5 Interaction of the Three Levels of Discretization

Recall that three different levels of discretization were necessary to reduce the continuous inverse boundary value problem (2.3-2.6) to the algebraic system of equations

$$\begin{Bmatrix} \underset{\sim}{f}(\underset{\sim}{U},\underset{\sim}{\lambda},\underset{\sim}{C}) \\ \underset{\sim}{g}(\underset{\sim}{U},\underset{\sim}{\lambda}) \end{Bmatrix} = \begin{Bmatrix} \underset{\sim}{P} \\ \underset{\sim}{\delta} \end{Bmatrix}. \tag{3.27}$$

These include a geometric discretization of the physical body and the measures of deformation, boundary conditions and loading, a discretization of the description of the deformed shape of the loaded body, and a discretization of the material functions. Each of these levels of discretization requires approximation of some type; therefore, equations (3.27) contain discretization errors from each of these three sources. When solving the discrete

inverse problem, the experimenter should keep in mind the relative sizes of these sorts of errors for his particular discretization scheme. For example, it is useless to have an extremely fine material mesh if the geometric mesh is very coarse; it is also useless to have an extremely fine geometric mesh if the experimental measurements used as input can be determined only very approximately.

In the course of this research numerous material identification problems based on the techniques of Sections 3.2-3.4 were studied. It was found that the sensitivity and physical accuracy of the governing equations (3.27) are extremely dependent upon how the experimenter chooses to discretize. Let us examine the effects of each level of discretization upon the solution of (3.27).

1) Geometric discretization follows the usual practices of linear elasticity applications of the finite element method. As the number of elements increases the discretization error decreases, and in the limit the solution $(\underset{\sim}{U},\underset{\sim}{\lambda})$ coincides with the continuous solution $U_1(x,y)$, $U_2(x,y)$, and $\lambda(x,y)$. In practice it is best to keep the number of nodes as small as possible, since the computational effort to solve (3.27) is proportional to the cube of the number of equations. Yet the mesh should be fine enough that errors in $\underset{\sim}{U}$ will be small compared to errors in the input measurements $\underset{\sim}{\delta}$. It is best to design the experiment in such a way that the strain distribution $\underset{\sim}{\varepsilon}(x,y)$ varies smoothly and without abruptness throughout a specimen with a geometric shape easily representable by the finite elements to be used. The example in Appendix D was quite accurately discretized with

only 36 elements; more than that number will probably be unnecessary in similar experimental situations.

2) The discretized description of the deformed body follows an intuitively obvious procedure of taking a finite number of measurements at various places on the surface of the body. If only a few measurements are taken it is possible that the discretization will be too coarse to adequately describe the shape of the loaded body. Hence, the equations (3.27) may be too flexible; the kinematic solution $(\underset{\sim}{U}, \underset{\sim}{\lambda})$ may be very unlike the deformed shape of the experimental body - especially if there are large inconsistencies in the input to which the solution $(\underset{\sim}{U}, \underset{\sim}{\lambda}, \underset{\sim}{C})$ must adjust itself in order to satisfy equations (3.27). For example, the body and system of measurements below

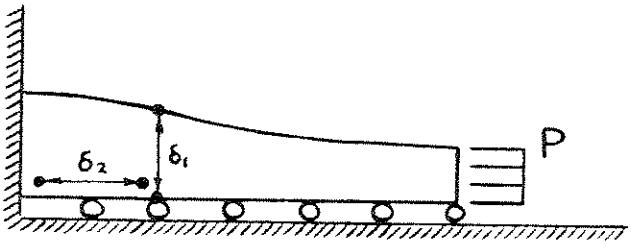

Fig. 3.19

leaves the loaded half of the body free to assume any shape it wishes (that satisfies force equilibrium and incompressibility constraints), thereby prejudicing the material identification in that part of the body. The locations of the input measurements must be chosen such that the general shape of the measured specimen is adequately defined.

The main difficulty with this level of discretization is that

the measurements will contain experimental errors, since they must be measured in the laboratory with instruments of limited accuracy. It is impossible to avoid introducing errors and inconsistencies into the set of equations

$$\underset{\sim}{g}(\underset{\sim}{u}, \underset{\sim}{\lambda}) = \underset{\sim}{\delta}. \tag{3.18}$$

The inverse boundary value problem is so incredibly sensitive by its very nature that measurement errors of even a fraction of a percent can cause equations (3.27) to be unstable and unsolvable. Therefore, it is extremely important to obtain good measurements and restrict their locations to places on the body where the inevitable experimental errors will do the least damage to the material identification. This problem is examined in detail in section 2 of Appendix B; the measurement system chosen there minimizes such instabilities. The best safeguard against poor results due to errors in input measurements is to have a large number of redundant measurements (every strain state represented by several elements in $\underset{\sim}{\delta}$) and use a least squares method to solve the indeterminate set of equations (3.27) which results when $\dim \underset{\sim}{\delta} > \dim \underset{\sim}{c}$. This procedure is developed in Chapter IV.

A thorough analysis of the method's stability when subjected to input errors is contained in section 2 of Appendix B (for direct solution of the discrete equations (3.27)) and in sections 1 and 3 of Appendix D (for a least squares solution of the discrete equations).

It is, of course, possible to simplify the algebra of equations (3.27) by measuring the displacement at every node in

the body and the extension ratio of every element, thus completely defining $(\underset{\sim}{U}, \underset{\sim}{\lambda})$ and simplifying the inverse boundary value problem to the set of equations

$$\underset{\sim}{f}_{EQ}(\underset{\sim}{C}) = \underset{\sim}{R} \tag{3.28}$$

which will be determinate if $\dim \underset{\sim}{f}_{EQ} = \dim \underset{\sim}{C}$ and indeterminate if $\dim \underset{\sim}{f}_{EQ} > \dim \underset{\sim}{C}$. In the determinate case (3.28) is a set of linear algebraic equations with the elements of $\underset{\sim}{C}$ as independent variables; hence, the solution $\underset{\sim}{C}$ is directly obtainable by any standard linear equation solving algorithm. Note that in effect this approach applies discretization directly to the inverse problem of Section 2.2, thus avoiding the inverse boundary value problem.

But this method has its drawback: in any realistic experimental situation the measured $\underset{\sim}{U}$ and $\underset{\sim}{\lambda}$ contain unavoidable experimental errors of considerable size compared to the size of the elements; large strain errors are introduced into each element and therefore into the equilibrium equations

$$\underset{\sim}{f}_{EQ}(\underset{\sim}{C}) = \underset{\sim}{R} \, , \tag{3.28}$$

making them unstable and the resulting solution $\underset{\sim}{C}$ worthless. Even least squares and other noise suppressing methods have been unsuccessful in smoothing out the inconsistencies that inevitably occur in (3.28). For an application of (3.2ó) to material identification the reader is referred to [23].

Thus, the system of equations (3.28) lacks the great advantage of the newly developed formulation (3.27) - that most elements

of $(\underset{\sim}{U}, \underset{\sim}{\lambda})$ are unspecified in the input data and therefore free to adjust themselves a bit so that a solution to the set of equations is possible. No strain errors are irrevocably fixed in any element; in the method of equations (3.28) large strain errors are irrevocably and directly fixed in each element. Also, the fact that an experimental measurement is defined over a length spanning several elements (instead of over just one element as in equations (3.28)) means that the input errors will give rise to smaller strain errors and inconsistencies in each element, since the magnitude of $\underset{\sim}{\delta}$ will be larger (and hence the relative sizes of the rounding errors of measuring the experiment will be smaller) and the intermediate nodes within the measured area can wander a bit to smooth out inconsistencies in $\underset{\sim}{\delta}$.

3) Material discretization offers remarkably few practical difficulties. It is usually possible to represent the functions $C_i(I_1, I_2)$ very accurately with very few degrees of freedom and the errors due to this level of discretization are minimal. However, when the material mesh is too coarse or inappropriately chosen, it may be impossible to converge to a good solution, as the examples in section 3 of Appendix C show quite clearly. A mesh that is very fine will not have discretization errors but could encourage the instabilities inherent in a system of approximate input measurements, as is discussed in section 3 of Appendix C. Also, if a part of the material mesh lies in an area of the (I_1, I_2) domain wherein none of the measurements of $\underset{\sim}{\delta}$ lie, those elements of $\underset{\sim}{C}$ will be indeterminate and undermine the whole solution $(\underset{\sim}{U}, \underset{\sim}{\lambda}, \underset{\sim}{C})$ of equation (3.27). For example, if the crosshatched

area in Figure 3.20 is the (I_1, I_2) domain of a certain experiment, and the material mesh is as shown, the variable C_4 is indeter-

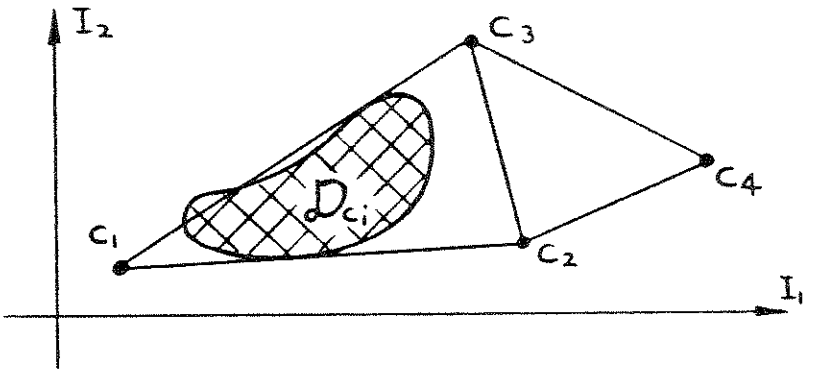

Fig. 3.20

minate. If the (I_1, I_2) domain of the tension tests in the appendices is the line shown below in Figure 3.21

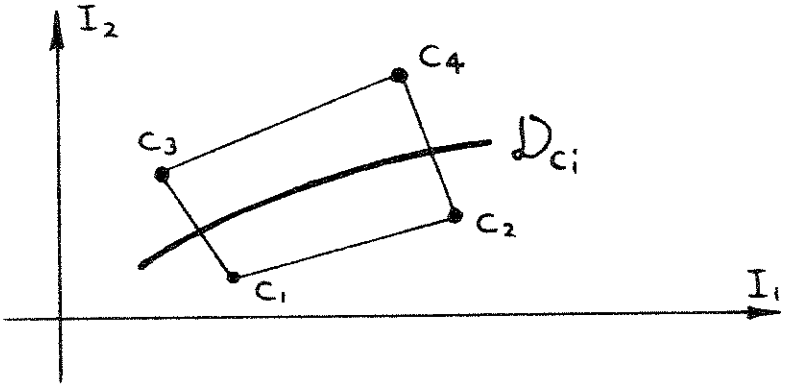

Fig. 3.21

then the 4 degree-of-freedom mesh shown is indeterminate, since the element is free to pivot around the domain D_{C_i}. A one-dimensional discretization must be chosen instead.

The material mesh must be chosen with the distribution of experimental measurements in mind in order to get a useful, stable material identification. See section 2 of Appendix B for a detailed discussion and several examples of this intimate relationship

between the material mesh and the locations of the experimental measurements.

3.6 Solution of Nonlinear Algebraic Equations

Discretization of the material identification inverse boundary value problem leads to the system of nonlinear algebraic equations (3.27). Solving such a system is a basic problem of numerical analysis; numerous methods are available [25,26]. In this section we shall develop and apply the method which seems most suitable for this type of problem - the Newton-Raphson method.

To illustrate the basic ideas behind the method, let us examine the single nonlinear algebraic equation with the single scalar independent variable X:

$$f(X) = 0 \tag{3.29}$$

If an initial guess X_0 is proposed for the solution X, increasingly better approximations to the solution can be obtained by use of the Newton-Raphson algorithm

$$X_{i+1} = X_i - \frac{f(X_i)}{\partial_X f(X_i)} \qquad i = 0,1,2,\ldots \tag{3.30a}$$

or equivalently,

$$X_{i+1} = X_i + \left[\partial_X f(X_i)\right]^{-1}\left(-f(X_i)\right) \qquad i = 0,1,2,\ldots \tag{3.30b}$$

This process can be represented graphically as in Figure 3.22. Algorithm (3.30) brings about convergence to the solution X by the use of the tangents of f. The tangents can be calculated analytically or by a numerical method. Finite differencing is a

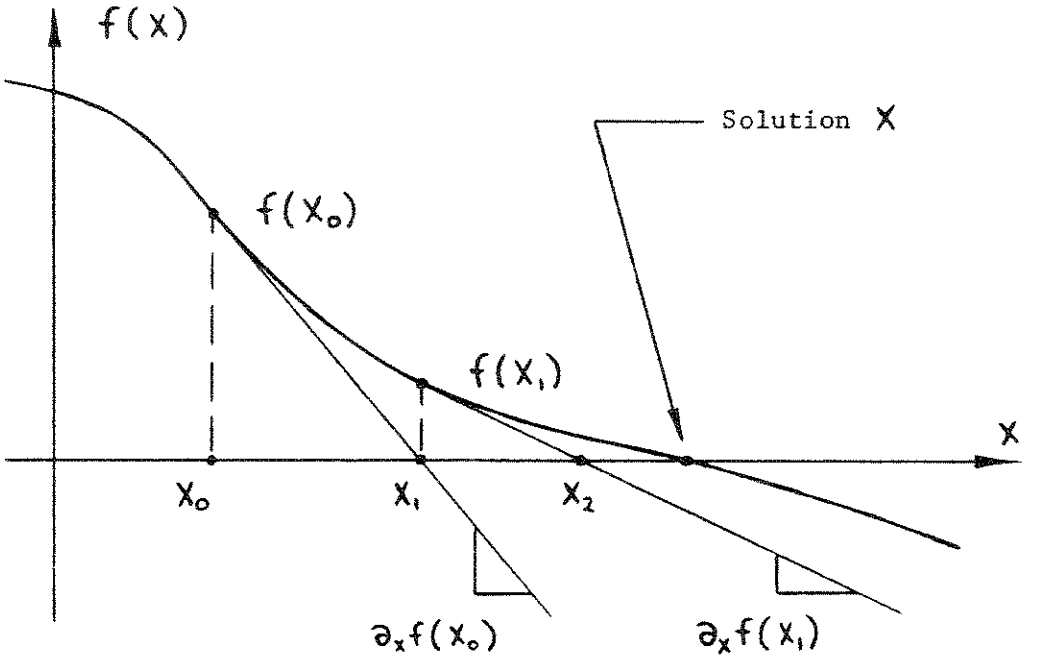

Fig. 3.22

particularly straightforward method and finds an approximation to the gradient $\partial_x f$ by the simple operation

$$\partial_x f(x) \doteq \frac{f(x+\Delta x) - f(x)}{\Delta x} \tag{3.31}$$

where Δx is very small. The procedure indicated by (3.31) can be visualized as in Figure 3.23.

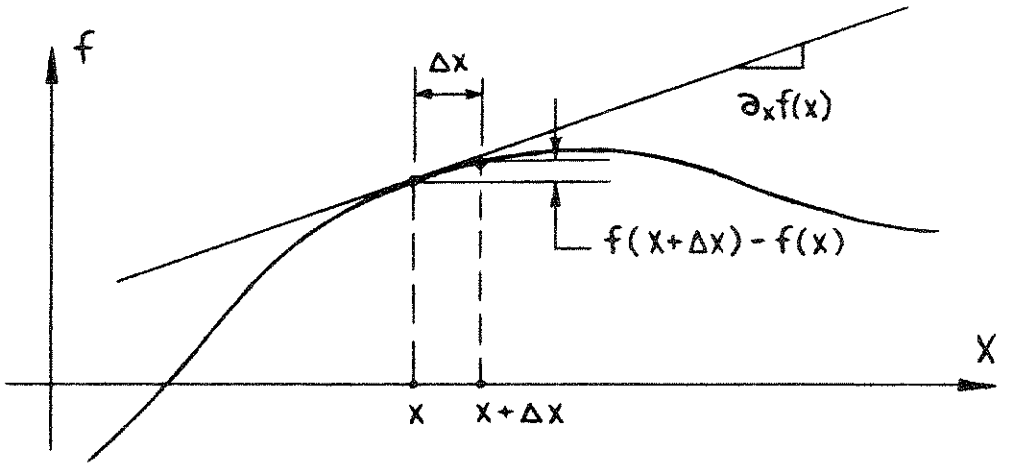

Fig. 3.23

A system of nonlinear equations in the n independent variables $\underset{\sim}{X}$, denoted by

$$\underset{\sim}{f}(\underset{\sim}{X}) = \underset{\sim}{0}, \tag{3.32}$$

can be solved (if a solution exists) by the n-dimensional analogue to (3.30)

$$\underset{\sim}{X}_{i+1} = \underset{\sim}{X}_i + \left[\nabla_{\underset{\sim}{X}} \underset{\sim}{f}(\underset{\sim}{X}_i)\right]^{-1}\left(-\underset{\sim}{f}(\underset{\sim}{X}_i)\right), \tag{3.33}$$

an iterative process where $i = 0,1,2,\ldots$. This version of the Newton-Raphson algorithm converges to the solution $\underset{\sim}{X}$ by following the various n-dimensional tangent hyperplanes defined in $\nabla_{\underset{\sim}{X}} \underset{\sim}{f}$ to the location $\underset{\sim}{X}$ which satisfies (3.32). The gradient $\nabla_{\underset{\sim}{X}} \underset{\sim}{f}$ at any point $\underset{\sim}{X}$ can be very simply approximated by the finite difference relation

$$\left[\nabla_{\underset{\sim}{X}} \underset{\sim}{f}(\underset{\sim}{X})\right]_{jk} \doteq \frac{f_j(\underset{\sim}{X} + \Delta X_k) - f_j(\underset{\sim}{X})}{\Delta X_k} \tag{3.34}$$

where $\nabla_{\underset{\sim}{X}} \underset{\sim}{f}(\underset{\sim}{X})$ is an $n \times n$ gradient matrix.

The Newton-Raphson algorithm (3.33) can be directly applied to the various systems of equations resulting from discretization of boundary value problems. For example, geometric discretization (Section 3.2) of the forward-direction plane stress boundary value problem (1.75-1.78) leads to the discrete set of equations (3.7),

$$\begin{Bmatrix} \underset{\sim}{f}_{EQ}(\underset{\sim}{U}, \underset{\sim}{\lambda}) \\ \underset{\sim}{f}_{INC}(\underset{\sim}{U}, \underset{\sim}{\lambda}) \end{Bmatrix} = \begin{Bmatrix} \underset{\sim}{R} \\ \underset{\sim}{1} \end{Bmatrix}. \tag{3.7}$$

The appropriate form of the Newton-Raphson formula (3.33) which

solves these equations is

$$\begin{Bmatrix} \underset{\sim}{\upsilon} \\ \underset{\sim}{\lambda} \end{Bmatrix}_{i+1} = \begin{Bmatrix} \underset{\sim}{\upsilon} \\ \underset{\sim}{\lambda} \end{Bmatrix}_{i} + \begin{bmatrix} \nabla_{\underset{\sim}{\upsilon}} \underset{\sim}{f}_{EQ} & \nabla_{\underset{\sim}{\lambda}} \underset{\sim}{f}_{EQ} \\ \nabla_{\underset{\sim}{\upsilon}} \underset{\sim}{f}_{INC} & \nabla_{\underset{\sim}{\lambda}} \underset{\sim}{f}_{INC} \end{bmatrix}_{i}^{-1} \begin{Bmatrix} \underset{\sim}{R} - \underset{\sim}{f}_{EQ}(\underset{\sim}{\upsilon}_i, \underset{\sim}{\lambda}_i) \\ \underset{\sim}{1} - \underset{\sim}{f}_{INC}(\underset{\sim}{\upsilon}_i, \underset{\sim}{\lambda}_i) \end{Bmatrix}. \tag{3.35}$$

The gradient is approximated very simply by finite difference operators:

$$\left[\nabla_{\underset{\sim}{\upsilon}} \underset{\sim}{f}_{EQ}(\underset{\sim}{\upsilon}, \underset{\sim}{\lambda})\right]_{jk} \doteq \frac{f_{EQ_j}(\underset{\sim}{\upsilon} + \Delta\upsilon_k, \underset{\sim}{\lambda}) - f_{EQ_j}(\underset{\sim}{\upsilon}, \underset{\sim}{\lambda})}{\Delta\upsilon_k} \tag{3.36a}$$

$$\left[\nabla_{\underset{\sim}{\lambda}} \underset{\sim}{f}_{EQ}(\underset{\sim}{\upsilon}, \underset{\sim}{\lambda})\right]_{jk} \doteq \frac{f_{EQ_j}(\underset{\sim}{\upsilon}, \underset{\sim}{\lambda} + \Delta\lambda_k) - f_{EQ_j}(\underset{\sim}{\upsilon}, \underset{\sim}{\lambda})}{\Delta\lambda_k} \tag{3.36b}$$

$$\left[\nabla_{\underset{\sim}{\upsilon}} \underset{\sim}{f}_{INC}(\underset{\sim}{\upsilon}, \underset{\sim}{\lambda})\right]_{jk} \doteq \frac{f_{INC_j}(\underset{\sim}{\upsilon} + \Delta\upsilon_k, \underset{\sim}{\lambda}) - f_{INC_j}(\underset{\sim}{\upsilon}, \underset{\sim}{\lambda})}{\Delta\upsilon_k} \tag{3.36c}$$

$$\left[\nabla_{\underset{\sim}{\lambda}} \underset{\sim}{f}_{INC}(\underset{\sim}{\upsilon}, \underset{\sim}{\lambda})\right]_{jk} \doteq \frac{f_{INC_j}(\underset{\sim}{\upsilon}, \underset{\sim}{\lambda} + \Delta\lambda_k) - f_{INC_j}(\underset{\sim}{\upsilon}, \underset{\sim}{\lambda})}{\Delta\lambda_k}. \tag{3.36d}$$

If the gradient is calculated with the aid of a computer, $\Delta\upsilon_k$ and $\Delta\lambda_k$ can be made extremely small; hence, actual application of (3.36) results in a virtually exact determination of the gradient at $(\underset{\sim}{\upsilon}, \underset{\sim}{\lambda})$.

The gradient in (3.35) is the "tangent stiffness" of the structural system modelled by (3.7) at the deformed configuration $(\underset{\sim}{\upsilon}, \underset{\sim}{\lambda})$. If the tangent stiffness of a structural system is derived directly from a variational principle, it will be a symmetric, positive-definite matrix. However, (3.7) is not based directly on the incompressible elastic variational functional (1.68d), since in the derivation of the plane stress boundary value problem (1.75-1.78) the hydrostatic pressure was made a

dependent field variable by merging the plane stress equation (1.69) into the other field equations. Therefore, the gradient

$$\begin{bmatrix} \nabla_{\underset{\sim}{u}} \underset{\sim}{f}_{EQ} & \nabla_{\underset{\sim}{\lambda}} \underset{\sim}{f}_{EQ} \\ \nabla_{\underset{\sim}{u}} \underset{\sim}{f}_{INC} & \nabla_{\underset{\sim}{\lambda}} f_{INC} \end{bmatrix} \tag{3.37}$$

is unsymmetric, and the inversion specified in (3.35) must be performed on an unsymmetric matrix.

It is possible to reformulate the plane stress boundary value problem in a way that preserves the symmetry of the tangent stiffness. Let both extension ratio $\lambda(X,Y)$ and hydrostatic pressure $h(X,Y)$ be retained as independent field variables, and establish the functional

$$\Phi(\underset{\sim}{u},\lambda,h) = \int_{\mathcal{B}_K} \hat{W}\,dV - \int_{\mathcal{B}_K} (\det \underset{\sim}{C} - 1)\,h\,dV$$
$$- \int_{\mathcal{B}_K} \rho_K \underset{\sim}{b}\cdot\underset{\sim}{u}\,dV - \int_{\partial\mathcal{B}_K^{\sigma}} \hat{\underset{\sim}{t}}_K \cdot \underset{\sim}{u}\,dS - \int_{\mathcal{B}_K} P_{33}\lambda\,dV. \tag{3.38}$$

Note that this functional includes the incompressibility constraint condition

$$\det \underset{\sim}{C}(X,Y) = 1 \qquad \forall (X,Y) \in \mathcal{B}_K \tag{3.39}$$

and the plane stress condition

$$P_{33}(\underset{\sim}{X}) = 0 \qquad \forall \underset{\sim}{X} \in \mathcal{B}_K. \tag{3.40}$$

Finite element geometric discretization (as in Section 3.2) and differentiation with respect to each discrete nodal variable produce the algebraic equations that describe the boundary value

problem,

$$\nabla_{\underset{\sim}{u}}\Phi(\underset{\sim}{u},\underset{\sim}{\lambda},\underset{\sim}{h}) = \underset{\sim}{f}_{EQ}(\underset{\sim}{u},\underset{\sim}{\lambda},\underset{\sim}{h}) - \underset{\sim}{R} = \underset{\sim}{0} \qquad (3.41a)$$

$$\nabla_{\underset{\sim}{\lambda}}\Phi(\underset{\sim}{u},\underset{\sim}{\lambda},\underset{\sim}{h}) = \underset{\sim}{f}_{PLST}(\underset{\sim}{u},\underset{\sim}{\lambda},\underset{\sim}{h}) = \underset{\sim}{0} \qquad (3.41b)$$

$$\nabla_{\underset{\sim}{h}}\Phi(\underset{\sim}{u},\underset{\sim}{\lambda},\underset{\sim}{h}) = \underset{\sim}{f}_{INC}(\underset{\sim}{u},\underset{\sim}{\lambda}) - \underset{\sim}{1} = \underset{\sim}{0}. \qquad (3.41c)$$

The gradient of this system of equations is related to the discretized variational functional $\Phi(\underset{\sim}{u},\underset{\sim}{\lambda},\underset{\sim}{h})$ by

$$\begin{bmatrix} \nabla_{\underset{\sim}{u}}\underset{\sim}{f}_{EQ} & \nabla_{\underset{\sim}{\lambda}}\underset{\sim}{f}_{EQ} & \nabla_{\underset{\sim}{h}}\underset{\sim}{f}_{EQ} \\ \nabla_{\underset{\sim}{u}}\underset{\sim}{f}_{PLST} & \nabla_{\underset{\sim}{\lambda}}\underset{\sim}{f}_{PLST} & \nabla_{\underset{\sim}{h}}\underset{\sim}{f}_{PLST} \\ \nabla_{\underset{\sim}{u}}\underset{\sim}{f}_{INC} & \nabla_{\underset{\sim}{\lambda}}\underset{\sim}{f}_{INC} & \nabla_{\underset{\sim}{h}}\underset{\sim}{f}_{INC} \end{bmatrix} = \begin{bmatrix} \nabla_{\underset{\sim}{u}}\nabla_{\underset{\sim}{u}}\Phi & \nabla_{\underset{\sim}{\lambda}}\nabla_{\underset{\sim}{u}}\Phi & \nabla_{\underset{\sim}{h}}\nabla_{\underset{\sim}{u}}\Phi \\ \nabla_{\underset{\sim}{u}}\nabla_{\underset{\sim}{\lambda}}\Phi & \nabla_{\underset{\sim}{\lambda}}\nabla_{\underset{\sim}{\lambda}}\Phi & \nabla_{\underset{\sim}{h}}\nabla_{\underset{\sim}{\lambda}}\Phi \\ \nabla_{\underset{\sim}{u}}\nabla_{\underset{\sim}{h}}\Phi & \nabla_{\underset{\sim}{\lambda}}\nabla_{\underset{\sim}{h}}\Phi & \nabla_{\underset{\sim}{h}}\nabla_{\underset{\sim}{h}}\Phi \end{bmatrix} \qquad (3.42)$$

and is obviously symmetric.

The set of equations that defines the discretized version of the plane stress inverse boundary value problem (2.3-2.6) is

$$\begin{Bmatrix} \underset{\sim}{f}_{EQ}(\underset{\sim}{u},\underset{\sim}{\lambda},\underset{\sim}{c}) \\ \underset{\sim}{f}_{INC}(\underset{\sim}{u},\underset{\sim}{\lambda}) \\ \underset{\sim}{g}(\underset{\sim}{u},\underset{\sim}{\lambda}) \end{Bmatrix} = \begin{Bmatrix} \underset{\sim}{R} \\ \underset{\sim}{1} \\ \underset{\sim}{\delta} \end{Bmatrix}, \qquad (3.43)$$

as derived in Section 3.4. The appropriate Newton-Raphson solution algorithm is

$$\begin{Bmatrix} \underset{\sim}{u} \\ \underset{\sim}{\lambda} \\ \underset{\sim}{c} \end{Bmatrix}_{i+1} = \begin{Bmatrix} \underset{\sim}{u} \\ \underset{\sim}{\lambda} \\ \underset{\sim}{c} \end{Bmatrix}_{i} + \begin{bmatrix} \nabla_{\underset{\sim}{u}}\underset{\sim}{f}_{EQ} & \nabla_{\underset{\sim}{\lambda}}\underset{\sim}{f}_{EQ} & \nabla_{\underset{\sim}{c}}\underset{\sim}{f}_{EQ} \\ \nabla_{\underset{\sim}{u}}\underset{\sim}{f}_{INC} & \nabla_{\underset{\sim}{\lambda}}\underset{\sim}{f}_{INC} & \underset{\sim}{0} \\ \nabla_{\underset{\sim}{u}}\underset{\sim}{g} & \nabla_{\underset{\sim}{\lambda}}\underset{\sim}{g} & \underset{\sim}{0} \end{bmatrix}_{i}^{-1} \begin{Bmatrix} \underset{\sim}{R} - \underset{\sim}{f}_{EQ}(\underset{\sim}{u}_i,\underset{\sim}{\lambda}_i,\underset{\sim}{c}_i) \\ \underset{\sim}{1} - \underset{\sim}{f}_{INC}(\underset{\sim}{u}_i,\underset{\sim}{\lambda}_i) \\ \underset{\sim}{\delta} - \underset{\sim}{g}(\underset{\sim}{u}_i,\underset{\sim}{\lambda}_i) \end{Bmatrix}, \qquad (3.44)$$

where the elements of the gradient are approximated by finite differencing as in (3.36). For example,

$$\left[\nabla_{\underset{\sim}{C}} \underset{\sim}{f}_{EQ}(\underset{\sim}{U},\underset{\sim}{\lambda},\underset{\sim}{C})\right]_{jk} \doteq \frac{f_{eqj}(\underset{\sim}{U},\underset{\sim}{\lambda},\underset{\sim}{C}+\Delta C_k)-f_{eqj}(\underset{\sim}{U},\underset{\sim}{\lambda},\underset{\sim}{C})}{\Delta C_k}. \quad (3.45)$$

Note that each iteration of the Newton-Raphson method involves solving the system of linear algebraic equations (3.44). Gauss elimination [25] or any other standard method of solving a general unsymmetric set of equations is suitable. If the forward-direction boundary value problem equations (3.35) can be expressed in terms of a symmetric gradient, a time-saving symmetric equation-solving algorithm could be used. However, the gradient (3.44) of the inverse problem is always unsymmetric - even if the tangent stiffness is symmetric.

To start the Newton-Raphson iteration some initial guess for the solution, $(\underset{\sim}{U}_o, \underset{\sim}{\lambda}_o, \underset{\sim}{C}_o)$, is necessary. The most consistent method of choosing this starting value is to estimate $C_1(I_1, I_2)$ and $C_2(I_1, I_2)$ - preferably on the basis of some simple, crude experiment, such as the uniaxial tension test discussed in Section 2.3. Then these approximate material functions are used to solve the forward-direction boundary value problem (3.8) in order to obtain $\underset{\sim}{U}_o$ and $\underset{\sim}{\lambda}_o$. Expressing the estimated $C_i(I_1, I_2)$ in terms of the finite element material coordinate functions determines $\underset{\sim}{C}_o$. Some criterion based on a norm

$$\|(\underset{\sim}{C}_{i+1} - \underset{\sim}{C}_i)\|$$

could be used to stop the iteration when convergence occurs.

A computer program utilizing this method of solving the inverse boundary value problem equations (3.43) was developed and all the material identification examples in Appendices A through D are solved by means of it. Note that very rapid convergence occurs in all but the most poorly designed problems - even if a very rough guess for $(\underset{\sim}{U}_o, \underset{\sim}{\lambda}_o, \underset{\sim}{C}_o)$ is used to start the iteration process. If convergence problems arise, the cause is usually that the governing equations (3.43) have no solution, rather than difficulties in applying the Newton-Raphson algorithm (3.44).

Nonlinear equations present a host of problems not encountered with linear equations. The existence and uniqueness of a solution is not assured - even with a "determinate" system of n equations in n unknowns. That is, a general system of nonlinear equations

$$\underset{\sim}{f}(\underset{\sim}{X}) = \underset{\sim}{0} \tag{3.32}$$

can have no solution, a unique solution, or many solutions. However, the equations

$$\begin{Bmatrix} \underset{\sim}{f}(\underset{\sim}{U}, \underset{\sim}{\lambda}, \underset{\sim}{C}) \\ \underset{\sim}{g}(\underset{\sim}{U}, \underset{\sim}{\lambda}) \end{Bmatrix} = \begin{Bmatrix} \underset{\sim}{P} \\ \underset{\sim}{\delta} \end{Bmatrix} \tag{3.27}$$

will always have a physically meaningful solution (if they contain no discretization or modelling errors) since they are based on a real physical situation which obviously has a solution $\underset{\sim}{U}(\underset{\sim}{X})$, $\lambda(\underset{\sim}{X})$ and $C_i(I_1, I_2)$. However, any error at all in any part of the formulation of the equations can introduce enough inconsistencies that no value of $(\underset{\sim}{U}, \underset{\sim}{\lambda}, \underset{\sim}{C})$ will satisfy equations

(3.27); hence, the Newton-Raphson iteration process will diverge. This situation is encountered very frequently (see Appendices A and B) and is one of the reasons the least squares approach of Chapter IV is developed, since it is capable of finding a "best" solution when no exact solution exists.

Another difficulty is that often more than one solution to equations (3.27) exist. If the initial guess for $(\underset{\sim}{U}, \underset{\sim}{\lambda}, \underset{\sim}{\zeta})$ is too far from the physically meaningful solution, the Newton-Raphson algorithm may converge to some other value $(\underset{\sim}{U}, \underset{\sim}{\lambda}, \underset{\sim}{\zeta})$ that satisfies the algebraic equations but is physically meaningless. However, this phenomenon has not been encountered in the examples tested in the appendices - even though very crude guesses for the material functions were often used to start the iterative process. Examples so poorly discretized that no physically meaningful solution existed that could solve (3.27) responded to identification attempts either by diverging or by converging to a set $(\underset{\sim}{U}, \underset{\sim}{\lambda}, \underset{\sim}{\zeta})$ that solves the equations but is unrelated to the experiment.

IV. IDENTIFICATION BY THE LEAST SQUARES TECHNIQUE

4.1 Introduction

The material identification algorithms studied in the previous chapters are not suitable for use in real experimental situations. All involve a determinate system of equations in which the dimension of the material discretization is the same as the number of observations on the specimen. If there are any experimental errors in the input measurements poor identification or divergence usually results. The examples in Appendix B point out this shortcoming very clearly. It is the extreme sensitivity of the inverse boundary value problem of nonlinear elasticity that causes such instability in the algebraic equations resulting from discretization, rather than any instabilities inherent in the choice of a finite element approach.

Therefore, in this chapter we shall develop methods of describing and solving the inverse problem which will be stable for any physically reasonable set of experimental measurements.

Let the vector of exact errorless measured displacements be denoted by $\underset{\sim}{\delta}$ and the vector of actually measured displacements be denoted by $\underset{\sim}{\delta}^*$. The "noise" in $\underset{\sim}{\delta}^*$ causes the corresponding solution $(\underset{\sim}{u}, \underset{\sim}{\lambda}, \underset{\sim}{c})^*$ of the system of equations

$$\begin{Bmatrix} \underset{\sim}{f}(\underset{\sim}{u}, \underset{\sim}{\lambda}, \underset{\sim}{c}) \\ g(\underset{\sim}{u}, \underset{\sim}{\lambda}) \end{Bmatrix} = \begin{Bmatrix} \underset{\sim}{P} \\ \underset{\sim}{\delta}^* \end{Bmatrix} \tag{4.1}$$

to differ from the solution $(\underset{\sim}{u}, \underset{\sim}{\lambda}, \underset{\sim}{c})$ of the system of equations defined by the exact $\underset{\sim}{\delta}$. Since, as already mentioned

earlier in this section, the system of equations (4.1) is extremely sensitive, even very small amounts of noise in $\underset{\sim}{\delta}^*$ will cause a very poor solution $(\underset{\sim}{u}, \underset{\sim}{\lambda}, \underset{\sim}{c})^*$ if (4.1) is solved directly. To effect a solution closer to the true solution $(\underset{\sim}{u}, \underset{\sim}{\lambda}, \underset{\sim}{c})$ a method must be developed to suppress the noise in the input data $\underset{\sim}{\delta}^*$. This is a well-known basic problem of signal processing; numerous methods are available. In this chapter we shall develop one of the simpler methods - the least squares method.

The basic idea of the least squares method is that $\dim \underset{\sim}{\delta}^*$ is made very large, so that the system of equations (4.1) is over-determined. Then the solution $(\underset{\sim}{u}, \underset{\sim}{\lambda}, \underset{\sim}{c})$ which most closely satisfies the indeterminate version of (4.1) is sought.

4.2 Derivation of Least Squares Method

The equations considered in the previous chapters,

$$\begin{Bmatrix} \underset{\sim}{f}(\underset{\sim}{u}, \underset{\sim}{\lambda}, \underset{\sim}{c}) \\ \underset{\sim}{g}(\underset{\sim}{u}, \underset{\sim}{\lambda}) \end{Bmatrix} = \begin{Bmatrix} \underset{\sim}{P} \\ \underset{\sim}{\delta} \end{Bmatrix}, \tag{4.2}$$

are a determinate system of equations, with $\dim \underset{\sim}{c}$ equal to $\dim \underset{\sim}{\delta}$. If more measurements are added to the system without increasing the complexity of the material discretization, $\dim \underset{\sim}{c}$ becomes less than $\dim \underset{\sim}{\delta}$ and the system of equations (4.2) is indeterminate. These equations cannot be solved exactly, but a "best" solution that most nearly satisfies the system of equations can be determined through the well-known least squares technique. This approach finds the combination of independent variables that minimizes the error norm of the system; that is, it finds the

value of $(\underset{\sim}{\upsilon}, \underset{\sim}{\lambda}, \underset{\sim}{\varsigma})$ such that

$$\|(\underset{\sim}{f}(\underset{\sim}{\upsilon},\underset{\sim}{\lambda},\underset{\sim}{\varsigma}) - \underset{\sim}{P})\| + \|(\underset{\sim}{g}(\underset{\sim}{\upsilon},\underset{\sim}{\lambda}) - \underset{\sim}{\delta})\| = \min. \tag{4.3}$$

The norm referred to here is the L_2-norm defined by

$$\| \underset{\sim}{X} \| = \sqrt{(X_1^2 + X_2^2 + \ldots + X_n^2)} \, . \tag{4.4}$$

Physically, by the least squares method we find the displacement and material solution that comes closest to satisfying the equilibrium equations, incompressibility equations, and experimental measurement constraint equations that describe the inverse problem. The measure of "closeness to the solution" is defined by the norm in equation (4.3).

To find the set $(\underset{\sim}{\upsilon}, \underset{\sim}{\lambda}, \underset{\sim}{\varsigma})$ which minimizes this norm, we convert the indeterminate set of equations to a determinate system of equations. It is possible to derive the set of nonlinear equations which minimizes the error norm; however, it is vastly simpler analytically to find the least squares set of determinate equations for each step of Newton-Raphson iteration applied to the natural set of equations. That is, if the indeterminate linear system of equations which constitutes the $i^{\underline{th}}$ Newton-Raphson iteration is the m x n system (where m equals $\dim \underset{\sim}{f} + \dim \underset{\sim}{g}$, and n equals $\dim \underset{\sim}{f} + \dim \underset{\sim}{\varsigma}$)

$$\begin{bmatrix} \nabla_{\underset{\sim}{\upsilon}} \underset{\sim}{f} & \nabla_{\underset{\sim}{\lambda}} \underset{\sim}{f} & \nabla_{\underset{\sim}{\varsigma}} \underset{\sim}{f} \\ \nabla_{\underset{\sim}{\upsilon}} \underset{\sim}{g} & \nabla_{\underset{\sim}{\lambda}} \underset{\sim}{g} & \underset{\sim}{0} \end{bmatrix}_i \begin{Bmatrix} \underset{\sim}{\Delta\upsilon} \\ \underset{\sim}{\Delta\lambda} \\ \underset{\sim}{\Delta\varsigma} \end{Bmatrix}_i = \begin{Bmatrix} \underset{\sim}{P} - \underset{\sim}{f}(\underset{\sim}{\upsilon},\underset{\sim}{\lambda},\underset{\sim}{\varsigma}) \\ \underset{\sim}{\delta} - \underset{\sim}{g}(\underset{\sim}{\upsilon},\underset{\sim}{\lambda}) \end{Bmatrix}_i \tag{4.5}$$

then the linear system of equations which defines the best solution in the least squares sense to equations (4.5) is given by

$$\begin{bmatrix} \nabla_{\underset{\sim}{v}} \underset{\sim}{f}^T & \nabla_{\underset{\sim}{v}} \underset{\sim}{g}^T \\ \nabla_{\underset{\sim}{\lambda}} \underset{\sim}{f}^T & \nabla_{\underset{\sim}{\lambda}} \underset{\sim}{g}^T \\ \nabla_{\underset{\sim}{c}} \underset{\sim}{f}^T & \underset{\sim}{0} \end{bmatrix}_i \begin{bmatrix} \nabla_{\underset{\sim}{v}} \underset{\sim}{f} & \nabla_{\underset{\sim}{\lambda}} \underset{\sim}{f} & \nabla_{\underset{\sim}{c}} \underset{\sim}{f} \\ \nabla_{\underset{\sim}{v}} \underset{\sim}{g} & \nabla_{\underset{\sim}{\lambda}} \underset{\sim}{g} & \underset{\sim}{0} \end{bmatrix}_i \begin{Bmatrix} \underset{\sim}{\Delta v} \\ \underset{\sim}{\Delta \lambda} \\ \underset{\sim}{\Delta c} \end{Bmatrix}_i = \begin{bmatrix} \nabla_{\underset{\sim}{v}} \underset{\sim}{f}^T & \nabla_{\underset{\sim}{v}} \underset{\sim}{g}^T \\ \nabla_{\underset{\sim}{\lambda}} \underset{\sim}{f}^T & \nabla_{\underset{\sim}{\lambda}} \underset{\sim}{g}^T \\ \nabla_{\underset{\sim}{c}} \underset{\sim}{f}^T & \underset{\sim}{0} \end{bmatrix}_i \begin{Bmatrix} \underset{\sim}{P} - \underset{\sim}{f}(\underset{\sim}{v}, \underset{\sim}{\lambda}, \underset{\sim}{c}) \\ \underset{\sim}{\delta} - \underset{\sim}{g}(\underset{\sim}{v}, \underset{\sim}{\lambda}) \end{Bmatrix}_i . \quad (4.6)$$

This is an n x n system of symmetric linear equations (where n equals $\dim \underset{\sim}{f} + \dim \underset{\sim}{c}$) and is equivalent to the $i^{\underline{th}}$ iteration Newton-Raphson equations of the nonlinear least squares equations had they been derived at the onset. The application of equations (4.6) (for i = 1, 2, 3,...) is equivalent to minimizing a non-quadratic functional $\mathcal{F}(\underset{\sim}{v}, \underset{\sim}{\lambda}, \underset{\sim}{c})$ with respect to each variable in $(\underset{\sim}{v}, \underset{\sim}{\lambda}, \underset{\sim}{c})$ and supplies the best solution - in the least squares sense - to the indeterminate set of m equations in n variables,

$$\begin{Bmatrix} \underset{\sim}{f}(\underset{\sim}{v}, \underset{\sim}{\lambda}, \underset{\sim}{c}) \\ \underset{\sim}{g}(\underset{\sim}{v}, \underset{\sim}{\lambda}) \end{Bmatrix} = \begin{Bmatrix} \underset{\sim}{P} \\ \underset{\sim}{\delta} \end{Bmatrix} . \quad (4.2)$$

If the equations (4.2) are determinate (<u>i.e.</u>, m = n) the least squares method will converge to the same solution as the direct solution technique. The direct solution method (as developed in Chapter III) can be considered a special case of this more general least squares approach.

4.3 Weighted Least Squares Technique

In the direct solution of the determinate set of equations

$$\begin{Bmatrix} \omega_1 \cdot \underset{\sim}{f}(\underset{\sim}{u},\underset{\sim}{\lambda},\underset{\sim}{c}) \\ \omega_2 \cdot \underset{\sim}{g}(\underset{\sim}{u},\underset{\sim}{\lambda}) \end{Bmatrix} = \begin{Bmatrix} \omega_1 \cdot \underset{\sim}{P} \\ \omega_2 \cdot \underset{\sim}{\delta} \end{Bmatrix} \tag{4.7}$$

the weighting factors ω_1 and ω_2 can take any values (other than zero) without affecting the solution. But if the system is indeterminate and is to be solved by the least squares method, the relative sizes of ω_1 and ω_2 will greatly affect what value of $(\underset{\sim}{u}, \underset{\sim}{\lambda}, \underset{\sim}{c})$ is the "best" solution to the system. In other words, the value of $(\underset{\sim}{u}, \underset{\sim}{\lambda}, \underset{\sim}{c})$ which minimizes the error norm

$$\| \omega_1 \cdot (\underset{\sim}{f}(\underset{\sim}{u},\underset{\sim}{\lambda},\underset{\sim}{c}) - \underset{\sim}{P}) \| + \| \omega_2 \cdot (\underset{\sim}{g}(\underset{\sim}{u},\underset{\sim}{\lambda}) - \underset{\sim}{\delta}) \| \tag{4.8}$$

will depend on the values of ω_1 and ω_2.

The three most obvious weighting combinations for the equations (4.7) illustrate this point well.

Case 1: Let $\omega_1 >> \omega_2$, such that the magnitude of the equilibrium equations and incompressibility equations (the equations $\omega_1 \cdot \underset{\sim}{f} = \omega_1 \cdot \underset{\sim}{P}$) is several orders of magnitude greater than that of the input measurement constraint equations (the equations $\omega_2 \cdot \underset{\sim}{g} = \omega_2 \cdot \underset{\sim}{\delta}$). Consequently, the component

$$\| \omega_1 \cdot (\underset{\sim}{f} - \underset{\sim}{P}) \|$$

of the total error norm (4.8) will be very large relative to the component

$$\| \omega_2 \cdot (\underset{\sim}{g} - \underset{\sim}{\delta}) \|$$

if there is any error at all in satisfying the equilibrium and incompressibility equations - even if the input measurement constraint equations are very poorly satisfied. The effect, therefore, is that in the limit as $\omega_1/\omega_2 \rightarrow \infty$ the equilibrium and incompressibility equations will be satisfied exactly and the input measurement constraint equations will be satisfied to the maximum extent possible in the least squares sense. If the inverse problem to be solved has a very fine geometric mesh and very accurately determined boundary conditions and loading, but has input measurements of uncertain exactness, this weighting choice will yield the best material identification since only the part of the problem likely to contain inconsistencies (the equations $\underset{\sim}{g} - \underset{\sim}{\delta}$) will be solved in a least squares sense. The remainder will be solved exactly. See the second section of Appendix C for experimental verification of this expectation.

Case 2: Let $\omega_2 >> \omega_1$, such that

$$\| \omega_2 \cdot (\underset{\sim}{g} - \underset{\sim}{\delta}) \| \;>>\; \| \omega_1 \cdot (\underset{\sim}{f} - \underset{\sim}{P}) \| \qquad (4.9)$$

if there is any error at all in satisfying the experimental measurement constraint equations. As $\omega_2/\omega_1 \rightarrow \infty$, this type of weighting choice will force the material identification algorithm to satisfy exactly all the input measurements, no matter how inconsistent and full of experimental error they may be. The force equilibrium and incompressibility equations will be satisfied to the maximum extent possible - in the least

squares sense. This weighting choice is suitable for the solution of an inverse problem with very accurate input measurements but a coarse finite element mesh or boundary conditions of uncertain accuracy.

Case 3: Adjust ω_1 and ω_2 such that

$$\| \omega_1 \cdot (\underset{\sim}{f} - \underset{\sim}{P}) \|$$

is about the same magnitude as

$$\| \omega_2 \cdot (\underset{\sim}{g} - \underset{\sim}{\delta}) \| .$$

This forces the algorithm to choose a $(\underset{\sim}{u}, \underset{\sim}{\lambda}, \underset{\sim}{\varepsilon})$ that best satisfied all the equations defining the inverse problem.

In a real experimental situation the best choice of weighting factors is probably that which forces a fairly accurate solution to the equilibrium and incompressibility equations but allows some imbalance if large inconsistencies in the boundary conditions or loading approximations demand it. The input measurement constraint equations are weighted much more lightly than the others, since this is the part of the characterization of the inverse problem most likely to be in error. Careful design can avoid most modelling errors, but the measuring of the deformation of a laboratory specimen cannot be achieved without some inconsistency. For the examples of Appendices C and D it happens that the natural weighting of the system of equations ($\omega_1 = \omega_2 = 1$) gives excellent results. However, for problems of different dimensions or mesh size or type of

strain measure used as input, it is possible that different weighting factors would be needed to produce good material identifications.

A more consistent approach to specifying the numerical values of weighting factors is to normalize the system of equations (4.7) before weighting them, since the magnitudes of the various elements of $\underset{\sim}{f}$ will depend on the units chosen to measure force, the type of geometric mesh chosen, and many other factors - factors which influence the magnitude of ω_1/ω_2. If (4.7) is normalized such that the average magnitude of the elements of $\underset{\sim}{P}$ is equal to the average magnitude of the elements of $\underset{\sim}{\delta}$, and if the weighting factors for this normalized system of equations are denoted by $\bar{\omega}_1$ and $\bar{\omega}_2$, the weighting of the discrete inverse problem can be expressed by $\bar{\omega}_1/\bar{\omega}_2$, a ratio unaffected by the dimensioning of any particular problem.

Of course, the vector equation we symbolize by

$$\underset{\sim}{f}(\underset{\sim}{u}, \underset{\sim}{\lambda}, \underset{\sim}{\varepsilon}) = \underset{\sim}{P} \tag{4.10}$$

is actually composed of two different types of scalar equations: 2 force equilibrium equations for each node and an incompressibility condition equation for each element. Theoretically, a different weighting factor should be chosen for each type of equation. That is, for the incompressible, isotropic plane stress examples considered in this dissertation the equations defining the problem are

$$\begin{Bmatrix} \omega_0 \cdot \underset{\sim}{f}_{EQ}(\underset{\sim}{v},\underset{\sim}{\lambda},\underset{\sim}{c}) \\ \omega_1 \cdot \underset{\sim}{f}_{INC}(\underset{\sim}{v},\underset{\sim}{\lambda}) \\ \omega_2 \cdot \underset{\sim}{g}(\underset{\sim}{v},\underset{\sim}{\lambda}) \end{Bmatrix} = \begin{Bmatrix} \omega_0 \cdot \underset{\sim}{R} \\ \omega_1 \cdot \underset{\sim}{1} \\ \omega_2 \cdot \underset{\sim}{\delta} \end{Bmatrix}. \qquad (4.11)$$

In section 2 of Appendix C the sensitivity of the solution of this set of equations to different choices of $(\omega_0,\omega_1,\omega_2)$ is carefully examined. The results (Table C.2 and Figure C.8) show that the solution is quite stable for any reasonably well-designed experimental situation. That is, all three cases described on pages 88-90 result in reasonable material identifications. The best identification - and theoretically the most sound balancing of equations (4.11) - was obtained from the choice

$$(\omega_0, \omega_1, \omega_2) = (1,100,1), \qquad (4.12a)$$

or (expressed in terms of weighting factors for a normalized system of equations)

$$(\bar{\omega}_0, \bar{\omega}_1, \bar{\omega}_2) = (1,1,0.01), \qquad (4.12b)$$

since the magnitude of the incompressibility equations was much smaller than that of the force equilibrium equations (note case E in Table C.2). All the examples in section 3 of Appendix C and in Appendix D are solved with this choice of weighting factors.

It is possible to exert even more control over the solution by using a different weighting factor for each experimental measurement. That is, we could let the input measurement con-

straint equations be

$$\begin{Bmatrix} \omega_{21} \cdot g_1(\underset{\sim}{\upsilon}, \underset{\sim}{\lambda}) \\ \omega_{22} \cdot g_2(\underset{\sim}{\upsilon}, \underset{\sim}{\lambda}) \\ \vdots \\ \omega_{2n} \cdot g_n(\underset{\sim}{\upsilon}, \underset{\sim}{\lambda}) \end{Bmatrix} = \begin{Bmatrix} \omega_{21} \cdot \delta_1 \\ \omega_{22} \cdot \delta_2 \\ \vdots \\ \omega_{2n} \cdot \delta_n \end{Bmatrix}, \tag{4.13}$$

where the weighting factors are largest for measurements most likely to have been accurately determined. For example, in the specimen and measurement system below

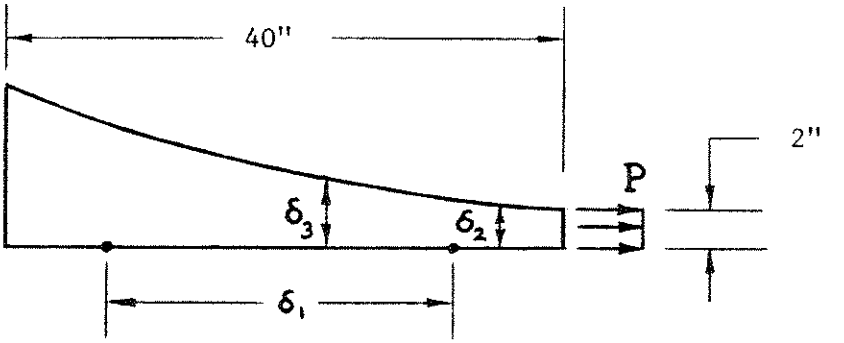

Fig. 4.1

δ_1 can be measured to extreme accuracy, but δ_2 and δ_3 are measurements of very small displacements and will probably contain errors of several percent. Hence the weighting of the equation

$$g_1(\underset{\sim}{\upsilon}, \underset{\sim}{\lambda}) = \delta_1 \tag{4.14}$$

should be greater than the weighting of the equations

$$g_2(\underset{\sim}{\upsilon}, \underset{\sim}{\lambda}) = \delta_2 \qquad (4.15)$$

$$g_3(\underset{\sim}{\upsilon}, \underset{\sim}{\lambda}) = \delta_3 \qquad (4.16)$$

if we want the material identification to reflect the superior credibility of measurement δ_1.

This refinement has not been exploited in the examples in the appendices, except in the very difficult 2 degree-of-freedom example in section 3 of Appendix C. It could be, though, a very important and useful modification of the least squares program presented here when it must be applied to actual experiments.

4.4 Analysis of Effectiveness of Least Squares Technique

Appendices C and D contain numerous examples of the behavior of the least squares technique when applied to test identification problems. Particularly noteworthy characteristics of the method are summarized in this section.

1) Least squares is a very powerful approach when very poor input data must be dealt with. The imbalance term

$$\underset{\sim}{g}(\underset{\sim}{\upsilon}, \underset{\sim}{\lambda}) - \underset{\sim}{\delta}$$

shows quite explicitly how each piece of input was received by the algorithm. If the system of equations was unable to use any particular measurement a large imbalance appears in the appropriate equation. In Appendix D a extremely large perturbation (20%) was introduced into one of the input measurements; the least squares algorithm immediately located it and showed how the material identification was being hurt by it (Figure D.12).

This is a vital feature of any method usable in practical experiments, where there will always be some poor measurements and often a good chance of a blunder in the input data.

2) Material identification is very little affected by reasonable experimental errors and inconsistencies in the input data, since there are many more measurements than material degrees of freedom. Only the average, overall information contained in the system of measurements is used, and measuring errors tend to cancel out each other if there are enough items of input. Even if some bias in the measuring method causes a non-Gaussian error distribution, the least squares algorithm is stable enough to find a material identification that reflects the bias - even if there are many physically illogical inconsistencies in the measurements. Note particularly the excellent stability of the examples of sections 1 and 3 of Appendix C - even with severely perturbed and inconsistent input - as contrasted with the instability of the examples in Appendix B solved by the direct solution of a determinate system of equations.

3) Divergence is not possible; there is always some value of $(\underset{\sim}{\upsilon}, \underset{\sim}{\lambda}, \underset{\sim}{\varsigma})$ that minimizes the error norm (4.3). Of course, if the input data are absurd the solution $(\underset{\sim}{\upsilon}, \underset{\sim}{\lambda}, \underset{\sim}{\varsigma})$ will be physically meaningless. But in practice no imaginable experiment should give data so poor that a meaningless identification results. It is nonetheless necessary to choose a reasonable first approximation to the material functions as the starting point for the Newton-Raphson iteration, since the method

will seek out a local minimum in the area of the initial guess of the material solution. If the initial guess is too far from the true material properties, the algorithm may converge to the wrong minimum of the error functional, and hence the wrong solution $(\underset{\sim}{\upsilon}, \underset{\sim}{\lambda}, \underset{\sim}{\varsigma})$. However, in the applications studied in the appendices this behavior was never encountered, even when very crude initial guesses were used. In real situations it should be possible to perform some kind of crude experiment to obtain the initial guess for the material functions.

Note in Appendix B the inferior stability of identification methods based on determinate systems of equations; the slightest inconsistency in input could cause divergence.

4) For very accurate input measurements the finer the material discretization, the better the material identification - as long as there are enough redundancies in the experimental measurements so that individual rounding errors cannot influence the solution much. In practice, best results are with $\dim \underset{\sim}{g}$ at least two or three times greater than $\dim \underset{\sim}{\varsigma}$. Of course, once the material discretization is fine enough to duplicate very closely the continuous material functions there is no further improvement in the identification. However, for input measurements with experimental errors and inconsistencies, fine material meshes tend to become much more unstable than coarse meshes. The best identification comes from using the coarsest discretization that is capable of reasonably representing the continuous material functions. Discretizations with more degrees of freedom than this give the system of equations unnecessary

freedom to adjust the material solution to experimental errors. This is a critical problem in experimental setups governed by an extremely sensitive inverse boundary value problem, such as the plane stress examples studied in the appendices. It requires much intuition to choose the best discretization to represent an unknown material. Too rigid a mesh may so poorly represent the material functions that only a very unreasonable material solution can best satisfy the equations describing the problem, while too fine a mesh can be too sensitive to experimental inaccuracies in input.

From experience with the examples in the appendices it has been found that an initial discretization of 2 degrees of freedom for a function suspected of being constant or fairly linear over the strain range of the experiment, and 3 degrees of freedom for functions suspected of having some curvature, is quite stable. From the information contained in the identification based on this first discretization choice, a more appropriate second discretization can be chosen and the problem solved again. This process can be repeated until the shapes and magnitudes of the material functions are understood. This is precisely the strategy used to solve the example discussed in Appendix D.

Section 3 of Appendix C examines a large number of types of material discretization and analyzes the stability of each. Reasonably stable identifications resulted from every material discretization choice, even the extremely poor ones.

No examples were tested with two-dimensional material

discretizations, but it is to be expected that great care would have to be taken to ensure stability. It may be easier in actual practice to choose experimental configurations with strain invariant ranges that permit a one-dimensional discretization. Superposing the results of several such experiments will give the material characterization over the entire (I_1, I_2) plane.

5) The weighted least squares method gives the experimenter much freedom in emphasizing whatever aspects of the experimental situation seem most reliably describable; equations in the system likely to be inaccurate can be given smaller weighting factors. This idea could be internalized into the computer program. For example, the material identification problem could be solved with a constant weighting factor for all experimental measurements to determine $g_i(\underline{c}) - \delta_i$ for each measurement i. This shows where measurement errors were most probable and permits the choosing of a new set of weighting factors in order to obtain an identification that ignores the worst inconsistencies in the input measurements.

Also important is the capability to deemphasize any inconsistencies that turn up in certain parts of the geometric or material mesh. For example, if the algorithm finds that the idealized boundary conditions of the finite element model very poorly approximate the clamped boundaries of the actual experiment and are causing large imbalances in the force equilibrium equations, it is possible to decrease the weighting factor for the force equilibrium equations at those particular nodes close

to the boundary, thus exempting those equations from having to satisy equilibrium as closely as the other force equilibrium equations in the body. This protects the solution $(\underset{\sim}{u}, \underset{\sim}{\lambda}, \underset{\sim}{c})$ from the adverse effects of being forced to satisfy equations derived from inaccurate modelling.

6) The material identification is not very sensitive to the exact location of the nodes of the material mesh relative to the strain invariant ranges covered by the various measurements. The pivoting problem discussed in section 3 of Appendix B cannot occur, since there are many more measurements than degrees of freedom in the material mesh. It is, of course, necessary that measurements exist somewhere in the range of each material degree of freedom to prevent that material variable from being indeterminate. The best stability seems to result from a fairly even distribution of measurements (as done in the example of Appendix D), since in this case all parts of the material identification's strain range are emphasized equally. If in a certain strain range it is particularly vital to obtain an exact identification of the material functions one can concentrate the experimental measurements in the parts of the specimen experiencing that magnitude of strain. This will force the algorithm to adjust the identified material functions in other less important strain ranges to account for experimental errors - leaving a virtually perfect material identification in the most important strain range.

7) Using the least squares method does not increase unreasonably the computational effort needed to identify a material. The

rectangular gradient matrix is found in exactly the same way as the square gradient matrix of Chapter III. The matrix multiplications (4.6) are straightforward and not too costly. The resulting system of equations is symmetric (unlike the determinate system of equations) and can be economically solved with a symmetric equation solving algorithm, thus largely compensating for the matrix multiplications necessary to obtain the least squares system of equations. The least squares examples in Appendix C cost on the average 40% more computational effort than the corresponding examples solved with a determinate set of equations.

V. GENERALIZED THERMOMECHANICAL MATERIAL IDENTIFICATION

5.1 Introduction

The detailed development of this material identification technique has made use of the particular case of isotropic, incompressible elastic materials in a state of plane stress, since the inverse boundary value problem (2.3-2.6) associated with this particular case is relatively simple and permits a clear and intuitive explanation of the technique. However, the method is completely general and in this chapter we shall briefly indicate how it might be used to identify general thermomechanical materials. Also, the method's application to a few important special situations - such as compressible elastic materials in states of plane stress - will be discussed in some detail.

5.2 General Thermomechanical Material

The inverse boundary value problem associated with the identification of general thermomechanical materials was outlined in Section 2.2 (pages 31-32). Discretization of this inverse boundary value problem was discussed in Section 3.1 (pages 43-45). Let finite element discretization of the kinematic variables $\underset{\sim}{\chi}(\underset{\sim}{X},t)$ and $\Theta(\underset{\sim}{X},t)$ be indicated by the same notation used previously in (3.1):

$$\chi_1(\underset{\sim}{X},t) \doteq \sum_{i=1}^{n_1} \alpha_i \varphi_i(\underset{\sim}{X},t) \tag{5.1a}$$

$$\chi_2(\underset{\sim}{X},t) \doteq \sum_{i=n_1+1}^{n_2} \alpha_i \varphi_i(\underset{\sim}{X},t) \tag{5.1b}$$

$$\chi_3(\underset{\sim}{X},t) \doteq \sum_{i=n_2+1}^{n_3} \alpha_i \varphi_i(\underset{\sim}{X},t) \tag{5.1c}$$

$$\theta(\underset{\sim}{x},t) \doteq \sum_{i=1}^{n_4} \Theta_i \psi_i(\underset{\sim}{x},t). \tag{5.1d}$$

Substitution of (5.1) into the general variational principle and field equations that define the general thermomechanical forward-direction boundary value problem results in a set of (n_3+n_4) nonlinear algebraic equations

$$\underset{\sim}{f}(\underset{\sim}{\alpha},\underset{\sim}{\Theta}) = \underset{\sim}{P}. \tag{5.2}$$

A more detailed discussion of the types of variational functionals which lead to (5.2) when discretized and minimized can be found in [1,10,27,28].

The observed motion and temperature history (2.1) are discretized by specifying q_1 measured deformations and temperatures (at various space-time points $(\underset{\sim}{x},t)$) and expressing these observed measurements in terms of the generalized coordinates $\underset{\sim}{\alpha}$ and $\underset{\sim}{\Theta}$ defined by (5.1). That is, conditions (2.1) are expressed by the q_1 discrete equations

$$\underset{\sim}{g}(\underset{\sim}{\alpha},\underset{\sim}{\Theta}) = \underset{\sim}{\delta}. \tag{5.3}$$

The general thermomechanical material operator (1.28) can be discretized as previously indicated in (3.2), i. e.,

$$\hat{\psi}(\underset{\sim}{C},\theta) \doteq \sum_{i=1}^{m_1} c_i \phi_i(\underset{\sim}{C},\theta) \tag{5.4a}$$

$$\hat{\eta}(\underset{\sim}{C},\theta) \doteq \sum_{i=m_1+1}^{m_2} c_i \phi_i(\underset{\sim}{C},\theta) \tag{5.4b}$$

$$\underset{\sim}{\hat{T}}(\underset{\sim}{C},\theta) \doteq \sum_{i=m_2+1}^{m_3} c_i \underset{\sim}{\phi}_i(\underset{\sim}{C},\theta) \tag{5.4c}$$

$$\hat{\underset{\sim}{Q}}(\underset{\sim}{C},\theta,\underset{\sim}{G}) \doteq \sum_{i=m_3+1}^{m_4} c_i \underset{\sim}{\phi}_i(\underset{\sim}{C},\theta,\underset{\sim}{G}). \tag{5.4d}$$

Applying this parameterization to the continuous material operators in equations (5.2), we obtain the set of $(n_3+n_4+q_1)$ algebraic equations that fully discretizes the inverse boundary value problem,

$$\begin{aligned} \underset{\sim}{f}(\underset{\sim}{\alpha},\underset{\sim}{\Theta},\underset{\sim}{C}) &= \underset{\sim}{P} \\ \underset{\sim}{g}(\underset{\sim}{\alpha},\underset{\sim}{\Theta}) &= \underset{\sim}{\delta} . \end{aligned} \tag{5.5}$$

Solution of (5.5) follows directly from the methods developed in Chapters III and IV.

Note that the usual difficulties of solving an inverse problem are encountered. The domain $(\underset{\sim}{C},\Theta,\underset{\sim}{G})$ of the material response operators $\hat{\psi}$, $\hat{\eta}$, $\underset{\sim}{\mathcal{T}}$, and $\hat{\underset{\sim}{Q}}$ must be known before discretization is possible. And the large number of degrees of freedom in $\underset{\sim}{C}$ makes the algebraic equations (5.5) very sensitive. Moreover, including the time variable in (5.1) makes it necessary that the dimension of $\underset{\sim}{\alpha}$ and $\underset{\sim}{\Theta}$ be very large - probably too large for an economically feasible solution of (5.5).

5.3 Compressible Materials in a State of Plane Stress

The physical experiments described in the appendices are suitable for the identification of compressible materials as well as incompressible materials. But a different set of equations will describe the system. The three-dimensional boundary value problem for elastic compressible materials (1.57-1.59) can be transformed into a two-dimensional boundary value problem by means of the plane stress assumptions (1.69) if the body is a thin planar sheet unloaded on its surfaces. A new set of field

equations can be derived by direct substitution of these plane stress assumptions into the three-dimensional field equations (1.57) expressed in terms of Lagrangian strain and displacement:

$$((\underset{\sim}{I} + \nabla\underset{\sim}{u})\cdot\underset{\sim}{P})\cdot\nabla + \rho_K \underset{\sim}{b} = \underset{\sim}{0} \tag{5.6a}$$

$$\underset{\sim}{C} = 2\underset{\sim}{E} + \underset{\sim}{I} \tag{5.6b}$$

$$\underset{\sim}{E} = \tfrac{1}{2}\left[\nabla\underset{\sim}{u} + \nabla\underset{\sim}{u}^T + \nabla\underset{\sim}{u}^T\cdot\nabla\underset{\sim}{u}\right] \tag{5.6c}$$

$$\begin{aligned}\underset{\sim}{P} = {} & 2C_1(I_1,I_2,I_3)\begin{bmatrix}1 & 0\\ 0 & 1\end{bmatrix} \\ & + 2C_2(I_1,I_2,I_3)\begin{bmatrix}C_{22}+\lambda^2 & -C_{12}\\ -C_{12} & C_{11}+\lambda^2\end{bmatrix} + 2C_3(I_1,I_2,I_3)\begin{bmatrix}C_{22}\lambda^2 & -C_{12}\lambda^2\\ -C_{12}\lambda^2 & C_{11}\lambda^2\end{bmatrix}\end{aligned} \tag{5.6d}$$

$$2\left\{C_1(I_i) + (C_{11}+C_{22})C_2(I_i) + (C_{11}C_{22}-C_{12}^2)C_3(I_i)\right\} = 0, \tag{5.6e}$$

where the last equation represents the plane stress condition $P_{33} = 0$. All the field equations are defined over the two-dimensional domain $\mathcal{B}_K$, with appropriate boundary conditions defined on $\partial\mathcal{B}_K$. The plane stress assumption also results in the following simplified forms for the strain invariants and strain tensor:

$$I_1 = C_{11} + C_{22} + \lambda^2 \tag{5.7a}$$

$$I_2 = (C_{11}+C_{22})\lambda^2 + C_{11}C_{22} - C_{12}^2 \tag{5.7b}$$

$$I_3 = \lambda^2(C_{11}C_{22} - C_{12}^2) \tag{5.7c}$$

$$\underset{\sim}{C} = \begin{bmatrix} C_{11} & C_{12} & 0\\ C_{12} & C_{22} & 0\\ 0 & 0 & \lambda^2\end{bmatrix} \tag{5.8}$$

where λ is the extension ratio in the z-direction. Introduction of the minimum potential energy theorem replaces (5.6a) and the traction boundary condition. Therefore, the inverse boundary value problem for a compressible material in a state of plane stress is as follows: for a body represented by domain $\mathcal{B}_{\underset{\sim}{K}}$, with body force $\underset{\sim}{b}(\underset{\sim}{X})$ and a description (through a finite set of experimental measurements) of the deformed configuration

$$\underset{\sim}{U}(x,y) = \hat{\underset{\sim}{U}}(x,y) \tag{5.9a}$$

$$\lambda(x,y) = \hat{\lambda}(x,y), \tag{5.9b}$$

find the material functions $C_1(I_1, I_2, I_3)$, $C_2(I_1, I_2, I_3)$, $C_3(I_1, I_2, I_3)$ and the mechanical state $R(x,y) : \{\underset{\sim}{U}, \underset{\sim}{E}, \underset{\sim}{C}, I_1, I_2, I_3, \lambda, \underset{\sim}{P}\}$ that satisfy at all (X,Y) in $\mathcal{B}_{\underset{\sim}{K}}$ the field equations

$$\underset{\sim}{E} = \tfrac{1}{2}\left[\nabla\underset{\sim}{U} + \nabla\underset{\sim}{U}^T + \nabla\underset{\sim}{U}^T \cdot \nabla\underset{\sim}{U}\right] \tag{5.10a}$$

$$\underset{\sim}{C} = 2\underset{\sim}{E} + \underset{\sim}{I} \tag{5.10b}$$

$$\underset{\sim}{P} = 2C_1(I_i)\begin{bmatrix}1 & 0\\ 0 & 1\end{bmatrix} + 2C_2(I_i)\begin{bmatrix}C_{22}+\lambda^2 & -C_{12}\\ -C_{12} & C_{11}+\lambda^2\end{bmatrix} + 2C_3(I_i)\begin{bmatrix}C_{22}\lambda^2 & -C_{12}\lambda^2\\ -C_{12}\lambda^2 & C_{11}\lambda^2\end{bmatrix} \tag{5.10c}$$

$$2\left\{C_1(I_i) + (C_{11}+C_{22})C_2(I_i) + (C_{11}C_{22}-C_{12}^2)C_3(I_i)\right\} = 0 \tag{5.10d}$$

$$I_1 = C_{11} + C_{22} + \lambda^2 \tag{5.10e}$$

$$I_2 = (C_{11}+C_{22})\lambda^2 + C_{11}C_{22} - C_{12}^2 \tag{5.10f}$$

$$I_3 = \lambda^2 (C_{11}C_{22} - C_{12}^2), \tag{5.10g}$$

satisfy the boundary condition

$$\underset{\sim}{u}(x,y) = \hat{\underset{\sim}{u}}(x,y) \qquad \forall (x,y) \in \partial \mathcal{B}_{\underset{\sim}{K}}^{1}, \tag{5.10h}$$

and satisfy the minimum potential energy theorem

$$\delta \Phi(\underset{\sim}{u}) = \frac{1}{2}\int_{\mathcal{B}_K} \underset{\sim}{P} : \delta \underset{\sim}{C}\, dV - \int_{\mathcal{B}_K} \rho_K \underset{\sim}{b} \cdot \delta \underset{\sim}{u}\, dV - \int_{\partial \mathcal{B}_K} \hat{\underset{\sim}{t}}_K \cdot \delta \underset{\sim}{u}\, dS = 0. \tag{5.10i}$$

When a two-dimensional finite element discretization

$$\underset{\sim}{u}(x,y) \doteq \sum_{i=1}^{n} \underset{\sim}{u}_i \varphi_i(x,y) \tag{5.11a}$$

$$\lambda(x,y) \doteq \sum_{i=1}^{m} \lambda_i \psi_i(x,y) \tag{5.11b}$$

is chosen and substituted into the field equations (5.10a-g) and the virtual work equation (5.10i), a nonlinear system of algebraic equations results:

$$\underset{\sim}{f}_{EQ}(\underset{\sim}{u}, \underset{\sim}{\lambda}) = \underset{\sim}{R} \tag{5.12a}$$

$$\underset{\sim}{f}_{PLST}(\underset{\sim}{u}) = \underset{\sim}{0}. \tag{5.12b}$$

with each variable representing an x- or y-component of nodal displacement or an element extension ratio. For the elements illustrated in Figure 3.2, the system (5.12) is composed of two force equilibrium equations for each node of the finite element mesh and one plane stress assumption equation for each element, and can be represented more compactly by the single vector

equation

$$\underset{\sim}{f}(\underset{\sim}{u},\underset{\sim}{\lambda}) = \underset{\sim}{P}. \tag{5.13}$$

If a number of experimental measurements are taken and the material functions discretized by means of the finite element expansions

$$C_1(I_1,I_2,I_3) \doteq \sum_{i=1}^{o} c_i \phi_i(I_1,I_2,I_3) \tag{5.14a}$$

$$C_2(I_1,I_2,I_3) \doteq \sum_{i=o+1}^{p} c_i \phi_i(I_1,I_2,I_3) \tag{5.14b}$$

$$C_3(I_1,I_2,I_3) \doteq \sum_{i=p+1}^{r} c_i \phi_i(I_1,I_2,I_3), \tag{5.14c}$$

the final form of the discrete inverse boundary value problem is

$$\begin{Bmatrix} \underset{\sim}{f}(\underset{\sim}{u},\underset{\sim}{\lambda},\underset{\sim}{c}) \\ \underset{\sim}{g}(\underset{\sim}{u},\underset{\sim}{\lambda}) \end{Bmatrix} = \begin{Bmatrix} \underset{\sim}{P} \\ \underset{\sim}{\delta} \end{Bmatrix}, \tag{5.15}$$

the same type of algebraic system dealt with throughout this dissertation and hence solvable by exactly the same methods developed in Chapters III and IV.

However, the finite element discretization of the material functions is considerably more complex, since there are now three functions of three independent variables. Considerable ingenuity must be exercised to choose an experimental situation that will involve only a small portion of the total three-dimensional (I_1, I_2, I_3) domain, so that a one-dimensional or two-dimensional discretization of each function is possible. For example, with a compressible material the tension experiment of Appendix D will probably have a strain invariant distribution

which is a curved line in the (I_1, I_2, I_3) space, and will probably resemble a three-dimensionalized Figure D.5. Hence, a 7 degree-of-freedom, one-dimensional discretization (shown below in Figure 5.1 with I_1 as the independent variable) would be a good possi-

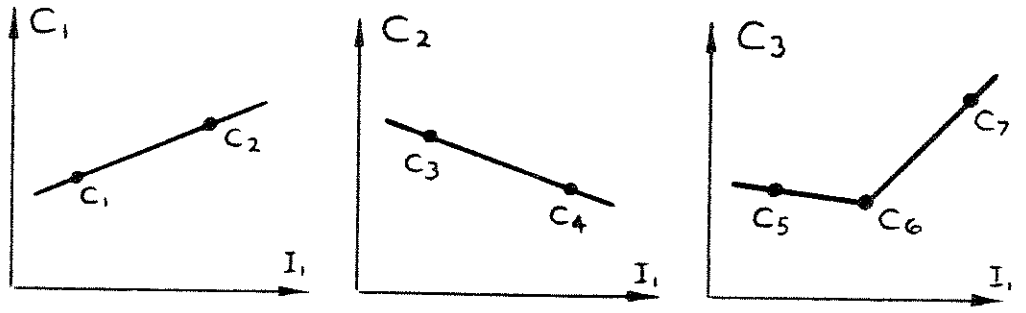

Fig. 5.1

bility to start the identification process. Fully general three-dimensional finite element material discretizations are theoretically possible, of course, but stability could be a problem if the experimental measurement locations are not evenly distributed throughout the domain covered by the material mesh. Virtually nothing is known about the shapes and relative magnitudes of the compressible material functions or about the sensitivity of the continuous inverse boundary value problem itself.

5.4 Compressible Materials in Three-dimensional States of Stress

If a more complicated experimental specimen which cannot be adequately represented by means of a two-dimensional plane stress model is tested, analysis must be based on the fully general three-dimensional field equations for a compressible elastic body (1.57-1.60). A three-dimensional finite element mesh is chosen,

$$u_1(x,y,z) \doteq \sum_{i=1}^{n} u_{1i}\varphi_i(x,y,z) \tag{5.16a}$$

$$u_2(x,y,z) \doteq \sum_{i=1}^{n} u_{2i}\varphi_i(x,y,z) \tag{5.16b}$$

$$u_3(x,y,z) \doteq \sum_{i=1}^{n} u_{3i}\varphi_i(x,y,z), \tag{5.16c}$$

and the discrete system of equations derived by direct substitution into the field equations (1.57a), (1.60) and the virtual work theorem (5.10i). This global system is composed simply of three force equilibrium equations for each node in the three-dimensional geometric mesh and can be represented by

$$\underset{\sim}{f}(\underset{\sim}{u}) = \underset{\sim}{P}. \tag{5.17}$$

Measurements can be taken anywhere on the surface of the body. The finite element material mesh (5.14) is chosen as in Section 5.3. The final set of equations describing the discretized inverse problem are

$$\begin{Bmatrix} \underset{\sim}{f}(\underset{\sim}{u},\underset{\sim}{c}) \\ \underset{\sim}{g}(\underset{\sim}{u}) \end{Bmatrix} = \begin{Bmatrix} \underset{\sim}{P} \\ \underset{\sim}{\delta} \end{Bmatrix} \tag{5.18}$$

and can be solved with the same methods discussed in previous chapters.

A three-dimensional problem does not force a more complicated algebraic situation or a more complicated material discretization. The main difficulty with three-dimensional experimental situations is that a very large number of elements and nodes is needed to adequately represent the geometry and displacement patterns of the experiment; as a result, the solution time often

increases prohibitively.

5.5 Incompressible Materials in Three-dimensional States of Strain

To identify material functions very accurately over their complete (I_1, I_2) domain it may be necessary to conduct some experiments with very complicated strain states and geometric shapes. This will necessitate using the general incompressible elastic field equations and variational principle (1.68) and setting up a three-dimensional finite element displacement discretization

$$v_1(x,y,z) \doteq \sum_{i=1}^{n} v_{1i}\varphi_i(x,y,z) \tag{5.19a}$$

$$v_2(x,y,z) \doteq \sum_{i=1}^{n} v_{2i}\varphi_i(x,y,z) \tag{5.19b}$$

$$v_3(x,y,z) \doteq \sum_{i=1}^{n} v_{3i}\varphi_i(x,y,z), \tag{5.19c}$$

a hydrostatic pressure finite element discretization

$$h(x,y,z) \doteq \sum_{i=1}^{\ell} h_i\psi_i(x,y,z), \tag{5.19d}$$

and the same material discretization used previously in the plane stress problem

$$C_1(I_1,I_2) \doteq \sum_{i=1}^{m} c_i\phi_i(I_1,I_2) \tag{5.20a}$$

$$C_2(I_1,I_2) \doteq \sum_{i=m+1}^{p} c_i\phi_i(I_1,I_2). \tag{5.20b}$$

Substituting the finite element approximations (5.19) into the field equations (1.68) forms a global system of three equations for each node of the three-dimensional geometric mesh and one incompressibility constraint equation for each element:

$$\begin{Bmatrix} \underset{\sim}{f}_{EQ}(\underset{\sim}{U},\underset{\sim}{h}) \\ \underset{\sim}{f}_{INC}(\underset{\sim}{U}) \end{Bmatrix} = \begin{Bmatrix} \underset{\sim}{R} \\ \underset{\sim}{1} \end{Bmatrix} \tag{5.21}$$

or more compactly

$$\underset{\sim}{f}(\underset{\sim}{U},\underset{\sim}{h}) = \underset{\sim}{P}. \tag{5.22}$$

Experimental measurements can be taken anywhere on the surface of the specimen. The final set of discrete equations for the inverse problem is

$$\begin{Bmatrix} \underset{\sim}{f}(\underset{\sim}{U},\underset{\sim}{h},\underset{\sim}{c}) \\ \underset{\sim}{g}(\underset{\sim}{U}) \end{Bmatrix} = \begin{Bmatrix} \underset{\sim}{P} \\ \underset{\sim}{\delta} \end{Bmatrix} \tag{5.23}$$

and is solved in the usual way, as described in Chapter IV. No complications result except the usual increase in the number of nodes needed to effect a sufficiently accurate geometric discretization.

5.6 Incompressible Materials in a State of Plane Strain

If all deformation in an experiment is limited to the $(x\text{-}y)$ plane, the boundary value problem can be simplified by use of the plane strain assumption

$$\underset{\sim}{C} = \begin{bmatrix} C_{11} & C_{12} & 0 \\ C_{12} & C_{22} & 0 \\ 0 & 0 & 1 \end{bmatrix}, \tag{5.24}$$

which when substituted into the three-dimensional field equations (1.64) results in a new system of field equations defined over a

two-dimensional domain, i. e.,

$$\left((\underset{\sim}{I} + \nabla\underset{\sim}{u})\cdot\underset{\sim}{P}\right)\cdot\nabla + \rho_R \underset{\sim}{b} = \underset{\sim}{0} \tag{5.25a}$$

$$\underset{\sim}{C} = 2\underset{\sim}{E} + \underset{\sim}{I} \tag{5.25b}$$

$$\underset{\sim}{E} = \tfrac{1}{2}\left[\nabla\underset{\sim}{u} + \nabla\underset{\sim}{u}^T + \nabla\underset{\sim}{u}^T\cdot\nabla\underset{\sim}{u}\right] \tag{5.25c}$$

$$\underset{\sim}{P} = 2C_1(I_1,I_2)\begin{bmatrix}1 & 0\\ 0 & 1\end{bmatrix} + 2C_2(I_1,I_2)\begin{bmatrix}C_{22}+1 & -C_{12}\\ -C_{12} & C_{11}+1\end{bmatrix} - \frac{h}{C_{11}C_{22}-C_{12}^2}\begin{bmatrix}C_{22} & -C_{12}\\ -C_{12} & C_{11}\end{bmatrix} \tag{5.25d}$$

$$P_{33} = 2C_1(I_1,I_2) + 2C_2(I_1,I_2)\left[C_{11} + C_{22}\right] - h \tag{5.25e}$$

$$\det\underset{\sim}{C} = C_{11}C_{22} - C_{12}^2 = 1 \tag{5.25f}$$

with strain invariants given by

$$I_1 = C_{11} + C_{22} + 1 \tag{5.25g}$$

$$I_2 = C_{11} + C_{22} + C_{11}C_{22} - C_{12}^2 . \tag{5.25h}$$

If the usual finite element discretizations for displacement and hydrostatic pressure variables

$$u_1(x,y) \doteq \sum_{i=1}^{n} u_{1i}\varphi_i(x,y) \tag{5.26a}$$

$$u_2(x,y) \doteq \sum_{i=1}^{n} u_{2i}\varphi_i(x,y) \tag{5.26b}$$

$$h(x,y) \doteq \sum_{i=1}^{\ell} h_i\psi_i(x,y) \tag{5.26c}$$

are substituted into field equations (5.25b-e) and the generalized minimum potential energy theorem (1.68d), there results the

system of algebraic equations

$$\begin{Bmatrix} \underset{\sim}{f}_{EQ}(\underset{\sim}{U}, \underset{\sim}{h}) \\ \underset{\sim}{f}_{INC}(\underset{\sim}{U}) \end{Bmatrix} = \begin{Bmatrix} \underset{\sim}{R} \\ \underset{\sim}{1} \end{Bmatrix}, \tag{5.27}$$

composed of two force equilibrium equations for each node of the two-dimensional geometric mesh and one incompressibility constraint equation for each element. This is usually condensed to the form

$$\underset{\sim}{f}(\underset{\sim}{U}, \underset{\sim}{h}) = \underset{\sim}{P}. \tag{5.28}$$

With the usual incompressible material mesh

$$C_1(I_1, I_2) \doteq \sum_{i=1}^{p} c_i \phi_i(I_1, I_2) \tag{5.29a}$$

$$C_2(I_1, I_2) \doteq \sum_{i=p+1}^{m} c_i \phi_i(I_1, I_2) \tag{5.29b}$$

and a system of experimental measurements, we have the discrete inverse boundary value problem in the familiar form

$$\begin{Bmatrix} \underset{\sim}{f}(\underset{\sim}{U}, \underset{\sim}{h}, \underset{\sim}{c}) \\ \underset{\sim}{g}(\underset{\sim}{U}) \end{Bmatrix} = \begin{Bmatrix} \underset{\sim}{P} \\ \underset{\sim}{\delta} \end{Bmatrix} \tag{5.30}$$

which is solvable by the methods developed in Chapters III and IV.

REFERENCES

1. Truesdell, C. and Noll, W., "The Nonlinear Field Theories of Mechanics," Ency. of Physics, Vol. III/3, Springer-Verlag, 1965.

2. Leigh, D. C., "Nonlinear Continuum Mechanics," McGraw-Hill, 1968.

3. Jaunzemis, W., "Continuum Mechanics," Macmillan, 1967.

4. Rivlin, R. S. and Saunders, D. W., "Large Deformations of Elastic Materials, VII. Experiments on the Deformation of Rubber," Phil. Trans. Roy. Soc., London, A, 243, 1951.

5. Obata, Y., Kawabata, S. and Kawai, H., "Mechanical Properties of Natural Rubber Vulcanizates in Finite Deformation," J. Polymer Science, 8, 1970.

6. Alexander, H., "A Constitutive Relation for Rubber-Like Materials," Int. J. Engng. Sci., Vol. 6, 1968.

7. Oden, J. T. and Key, J. E., "Analysis of Finite Deformations of Elastic Solids by the Finite Element Method," IUTAM Symposium of Elastic Structures, Liege, Belgium, August, 1970.

8. Oden, J. T., "Finite Plane Strain of Incompressible Elastic Solids by the Finite Element Method," The Aeronautical Quarterly, August 1968.

9. Oden, J. T., "Finite Element Analysis of Nonlinear Problems in the Dynamical Theory of Coupled Thermoelasticity," Nuclear Engineering and Design, 10, 1969.

10. Lu, C., "Nonlinear Theory of Thermoelasticity," Ph. D. Dissertation, Graduate Division, Univ. of Calif. (Berkeley) 1971.

11. Block, H. D., "Introduction to Tensor Analysis," Merrill, 1962.

12. Fung, Y. C., "Foundations of Solid Mechanics," Prentice-Hall, 1965.

13. Nemat-Nasser, S. and Shatoff, H. D., "A Consistant Numerical Method for the Solution of Nonlinear Elasticity Problems at Finite Strains," Tech. Report No. 2, Dept. Aero. Mech. Engng. Sci., Univ. of Calif. (San Diego) January, 1970.

14. Coleman, B. D. and Gurtin, M. E., "Thermodynamics with Internal State Variables," J. Chem. Phys., 47, 1967.

15. Green, A. E. and Adkins, J. E., "Large Elastic Deformations," Clarendon Press, Oxford, England, 1960.

16. Treloar, L. R. G., "The Physics of Rubber Elasticity," Oxford University Press, 1958.

17. Mooney, M., "A Theory of Large Elastic Deformation," J. Appl. Phys., 11, 1940.

18. Miklin, S. G., "Variational Methods in Mathematical Physics," Pergamon Press, Oxford, 1964.

19. Bellman, R. and Kalaba, R., "Quasilinearization and Nonlinear Boundary Value Problems," American Elsevier, New York, 1965.

20. Angel, E., "Discrete Invariant Imbedding and Elliptic Boundary Value Problems over Irregular Regions," J. Math. Anal. Appl., 23, 1968.

21. Zienciewicz, O. C., "The Finite Element Method in Engineering Science," McGraw-Hill, London, 1971.

22. Oden, J. T., "Finite Elements of Nonlinear Continua," McGraw-Hill, 1972.

23. Kavanaugh, K. T., "The Finite Element Analysis of Physically and Kinematically Nonlinear Elastic Solids," Ph. D. Dissertation, Graduate Division, Univ. of Calif. (Berkeley) 1969.

24. Pister, K. S., "Mathematical Modeling for Structural Analysis and Design," Nuclear Engineering and Design, 18, 1972.

25. Ralston, A., "A First Course in Numerical Analysis," McGraw-Hill, 1965.

26. Isaacson, E. and Keller, H. B., "Analysis of Numerical Methods," John Wiley & Sons, 1966.

27. Gurtin, M. E., "Variational Principles for Linear Elastodynamics," Arch. Rat. Mech. Anal., 16, 1964.

28. Nickell, R. E. and Sackman, J. L., "Variational Principles for Linear Coupled Thermoelasticity," Quarterly Appl. Math., 26, 1968.

29. Dong, R. G., Pister, K. S. and Dunham, R. S., "Mechanical Characterization of Nonlinear Viscoelastic Solids for Iterative Solution of Boundary Value Problems," Acta Mechanica, 9, 1970.

APPENDICES

To test the methods developed in this dissertation a number of material identification experiments were simulated by computer. Rather than breaking the flow of the main body of the dissertation with lengthy descriptions of these experiments and analysis of the results derived from them, we have put off detailed discussion until the appendices. Many of the conclusions already mentioned stem directly from observing the behavior of these experiments.

Appendix A: Identification of an isotropic, incompressible elastic material by means of a spatial finite element discretization

$$C_i(x,y) \doteq \sum_{j=1}^{n} c_j \varphi_j(x,y)$$

is examined. The material discretization has one degree of freedom for each experimental measurement used as input.

Appendix B: Use of a direct finite element material discretization

$$C_i(I_1,I_2) \doteq \sum_{j=1}^{n} c_j \varphi_j(I_1,I_2)$$

in situations where there is one material parameter for each experimental input measurement is examined. That is, the method of Chapter III is used; no effort is made to suppress noise in the input measurements $\underset{\sim}{\delta}$.

Appendix C: Several applications of the least squares technique of Chapter IV are examined in great detail. Effects of different

types of noise in $\underset{\sim}{\delta}$, different weighting schemes for the algebraic equations, and different types of material meshes are studied.

Appendix D: An identification experiment using geometric and material meshes fine enough to be effective in an actual physical experiment is developed. The precise procedure an experimenter must follow when applying this identification method is fully described.

APPENDIX A

Chapter III developed material identification techniques based on the direct solution of the determinate set of equations

$$\begin{Bmatrix} \underset{\sim}{f}(\underset{\sim}{v},\underset{\sim}{\lambda},\underset{\sim}{c}) \\ \underset{\sim}{g}(\underset{\sim}{v},\underset{\sim}{\lambda}) \end{Bmatrix} = \begin{Bmatrix} \underset{\sim}{P} \\ \underset{\sim}{\delta} \end{Bmatrix} . \tag{A.1}$$

That is, the equations contained one experimental measurement (equation in $\underset{\sim}{g}$) for each material degree of freedom (element of $\underset{\sim}{c}$). In this appendix we shall examine some examples in which the material functions are discretized with respect to spatial variables; that is, we shall let

$$c_i(x,y) \doteq \sum_{j=1}^{n} c_j \phi_j(x,y) . \tag{A.2}$$

In Appendix B we shall examine several examples in which the material is discretized with respect to strain invariants:

$$c_i(I_1,I_2) \doteq \sum_{j=1}^{n} c_j \phi_j(I_1,I_2) . \tag{A.3}$$

For this experiment a sheet of isotropic, incompressible elastic material was subjected to the loading and boundary conditions shown below in Figure A.1.

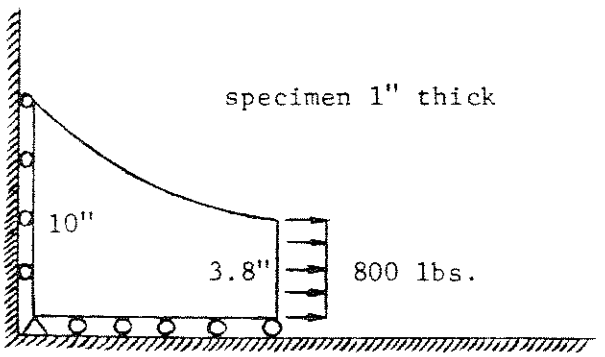

Fig. A.1

The experiment was modelled using the plane stress assumptions and a 16 element finite element mesh, as shown in Figure A.2.

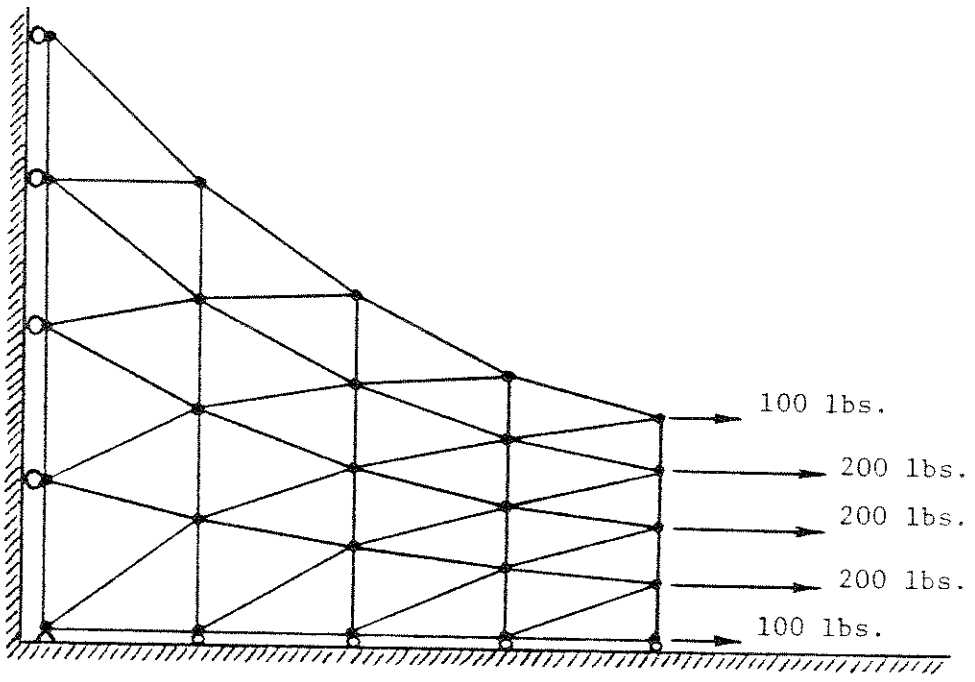

Fig. A.2

The experimental measurements used as input were obtained by solving this 16 element model in the forward direction using

$$C_1(I_1, I_2) = 80\, e^{0.25(I_1-3)} \text{ psi.} \qquad \text{(A.4a)}$$

and

$$C_2(I_1, I_2) = 20 \text{ psi.} \qquad \text{(A.4b)}$$

and choosing the 18 measurements diagrammed in Figure A.3. Therefore, all errors due to the coarseness of the finite element mesh are automatically avoided in this test example. However, a comparison of the 8 element solution with the 16 element solution shows a maximum difference in displacements of 0.02 inch, so even this simple 16 element model is very close to the continuous solution.

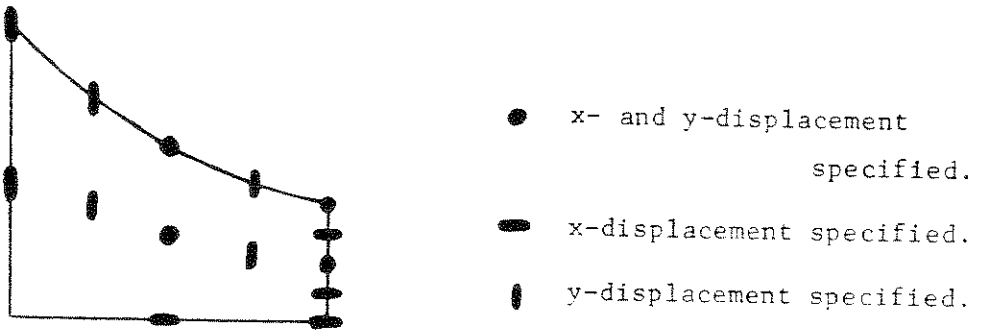

Fig. A.3

The material mesh indicated in Figure A.4 was chosen for both $C_1(x,y)$ and $C_2(x,y)$ to best utilize the 18 degrees of freedom permitted by the 18 measurements specified. In Figure A.5 the

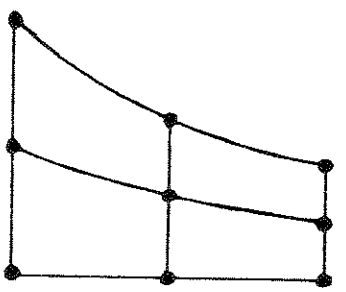

Fig. A.4

undeformed and deformed shapes of the experiment are compared.

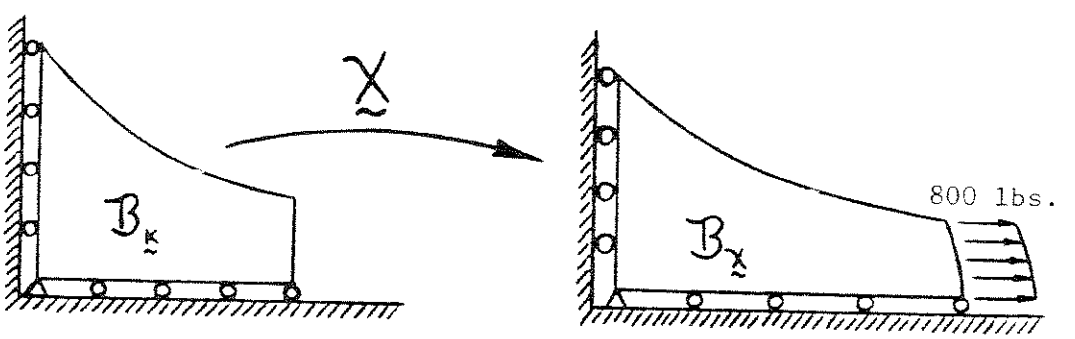

Fig. A.5

Strains vary from almost zero to 54%. The strain invariants I_1 and I_2 vary from 3.01 to 3.46, as shown in Figure A.6.

To start the iterative solution process an initial guess

$$C_1(I_1, I_2) = 100 \text{ psi.}$$
$$C_2(I_1, I_2) = 0 \text{ psi.} \qquad (A.5)$$

was used. Then the forward-direction solution required the inversion of a system of 75 nonlinear equations to get a starting point $\underset{\sim}{U}_o$ and $\underset{\sim}{C}_o$ for the inverse problem. This inverse problem required 5 Newton-Raphson iterations upon a set of 93 nonlinear equations. Almost a minute of CDC 6400 computer time was needed.

For the first solution attempt the 18 input measurements were exact and without experimental error. Nevertheless, the sensitivity of this method of solution was so great that convergence was not obtained; apparently no solution $\{\underset{\sim}{U}, \underset{\sim}{\lambda}, \underset{\sim}{C}\}$ was capable of satisfying all 93 equations. However, both the second and third iterates almost balance the equations, so the resulting identifications are plotted in Figures A.7 and A.8. When the data from both iterations are combined (Figure A.9) and a curve passed through the distribution by some averaging process (such as a least squares technique), it is possible to identify the two material functions with reasonable accuracy.

Two other attempts were made to solve the problem. One used input measurement data rounded off to 0.01 inch, and the other used input data rounded off to 0.001 inch. Immediate divergence was the result in both cases and absolutely no information about the material functions was obtained.

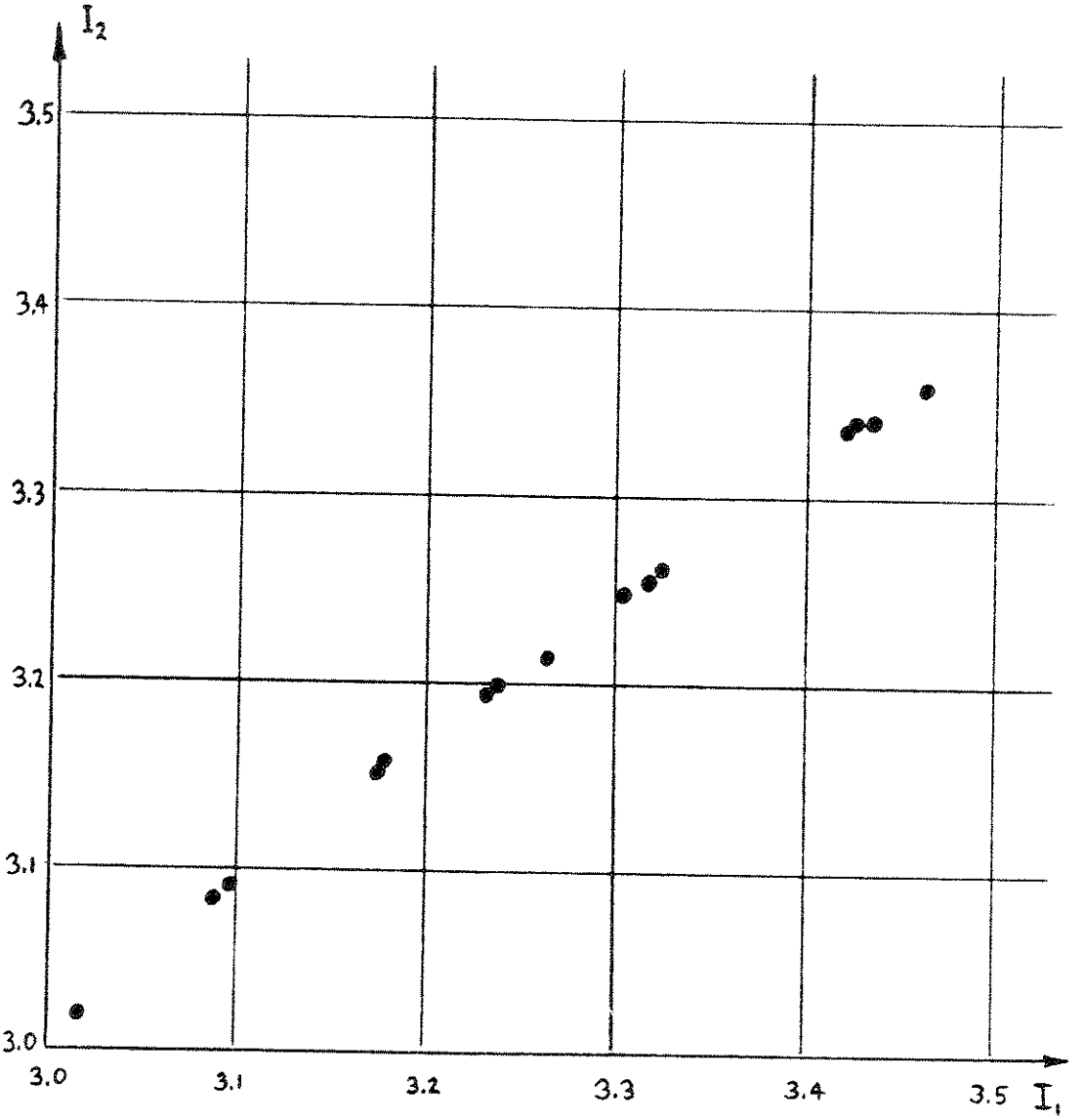

DOMAIN OF MATERIAL OPERATOR

(VALUE OF (I_1, I_2) IN EACH ELEMENT OF THE BODY)

Fig. A.6

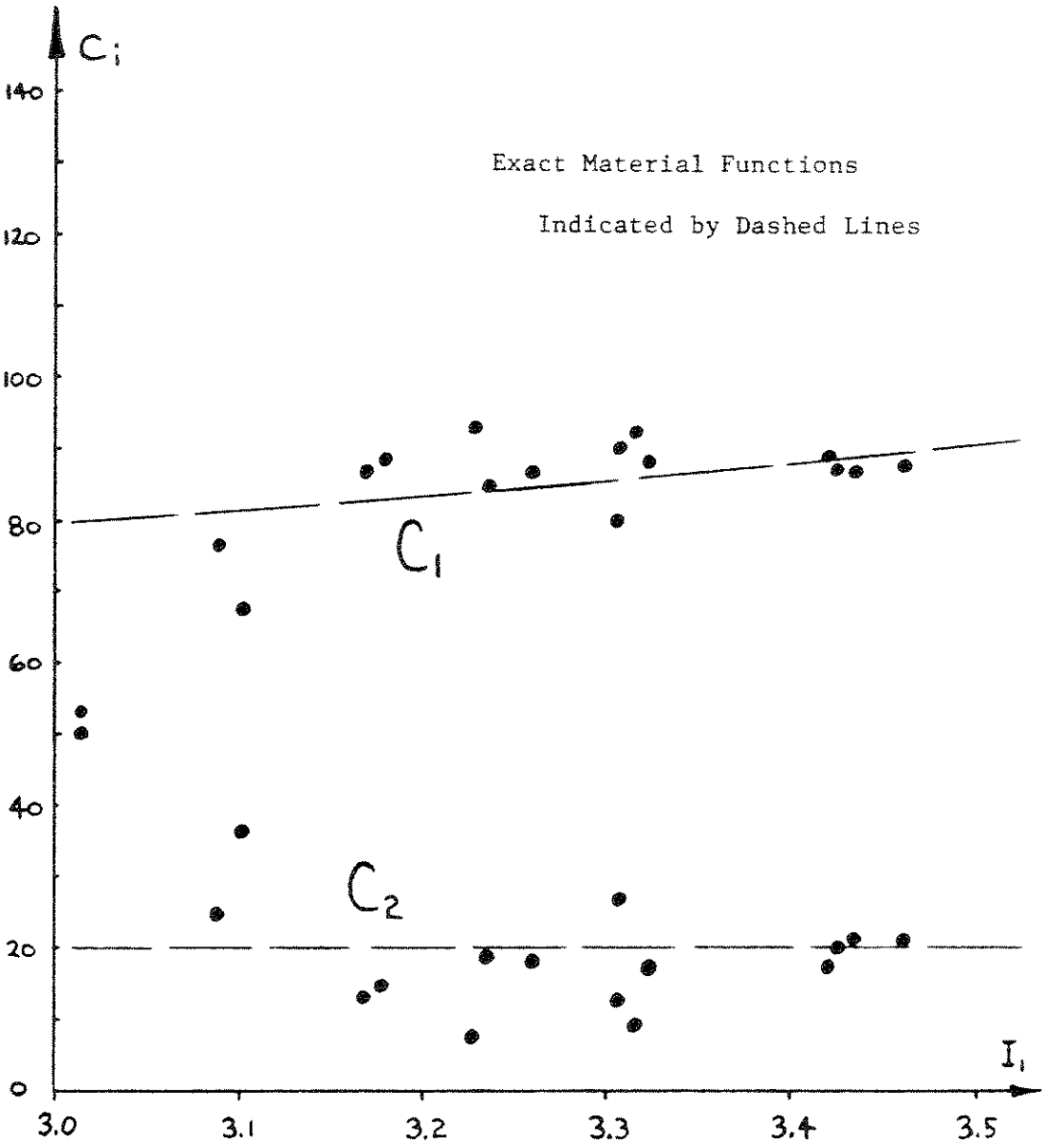

MATERIAL IDENTIFICATION OF

SECOND ITERATION

Fig. A.7

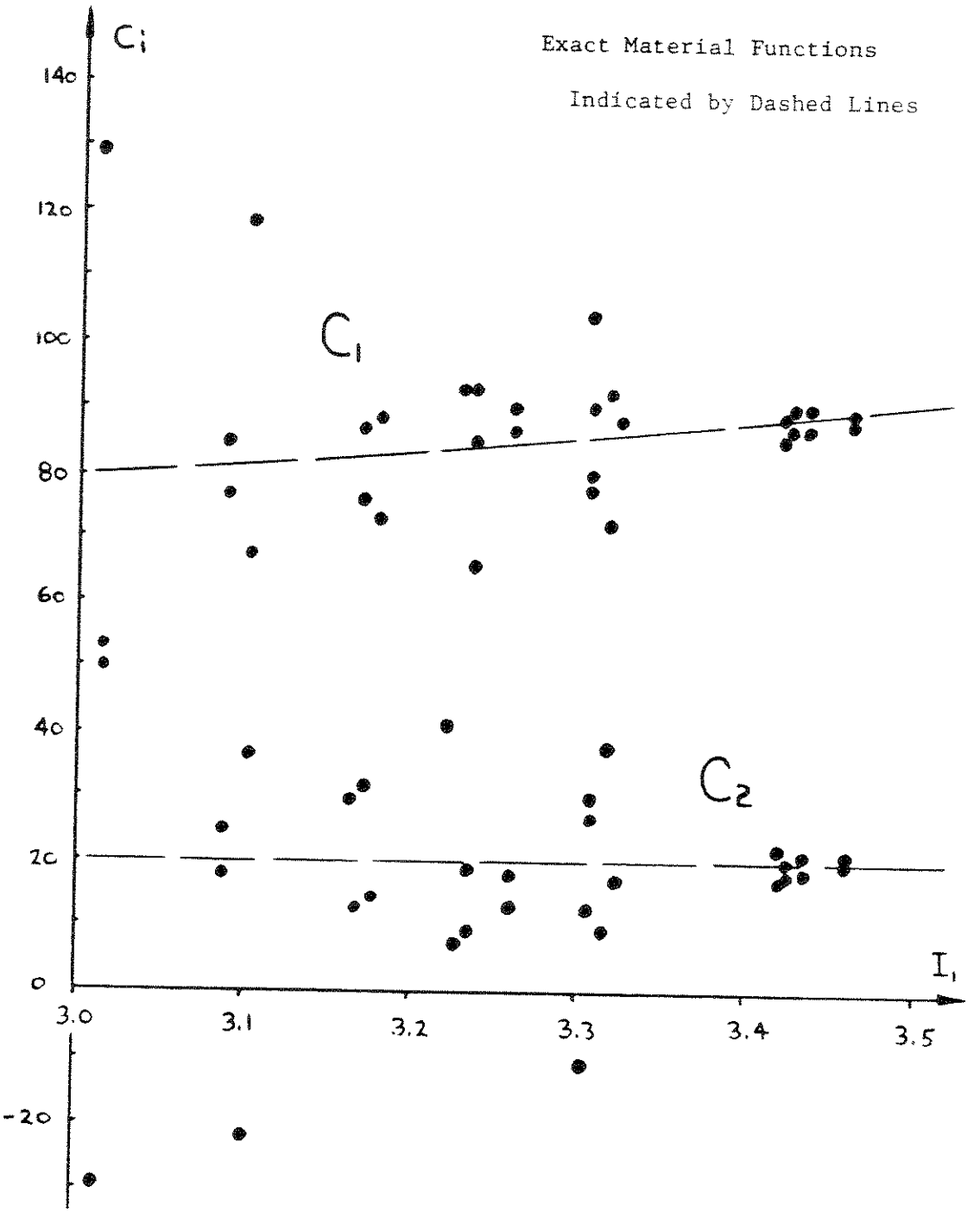

MATERIAL IDENTIFICATION RESULTING FROM

COMBINING SECOND AND THIRD ITERATIONS

Fig. A.9

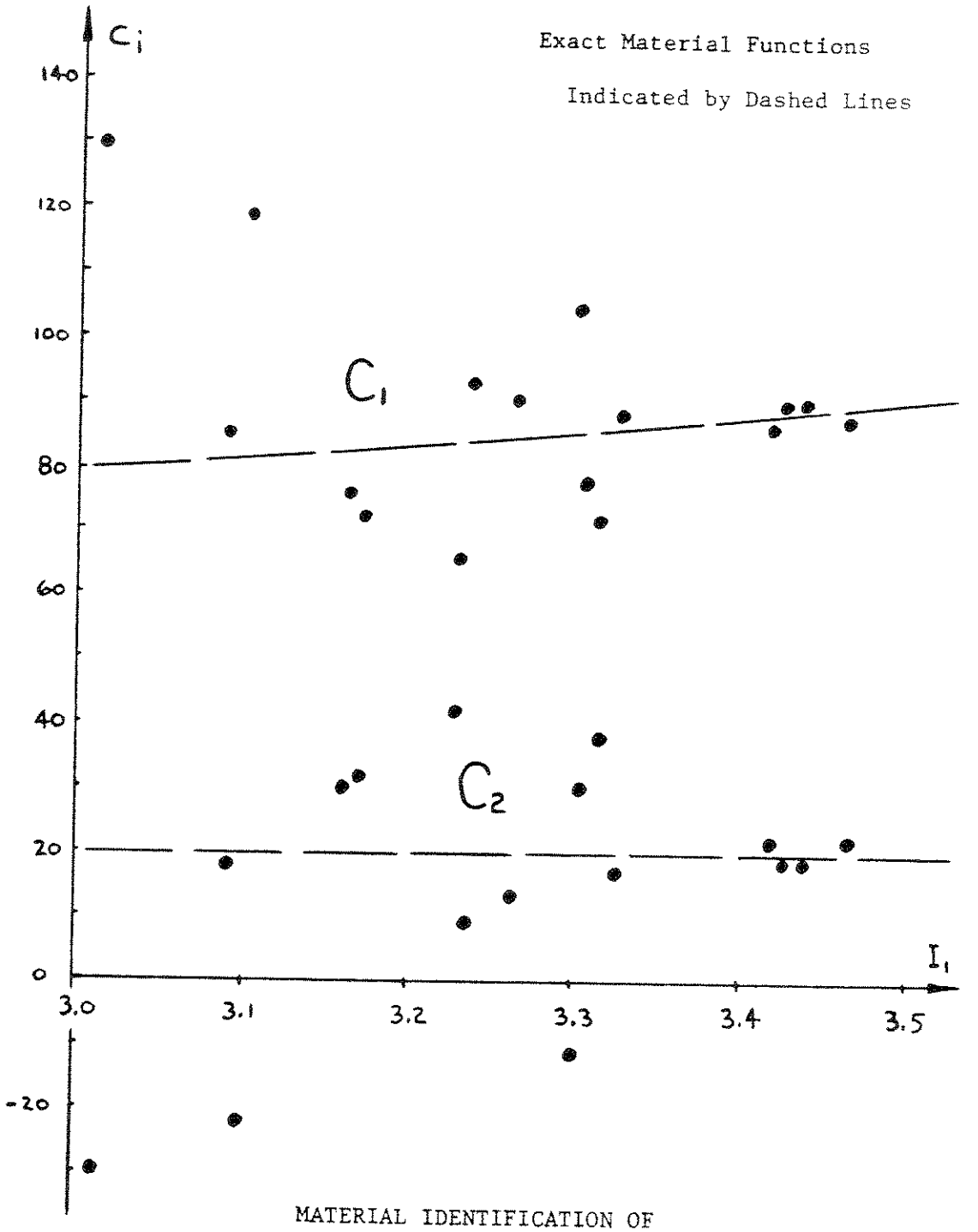

MATERIAL IDENTIFICATION OF

THIRD ITERATION

Fig. A.8

Although it is true that the spatial discretization technique could be tested on less sensitive examples and perhaps good identifications somehow obtained, the conclusion reached by comparing the results of this appendix with the results in Appendix B is that spatial discretization leads to unstable solutions and is not as promising an approach to material identification algorithms as the direct discretization of $C_i(I_1, I_2)$. This is especially apparent when experimental errors are introduced into the input data.

APPENDIX B

In this appendix we shall examine a number of examples of material identification in which the material functions are discretized with respect to strain invariants. All the examples here lead to a determinate set of equations which are solved directly without benefit of a least squares algorithm.

B.1 16 Element Example

Let us resolve the example of Appendix A (discretization applied to $C_i(x,y)$) by discretizing $C_i(I_1, I_2)$. Refer to Figures A.1 and A.2 for the description of the geometry of the problem. Figure A.6 shows that only a very limited portion of the strain invariant space comes to be used in this particular experiment. Hence a one-dimensional discretization will suffice. For the first material function choose the 4 degrees of freedom indicated in Figure B.1.

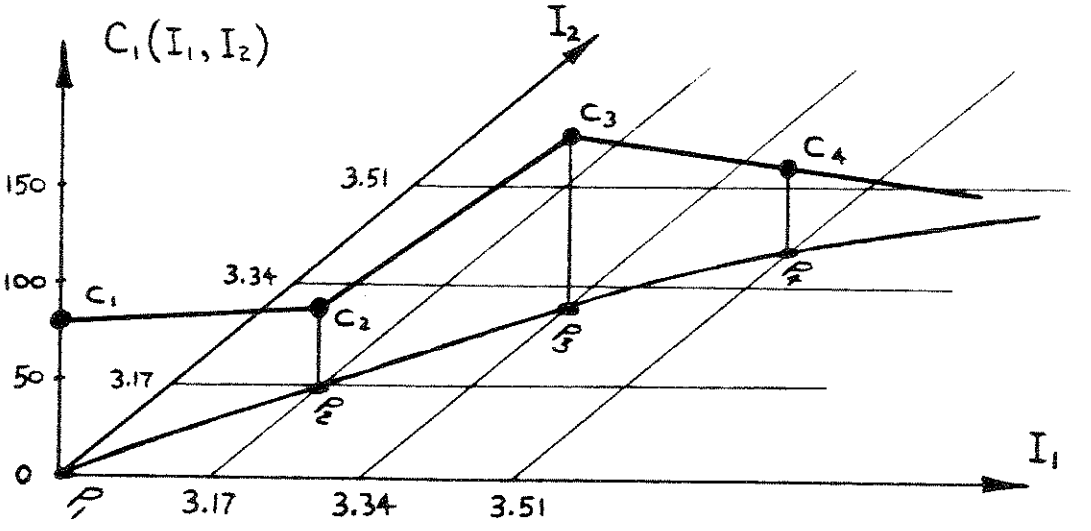

Fig. B.1

That is, the nodes of the discretization for each material function are chosen as follows:

ρ_1 set at $(I_1, I_2) = (3.000, 3.000)$

ρ_2 set at $(I_1, I_2) = (3.167, 3.148)$

ρ_3 set at $(I_1, I_2) = (3.340, 3.275)$

ρ_4 set at $(I_1, I_2) = (3.510, 3.395)$,

with the finite element interpolation functions linear in I_1 and constant in I_2. Let us graphically represent this type of discretization as shown below in Figure B.2.

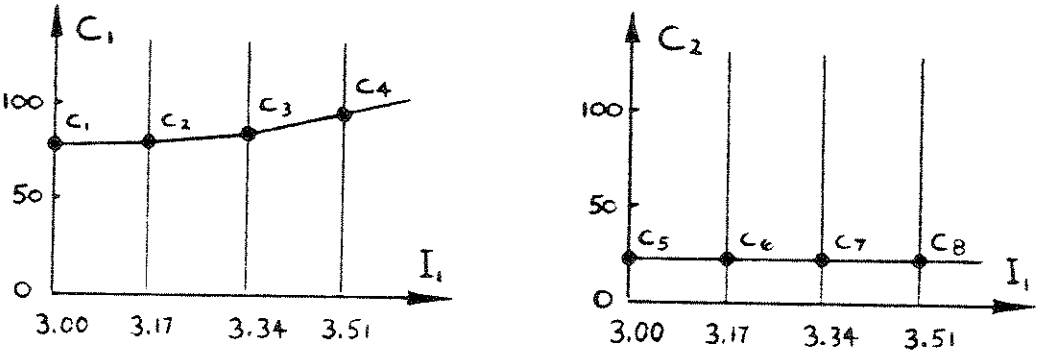

Fig. B.2

Choose the 8 measurements indicated in Figure B.3 to serve as input.

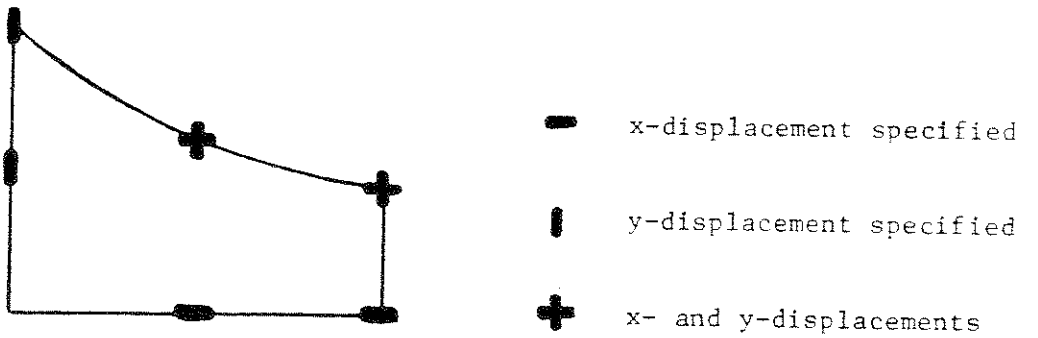

Fig. B.3

The first solution attempt used exact measurements as input data; the resulting identification is plotted in Figure B.4. The second solution attempt used measurements rounded off to 0.001 inch; the resulting identification is plotted in Figure B.5. The third solution attempt used measurements rounded off to 0.01 inch and resulted in divergence; no worthwhile information about the material functions was obtained.

A comparison of Figure B.4 with Figure A.9 shows the superiority of techniques utilizing the direct discretization of $C_i(I_1, I_2)$. This approach guarantees continuity in the material functions and requires fewer material degrees of freedom to closely approximate the material functions. Hence it is far more stable, especially when there is noise in the input data, as there will always be in any real experimental situation.

B.2 36 Element Example

In this section we shall study how different types of discretization choices and different degrees of accuracy in measuring the input data affect the algorithm's ability to identify the material. But to do this an experimental setup less sensitive than the one in Section B.1 must be chosen. We shall use the 36 element rubber sheet described in Appendix D, as illustrated in Figures D.1 through D.3. This experiment avoids the worst sensitivities of the 16 element experiment for the following reasons:

1) The geometric mesh is larger and permits several elements to be located between measurement points, permitting the system

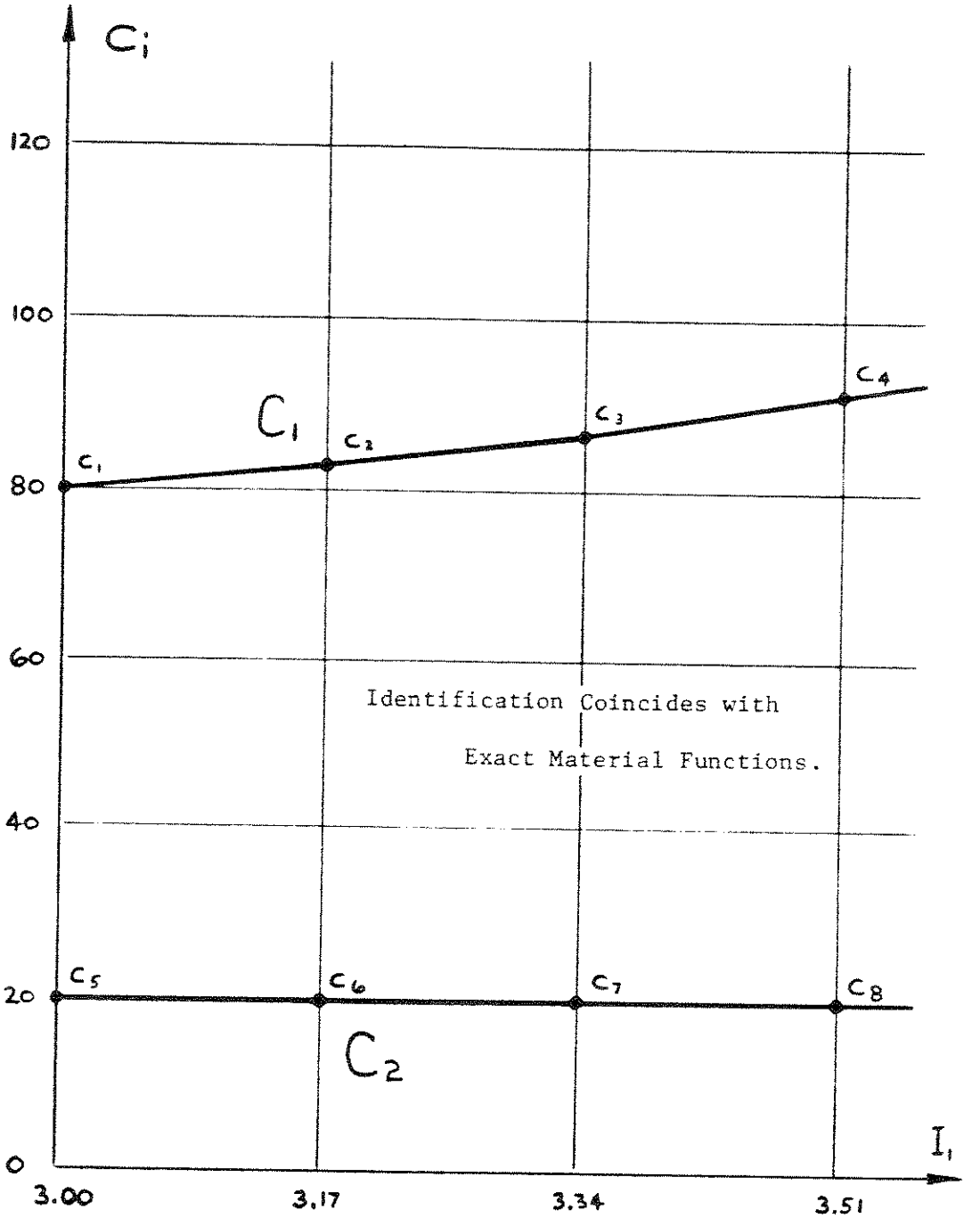

MATERIAL IDENTIFICATION

WITH EXACT INPUT MEASUREMENTS

Fig. B.4

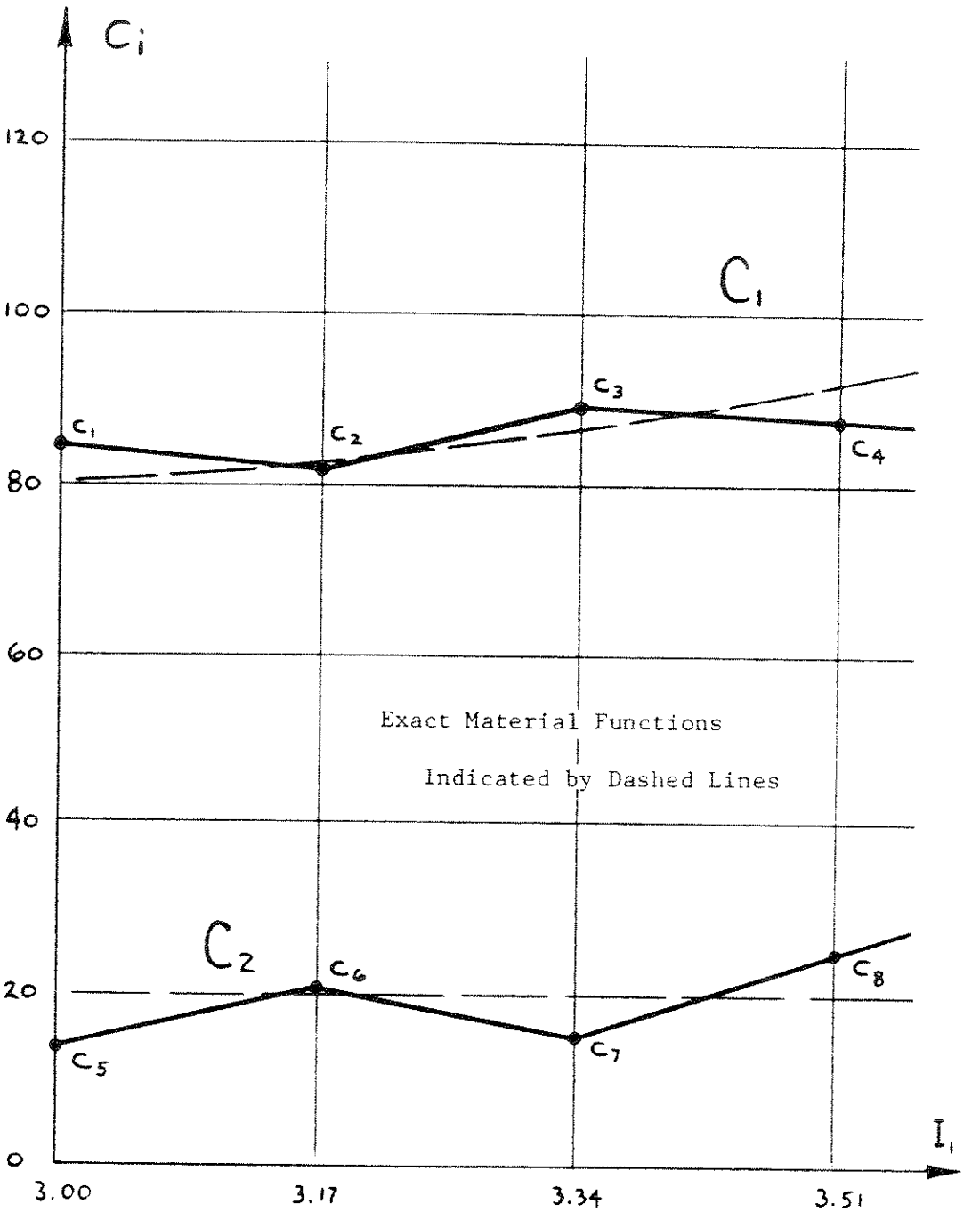

MATERIAL IDENTIFICATION

WITH ALL INPUT MEASUREMENTS ACCURATE TO 0.001"

Fig. B.5

more freedom to adjust itself to experimental inaccuracies in the input data.

2) The measurements used as input are not taken relative to any clamped boundary, but are the relative displacement changes between pairs of nodes far enough away from the clamps to avoid their complications.

3) The whole experiment is in a higher strain range, making the inverse problem less sensitive. No measurements are specified in low strain areas, since any experimental noise in such measurements would give rise to large errors in strain, as was encountered in the 16 element example.

Also, to further stabilize the solution, only one degree of freedom will be permitted in $C_1(I_1, I_2)$. Two different 5 degree-of-freedom discretizations will be tested:

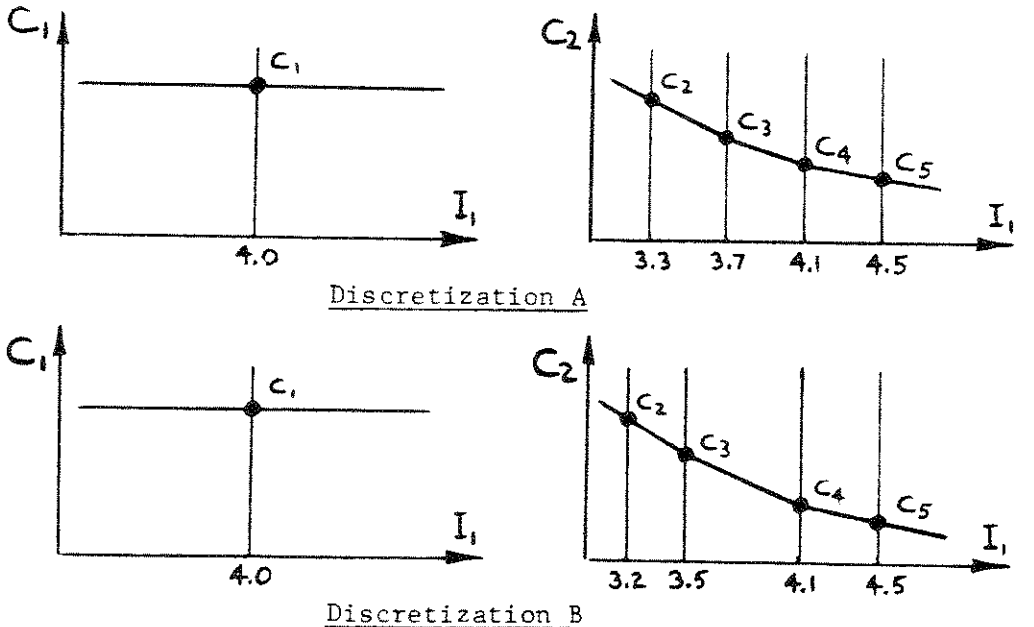

Fig. B.6

Four different input accuracies will be tested:

1) All 5 measurements are exact. This serves as a test of the adequacy of the 5 degree-of-freedom mesh chosen.

2) All 5 measurements are rounded off to the nearest hundredth of an inch. This simulates the kind of input accuracy obtainable from a well conducted experimental situation.

3) One 0.01 inch perturbation is introduced into one of the 5 measurements; the other 4 are rounded off to the nearest hundredth of an inch. This tests the method's sensitivity to larger errors in experimental measuring.

4) Two 0.01 inch perturbations are introduced. This causes even greater inconsistencies in the input data.

These measurements and their locations on the body are shown in Table B.1. The resulting identifications (using an initial guess of $C_1 = 25.0$ psi. and $C_2 = 7.0$ psi.) are tabulated in Table B.2 and plotted in Figures B.7 through B.11. Note that the identifications based on exact input data are not plotted, since they correspond almost exactly to the true material functions. Note also that for discretization A the fourth input case resulted in divergence, but to show the kind of information obtainable from such a situation, the first four iterates are shown in Figure B.9. The third iteration comes closest to satisfying the system of equations, so it would serve best as a material identification.

Both discretization schemes result in good identifications

Numbered points identify nodes of 36 element geometric mesh.

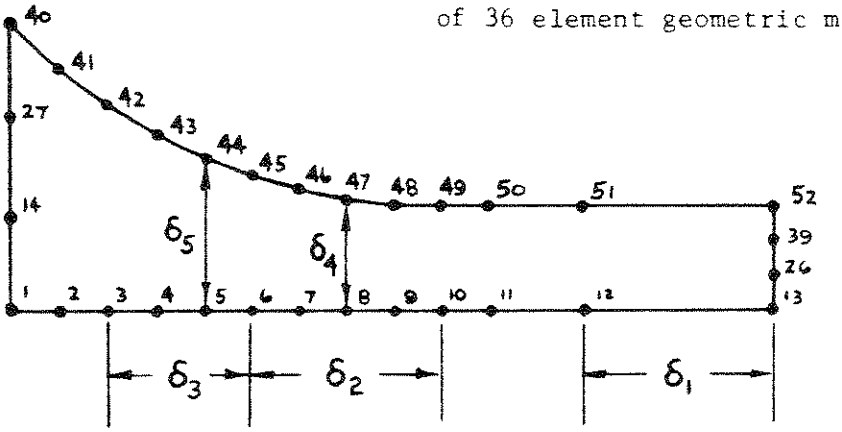

Locations of the 5 Input Measurements Chosen

$$\delta_1 = U_{13} - U_{12} \qquad \delta_2 = U_{10} - U_6 \qquad \delta_3 = U_6 - U_3$$

$$\delta_4 = V_{47} - V_8 \qquad \delta_5 = V_{44} - V_5$$

Case 1: Exact Measurements Used as Input Data.
Case 2: Measurements of 0.01" Accuracy Used as Input Data.
Case 3: One 0.01" Perturbation (at δ_3) in Input Data.
Case 4: Two 0.01" Perturbations (at δ_3 and δ_5) in Input Data.

Measurement Location	Input Measurements Used to Obtain Solution			
	case 1	case 2	case 3	case 4
δ_1	4.26483	4.26	4.26	4.26
δ_2	3.52194	3.52	3.52	3.52
δ_3	1.59771	1.60	1.61	1.61
δ_4	-0.68358	-0.68	-0.68	-0.68
δ_5	-0.58296	-0.58	-0.58	-0.59

INPUT DATA FOR 36 ELEMENT EXAMPLE

Table B.1

MATERIAL DISCRETIZATION CHOICE	ACCURACY OF INPUT MEASUREMENTS (see Table B.1)	MATERIAL IDENTIFICATION				
		C_1	C_2	C_3	C_4	C_5
A	Case 1: exact input	25.00	8.33	6.54	5.33	4.31
	Case 2: 0.01" accuracy	25.59	7.78	5.02	4.61	3.24
	Case 3: one 0.01" perturbation	25.16	8.64	4.73	5.73	4.04
	Case 4: two 0.01" perturbations	-	- DIVERGENCE		-	-
B	Case 1: exact input	25.00	8.70	7.44	5.33	4.31
	Case 2: 0.01" accuracy	25.78	8.66	5.48	4.16	2.89
	Case 3: one 0.01" perturbation	25.92	7.85	5.87	3.75	2.62
	Case 4: two 0.01" perturbations	25.44	11.61	4.58	5.09	3.53

Discretization A: Constant C_1 and 4 degrees of freedom in C_2 (nodes at I_1 =3.3, 3.7, 4.1, and 4.5)

Discretization B: Constant C_1 and 4 degrees of freedom in C_2 (nodes at I_1 =3.2, 3.5, 4.1, and 4.5)

36 ELEMENT EXAMPLE: MATERIAL IDENTIFICATIONS RESULTING FROM DIRECT SOLUTION OF DISCRETIZED EQUATIONS.

Table B.2

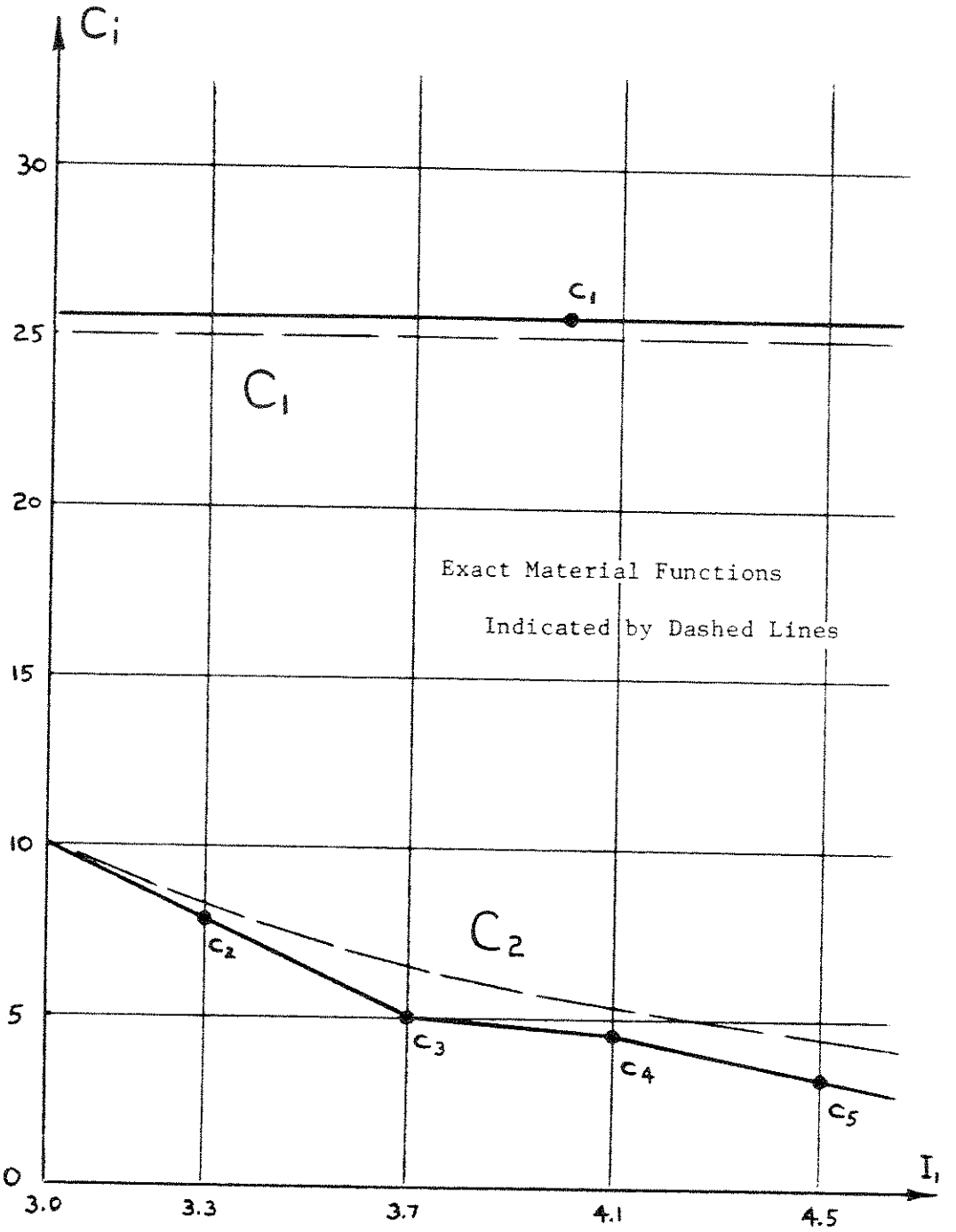

36 ELEMENT MATERIAL IDENTIFICATION EXAMPLE

MATERIAL DISCRETIZATION CASE A - INPUT MEASUREMENT CASE 2

Fig. B.7

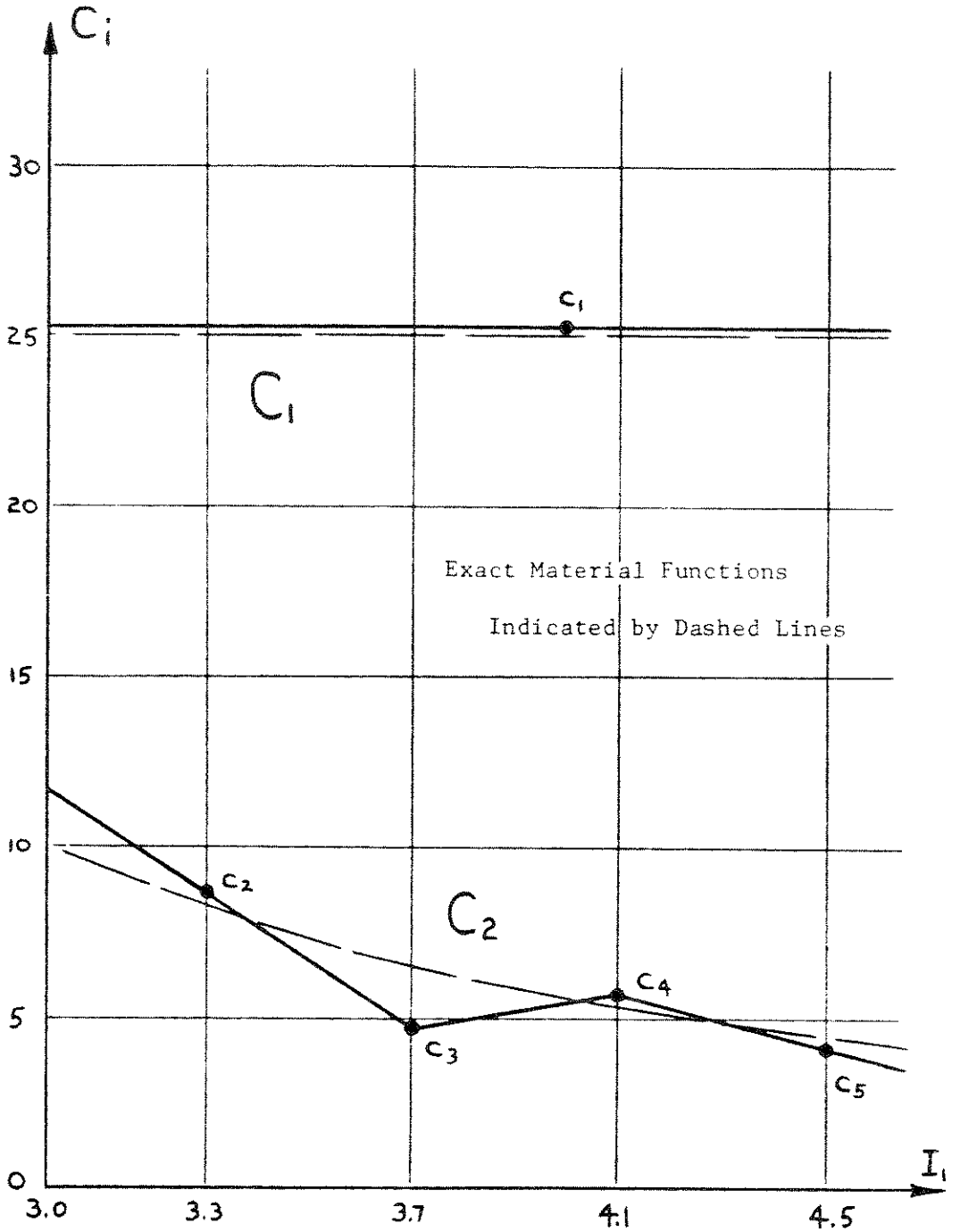

36 ELEMENT MATERIAL IDENTIFICATION EXAMPLE

MATERIAL DISCRETIZATION CASE A - INPUT MEASUREMENT CASE 3

Fig. B.8

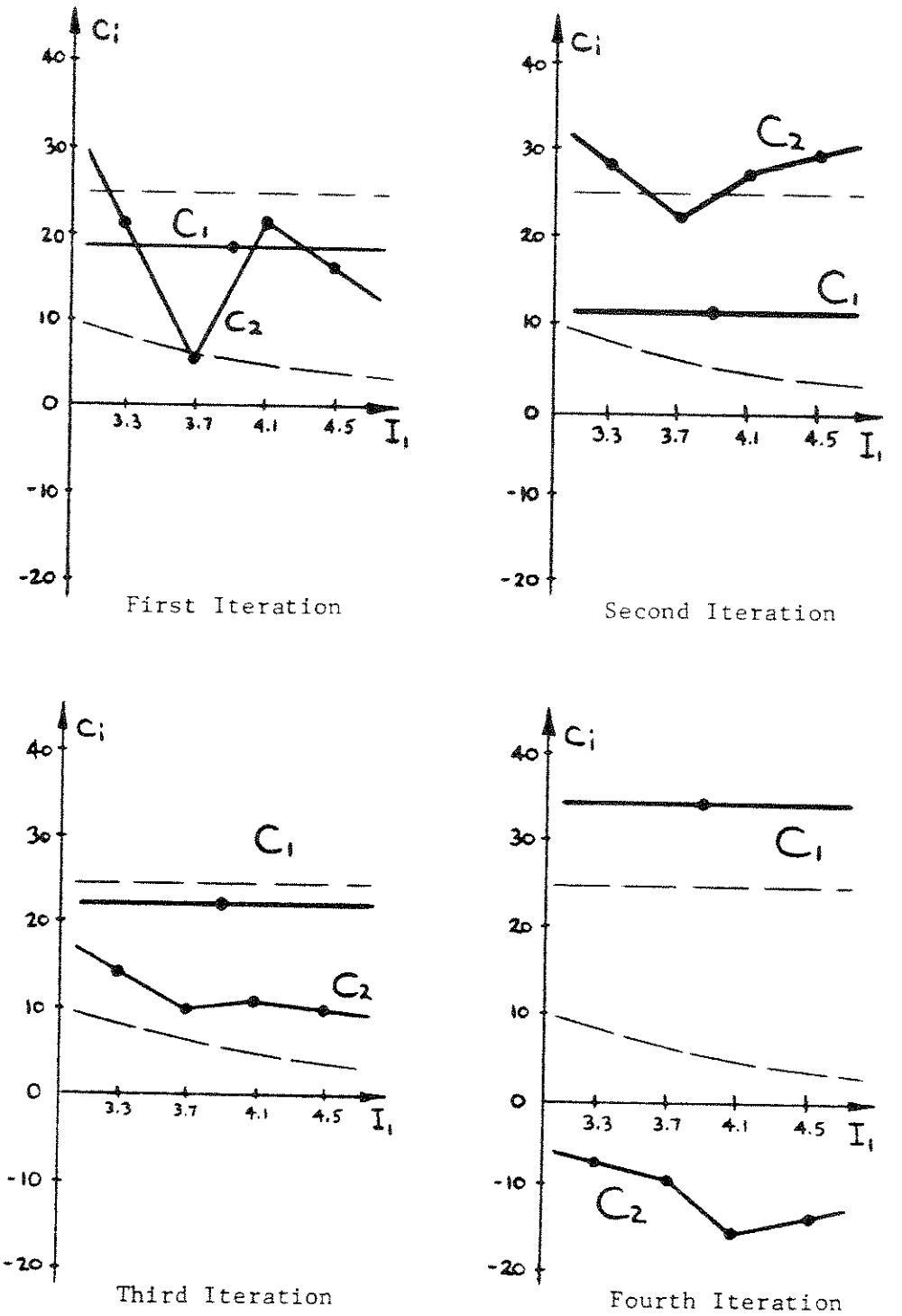

36 ELEMENT MATERIAL IDENTIFICATION EXAMPLE

MATERIAL DISCRETIZATION CASE A - INPUT MEASUREMENT CASE 4

Fig. B.9

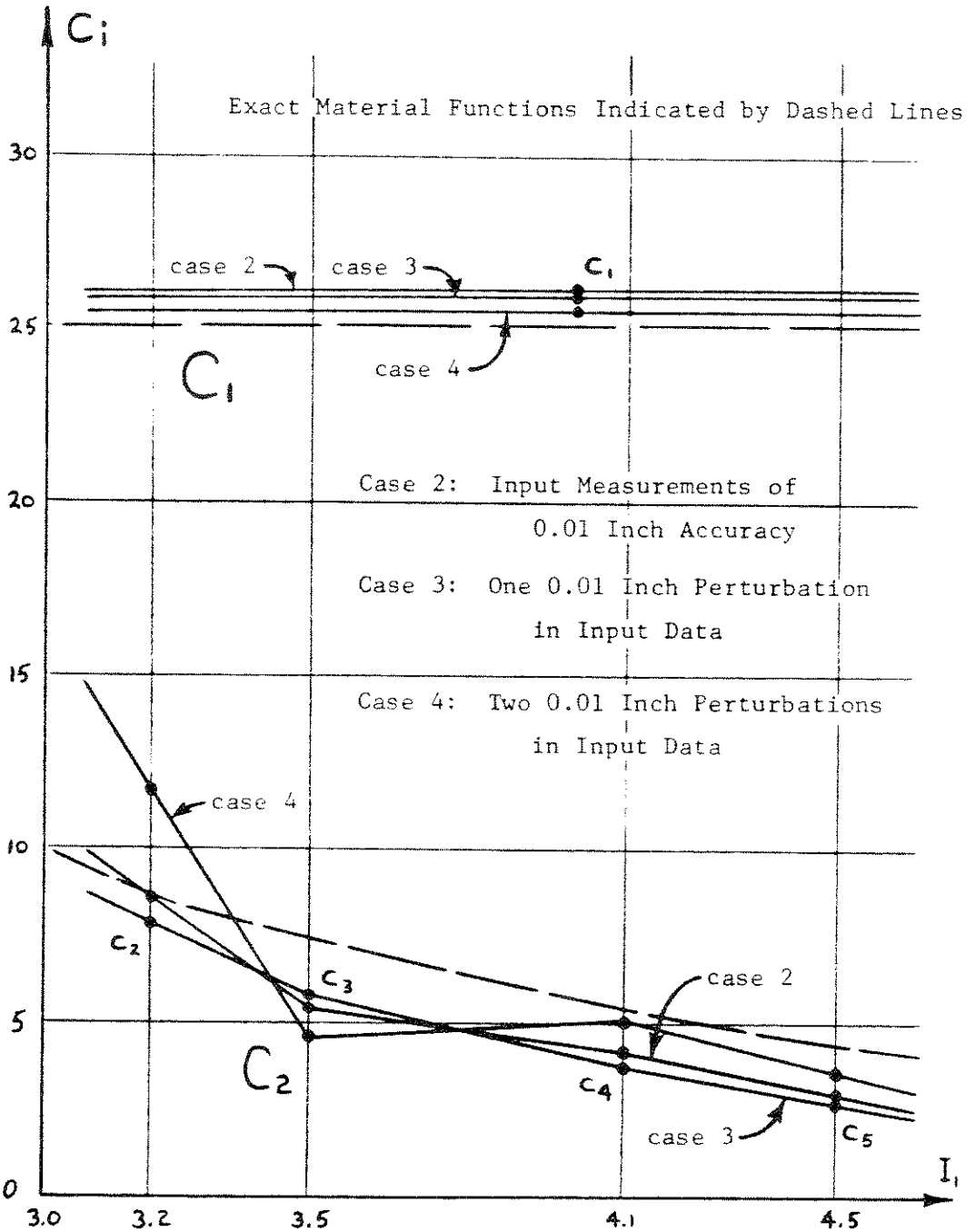

36 ELEMENT MATERIAL IDENTIFICATION EXAMPLE

MATERIAL DISCRETIZATION CASE B

Fig. B.10

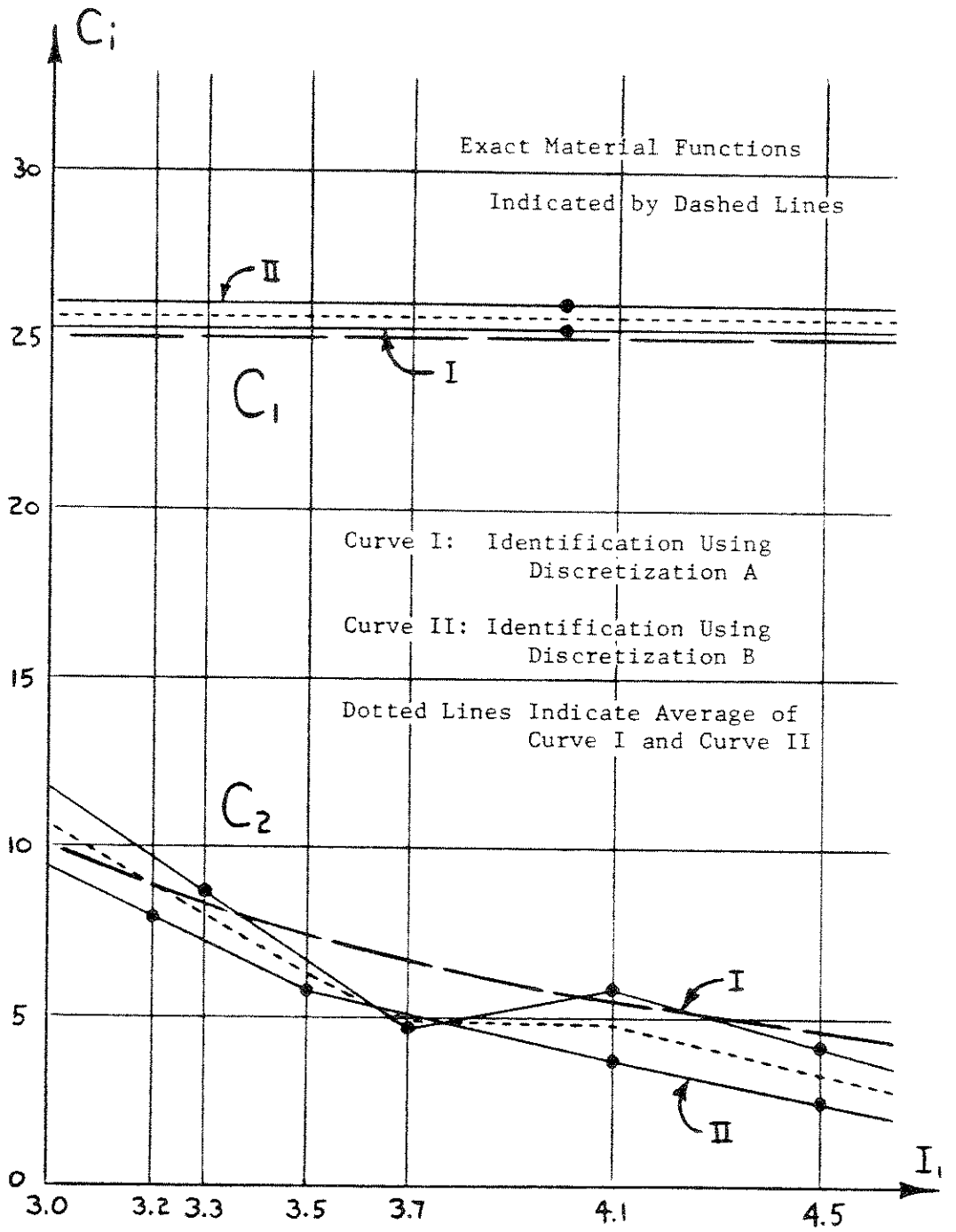

36 ELEMENT MATERIAL IDENTIFICATION EXAMPLE

INPUT MEASUREMENT CASE 3 - PERTURBATION AT δ_3

Fig. B.11

if accurate input data are used. However, if any significant inaccuracies exist in the measurements discretization B is much less likely to give unstable solutions. To understand the cause of this instability, examine the strain invariant range in the vicinity of each input measurement, as shown in Figure B.12.

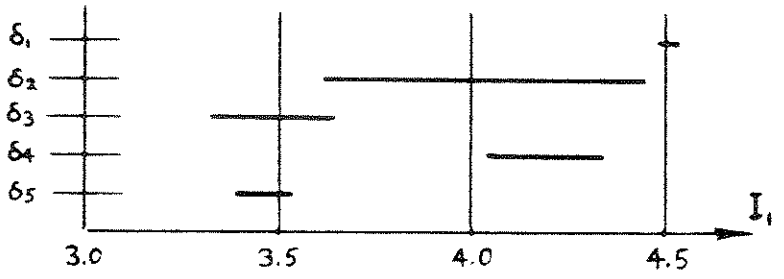

Fig. B.12

Compare the average value of each of these strain invariant ranges (which represent the five places in the I_1 domain where information about the material properties is given the algorithm) with the nodal points of the discretizations for C_2 :

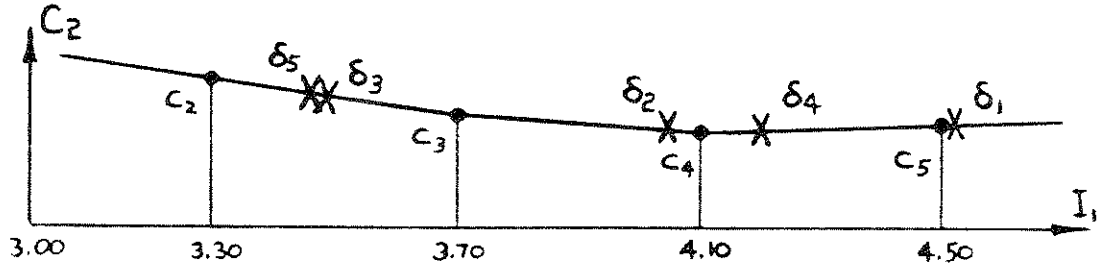

Discretization A

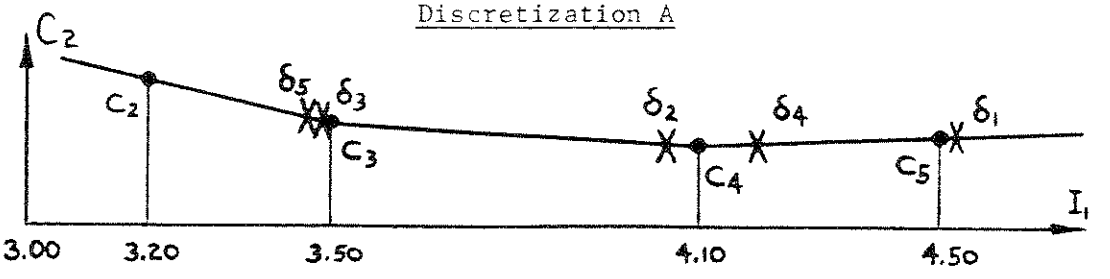

Discretization B

Fig. B.13

Note that much vacillation is possible in the solutions of discretization A, since the nodes corresponding to parameters C_2 and C_3 are not close to the areas where input data pins down the material solution. Hence considerable changes in the values of C_2 and C_3 are possible without much affecting the value the material function assumes at the points where data from the experimental measurements exists. This brings about an unstable situation; the system is too flexible and tends to diverge or find a physically unreasonable solution if it tries to adjust itself to inconsistencies in the input data. Discretization scheme B is much more appropriate for this particular system of input measurements; stable solutions result, as in Figure B.10, even for the poorest input data case.

Note how sensitive the identified material functions are to very small errors in input data, especially when there is just one item of input for each degree of freedom in the material discretization. Figure B.11 shows the identification for the third data case (0.01 inch perturbation introduced at δ_3) obtained by averaging the results from both discretization schemes. The I_1 range of measurement δ_3 is 3.35 - 3.65. The perturbed measurement is slightly larger than the actual measurement; hence it would be expected that in the range $3.35 < I_1 < 3.65$ the identification would indicate a less rigid material. The curve in Figure B.11 confirms this expectation. This behavior is a result of the extreme sensitivity of this type of inverse problem and can be overcome only by extremely accurate input measurements or the use of a method which reduces noise in the input data.

APPENDIX C

C.1 Sensitivity of Least Squares Method to Experimental Errors

In Chapter IV was discussed a material identification algorithm based on a least squares solution to the nonlinear equations describing the discretized problem. In this appendix this least squares algorithm will be tested on a large group of identification problems.

The experimental body to be considered is a rubber sheet loaded and supported as shown below in Figure C.1.

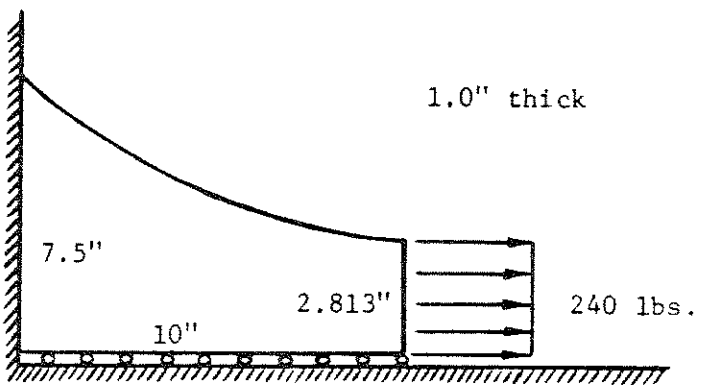

Fig. C.1

To describe this experiment the plane stress finite element model shown in Figure C.2 is used. To generate input data a Rivlin-Saunders material description is assumed. The particular material functions used are

$$C_1(I_1, I_2) = 25 \text{ psi.}$$
$$C_2(I_1, I_2) = 10\left(1 - \tfrac{5}{7}(I_2 - 3) + \tfrac{1}{7}(I_2 - 3)^2\right) \text{ psi.} \qquad (C.1)$$

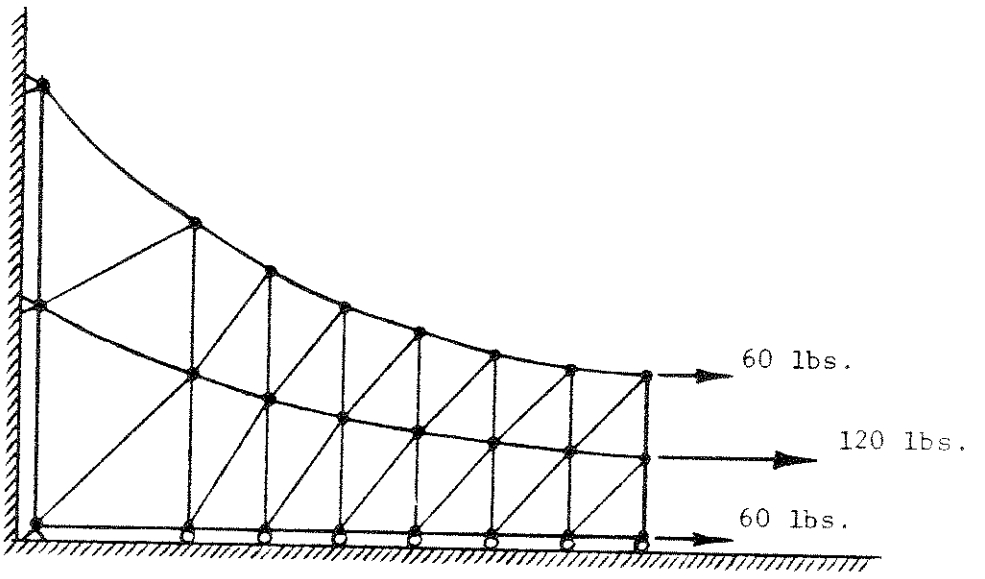

Fig. C.2

Solving the forward-direction boundary value problem using material functions (C.1) determines the full set of nodal displacements. From this the displacement which would be measured experimentally between any two nodes can be determined. For the first series of tests the eight measurement locations indicated in Figure C.3 were chosen.

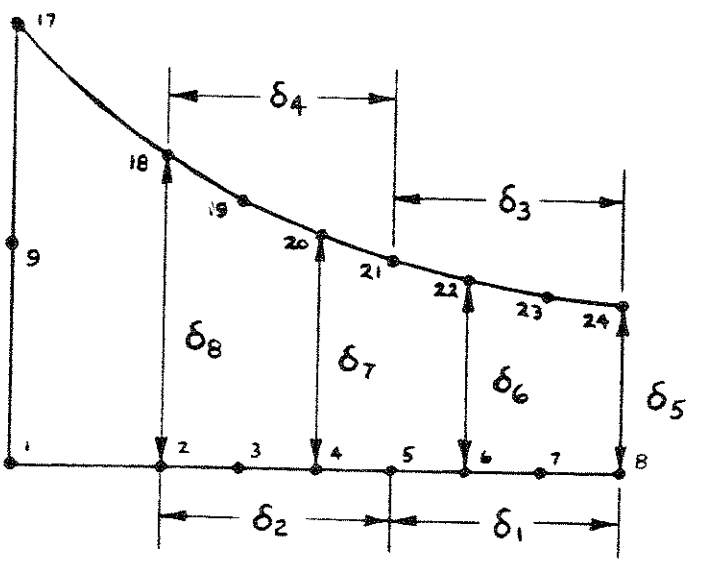

Fig. C.3

That is,

$$\begin{aligned}
\delta_1 &= u_8 - u_5 = 2.5415 \text{ in.} \\
\delta_2 &= u_5 - u_2 = 1.5896 \text{ in.} \\
\delta_3 &= u_{24} - u_{21} = 2.7963 \text{ in.} \\
\delta_4 &= u_{21} - u_{18} = 1.4641 \text{ in.} \\
\delta_5 &= v_{24} - v_8 = -0.6363 \text{ in.} \\
\delta_6 &= v_{22} - v_6 = -0.6537 \text{ in.} \\
\delta_7 &= v_{20} - v_4 = -0.5833 \text{ in.} \\
\delta_8 &= v_{18} - v_2 = -0.4126 \text{ in.}
\end{aligned} \tag{C.2}$$

where u_i is the x-displacement of node i and v_i is the y-displacement of node i. Note that in an actual experimental situation $u_i - u_j$ is simply the x-coordinate of the measured distance between node i and node j on the loaded test specimen minus the x-coordinate of the measured distance between node i and node j on the unloaded test specimen.

A four degree-of-freedom discretization was chosen for the material functions, as shown below in Figure C.4.

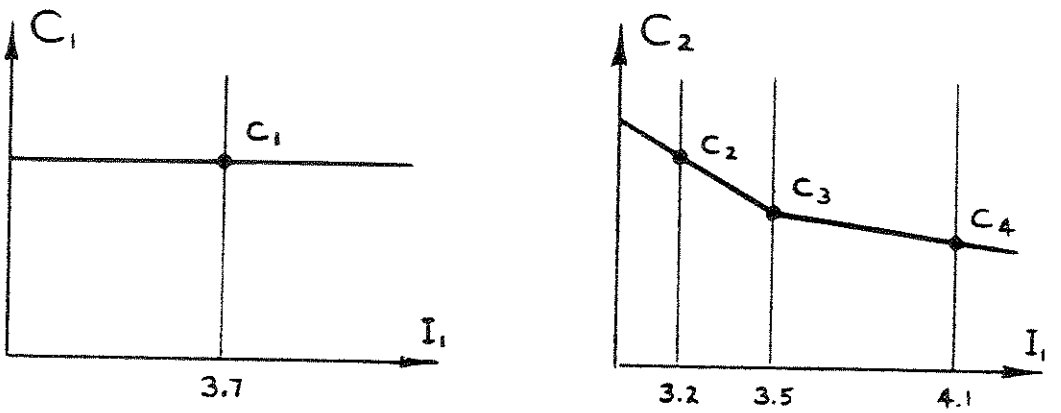

Fig. C.4

Hence this example results in the nonlinear equations

$$\begin{Bmatrix} \underset{\sim}{f}(\underset{\sim}{U},\underset{\sim}{\lambda},\underset{\sim}{C}) \\ \underset{\sim}{g}(\underset{\sim}{U},\underset{\sim}{\lambda}) \end{Bmatrix} = \begin{Bmatrix} \underset{\sim}{P} \\ \underset{\sim}{\delta} \end{Bmatrix} \tag{C.3}$$

a system of 60 equations (48 equilibrium equations, 14 incompressibility equations, 8 input measurement equations) in 56 independent variables (48 in $\underset{\sim}{U}$, 14 in $\underset{\sim}{\lambda}$, 4 in $\underset{\sim}{C}$). An approximation of $C_1(I_1, I_2)$ = 25 psi. and $C_2(I_1, I_2)$ = 7 psi. was used to start the Newton-Raphson iteration procedure.

The material identification problem was solved with three different sets of input data:

Case A The input measurements $\underset{\sim}{\delta}$ are the exact values determined by solving the forward-direction problem using the finite element mesh in Figure C.2 and the material functions (C.1). This eliminates the possibility of noise in the input measurements; therefore, this input case will test the adequacy of the four degree-of-freedom material discretization.

Case B The input measurements $\underset{\sim}{\delta}$ are rounded off to the nearest hundredth of an inch. This will determine the type of material identification possible using measurements of feasible experimental accuracy as input.

Case C Several large perturbations are introduced into the true value of $\underset{\sim}{\delta}$. Use of this perturbed $\underset{\sim}{\delta}$ will test the algorithm's capability to identify the material when very poor experimental measurements are used as input.

For purposes of comparison, this same test problem was solved without the least squares option. Of course, to avoid

overdetermining the system of equations only four observed input measurements could be used. Two cases were studied:

Case D Input $\underset{\sim}{\delta}$ is rounded off to the nearest hundredth of an inch.

Case E Input $\underset{\sim}{\delta}$ contains the same perturbations as in case C.

The numerical input data and the material identification output for these 5 cases are summarized in Table C.1.

The discretized material functions identified for cases B and C are plotted in Figure C.5. These results clearly show that the least squares approach gives an excellent identification even with very roughly measured input data.

Figure C.6 compares the material identification resulting from a least squares solution with 8 experimental measurements (case B) with the material identification resulting from direct solution with 4 experimental measurements (case D). In both cases the measurements are accurate to 0.01 inch and the identifications are good enough for practical engineering purposes. However, the plot shows that the least squares method gives a far more accurate identification; as is to be expected from the discussion in Chapter IV, the least squares solution is less sensitive to disturbance by rounding errors in the input data. In Figure C.7 the same two methods are compared using even rougher experimental data - rougher than what might be expected from a real experimental situation - and the superiority of the least squares approach is dramatically pointed out. In the direct solution approach (4 measurements, 4 degrees of freedom in the material discretization) any error in any of the 4 experimental

Input Measurement Accuracy		Case A	Case B	Case C	Case D	Case E
INPUT	δ_1	2.5415	2.5400	2.5300	2.5400	2.5300
	δ_2	1.5896	1.5900	1.6200	1.5900	1.6200
	δ_3	2.7963	2.8000	2.8000	-0.6700	-0.6800
	δ_4	1.4641	1.4600	1.4600	-0.5800	-0.5600
	δ_5	-0.6363	-0.6400	-0.6500		
	δ_6	-0.6567	-0.6500	-0.6500		
	δ_7	-0.5833	-0.5800	-0.5600		
	δ_8	-0.4126	-0.4100	-0.4100		
OUTPUT	C_1	25.069	25.030	24.710	25.652	20.909
	C_2	8.701	8.937	10.021	8.391	23.923
	C_3	7.291	7.288	6.823	6.234	7.283
	C_4	5.270	5.324	5.965	4.294	12.931

INPUT AND OUTPUT DATA FOR FIVE TESTS OF MATERIAL IDENTIFICATION ALGORITHM - 14 ELEMENT EXAMPLE

Table C.1

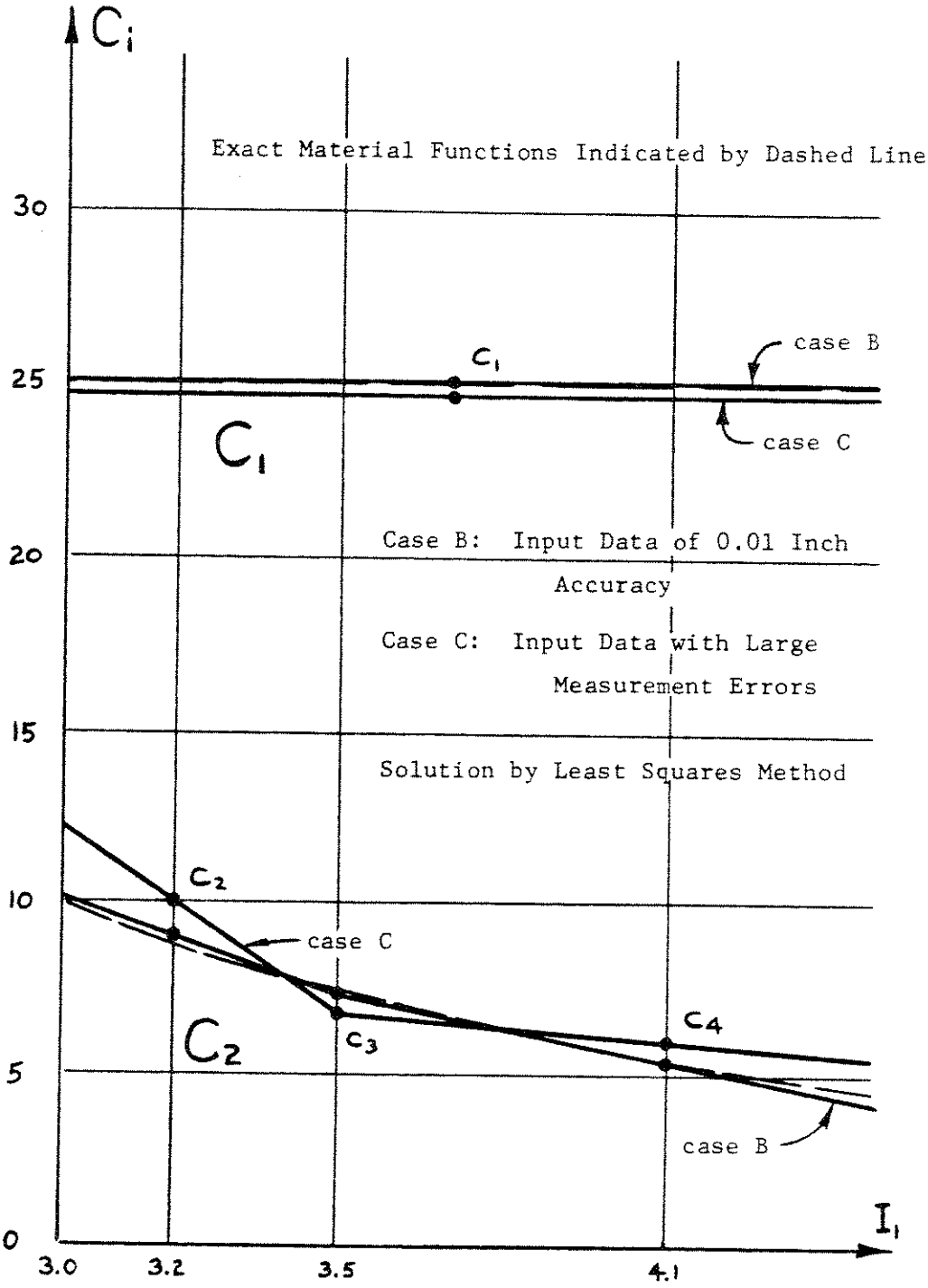

14 ELEMENT MATERIAL IDENTIFICATION EXAMPLE

INPUT DATA CASES B AND C

Fig. C.5

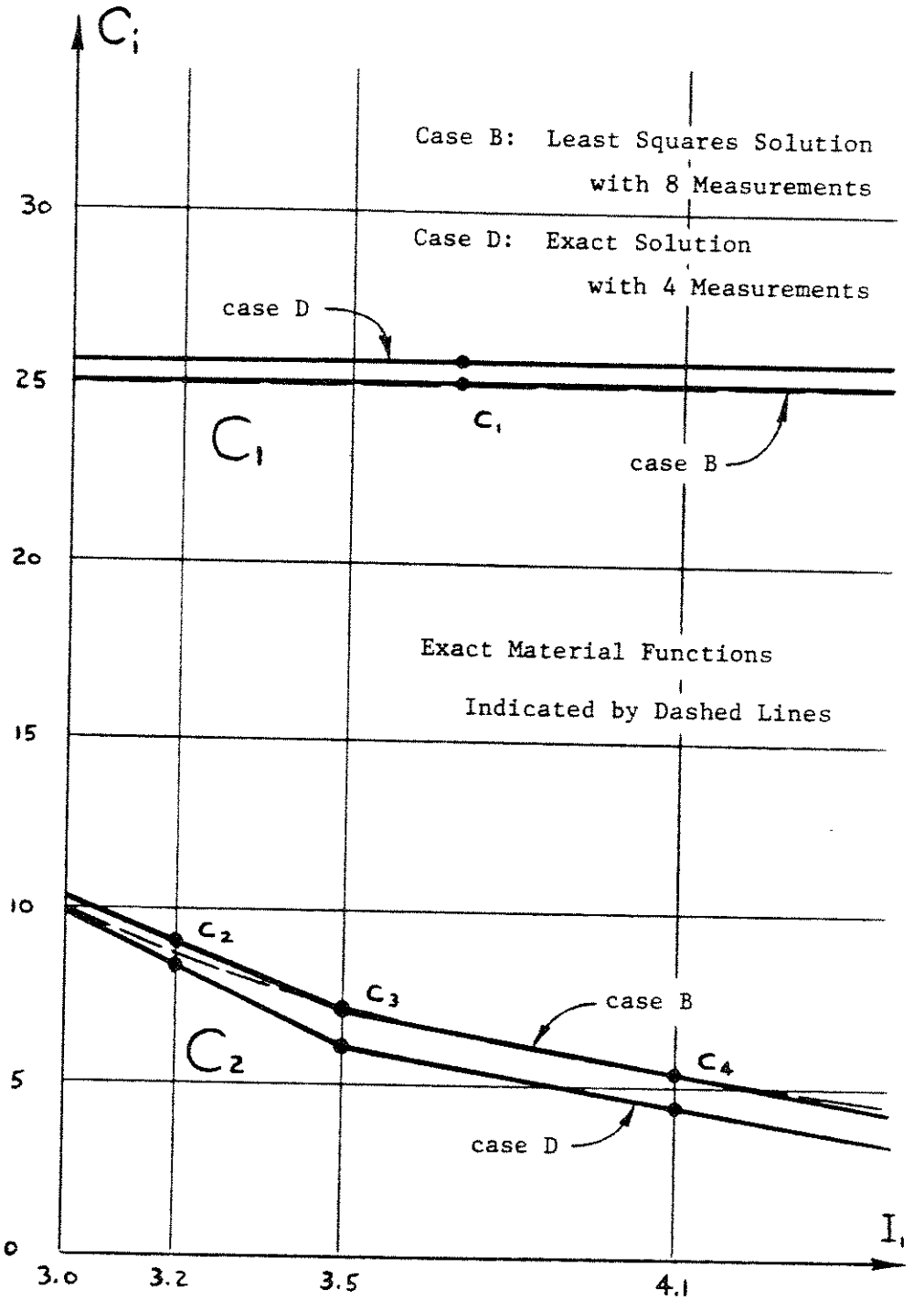

14 ELEMENT MATERIAL IDENTIFICATION EXAMPLE

INPUT DATA OF 0.01 INCH ACCURACY

Fig. C.6

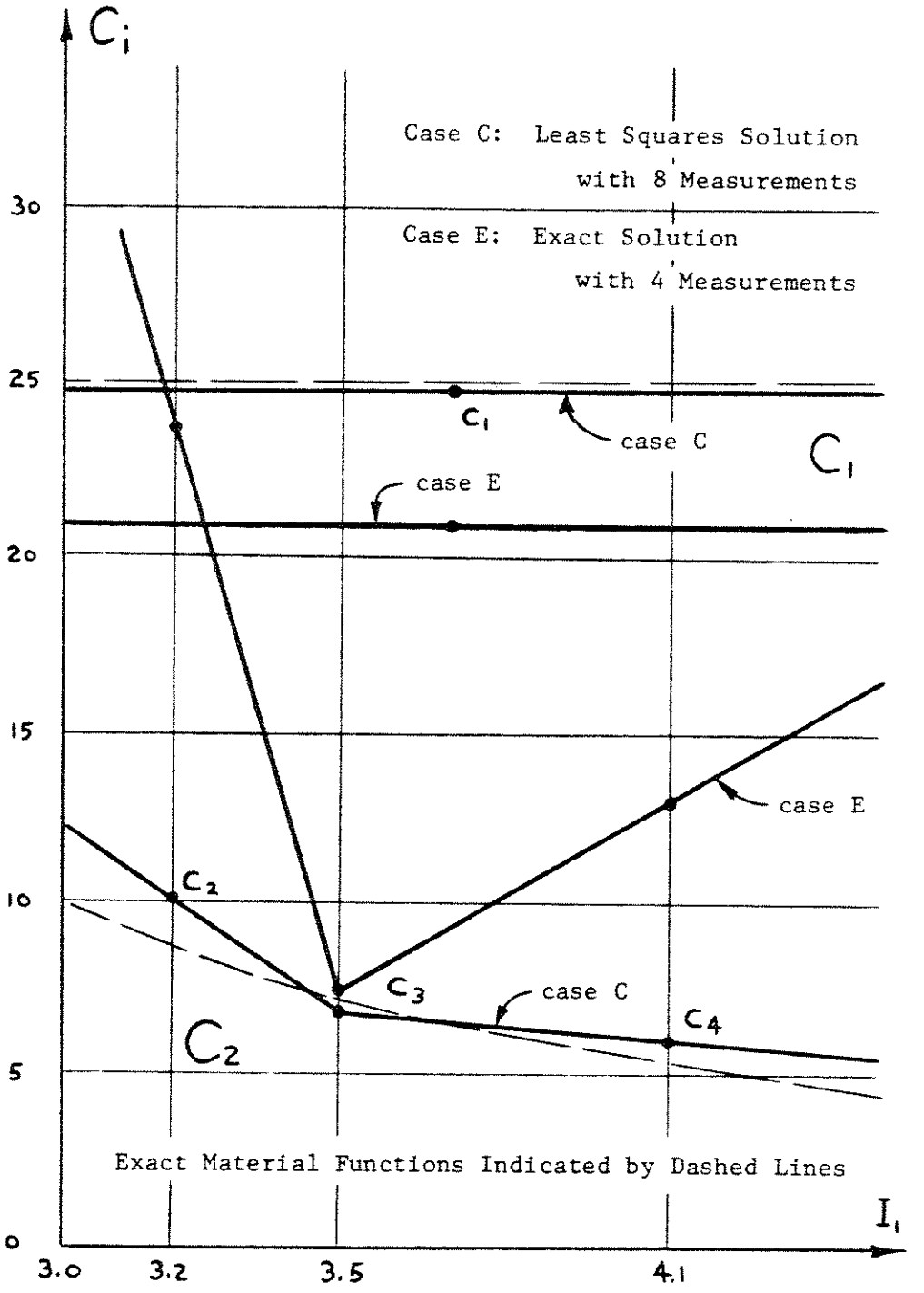

14 ELEMENT MATERIAL IDENTIFICATION EXAMPLE

INPUT DATA WITH LARGE MEASUREMENT ERRORS

Fig. C.7

measurements must be reflected in the material and displacement solution converged upon; hence an error in even one measurement can be sufficient to ruin the identification. But, as Figure C.7 shows, the least squares identification (8 measurements, 4 degrees of freedom in the material discretization) can ignore the effects of measurements that seem unreasonable or inconsistent with the rest of the measurements. For case C let us examine how closely the convergent solution satisfied the experimental measurements used as input:

$$\underset{\sim}{\delta} - \underset{\sim}{g}(\underset{\sim}{v}, \underset{\sim}{\lambda}) = \begin{Bmatrix} 0.006 \\ -0.010 \\ -0.003 \\ 0.003 \\ 0.016 \\ -0.009 \\ -0.025 \\ 0.007 \end{Bmatrix} . \qquad (C.4)$$

This corresponds quite closely with the error introduced into the input data, which is

$$\underset{\sim}{\delta}_{input} - \underset{\sim}{\delta}_{exact} = \begin{Bmatrix} 0.011 \\ -0.030 \\ -0.004 \\ 0.004 \\ 0.014 \\ -0.004 \\ -0.023 \\ -0.003 \end{Bmatrix} \qquad (C.5)$$

Thus exactly what was predicted in Chapter IV has occurred: the least squares algorithm has smoothed out the worst errors in the input data and has thereby protected the very delicate inverse problem from the shock of having to force its solution to account for all errors in the input data.

C.2 Weighting of Least Squares Equations

In Section 4.3 it was noted that the least squares solution to the equations

$$\begin{Bmatrix} \omega_0 \cdot \underset{\sim}{f}_{EQ}(\underset{\sim}{u}, \underset{\sim}{\lambda}, \underset{\sim}{c}) \\ \omega_1 \cdot \underset{\sim}{f}_{INC}(\underset{\sim}{u}, \underset{\sim}{\lambda}) \\ \omega_2 \cdot \underset{\sim}{g}(\underset{\sim}{u}, \underset{\sim}{\lambda}) \end{Bmatrix} = \begin{Bmatrix} \omega_0 \cdot \underset{\sim}{R} \\ \omega_1 \cdot \underset{\sim}{1} \\ \omega_2 \cdot \underset{\sim}{\delta} \end{Bmatrix} \tag{C.6}$$

will depend on the relative sizes of the weighting factors ω_0, ω_1, and ω_2. To complement the theoretical discussion in Chapter IV, let us reexamine case C of the previous section, using a number of different weighting schemes. Case C is a 14 element rubber sheet identified by taking 8 measurements and solving with a 4 degree-of-freedom material discretization. Large errors have been introduced into the 8 items of input data (as in Table C.1) so that poor choices of weighting factors will have a significant effect on the solution.

Table C.2 summarizes the results of solving the identification problem with 6 promising combinations of weighting factors. Shown are the material identification $\underset{\sim}{c}$ and how closely the least squares algorithm allowed each of the three different types of equations to be satisfied. That is, the largest element in each of the vectors

$$\begin{Bmatrix} \underset{\sim}{f}_{EQ}(\underset{\sim}{u}, \underset{\sim}{\lambda}, \underset{\sim}{c}) - \underset{\sim}{R} \\ \underset{\sim}{f}_{INC}(\underset{\sim}{u}, \underset{\sim}{\lambda}) - \underset{\sim}{1} \\ \underset{\sim}{g}(\underset{\sim}{u}, \underset{\sim}{\lambda}) - \underset{\sim}{\delta} \end{Bmatrix} \tag{C.7}$$

CASE	WEIGHTING FACTORS FOR DIMENSIONING OF 14 ELEMENT EXAMPLE			WEIGHTING FACTORS FOR NORMALIZED SYSTEM OF EQUATIONS (SEE SECTION 4.3)			MATERIAL IDENTIFICATION				MAXIMUM IMBALANCE IN EQUATIONS AT CONVERGENCE		
	ω_0	ω_1	ω_2	$\bar{\omega}_0$	$\bar{\omega}_1$	$\bar{\omega}_2$	C_1	C_2	C_3	C_4	Force Balance Equations	Incompress-ibility Equations	Input Data Equations
A	1	1	1	1	0.01	0.01	24.71	10.02	6.83	5.97	0.0002	0.002	0.025
B	1	1	100	1	0.01	1	25.46	8.73	6.71	4.48	0.02	0.2	0.0004
C	1	100	100	1	1	1	25.40	8.97	5.84	4.77	0.95	0.0008	0.015
D	1	100	10	1	1	0.1	24.72	10.01	6.81	5.96	0.02	0.00002	0.025
E	1	100	1	1	1	0.01	24.70	10.03	6.83	5.98	0.0002	0.0000002	0.025
F	1	100	0.1	1	1	0.001	24.70	10.03	6.83	5.98	0.000002	0.00000002	0.025

14 ELEMENT MATERIAL IDENTIFICATION EXAMPLE

LEAST SQUARES SOLUTION USING 6 WEIGHTING SCHEMES

Table C.2

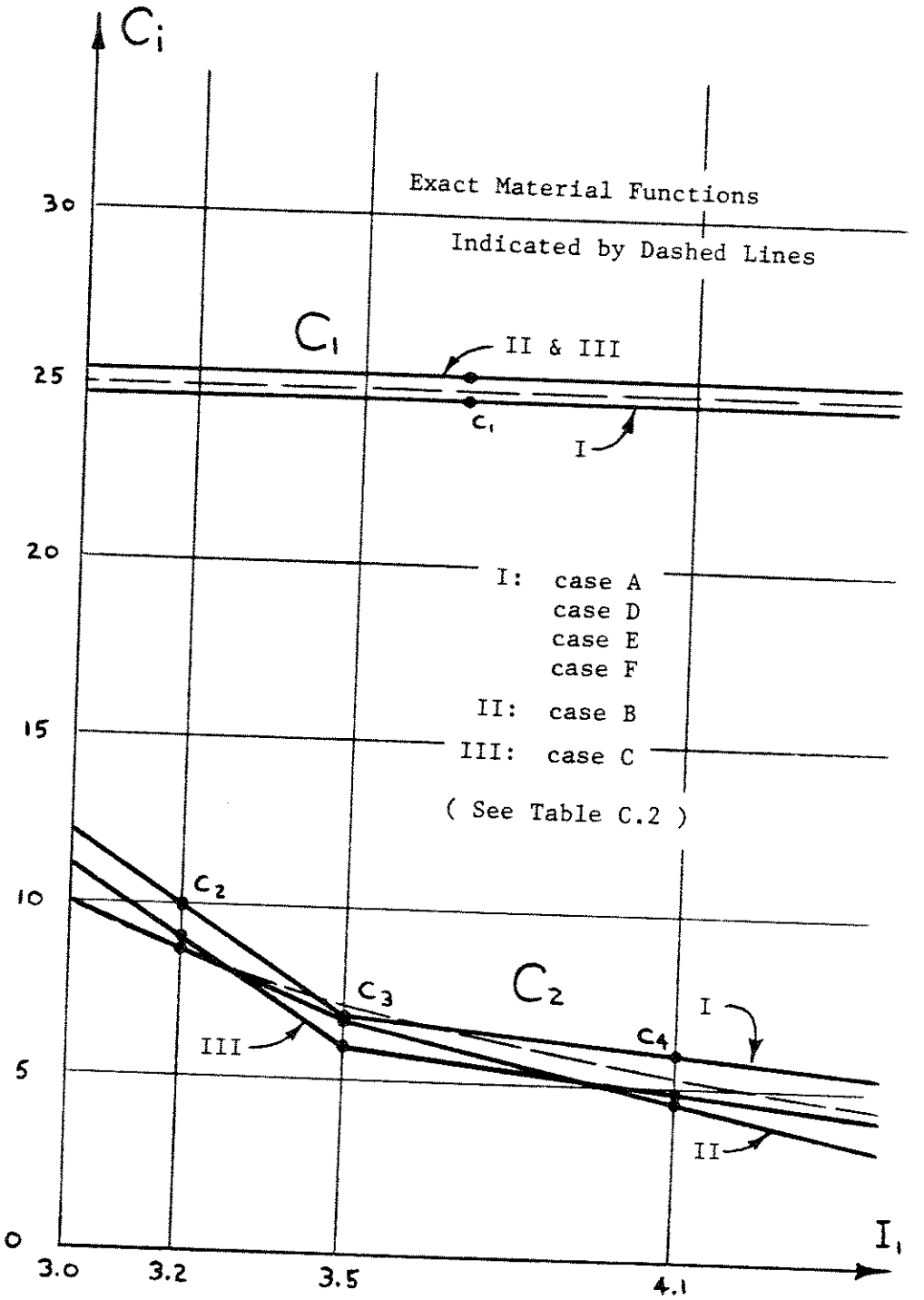

14 ELEMENT MATERIAL IDENTIFICATION EXAMPLE

EFFECT OF VARIOUS WEIGHTING SCHEMES UPON SOLUTION

Fig. C.8

at the convergent solution $(\underset{\sim}{u},\underset{\sim}{\lambda},\underset{\sim}{c})$ is shown in the last three columns of Table C.2. These identifications are plotted in Figure C.8.

The results confirm the theoretical predictions of Chapter IV: the best identifications result when the equations are weighted such that the measurement constraint equations are smallest and hence take up most of the experimental error introduced into the system. Cases A, D, E, and F are examples of this situation. In cases B and C the equilibrium or incompressibility equations are not weighted heavily enough and the resulting inaccuracies in satisfying those equations (and the accompanying overstrictness in satisfying the erroneous input measurements) disturb the excellence of the material identification.

C.3 Stability of Material Mesh

The accuracy and stability of the identification algorithm will depend very much on the number of nodes in the material mesh. In this section we shall reexamine the 14 element experiment used previously in this appendix using a large number of different material meshes and compare the resulting identifications. 19 measurements are used as input, as shown in Figure C.9. Two levels of experimental accuracy are considered: input to 0.01 inch accuracy (good data) and input with large perturbations (poor data), as shown in Figure C.10. Eight different material discretizations are tested:

1) 6 degrees of freedom (3 in C_1 , 3 in C_2) as shown in Figure C.11, a very rich and general mesh. It would probably

Small numbers refer to nodes of 14 element mesh.

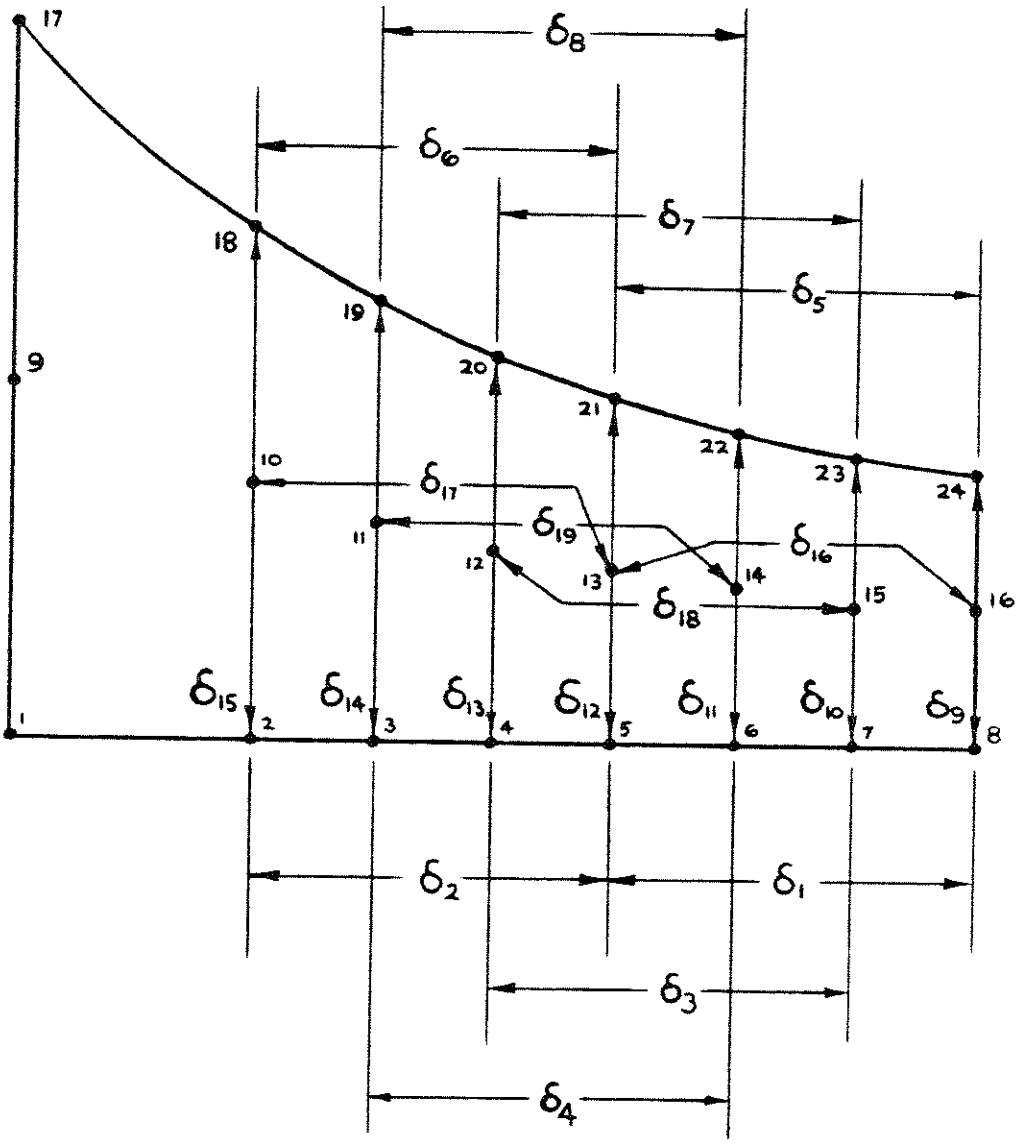

$\delta_1 = U_8 - U_5$ $\qquad$ $\delta_9 = V_{24} - V_8$

$\delta_2 = U_5 - U_2$ $\qquad$ $\delta_{10} = V_{23} - V_7$

$\delta_{17} = U_{16} - U_{13}$ $\qquad$ etc.

14 ELEMENT MATERIAL IDENTIFICATION EXAMPLE

LOCATIONS OF 19 EXPERIMENTAL MEASUREMENTS USED AS INPUT DATA

Fig. C.9

$$\underset{\sim}{\delta} = \begin{Bmatrix} 2.54 \\ 1.59 \\ 2.19 \\ 1.88 \\ 2.80 \\ 1.46 \\ 2.41 \\ 1.95 \\ -0.64 \\ -0.67 \\ -0.65 \\ -0.62 \\ -0.58 \\ -0.53 \\ -0.41 \\ 2.60 \\ 1.59 \\ 2.25 \\ 1.90 \end{Bmatrix} \qquad \underset{\sim}{\epsilon}_{\underset{\sim}{\delta}} = \begin{Bmatrix} -0.002 \\ 0.000 \\ -0.004 \\ 0.005 \\ 0.004 \\ -0.004 \\ -0.003 \\ 0.000 \\ -0.002 \\ 0.004 \\ 0.004 \\ 0.001 \\ 0.003 \\ -0.002 \\ 0.003 \\ -0.002 \\ 0.000 \\ 0.005 \\ 0.002 \end{Bmatrix} \qquad \underset{\sim}{\hat{\delta}} = \begin{Bmatrix} 2.53 \\ 1.62 \\ 2.19 \\ 1.85 \\ 2.80 \\ 1.45 \\ 2.44 \\ 1.95 \\ -0.65 \\ -0.65 \\ -0.65 \\ -0.61 \\ -0.58 \\ -0.55 \\ -0.41 \\ 2.63 \\ 1.59 \\ 2.24 \\ 1.91 \end{Bmatrix} \qquad \underset{\sim}{\epsilon}_{\underset{\sim}{\hat{\delta}}} = \begin{Bmatrix} -0.012 \\ 0.030 \\ -0.004 \\ -0.025 \\ -0.016 \\ -0.014 \\ 0.027 \\ 0.000 \\ -0.014 \\ 0.024 \\ 0.004 \\ 0.011 \\ 0.003 \\ -0.022 \\ 0.003 \\ 0.028 \\ 0.000 \\ -0.005 \\ 0.012 \end{Bmatrix}$$

$\underset{\sim}{\delta}$: Input Measurements of 0.01 Inch Accuracy

$\underset{\sim}{\epsilon}_{\underset{\sim}{\delta}}$: Rounding Errors in $\underset{\sim}{\delta}$

$\underset{\sim}{\hat{\delta}}$: Input Measurements with Large Perturbations

$\underset{\sim}{\epsilon}_{\underset{\sim}{\hat{\delta}}}$: Total Error (Rounding & Perturbation) in $\underset{\sim}{\hat{\delta}}$

14 ELEMENT MATERIAL IDENTIFICATION EXAMPLE

INPUT DATA AND INPUT DATA ACCURACY

Fig. C.10

be too rich for use in a first attempt to identify a material, but might be needed if both material functions show possibility of considerable curvature.

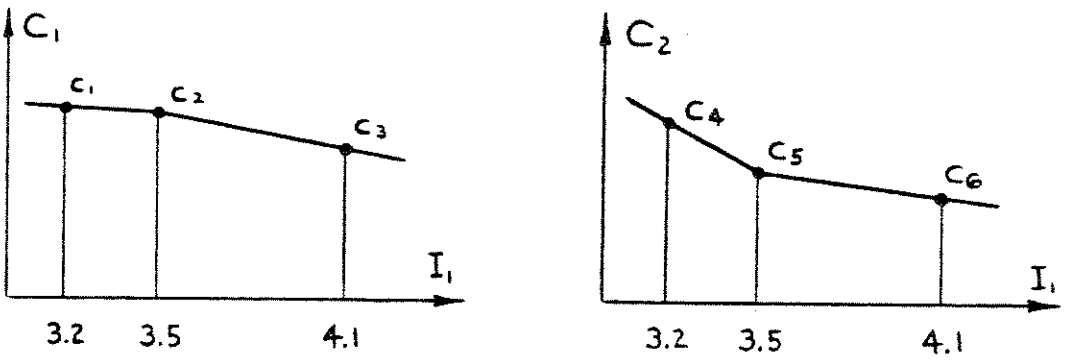

Fig. C.11

2) 6 degrees of freedom (2 in C_1, 4 in C_2) as shown in Figure C.12, a good mesh to use when nothing at all is known about the shape of the material functions. It permits representation of a highly nonlinear material with both material functions showing considerable variation with strain.

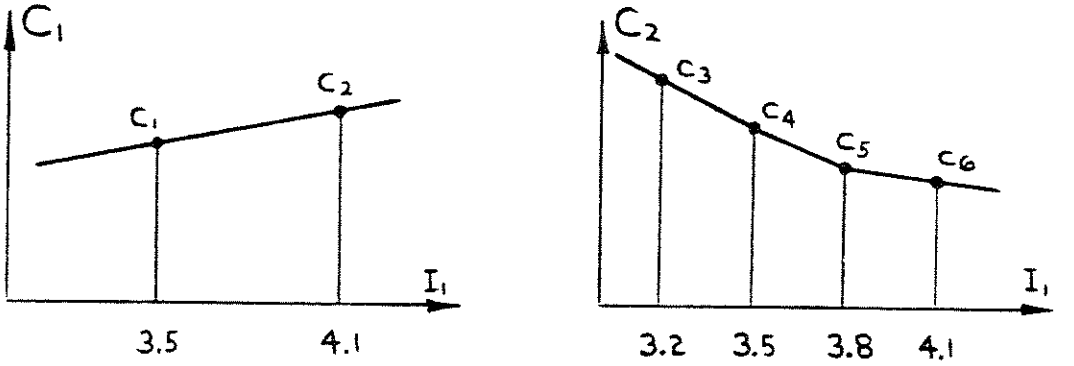

Fig. C.12

3) 5 degrees of freedom (2 in C_1, 3 in C_2), as shown in Figure C.13.

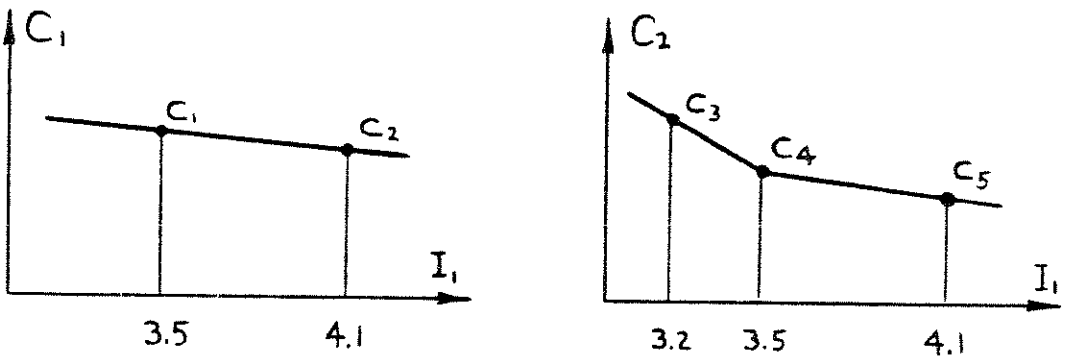

Fig. C.13

4) 4 degrees of freedom (1 in C_1, 3 in C_2) as shown in Figure C.14, a very stable discretization since C_1 is held constant. It is a wise choice when the input data are of uncertain accuracy and the material is such that C_1 is probably more or less constant. It is not necessary that C_1 be exactly constant, since C_2 will adjust somewhat to compensate.

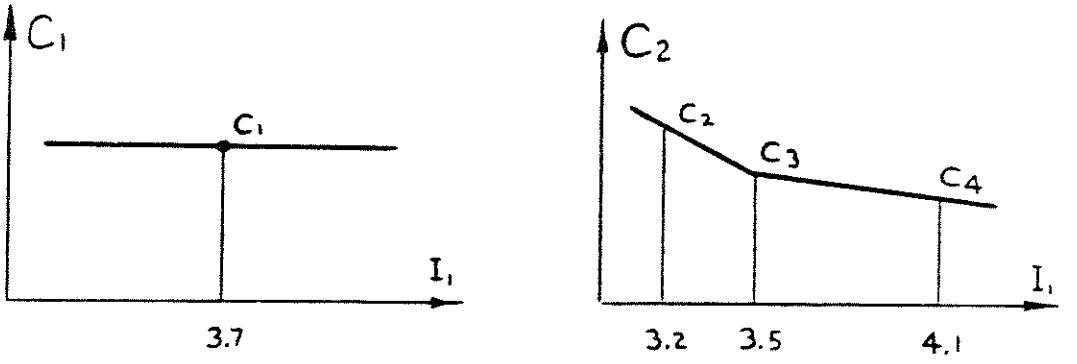

Fig. C.14

5) 3 degrees of freedom (1 in C_1, 2 in C_2) as shown in Figure C.15, a very rigid mesh that gives a good representation only if both material functions are quite linear. It is, however, extremely stable (if not accurate) and could be used to wring some sort of identification out of extremely poor experimental measurements.

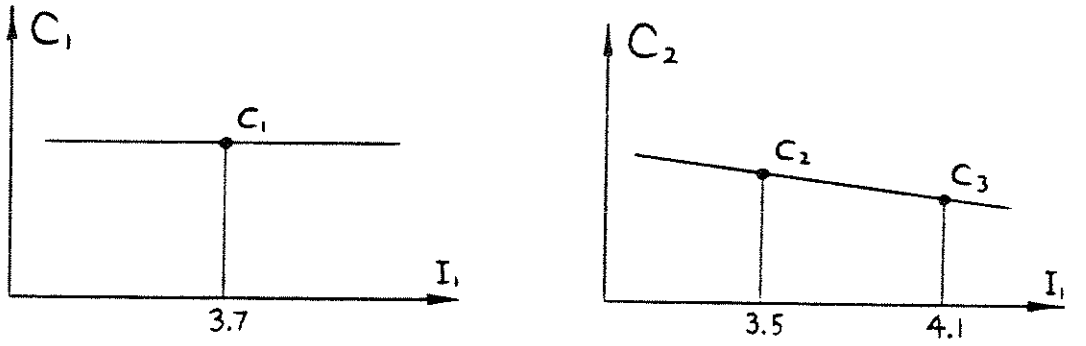

Fig. C.15

6) 2 degrees of freedom (1 in C_1, 1 in C_2) as shown in Figure C.16, an extremely coarse mesh that is unsuitable for anything except a truly Mooney-Rivlin material. Use of this mesh is a way to find the best approximation to the real material behavior over the strain range of the experiment in terms of two Mooney-Rivlin constants.

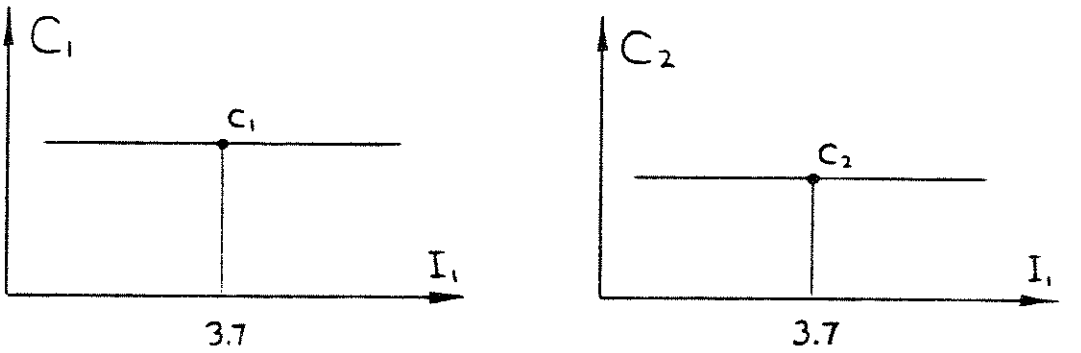

Fig. C.16

7) 3 degrees of freedom (2 in C_1, 1 in C_2) as shown in Figure C.17, a very inappropriate material mesh for the example being considered. It is included only as a test of the algorithm's behavior when it must work with an unsuitable material discretization.

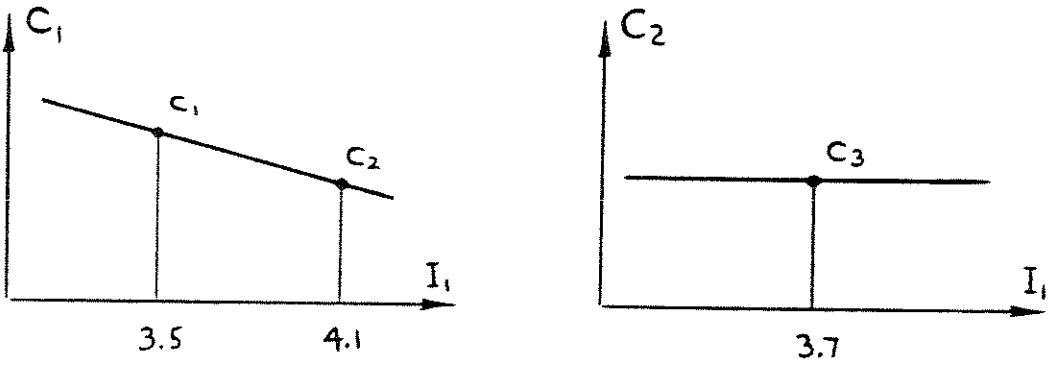

Fig. C.17

8) 4 degrees of freedom (2 in C_1, 2 in C_2) as shown in Figure C.18, suitable only for a material with linear material functions, since this mesh cannot account for any curvature in either material function.

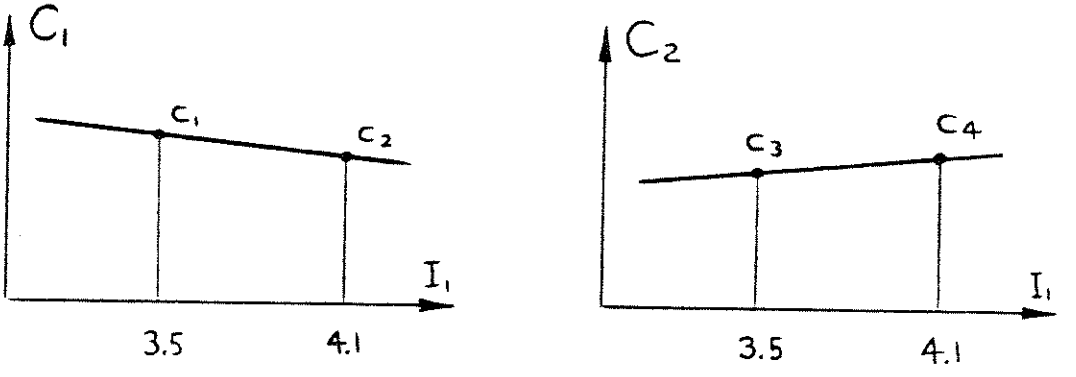

Fig. C.18

The material identifications for each of these material meshes are displayed in Table C.3 and plotted in Figures C.19-C.27. Note that the 2 degree-of-freedom case has been solved using two different weighting schemes.

A number of conclusions are immediately evident from these plots:

1) Figures C.19-C.22 show that accurate input data (case I in

ACCURACY OF DATA USED AS INPUT	MATERIAL DISCRETIZATION CASE (See pages 156 - 162)		MATERIAL IDENTIFICATION					
			C_1	C_2	C_3	C_4	C_5	C_6
19 measurements rounded off to 0.01 inch (see Fig. C.10)	1	6 DOF (3 in C_1, 3 in C_2)	24.26	25.74	25.22	10.01	6.18	5.03
	2	6 DOF (2 in C_1, 4 in C_2)	25.14	25.13	8.83	7.03	6.15	5.17
	3	5 DOF (2 in C_1, 3 in C_2)	25.21	25.13	8.67	6.97	5.17	
	4	4 DOF (1 in C_1, 3 in C_2)	25.13	8.81	7.08	5.16		
	8	4 DOF (2 in C_1, 2 in C_2)	23.89	25.03	9.05	5.30		
	5	3 DOF (1 in C_1, 2 in C_2)	24.88	7.64	5.56			
	7	3 DOF (2 in C_1, 1 in C_2)	25.04	23.80	7.44			
	6	2 DOF weighting case A	17.14	18.87				
	6	2 DOF weighting case B	19.76	15.12				
19 measurements with large perturbations (see Fig. C.10)	1	6 DOF (3 in C_1, 3 in C_2)	17.83	27.01	25.99	18.18	4.38	3.66
	2	6 DOF (2 in C_1, 4 in C_2)	22.73	25.06	13.42	10.30	8.37	5.17
	3	5 DOF (2 in C_1, 3 in C_2)	23.84	25.37	11.11	9.12	4.66	
	4	4 DOF (1 in C_1, 3 in C_2)	25.46	8.15	6.63	4.54		
	5	3 DOF (1 in C_1, 2 in C_2)	25.31	6.96	4.77			

14 ELEMENT EXAMPLE: MATERIAL IDENTIFICATIONS FOR VARIOUS MATERIAL DISCRETIZATION CHOICES

Table C.3

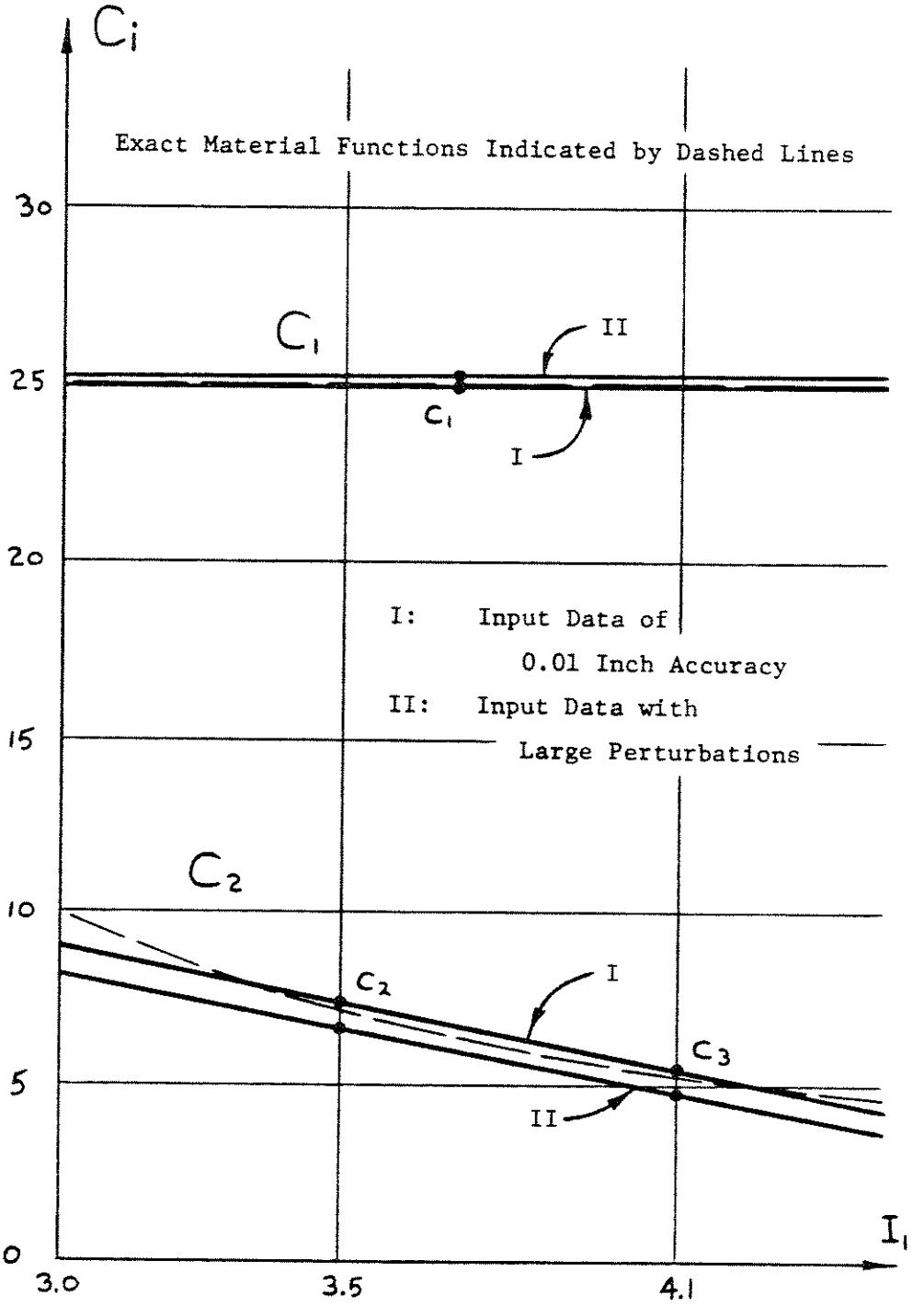

TEST OF MATERIAL MESH #5

1 DEGREE OF FREEDOM IN C_1, 2 DEGREES OF FREEDOM IN C_2

Fig. C.19

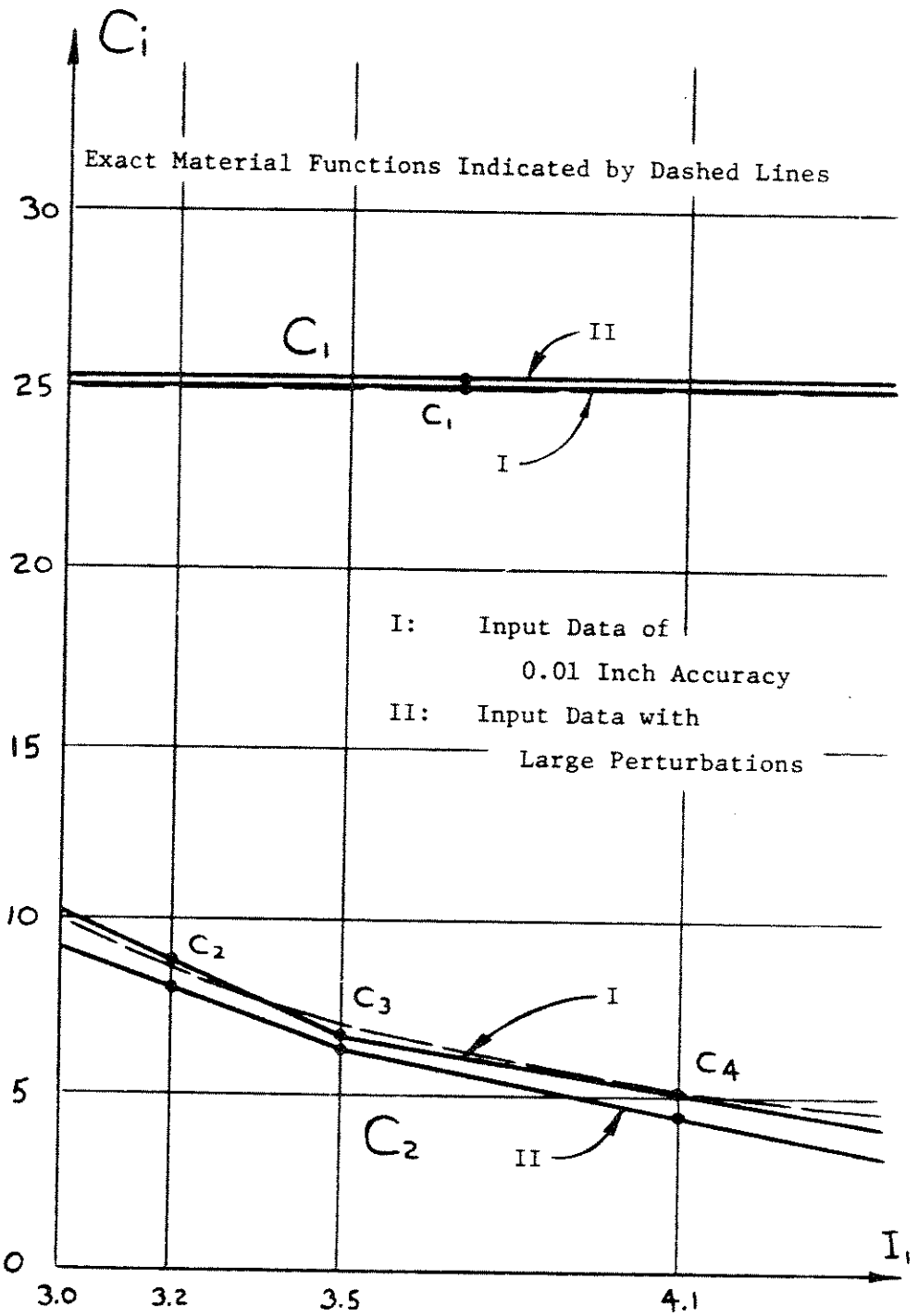

TEST OF MATERIAL MESH #4

1 DEGREE OF FREEDOM IN C_1, 3 DEGREES OF FREEDOM IN C_2

Fig. C.20

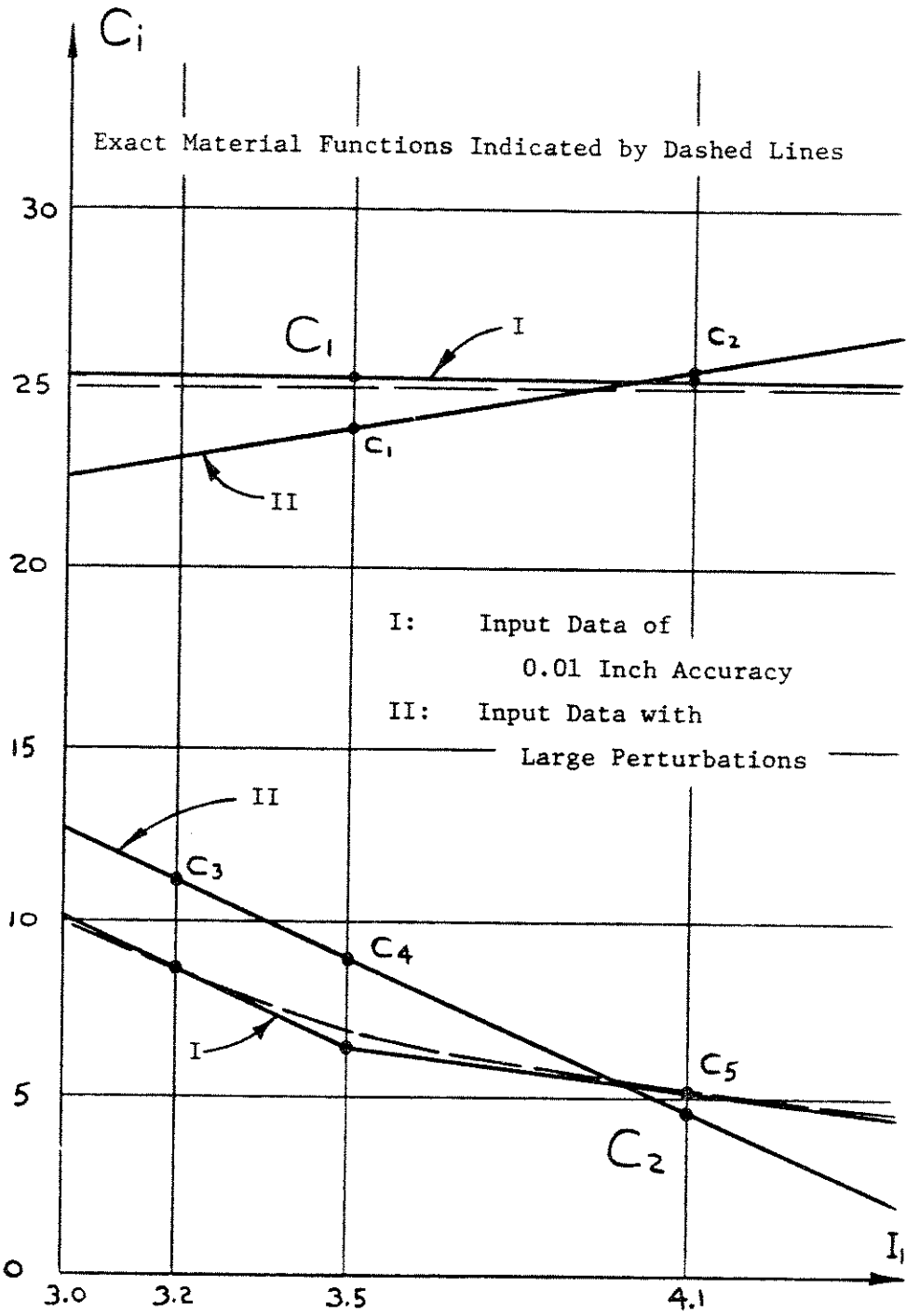

TEST OF MATERIAL MESH #3

2 DEGREES OF FREEDOM IN C_1, 3 DEGREES OF FREEDOM IN C_2

Fig. C.21

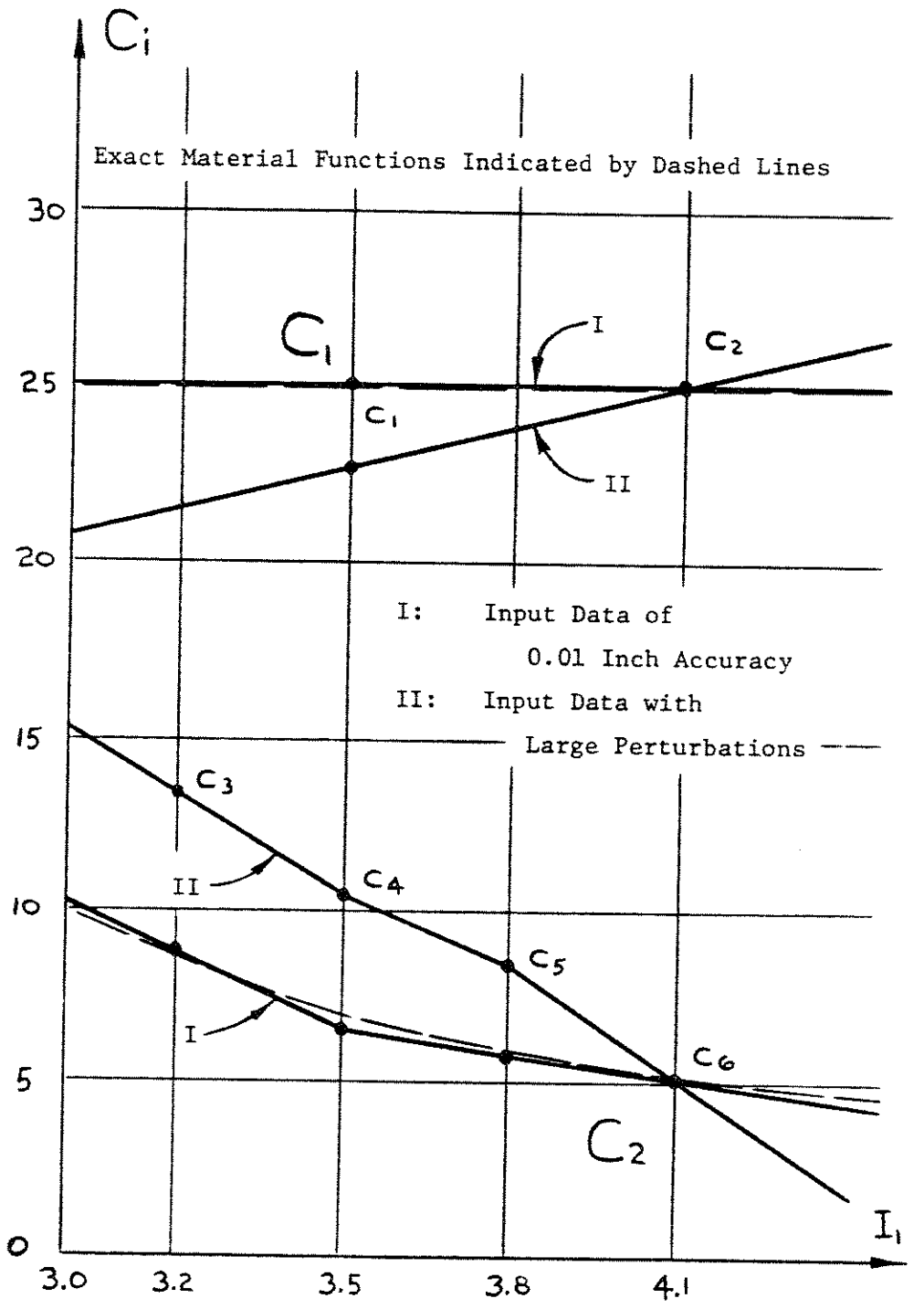

TEST OF MATERIAL MESH #2

2 DEGREES OF FREEDOM IN C_1, 4 DEGREES OF FREEDOM IN C_2

Fig. C.22

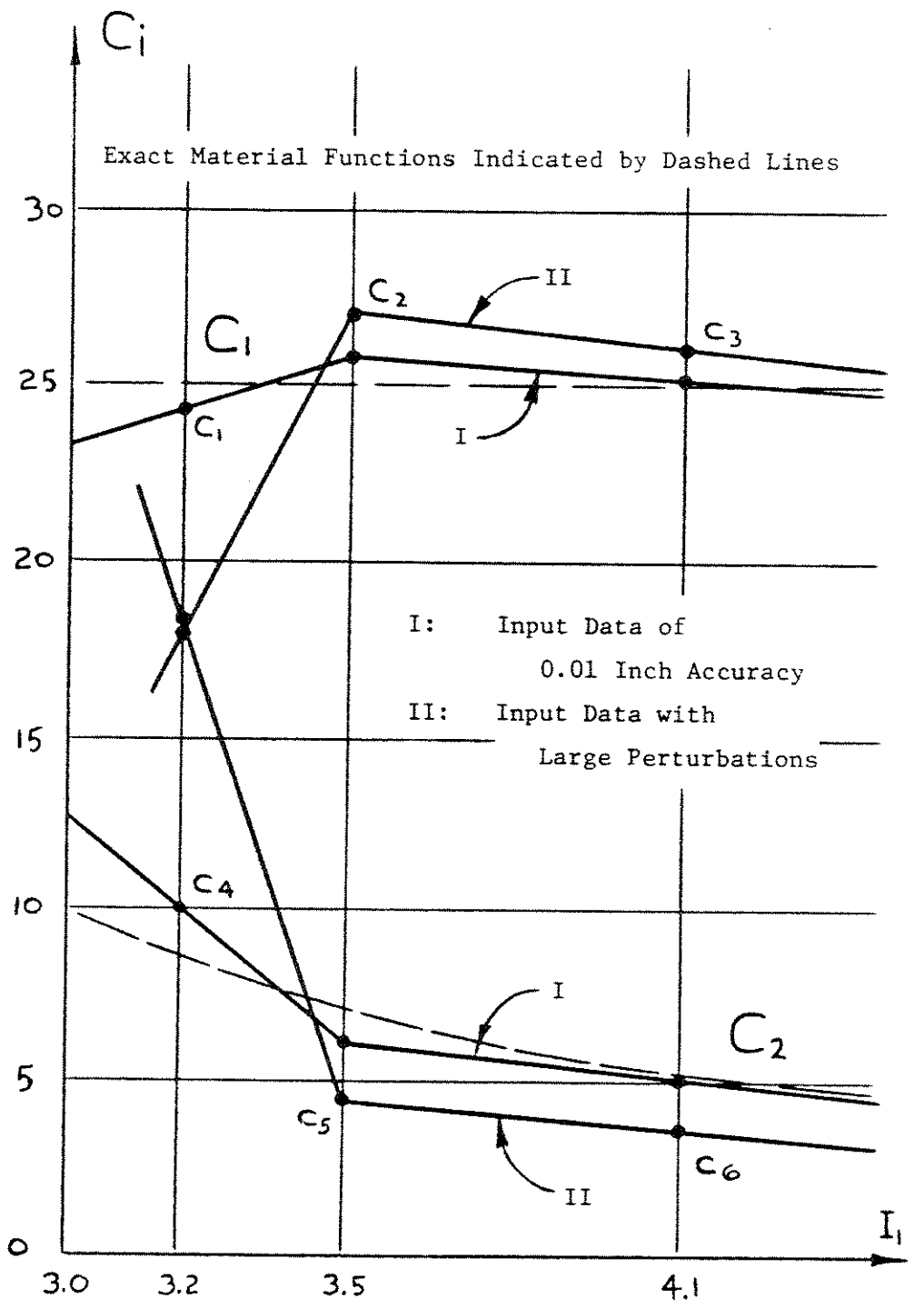

TEST OF MATERIAL MESH #1

3 DEGREES OF FREEDOM IN C_1 , 3 DEGREES OF FREEDOM IN C_2

Fig. C.23

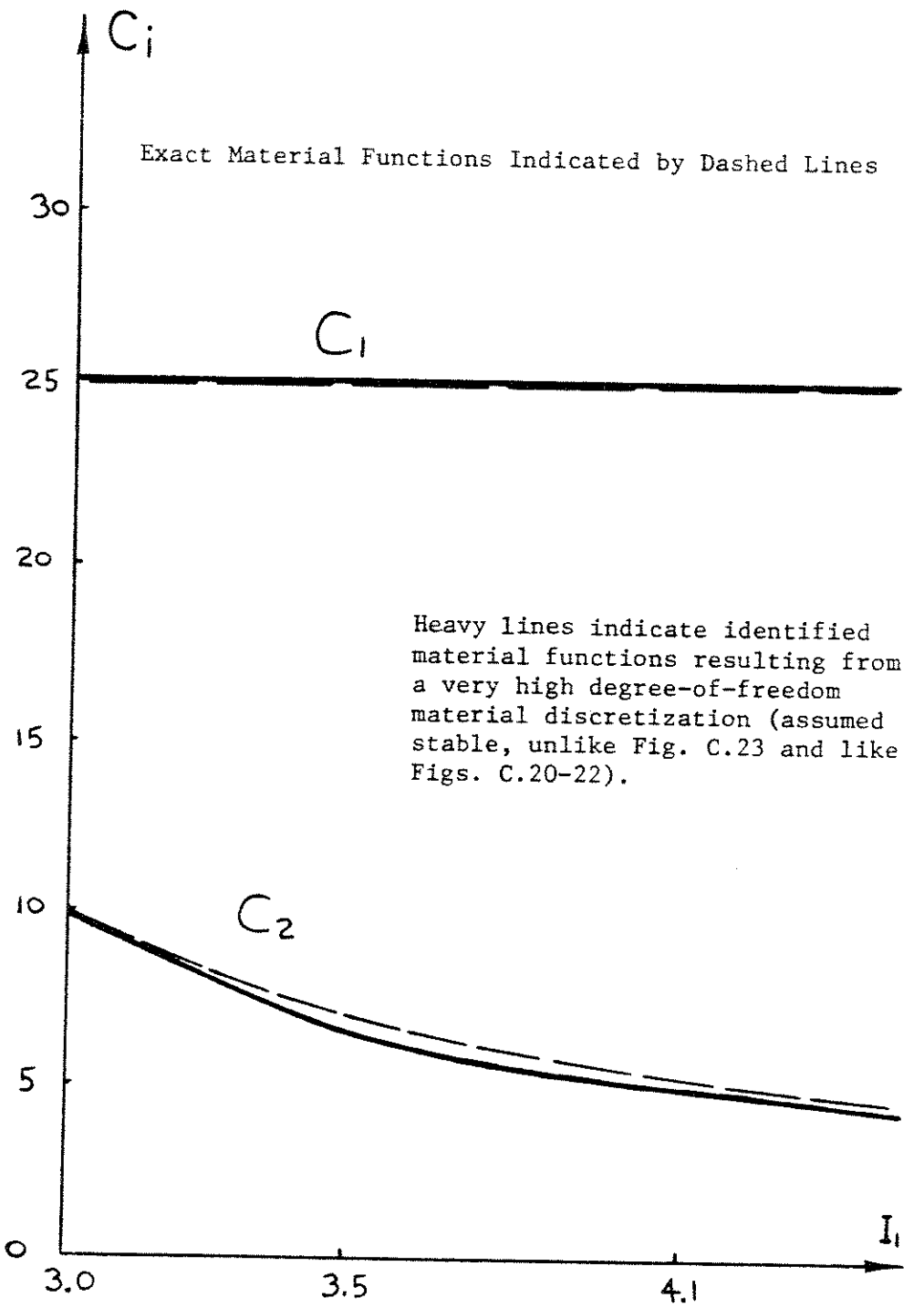

LIMITING MATERIAL IDENTIFICATION FOR

INPUT DATA OF 0.01 INCH ACCURACY

Fig. C.24

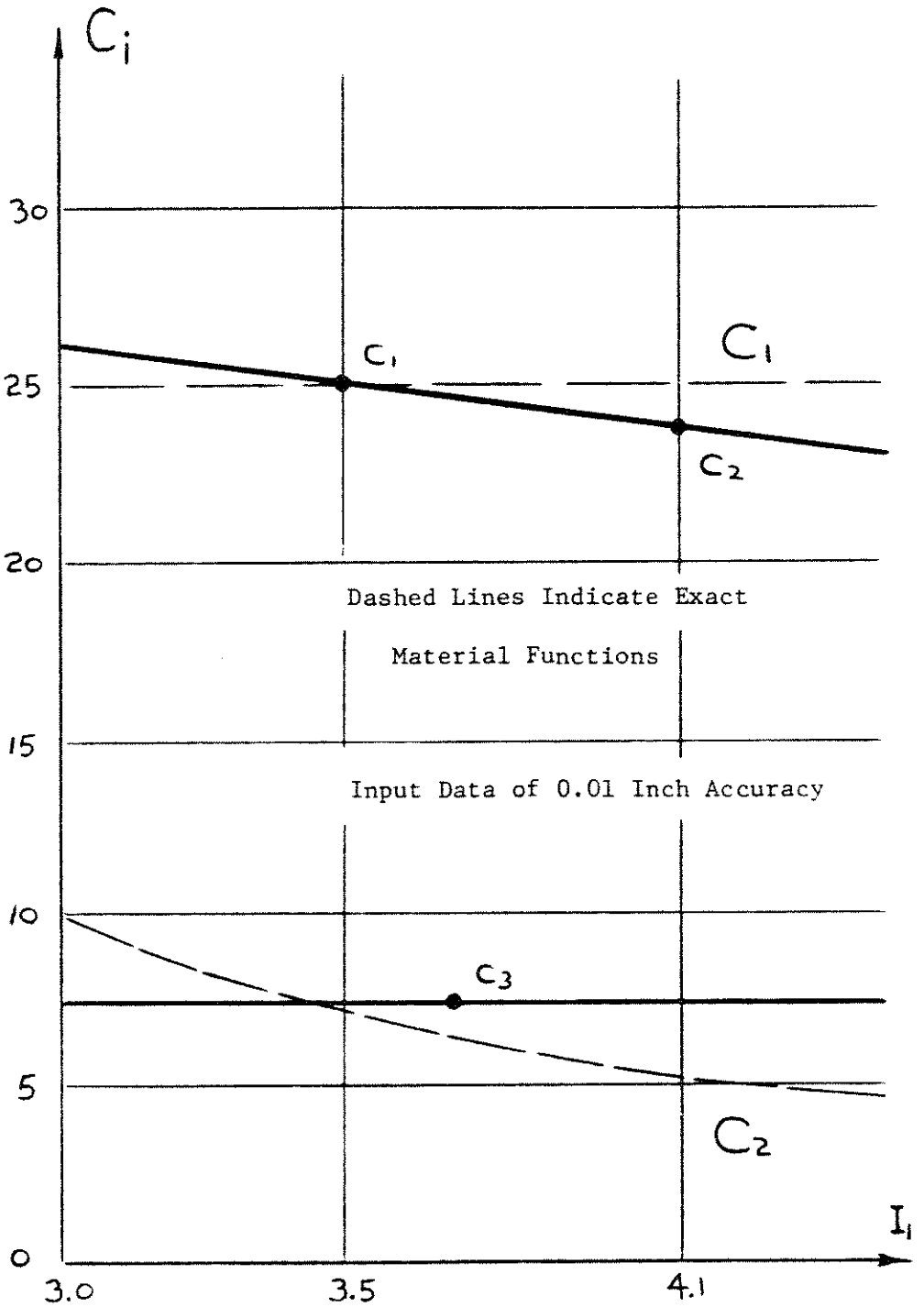

TEST OF MATERIAL MESH #7

2 DEGREES OF FREEDOM IN C_1, 1 DEGREE OF FREEDOM IN C_2

Fig. C.25

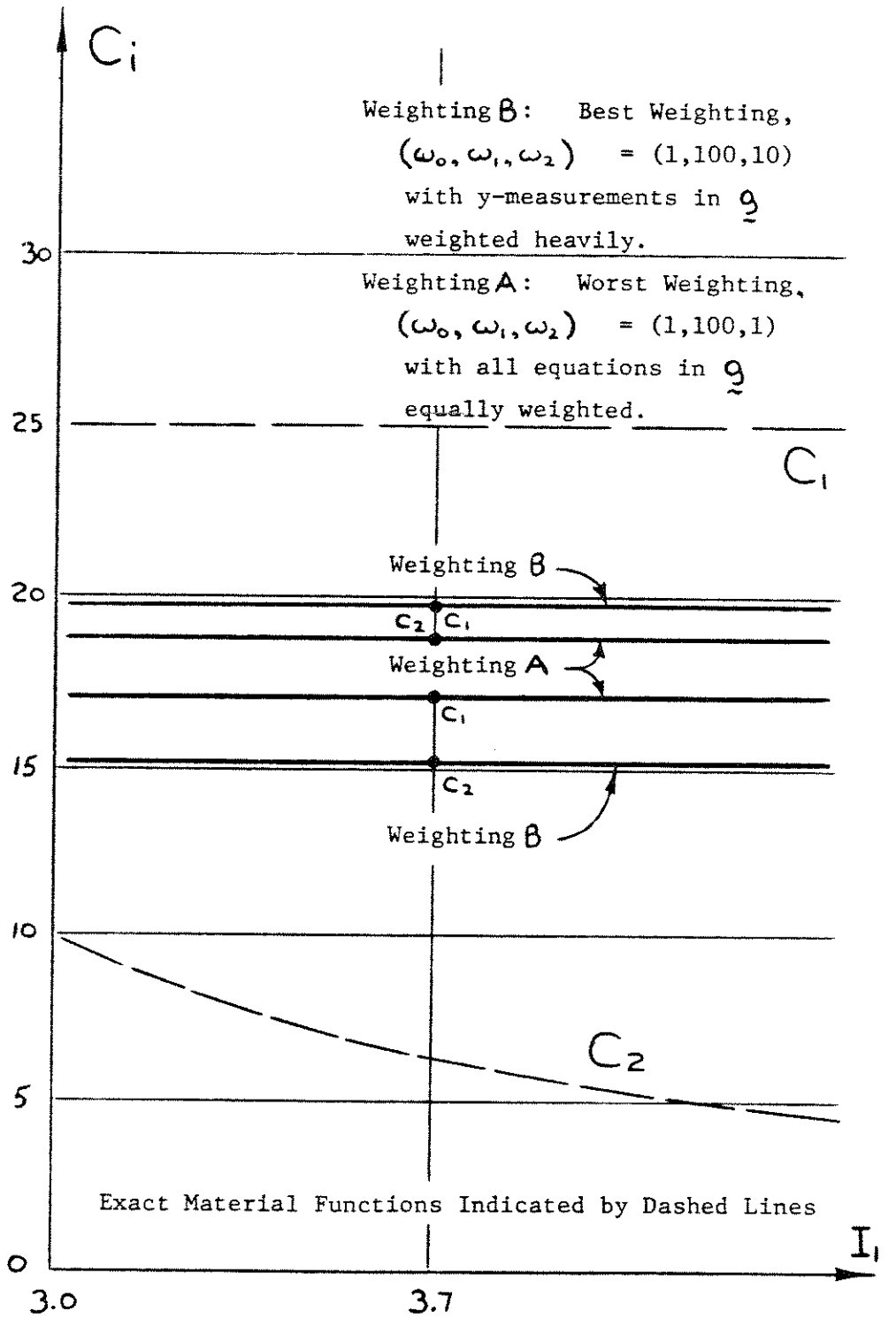

TEST OF MATERIAL MESH #6

1 DEGREE OF FREEDOM IN C_1, 1 DEGREE OF FREEDOM IN C_2

Fig. C.26

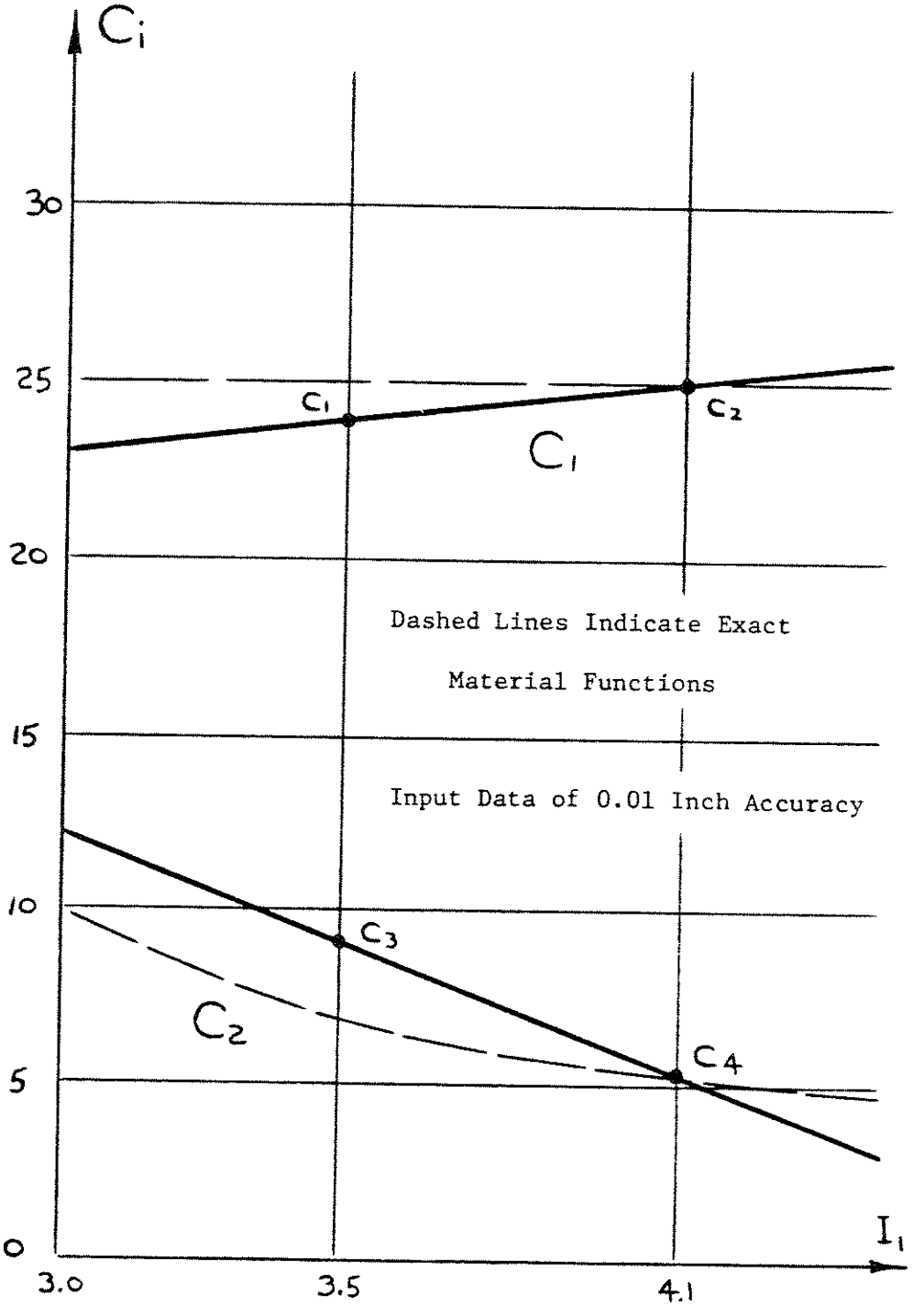

TEST OF MATERIAL MESH #8

2 DEGREES OF FREEDOM IN C_1 , 2 DEGREES OF FREEDOM IN C_2

Fig. C.27

the plots) effect an accurate identification with all the various material meshes tested. As the meshes become finer and more capable of very closely representing the curved shape of $C_2(I_2)$, the respective identifications approach the identification which would result from using an infinitely fine material mesh. This limiting value is shown in Figure C.24. As expected, it is different from the exact material functions, since the 19 measurements it is based on contain rounding errors which, when analyzed in the least squares sense, cause some error in the identified material functions no matter how fine the material mesh is. Of course, as the number of degrees of freedom in the material mesh approach the number of input measurements some instability of the type encountered with determinate systems of equations results. Figure C.23 shows the beginnings of this type of behavior.

An entirely different situation is encountered if the input measurements contain errors and inconsistencies. A mesh that is finer than necessary tends to give the system of equations excess freedom and the material identification suffers. Figures C.21-23 show this clearly. And a mesh that is too coarse, as in Figure C.26, is incapable of effecting good results. The best material identifications come from using the meshes in Figures C.19 and C.20, since there are as few material nodes as possible; the minimum number that can reasonably represent the continuous material functions is used and a very stable system of equations results.

2) In Figures C.25-27 are plotted the material identifications resulting when three very unsuitable choices of material meshes

are chosen. Note that the least squares method exerts such a stabilizing influence on the system of equations that reasonable results are possible. Note in Figure C.25 how the first material function is made to vary much like the second function would have if the material mesh had permitted it to, thus effecting a material identification quite usable for stress analysis. In Figure C.26 two different weighting schemes are used in an attempt to obtain a good solution (as discussed on pages 92-94) - one that weights all input data equally and one that weights the more delicate y-direction measurements more heavily to avoid excess drifting in that direction. (Much adjustment in $(\underset{\sim}{\upsilon}, \underset{\sim}{\lambda})$ is needed to compensate for so coarse a material mesh.) The second choice gave the better solution.

3) Note that in each material identification that shows significant error in $\underset{\sim}{\varepsilon}$ (Figures C.21-23), the errors are greatest in the low strain invariant range. This is to be expected since measurements taken in a low strain area tend to be more sensitive to measuring errors. In addition, the elastic field equations tend to be very sensitive when $I_1 < 3.5$. Another contributing factor is the shape of the specimen, which results in high strains over most of the area of the loaded specimen. Thus, the majority of the 19 input measurements lie in the high I_1 range, and the algorithm emphasizes the part of the identification within this high I_1 range.

4) Figures C.28 and C.29 compare the material identifications resulting from the use of different numbers of measurements in $\underset{\sim}{\delta}$.

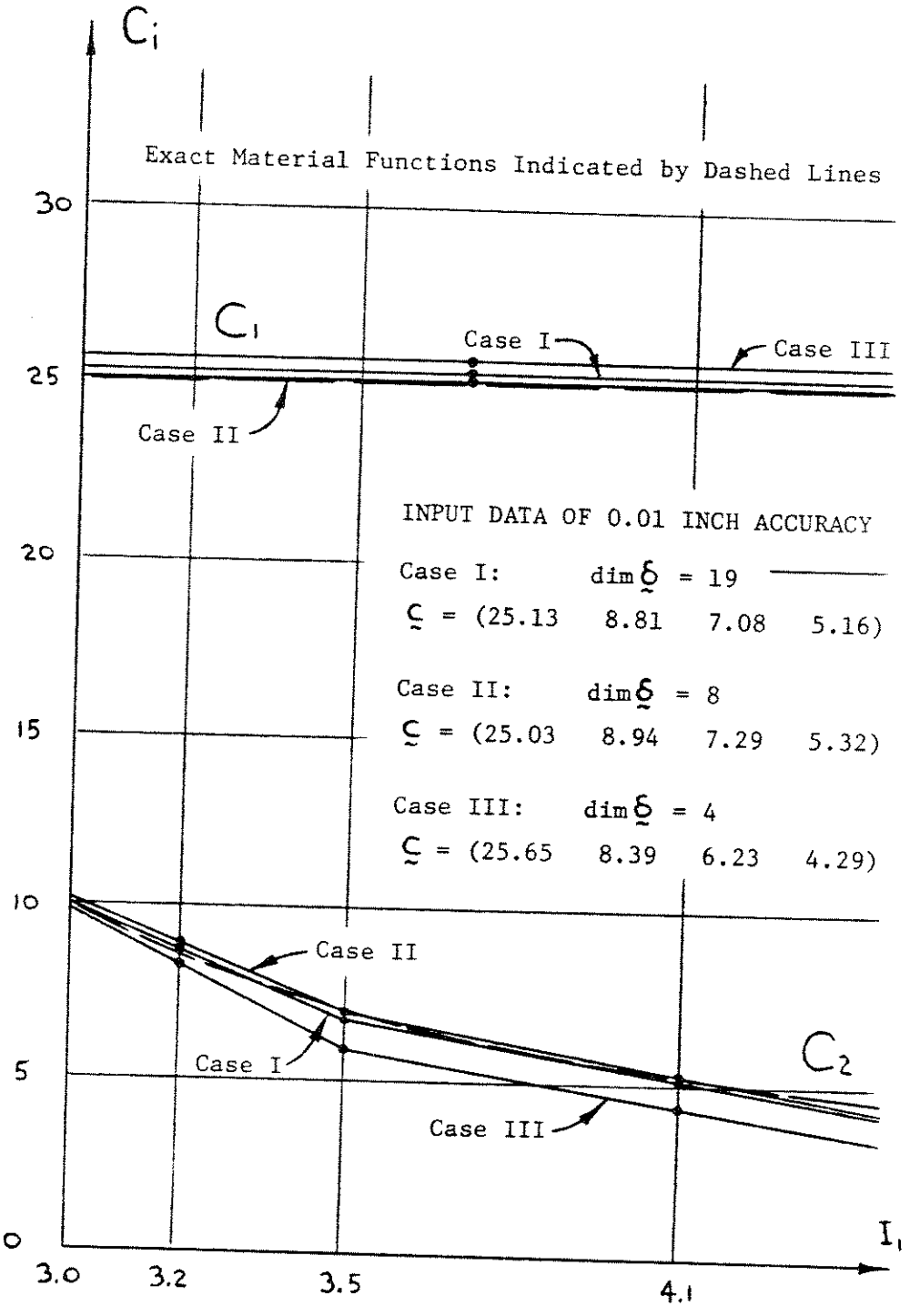

IDENTIFICATION WITH 4 MATERIAL DEGREES OF FREEDOM

USING 4, 8 & 19 INPUT MEASUREMENTS OF 0.01 INCH ACCURACY

Fig. C.28

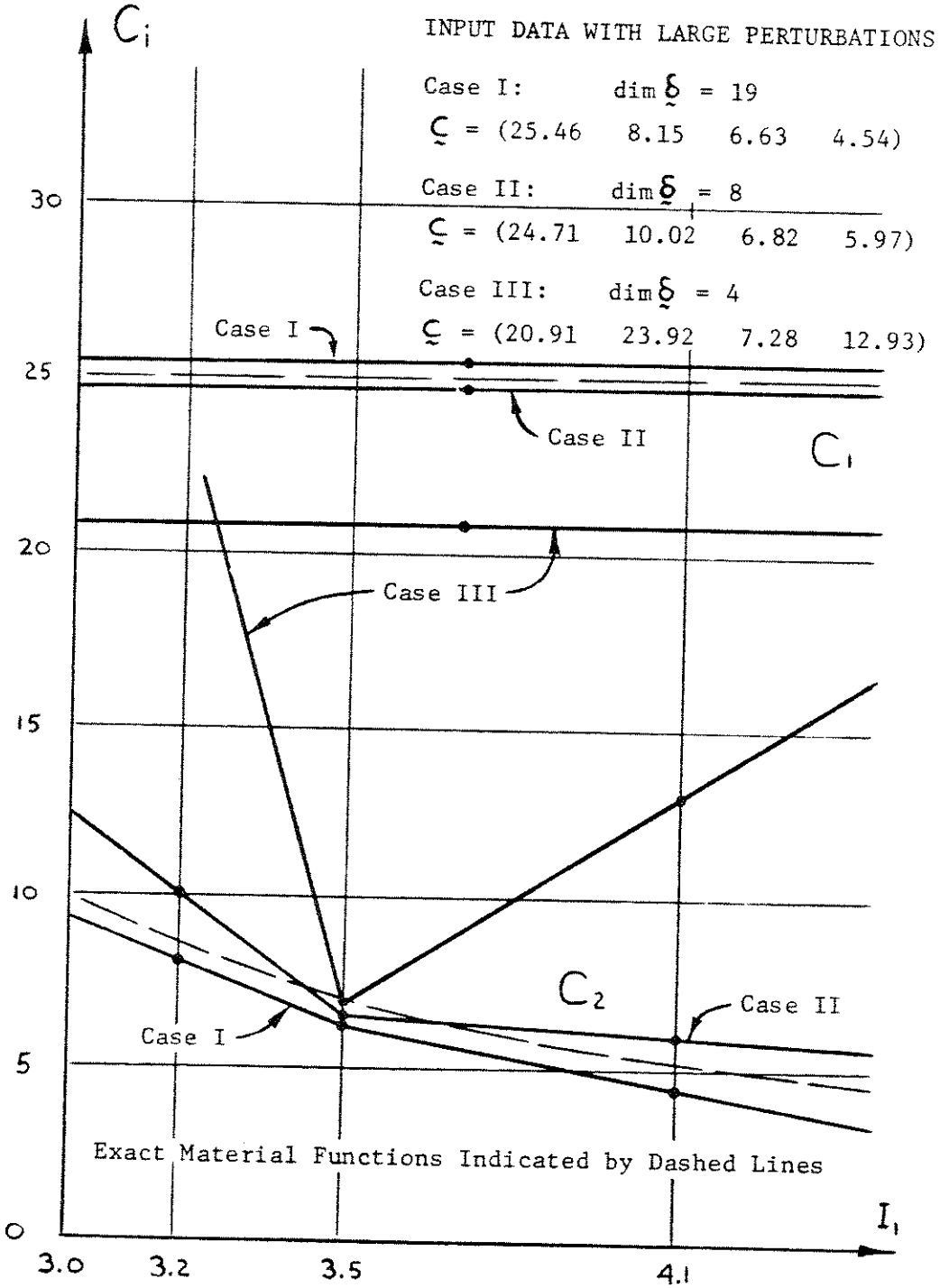

IDENTIFICATION WITH 4 MATERIAL DEGREES OF FREEDOM

USING 4, 8 & 19 INPUT MEASUREMENTS WITH LARGE PERTURBATIONS

Fig. C.29

A large $\underset{\sim}{\delta}$, with many redundancies in measuring, tends to stabilize the system of equations, especially when the system is based on poor input data as in Figure C.29.

APPENDIX D

In this appendix we will look at an example large enough to be suitable for an actual experimental situation. A rubber sheet subjected to nonhomogeneous stresses in the plane of the sheet is the experiment chosen. The shape of the sheet and its means of support are as shown in Figure D.1. For purposes of

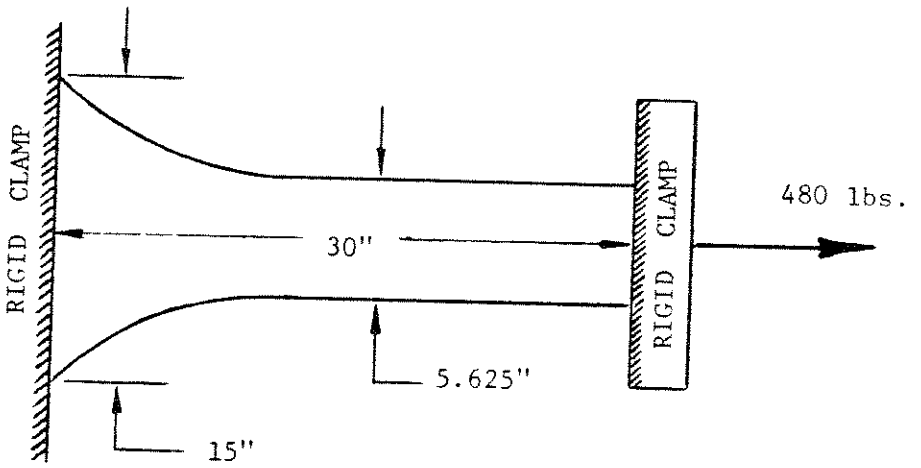

Fig. D.1

analysis this experimental setup can be represented by the two-dimensional plane stress model in Figure D.2.

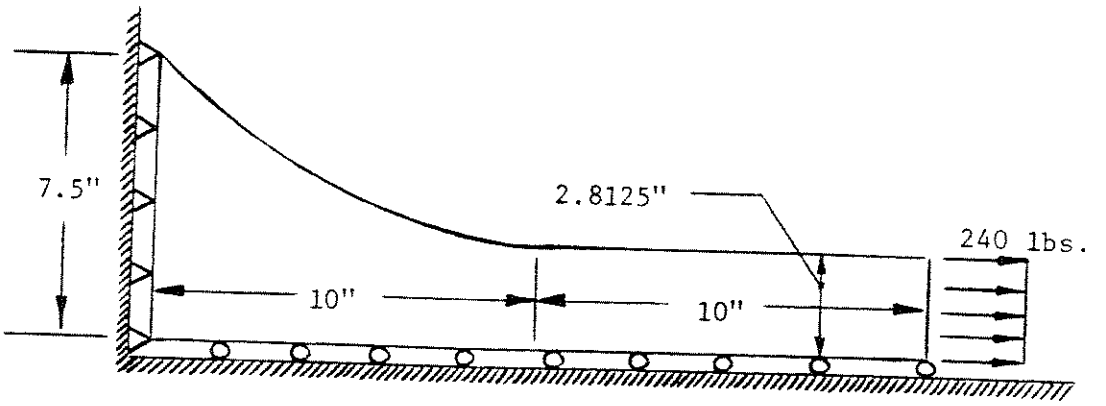

Fig. D.2

The sheet is discretized into 36 quadrilateral finite elements as shown in Figure D.3. This mesh and the material functions

$$C_1(I_1, I_2) = 25 \text{ psi.}$$
$$C_2(I_1, I_2) = 10\left(1-\tfrac{5}{7}(I_2-3)+\tfrac{1}{7}(I_2-3)^2\right) \text{ psi.} \qquad \text{(D.1)}$$

are used to solve the forward direction problem with the specified loading, and the deformed configuration thereby obtained is the basis for the measurements used as input in this simulated experimental situation. Solving this same problem with a 20 element mesh shows that a 36 element geometric discretization results in displacement errors of less than 0.005 inch and therefore is sufficiently accurate for this experiment. Figure D.4 plots by means of contours the value of I_1 at every point on the sheet; this information is needed to choose the best places in the body to take measurements. Figure D.5 shows the values of the variables I_1 and I_2 in each element of the body and tells us a priori which part of the I_1-I_2 plane is involved in the types of strain states encountered in this particular experiment. This indicates the domain of the material operator and makes possible the selection of an appropriate discretization for $C_1(I_1, I_2)$ and $C_2(I_1, I_2)$.

Of course, in an actual experiment we would have to determine the information in Figures D.4 and D.5 by solving the forward direction 36 element problem with an approximate $C_1(I_1, I_2)$ and $C_2(I_1, I_2)$. In this particular case a simple uniaxial tension test would be able to give a good approximation to the material functions. Even an extremely crude guess at $C_i(I_1, I_2)$ will

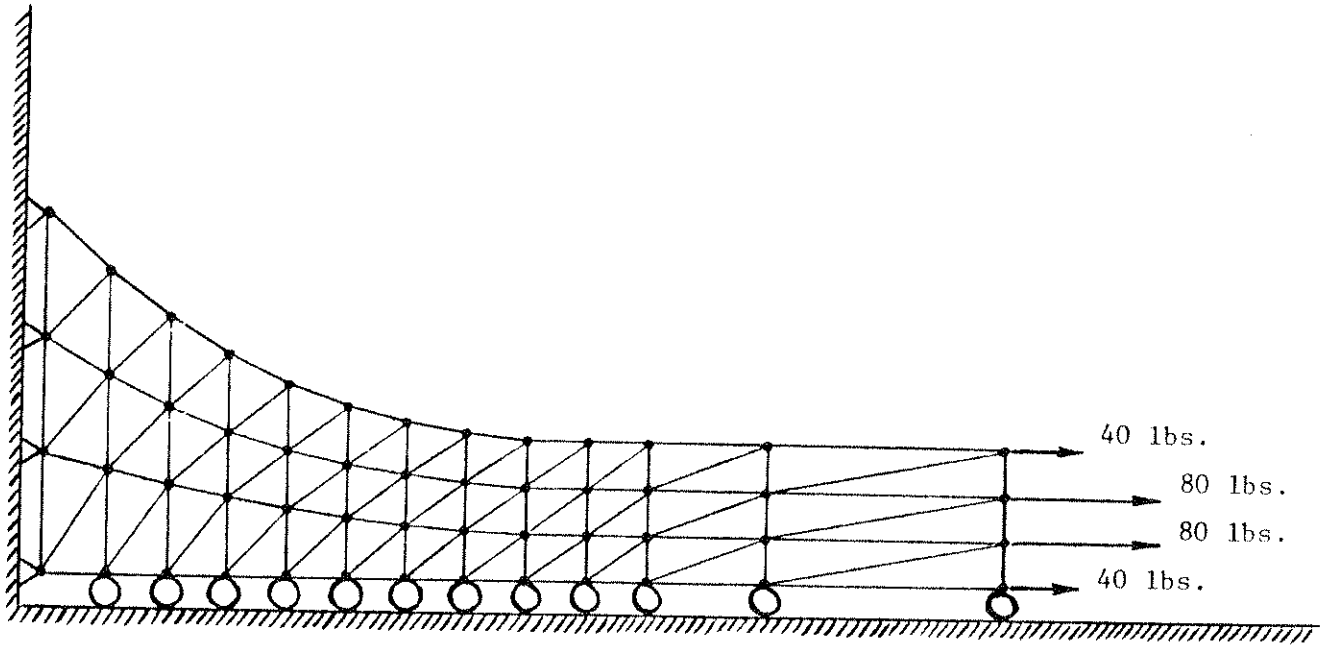

FINITE ELEMENT GEOMETRIC DISCRETIZATION

36 ELEMENT MESH

Fig. D.3

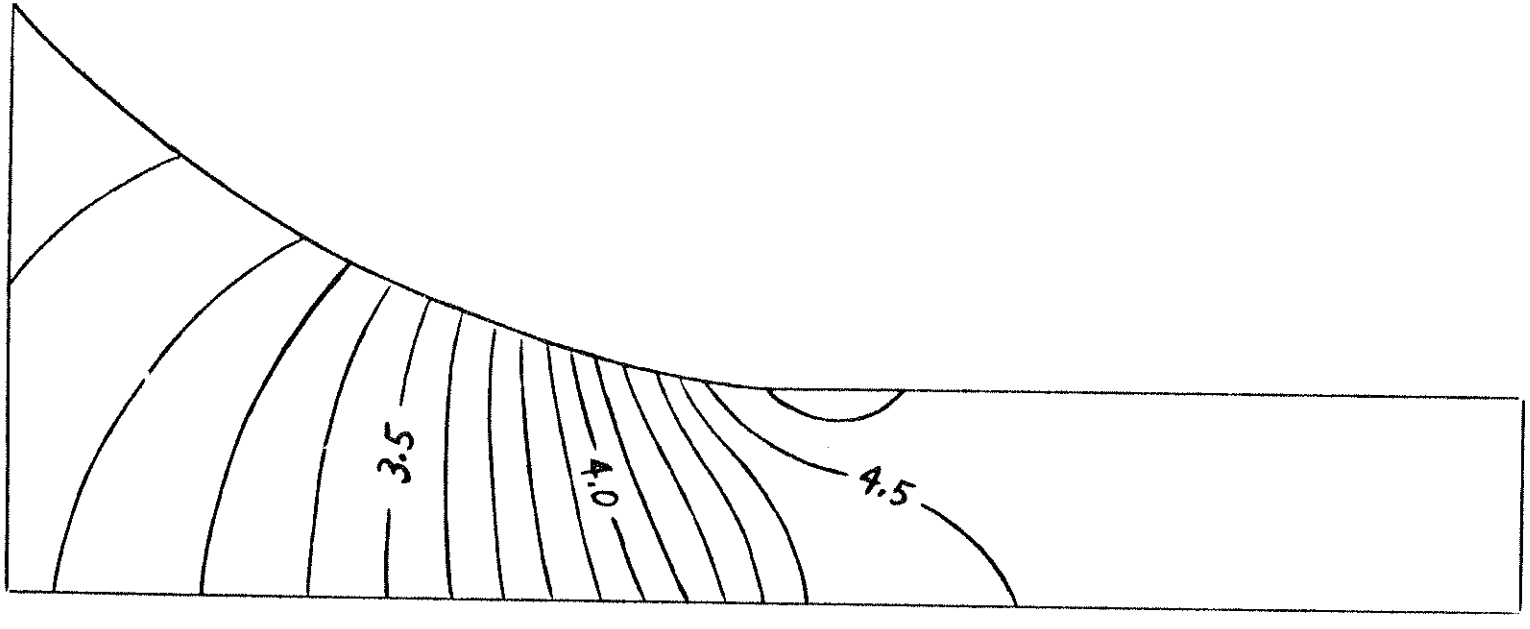

FIRST STRAIN INVARIANT DISTRIBUTION IN EXPERIMENTAL BODY

$I_1(x,y)$

Fig. D.4

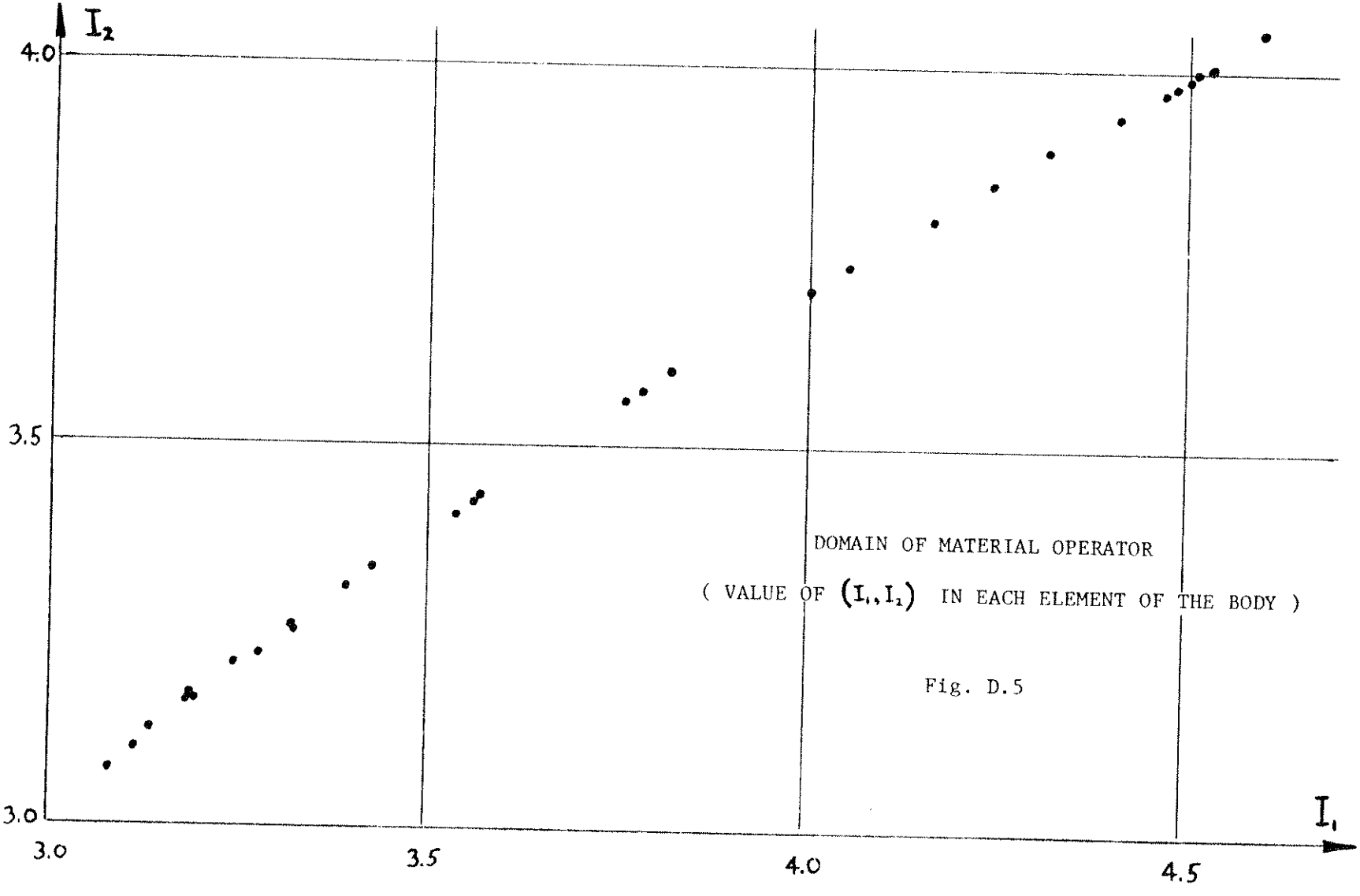

DOMAIN OF MATERIAL OPERATOR

(VALUE OF (I_1, I_2) IN EACH ELEMENT OF THE BODY)

Fig. D.5

give the experimenter a good idea of the strain invariant distribution to be expected in the experiment. And even a very crude guess at $C_i(I_1, I_2)$ will permit testing of the mesh to see if it's fine enough for the accuracy needed.

Twenty experimental measurements are to be used to identify the material, chosen as shown in Figure D.6. That is, the displacement changes between the 20 pairs of points indicated in Figure D.6 are computed from the forward direction solution of the 36 element model using the material functions (D.1). In an actual experiment, of course, these 20 items of input would be obtained by direct measurement of the deformed configuration of the test specimen.

The locations of these 20 measurements are chosen so that they quite evenly cover the strain range for which we want the identification to be valid. The strain range spanned by each input measurement is shown in Figure D.7 and is based on the I_1 spatial distribution plotted in Figure D.4. This particular set of measurements is suitable for a real experiment for the following reasons:

1) The effects of boundary conditions (which are difficult to calculate exactly because of the irregular action of the clamps) should not disturb the accuracy of the measurements. All measurements are somewhat away from the clamps and no item of input is based on the absolute location of any point in the body, but only upon relative distances between points.

2) All measurements are taken over as large a distance as

$\delta_1 = v_{13} - v_{11} = 6.39"$

$\delta_2 = v_{11} - v_8 = 3.01"$

$\delta_{11} = V_{52} - V_{13} = -0.75"$

etc.

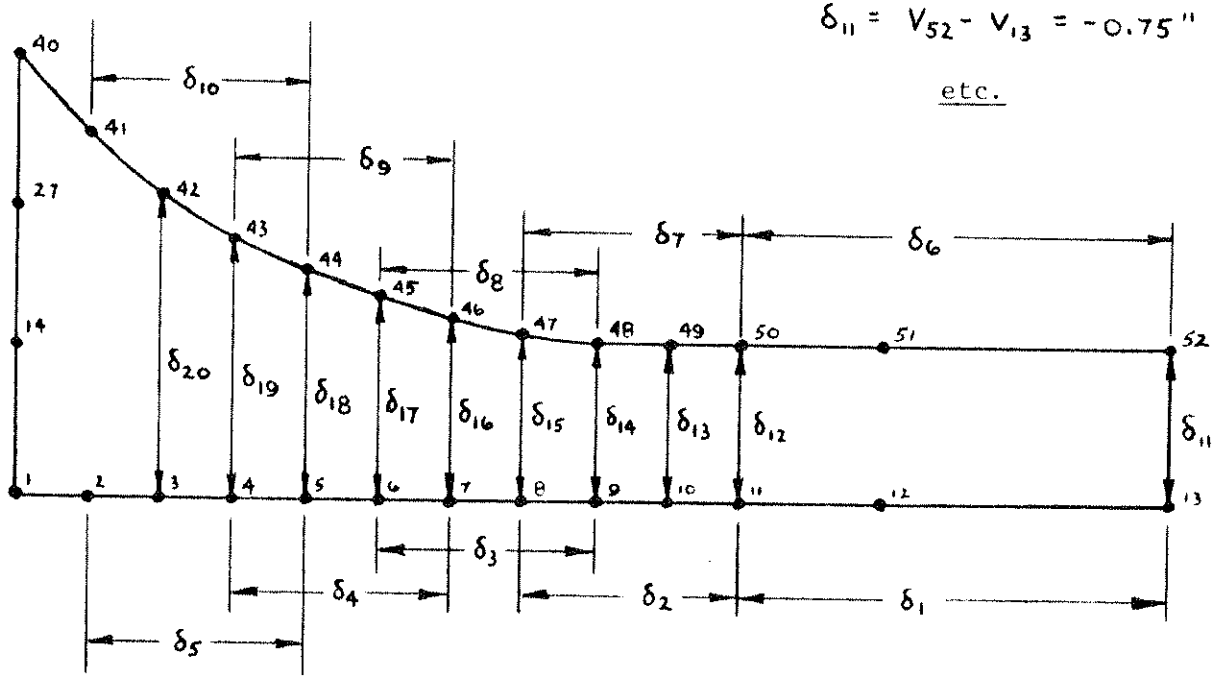

LOCATIONS OF 20 EXPERIMENTAL MEASUREMENTS USED AS INPUT DATA

Fig. D.6

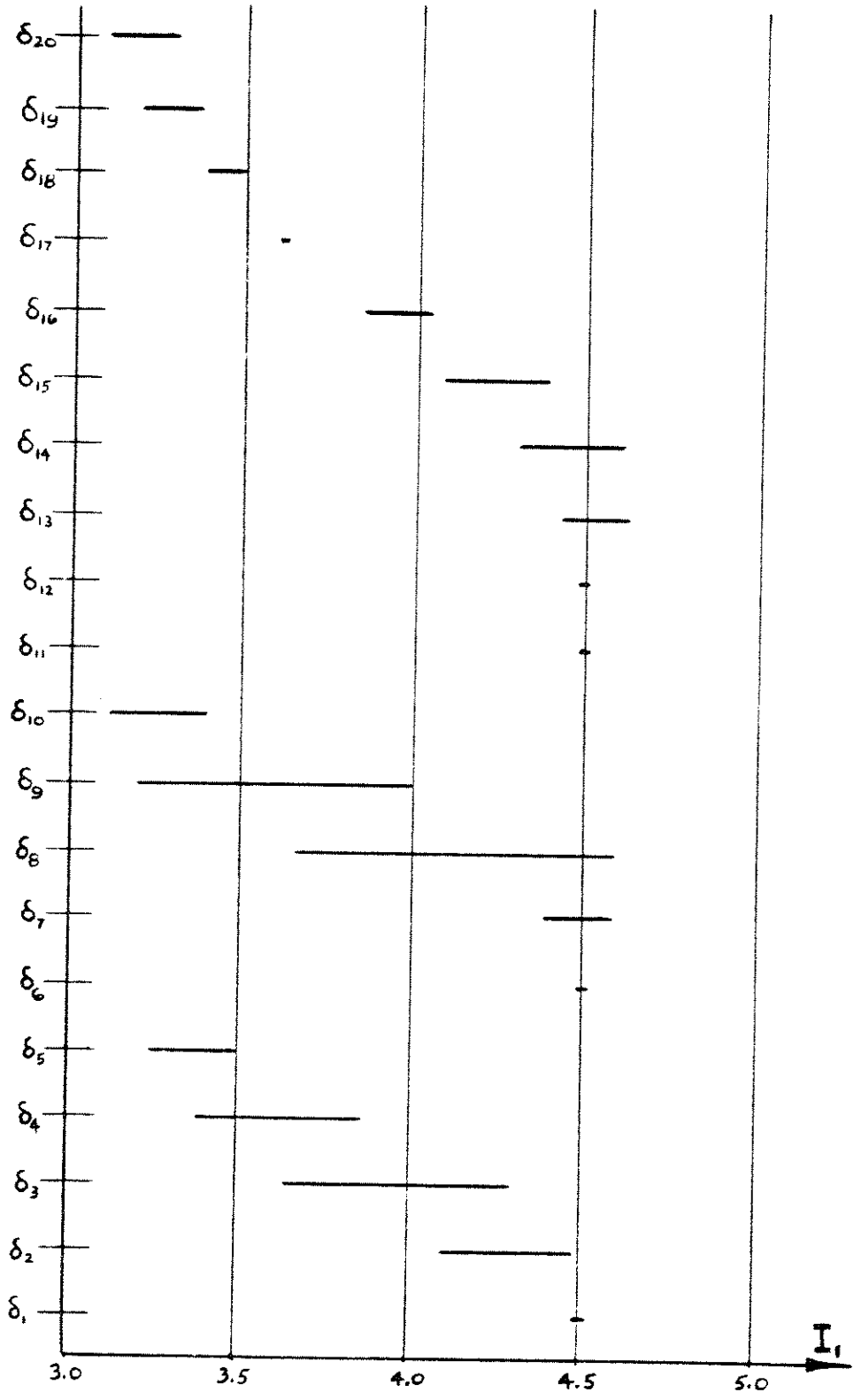

RANGE OF I_1 IN VICINITY OF EACH INPUT MEASUREMENT

Fig. D.7

possible so that experimental errors in measurement will be small relative to the magnitude of the input data. That is, care has been taken so that small experimental measurement errors will not give rise to sizeable errors in strain and hence introduce large errors into the identified material functions.

Figure D.5 shows that the domain of the material functions $C_1(I_1, I_2)$ and $C_2(I_1, I_2)$ involves only a very limited part of the full two-dimensional strain invariant space. A one-dimensional discretization with either I_1 or I_2 chosen as the independent variable is adequate for this experiment. A 6 degree-of-freedom discretization in I_1 is chosen, as shown below in Figure D.8:

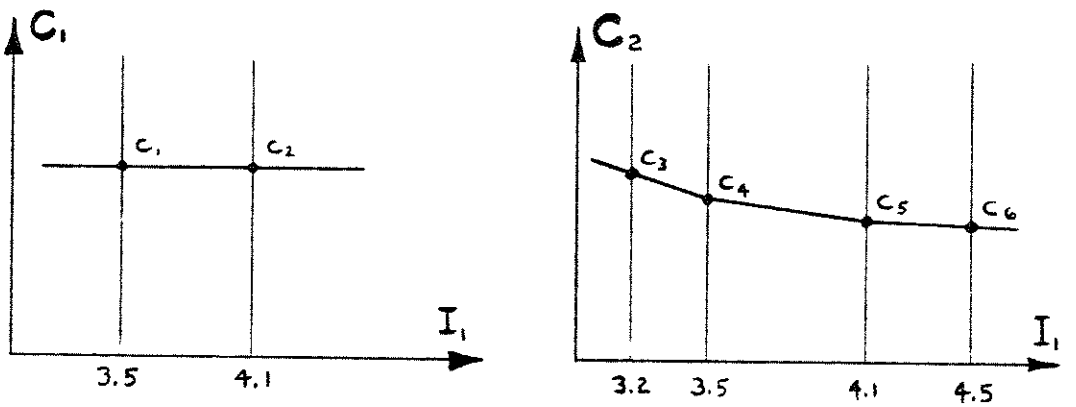

Fig. D.8

In a real experimental situation a great deal of intuition is needed to choose a good material discretization. There should be enough degrees of freedom to approximate closely the material functions; otherwise the algorithm may be forced to converge upon a very poor solution in order to best satisfy the 20 input measurements. And yet the mesh should not be much finer than

necessary, lest the solution become very sensitive to small experimental errors in the input data, as was discussed in Section 3 of Appendix C. Often a number of different discretizations must be attempted if no information about the shape of the material functions is available from earlier experiments.

These discretization choices lead to 160 nonlinear equations with 146 variables. The Newton-Raphson iteration is started with an estimate of C_1 = 25.0 psi. and C_2 = 7.0 psi. The weighting scheme used is $\{\omega_0, \omega_1, \omega_2\} = \{1, 100, 1\}$. The algorithm effected convergence after four iterations to the material parameters

$$\underset{\sim}{C} = \begin{Bmatrix} 25.20 \\ 25.82 \\ 9.08 \\ 7.06 \\ 4.01 \\ 2.05 \end{Bmatrix}, \tag{D.2}$$

and this identification is plotted in Figure D.9. Six minutes of CDC 6400 computer time was needed for this identification.

The resulting material characterization is quite good - certainly good enough for use in any kind of stress analysis problem. The results, however, are not as accurate as those of the 6 degree-of-freedom example in Appendix C (Figure C.21), probably because the roundoff errors in the input measurements have a distribution that is less Gaussian than those of the example in Appendix C. Note that the total stiffness measure - the term $\left(C_1 + \frac{1}{\lambda} C_2\right)$ - is very little in error; it is only the relative sizes of C_1 and C_2 that tend to be somewhat in error. However, this example shows that the least squares approach is

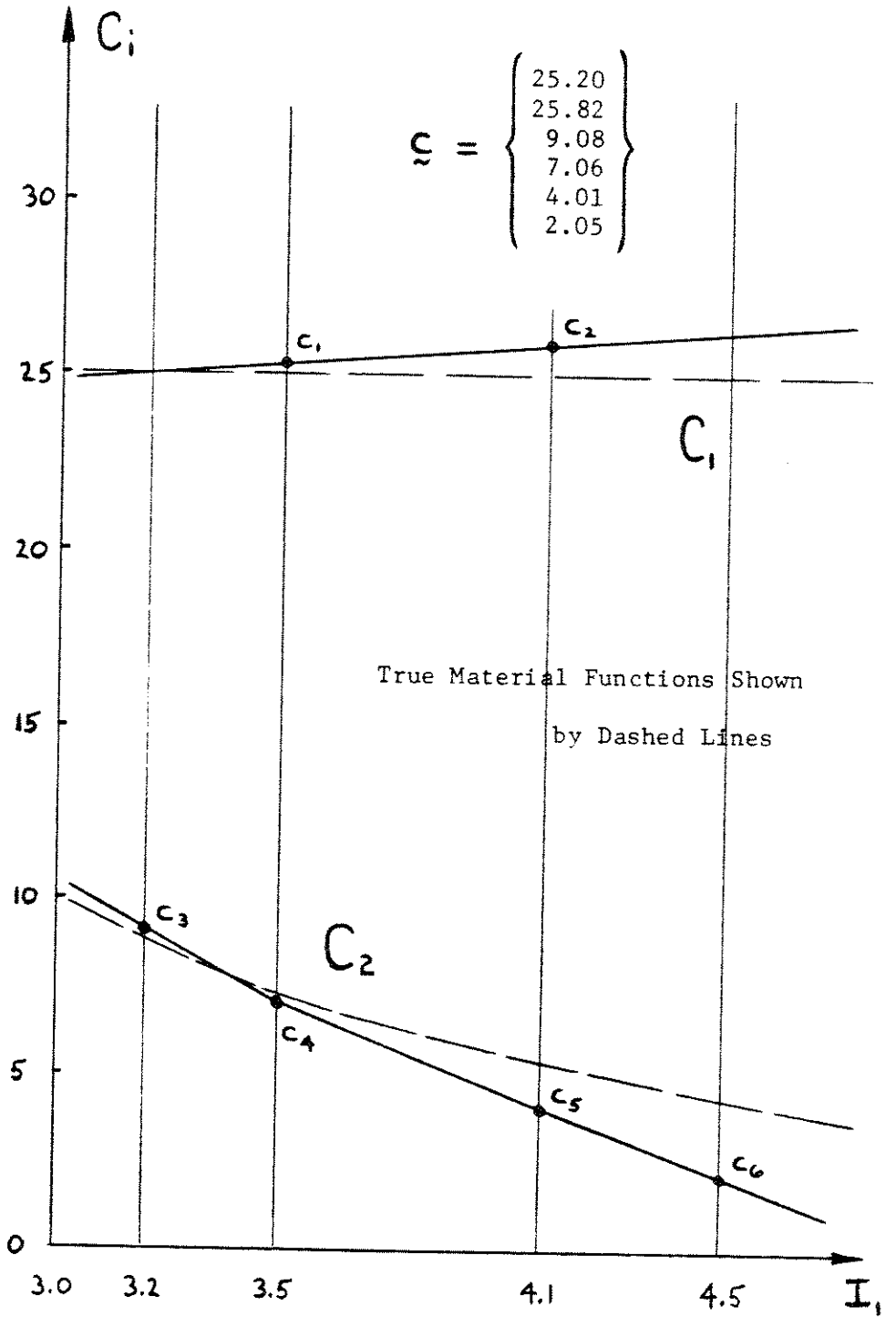

MATERIAL IDENTIFICATION FOR 36 ELEMENT EXPERIMENT

Fig. D.9

far more stable and gives infinitely more useful results than any method based on the direct solution of the equations governing the inverse problem.

The determining of the relative sizes of C_1 and C_2 is an extremely sensitive problem in an experiment with these particular states of strain. But conversely the forward direction solution of a stress analysis problem with these types of strain states is extremely insensitive to errors in the relative sizes of C_1 and C_2 ; it is only the total stiffness measure $(C_1 + \frac{1}{\lambda} C_2)$ that is really important. Hence the material functions identified will give virtually perfect results in boundary value problems within the strain invariant range over which the experiment was measured.

An excellent example of how considerable errors in the proportioning of the total stiffness between C_1 and C_2 will result in virtually no errors when the functions are used in solving stress analysis problems is the simple uniaxial stress state shown in Figure D.10.

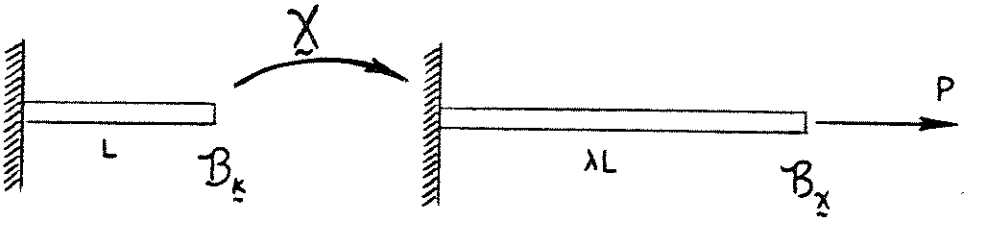

Fig. D.10

The stress constitutive equation governing this situation is

$$T_{11} = 2\left(\lambda - \frac{1}{\lambda^2}\right)\left(C_1 + \frac{1}{\lambda} C_2\right) \tag{D.3}$$

and the relation between extension ratio and the first strain invariant is

$$I_1 = \lambda^2 + \frac{2}{\lambda} . \qquad (D.4)$$

Assuming an extension ratio of 1.85 (and hence an I_1 of 4.50) the stress calculated using the exact material functions and the stress calculated using the approximate material functions just identified are charted below:

Material Functions Used To Solve for Stress:	C_1	C_2	T_{11}
Exact	25.00 psi	4.32 psi	85.1 psi
Identified (Figure D.9)	25.82 psi	2.05 psi	83.9 psi

That is, a 53% error in identifying the magnitude of C_2 led to only a 1.4% error in solving a stress analysis problem with it, and we can conclude that the material identification is quite sufficient for practical purposes.

In an actual experiment upon a specimen with unknown properties, the experimenter would use the results shown in Figure D.9 to optimize the material discretization. In this particular case Figure D.9 shows that C_1 is essentially a constant; hence a discretization with C_1 held constant might give better results. Figure D.11 illustrates the identification resulting from a 6 degree-of-freedom discretization (1 degree of freedom in C_1 and 5 degrees of freedom in C_2) using the same input data described in Figure D.6. This improved material mesh permits a virtually perfect identification of both material functions.

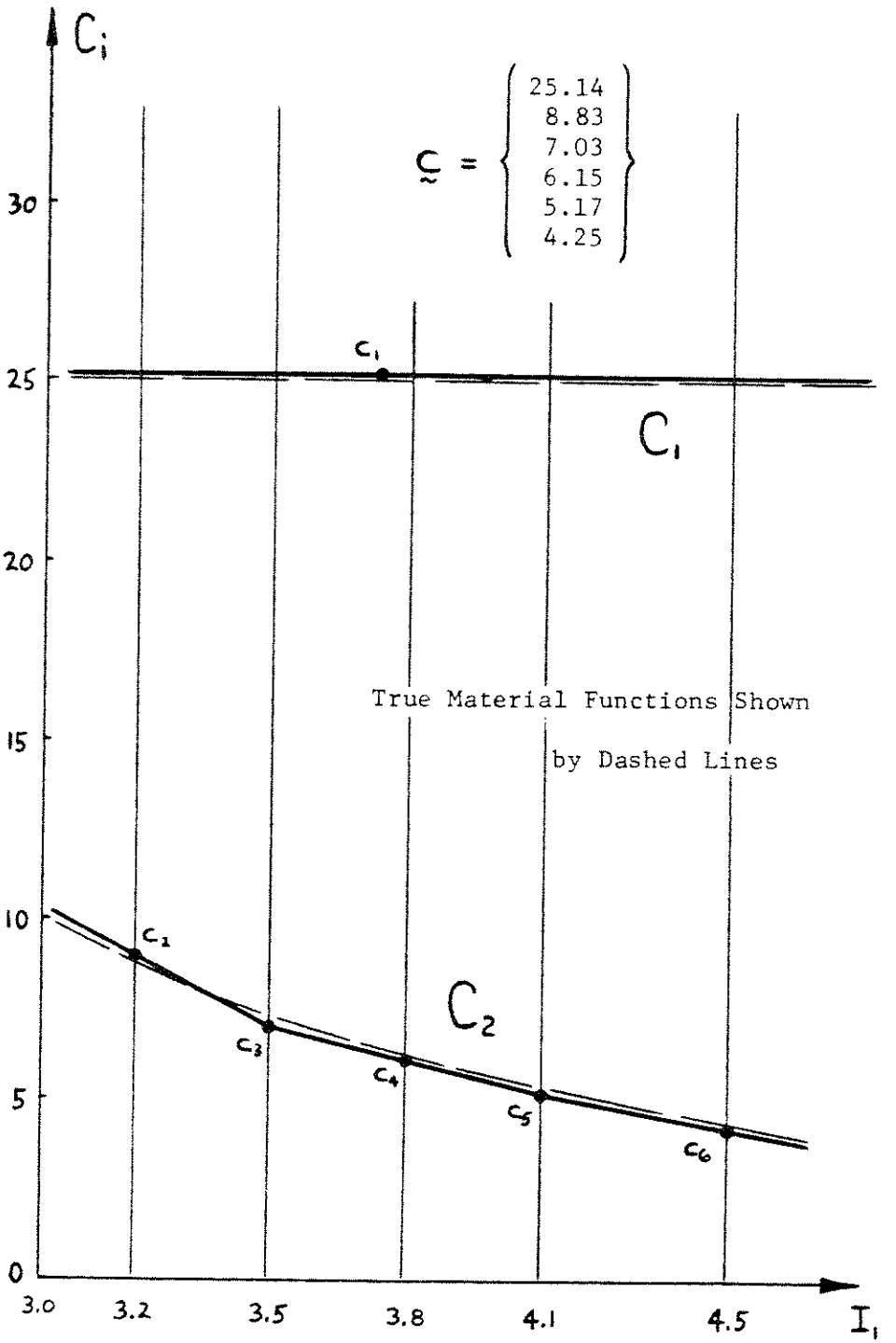

IMPROVED MATERIAL IDENTIFICATION FOR 36 ELEMENT EXPERIMENT

Fig. D.11

It would be useful to know how stable this identification technique is when a very large error or blunder accidentally occurs in the measured input data. To test for this, introduce an error of -0.33 inch in δ_5 (an error of 20%), leaving the other 19 measurements correct to the nearest hundredth inch. The resulting identification is shown in Figure D.12. A very fortunate buffering effect has been obtained by using a least squares averaging of the 20 items of input data to determine the 6 material degrees of freedom. The solution is quite reasonable: the only really significant error is in the range $I_1 < 3.50$, the strain range of the blundered measurement. An examination of how closely the least squares displacement solution corresponds to each of the 20 measurements used as input will pinpoint the location of the blunder. That is,

$$\underset{\sim}{\delta} - \underset{\sim}{g}(\underset{\sim}{\varrho}, \underset{\sim}{\lambda}) = \left\{ \begin{array}{r} 0.00 \\ 0.00 \\ -0.01 \\ 0.00 \\ -0.16 \\ 0.00 \\ 0.00 \\ 0.00 \\ 0.06 \\ 0.14 \\ 0.00 \\ 0.00 \\ 0.00 \\ 0.00 \\ 0.01 \\ 0.01 \\ 0.01 \\ -0.01 \\ -0.03 \\ -0.04 \end{array} \right\} \qquad \text{(D.5)}$$

shows the experimenter that there is some irregularity in the

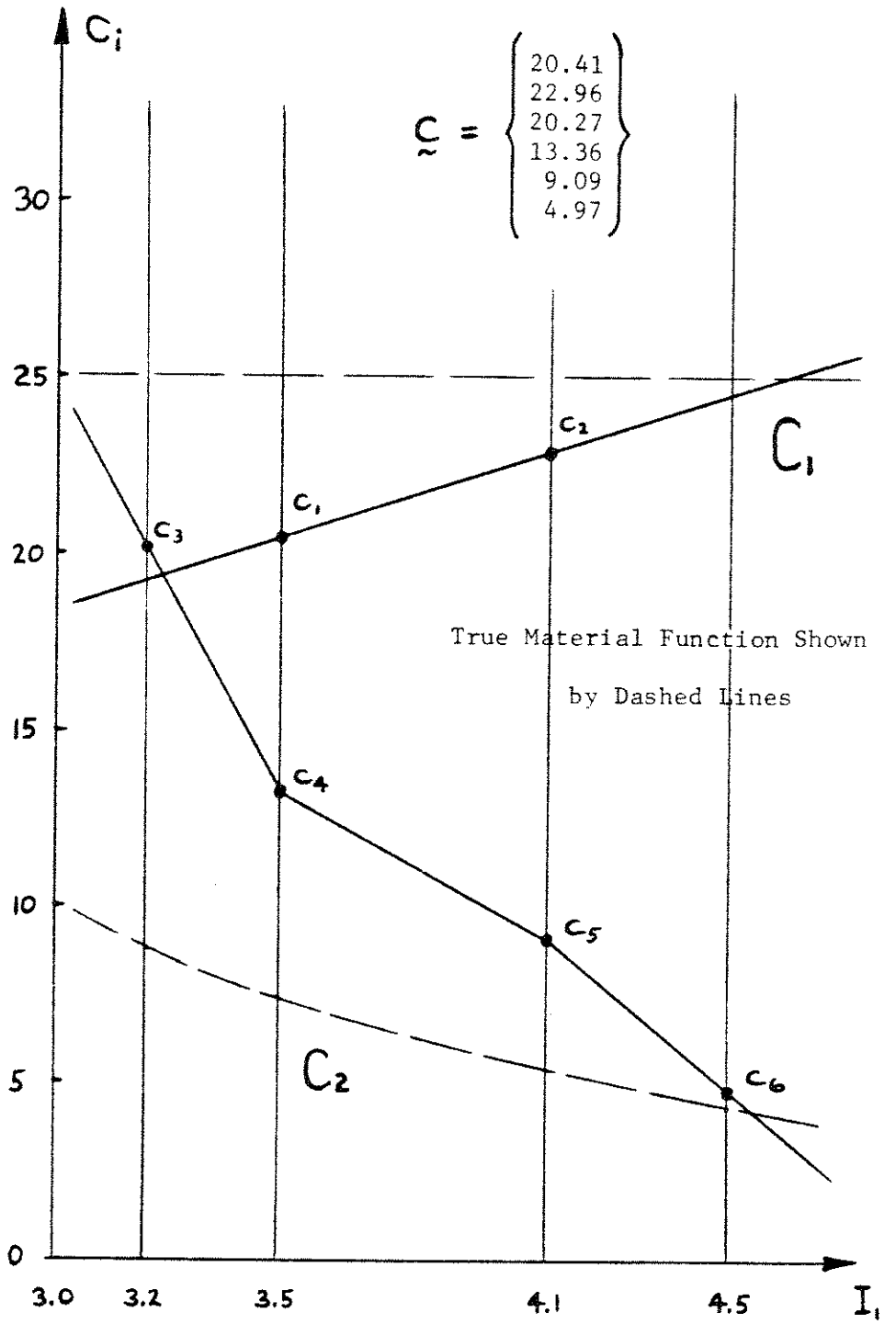

MATERIAL IDENTIFICATION WITH LARGE BLUNDER IN INPUT DATA

Fig. D.12